OFFSHORE SEDIMENT TRANSPORT AND EQUILIBRIUM BEACH PROFILES

This thesis is also published as Delft Hydraulics Laboratory Publication No. 131, 1974 and as Delft Hydraulics Laboratory Report M 918, Part 2, 1974

OFFSHORE SEDIMENT TRANSPORT AND EQUILIBRIUM BEACH PROFILES

PROEFSCHRIFT

TER VERKRIJGING VAN DE GRAAD VAN DOCTOR IN DE TECHNISCHE WETENSCHAPPEN AAN DE TECHNISCHE HOGESCHOOL DELFT, OP GEZAG VAN DE RECTOR MAGNIFICUS IR. H. B. BOEREMA, HOOGLERAAR IN DE AFDELING DER ELEKTROTECHNIEK, VOOR EEN COMMISSIE AANGEWEZEN DOOR HET COLLEGE VAN DEKANEN TE VERDEDIGEN OP WOENSDAG 18 DECEMBER 1974 TE 16.00 UUR

door

DIRK HERMANUS SWART

civiel ingenieur

geboren te Vishoek, Zuid-Afrika

W. D. MEINEMA B.V. – DELFT

Dit proefschrift is goedgekeurd door de promotor
prof. dr. ir. E.W. Bijker

Abstract

A predictive model, based on both model and prototype data, is developed to enable the computation of the offshore sediment transport on sandy beaches under wave action, as well as of the corresponding time-dependent and eventual equilibrium beach profiles.

Samenvatting

Een kwantitatief rekenmodel, gebaseerd op zowel model- als prototype-gegevens, is ontwikkeld voor het berekenen van het zeewaarts gerichte sediment-transport door golfactie op zandstranden en van de bijbehorende tijdsafhankelijke profielen en eventuele evenwichtsprofielen.

ACKNOWLEDGEMENTS

This thesis was prepared while the author was employed at the De Voorst Laboratory of the Delft Hydraulics Laboratory. The investigation reported herein was partly conducted under contract for the Dutch Ministry of Public Works (Rijkswaterstaat). The author is deeply indebted, both to the Management of the Laboratory for the possibility to conduct this study, and to the Ministry of Public Works for their consent to use the report of the investigation as a thesis. The support, interest and constructive critisism given by all the technical members of the Harbours and Coasts Branch, and especially by Ir. R. Reinalda, Chief of this Branch, during the preparation of this publication, is gratefully acknowledged. Data supplied by the United States Coastal Engineering Research Center were used to assist in the extrapolation of the model data to prototype conditions. The C.E.R.C.'s consent to use the data in this publication is highly appreciated.

CONTENTS

LIST OF SYMBOLS

LIST OF FIGURES

LIST OF FIGURES (continued)

LIST OF FIGURES (continued)

LIST OF TABLES

LIST OF PHOTOGRAPHS

LIST OF SYMBOLS

The most important symbols which have been used in the text are listed below. Those variables which have only been used locally have not been included. All symbols are also, in addition to this list, defined when they are used in the text for the first time.

a_0	amplitude of orbital excursion at the bed	L
C	concentration of suspended sediment	-
C_0	sediment concentration at a height z_0 above the bed	-
C_h	Chezy roughness coefficient	$L^{1/2}T^{-1}$
C_p	Hunt's porosity factor (< 1)	-
C_z	sediment concentration at a height z above the bed	-
d	actual water depth	L
d_b	actual water depth at point of wave breaking	L
D_{50}	median sediment particle diameter	L
E	wave energy per unit of surface area	MT^{-2}
f_w	Jonsson's wave friction factor for τ_{wm}	-
g	gravitational acceleration	LT^{-2}
h	still-water depth	L
h_0	upper limit of D-profile relative to still-water level	L
h_b	still-water depth at point of wave breaking	L
h_m	lower limit of D-profile relative to still-water level	L
H	wave height	L
H_0	deepwater wave height	L
H_b	breaking wave height	L
I	total volume of sediment in the coastal area	L^3
I_1	total volume of sediment in the onshore profile area	L^3
I_2	total volume of sediment in the offshore profile area	L^3
L_1	schematized onshore profile length	L
L_2	schematized offshore profile length	L
L_2-L_1	schematized length between the onshore and offshore profiles	L
L_e	schematized backshore length	L
L_t	schematized transition area length	L
m_0	initial beach slope at the still-water level	-
m_r	schematized equilibrium slope at the still-water level	-
p	breaker type	
p_B	ratio between orbital velocity at z = z' and that at the bed, as given by the 1st order wave theory, after Bijker	-

p_J	ratio between the orbital velocity at z = z' and that at the bed, as given by the 1st order wave theory, after Jonsson	-
q_y	Bakker's coastal constant	LT^{-1}
r	bed roughness	L
r(F(x),Y)	correlation coefficient	-
R_{yy}	radiation stress in direction perpendicular to the coastline	MT^{-2}
s_e	backshore constant	LT^{-1}
s_t	transition area constant	LT^{-1}
s_y	D-profile coastal constant	LT^{-1}
s_{y3}	value of s_y when $\delta_1 = 0$	LT^{-1}
s_{y4}	value of s_y when $\delta_1 = \delta$	LT^{-1}
s_{y2D}	value of s_y in the two-dimensional case	LT^{-1}
s_{y3D}	value of s_y in the three-dimensional case	LT^{-1}
s_{ym}	maximum value of s_y in the D-profile	LT^{-1}
S	sediment transport	L^2T^{-1} or L^3T^{-1}
S_{11}	upstream longshore transport capacity into onshore profile	L^3T^{-1}
S_{12}	downstream longshore transport capacity from onshore profile	L^3T^{-1}
S_{21}	upstream longshore transport capacity into offshore profile	L^3T^{-1}
S_{22}	downstream longshore transport capacity from offshore profile	L^3T^{-1}
S_b	bed load transport	L^2T^{-1}
S_e	backshore erosion rate	L^2T^{-1}
S_s	suspended load transport	L^2T^{-1}
S_t	transition area accretion rate	L^2T^{-1}
S_y	offshore transport rate at any location in D-profile	L^2T^{-1}
$\overline{S(d)}$	total onshore-offshore transport rate in coastal profile	L^2T^{-1}
t	time	T
T	wave period	T
u_0	orbital velocity at the bed	LT^{-1}
v	longshore current velocity	LT^{-1}
v_*	shear-stress velocity	LT^{-1}
V_b	sediment particle velocity at the bed	LT^{-1}
w	sediment particle fall velocity	LT^{-1}
W	equilibrium length between the onshore and offshore profiles	L
W_3	value of W when $\delta_1 = 0$	L
W_4	value of W when $\delta_1 = \delta$	L
W_e	total eroded length of the backshore	L
W_k	value of W at the k^{th} section in the D-profile	L
W_r	value of W at the water line	L
W_t	total growth of the transition area	L

y	horizontal ordinate relative to landward extremity of coastal area	L
Y	horizontal ordinate relative to the zero line	L
z	vertical ordinate	L
z_d	vertical ordinate of division between onshore and offshore profiles	L
z_{ik}	vertical ordinate of the i^{th} measuring point in the k^{th} section	L
Z	vertical ordinate relative to the reference level	L
Z_0	height of upper limit of D-profile relative to the reference level	L
Z_k	height of k^{th} section in the D-profile relative to the reference level	L
Z_m	height of lower limit of D-profile relative to the reference level	L
Z_r	height of still-water level relative to the reference level	L
α	slope	-
γ	breaker index	-
γ_p	breaker index for plunging breakers	-
γ_s	breaker index for spilling breakers	-
δ	total thickness of D-profile	L
δ_1	layer thickness of the onshore profile	L
δ_2	layer thickness of the offshore profile	L
δ_{2m}	offshore profile thickness where $s_y = s_{ym}$	L
δ_e	schematized backshore thickness	L
δ_t	schematized transition area thickness	L
Δ_{2m}	dimensionless offshore profile thickness where $s_y = s_{ym}$	-
Δ_m	absolute value of dimensionless position in the D-profile relative to Δ_{2m}	-
Δ_r	dimensionless position in the D-profile relative to the still-water level	-
$\Delta(..)$	small increment	..
ε	diffusion coefficient	L^2T^{-1}
$\bar{\xi}$	wave set-up, measured relative to the still-water level	L
$\bar{\xi}'$	wave set-up, measured relative to the actual water level	L
η	wave run-up, measured relative to the still-water level	L
$\mathcal{H}$	von Kármán's constant	-
λ	wave length	L

λ_0	deepwater wave length	L
μ	mean value	..
ρ_w	density of water	ML^{-3}
ρ_s	density of sediment	ML^{-3}
σ	standard deviation	..
τ_c	shear stress due to current action only	$ML^{-1}T^{-2}$
τ_w	shear stress due to wave action only	$ML^{-1}T^{-2}$
τ_{wc}	shear stress due to combined wave and current action	$ML^{-1}T^{-2}$
τ_{wm}	maximum value of τ_w	$ML^{-1}T^{-2}$

Subscripts

0	refers to conditions at the bed, or to deepwater conditions
b	refers to wave breaking
p	refers to plunging breakers
s	refers to spilling breakers
t	refers to time t

Chapter 1: Introduction

1.1 General

In order to design engineering structures which are to be built in the coastal environment, a detailed knowledge of the initial coastal regime is essential. In the design of such a maritime structure three clearly different aspects can be discerned, viz.:

(1) the structural design of the structure, to ensure that it can withstand the hydraulic forces exerted on it, such as forces due to wave action, current action, etc.,

(2) the design of the lay-out of the structure in such a way that it can be optimally used eventually,

and (3) the environmental design of the structure, i.e. such a positioning of the structure in the coastal environment, that the possible adverse effects on the surroundings, due to its building, are kept to a minimum. The building of the structure will lead to an adaptation of the hydraulic boundary conditions, such as the current pattern, wave height and direction, etc.. Accordingly the movement of bed material, both perpendicular and parallel to the coastline, will also change.

The optimal design will be that one in which the above-mentioned aspects are optimized. It is evident that in order to make an adequate design, the designer(s) should know which criteria will play a role in the evaluation of each of the above-mentioned three aspects.

The third aspect, i.e. the effect of a maritime structure on the surrounding coastal regime, will then offer the biggest problems. Qualitatively the coastal engineer can mostly give a reasonable indication of the type of changes that will be affected by the building of the structure. Such a qualitative answer can be backed by experience as well as by observations, either on site or in a small-scale model. The giving of a quantitative answer, however, is usually a much bigger problem, due to the inadequacies in the knowledge of the basic phenomena which could lead to the disturbance of the coastal equilibrium.

During the last few decades there has been an increased activity in the field of coastal engineering. The progress of the basic research is, however, hampered by the lack of adequate measuring techniques and devices. This situation is luckily changing, due to the increased research regarding the development of devices to measure water movement and sediment concentration under wave action. However, it will still take several years until all problems in the field of coastal engineering have been solved to such an extent that designs can be based on physically-justified analytical procedures.

The coastal engineer has another aid to assist in the designing of adequate structures, viz. the small-scale hydraulic model. Problems regarding sediment transport are mostly studied in a hydraulic model with a movable bed. Both the transport perpendicular to the coastline and that parallel to the coastline should be reproduced to scale in the model. Particularly due to the fact that the basic relationships between each of these transports and the boundary conditions are not exactly known, the interpretation of the results obtained from such movable bed models should be done with the utmost care. The model can then prove an invaluable guide to the coastal engineer.

It is thus of importance to continue the research in the field of the transport of bed material in the coastal environment. The basic knowledge regarding longshore transport is more advanced than that regarding onshore-offshore transport under wave action. In this report the last-mentioned phenomenon, i.e. the sediment transport under wave action in a direction perpendicular to the coastline, will be studied in more detail.

This investigation was partly done within the scope of an investigation into the effect of groynes on the coastal regime, commissioned by the Dutch Rijkswaterstaat and being performed in the De Voorst Laboratory of the Delft Hydraulics Laboratory, and partly as basic research of the Delft Hydraulics Laboratory. As such this dissertation will also be published as a report of the Delft Hydraulics Laboratory.

1.2 Scope of the study

In the previous section it was stated that at present the available measuring devices do not yet permit the measurement of momentary sediment concentrations and water velocities in a wave field with sufficient accuracy. Furthermore, neither the exact nature of the internal mechanism of sediment entrainment in a coastal environment, nor the exact interaction between the complicated water and sediment movement, is precisely known as yet. Consequently, it can be concluded that the problem of sediment transport under wave action in the onshore-offshore direction will not be solved by means of the internal mechanism in the direct future. For this reason the effect of the onshore-offshore transport on the profile will be schematized externally in this report. It will be shown that offshore sediment transport under wave action in the actual developing profile can be described with sufficient accuracy when the profile development is characterized into three different zones, each with its own characteristic transport mechanism, viz. (1) the backshore, above the wave run-up limit, (2) the real developing profile (called the D-profile in this report), where transport under wave action takes place and (3) a transition area, which is formed because the lower limit of the D-profile does normally not coincide with a horizontal bed. The sediment transport in this latter area is not necessarily negligible. The offshore transport taking place in the D-profile is the subject of this report; the time-dependent erosion of the backshore and growth of the transition area only serve as boundary conditions for the process in the D-profile.

In Chapter 2 an analysis is made of the internal mechanism, in order to lead to a schematization, which is as close as possible to the actual physical process. In Chapters 3 and 4 the schematization is worked out more thoroughly and derived in its final form. In Chapter 4.5 the area of applicability of the theory is derived and correlated to the available model and prototype data. The data used in this study are presented in Chapter 5. The bed material in all tests used for the evaluation in this report was sand, the median particle diameters ranged between 0.11 mm and 0.227 mm. As Bonnefille's formula [6], which was used to describe sediment entrainment, only applies to sand with a median diameter smaller than 0.7 mm, this diameter serves as an upper limit for the range of particle diameters to which the results of the

present investigation can be applied. As the number of tests in which onshore transport occurred is negligible, only tests in which offshore transport occurred were used in this study. The data were processed according to the developed schematization. The results are presented and evaluated in Chapter 6. The steps that are to be followed in the application of the method are summarized in Chapter 6.5. The main conclusions, following from the application of the schematization to the data, are given below in Chapter 1.3.

1.3 Conclusions

The principal conclusions of the investigation described in this report may be summarized as follows:

(1) The upper limit of the actual developing profile (called D-profile in this report) is related to the maximum wave run-up and is of the form given in equation (4.110).

(2) The lower limit of the D-profile is related to the beginning of movement of bed material under wave action and is of the form given in equation (4.125).

(3) The offshore transport at any location in the D-profile at any time t is proportional to the difference between the equilibrium profile form and the profile form at time t, according to equation (4.90). The application of equation (4.90) is described in Chapter 6.5.

(4) The sediment transports at the upper and lower limits of the D-profile are not necessarily negligible; these transports follow the same time-dependent variation as given by equation (4.90).

(5) The form of the dimensionless equilibrium D-profile is determined by the particle diameter according to equation (6.20).

(6) The horizontal scale of the equilibrium D-profile is determined by the absolute value of the deepwater wave height, the deepwater wave steepness and the particle diameter, according to equation (6.32).

(7) The equilibrium beach slope at the upper limit of the D-profile increases with increasing particle diameter, while the equilibrium slope at the lower limit of the D-profile decreases with increasing particle diameter.

(8) The equilibrium D-profile under three-dimensional conditions is as a first approximation equal to that under corresponding two-dimensional conditions.

(9) The rate of offshore transport under three-dimensional conditions is higher than under corresponding two-dimensional conditions, due to the increase in the average bed shear (equation (6.88)).

1.4 Recommendations

The results of the present study open the possibility to compute offshore sediment transport under either wave action only or combined wave and current action. However, it is recommended that in order to improve the accuracy of the computational method, a number of investigations be initiated, or continued, as the case may be.
As the median particle diameter of the bed material used in the study never exceeded 0.227 mm, it is suggested that tests be done with median particle diameters ranging between 0.227 and 0.7 mm. It should also be investigated if the principle of the physically-based empirical relationships found in this study can also be applied to the transport phenomena for coarser bed materials ($D_{50} \geqslant 0.7$ mm).

In order to improve the extrapolation of the small-scale test results to (full-scale) prototype conditions, model tests should be done in which the boundary conditions are closer to those occurring in prototype. This implies tests with a wave height in excess of one metre. An improvement of the quantity and quality of actual prototype measurements regarding onshore-offshore transport will be invaluable.

The tests described in this investigation were all performed with regular wave attack. As all prototype waves are by definition irregular, the study of coastal processes under irregular wave attack should get preference in future.

The number of three-dimensional tests used in the evaluation in this investigation is limited. More research should be done into the effect of the three-dimensionality of the wave and current pattern on the onshore-offshore sediment transport. Especially the internal mechanism of rip currents and their effect on the overall transport pattern should be the subject of increased research.

In future more tests should be done in which the initial profiles are flatter than the eventual equilibrium profiles, to ensure that onshore transport will occur. As the initial profile influences the wave breaking mechanism, which in turn determines the water movement in the breaker zone, a study regarding the mechanics of wave breaking will increase the insight into onshore-offshore sediment transport.

As in most of the above-mentioned investigations, the progress in the basic research regarding the vertical velocity profile, the entrainment of sediment and the sediment concentration distribution at any location in the profile is hampered by the lack of appropriate measuring devices and techniques.
Nevertheless, this basic research should be continued with the highest priority. When these basic problems have been fully solved, it will become possible to compute the sediment transport in onshore-offshore direction by means of the internal mechanism of sediment transport. Until that time the approach followed in this report can be used to compute the magnitude of the offshore sediment transport.

Chapter 2: Analysis

2.1 General

The onshore-offshore transport at any section in a non-equilibrium profile can be characterized as being a combination of bed load transport and suspended load transport. The amount of bed load is strongly influenced by the bottom shear stress and can be assumed as a first approximation to be equal to the sediment concentration immediately above the bed, multiplied by a layer thickness and by some characteristic particle velocity in the layer, which need not be equal to the actual water velocity at that location. The particle velocity of suspended load, on the other hand, is not so strongly influenced by the bottom. Suspended load can thus be found by integration of the momentary horizontal water velocity and the momentary sand concentration over the water depth, and averaging over the wave period (convection transport).

The character of the sediment load in a small-scale model is expected to be different from that in the prototype, as the bed roughness in a small-scale model has a relatively larger influence on the water movement in the nearshore area than in the (full-scale) prototype.

As the scale of the model decreases, i.e. as the model becomes bigger, the influence of the bed roughness on the water movement in the nearshore area will gradually decrease. This varying influence of the bed roughness will give rise to a scale effect in the reproduction of sediment transport phenomena. Observations learnt that the suspended load in a model can be classified into a few clearly different modes, viz.:

(1) During the passing of the wave crest, while relatively large landward-directed velocities occur, small vortices (containing sand in suspension) are formed on the downstream (landward) side of the ripples in a zone close to the sea bed, at a height of one to two ripple heights above the bed. When the wave trough passes, on the other hand, the seaward-directed velocity, mostly lower than the landward-directed velocity under the crest, but which occurs during a longer period of time, carries away the vortices in seaward direction.

(2) In a turbulent boundary layer above the zone described under (1), with a height of a few ripple heights, the vortices described under (1) are diffused.

(3) Two different modes of transport can be distinguished in the zone above the turbulent boundary layer. At any location outside the breaker zone the suspended load can be characterized by the convection transport, as stated earlier in this paragraph. Inside the breaker zone, where the wave motion is extremely non-linear, the situation is much more complicated, partly due to the unknown turbulence pattern, partly due to the presence of trapped air.

Onshore-offshore transport under wave action normally takes place in the nearshore region landwards of the location with a water depth of approximately two to three times the breaker depth.
In this chapter the above-mentioned complicated water movement and sediment concentration in the nearshore region will be simplified, in order to allow an evaluation of the long-term time-variation of onshore-offshore sediment transport. The results will be used to formulate some simplified assumptions regarding a schematization of onshore-offshore transport.

NOTE: It should be stressed that the aim of this chapter is not to solve the problem of onshore-offshore transport under wave action theoretically, but only to provide a firm base for a schematic representation of the problem.

2.2 Water movement

The velocity field developed during the shoaling and eventually during the breaking of the waves, is of the utmost importance when a study is made of the transport phenomena in the nearshore area. This velocity field under the wave is closely related to the wave form.
At present no single wave theory exists which adequately describes the wave form and velocity field under the wave in the whole area from deep water, through the breaker zone, to the water line.
The waves become extremely asymmetrical in the nearshore area, consequently the orbital motion under the wave also becomes asymmetrical.

Longuet-Higgins [33] showed theoretically that, in addition to the orbital motion, a mass-transport circulation cell can be expected to occur in the nearshore region outside the breaker zone, due to the asymmetry in the wave form. The mass-transport velocity in Longuet-Higgins' solution of the Navier-Stokes equations is in the direction of wave propagation near the bed and near the water surface, and in opposite direction at intermediate depths. Longuet-Higgins studied a case with constant water depth. In the present case with a sloping bottom his result can be summarized as follows:

$$v_{m2} = f\ (H,\ T,\ d/\lambda_0,\ z,\ P\ (t)) \tag{2.1}$$

where v_{m2} = mass-transport velocity outside the breaker zone (according to Longuet-Higgins [33]).

H = wave height

T = wave period

λ_0 = deepwater wave length

z = vertical coordinate, measured upwards from the bed

$P(t)$ = a time-dependent characteristic bottom profile quantity, left undefined for the time being. Later in this chapter the form of $P(t)$ will be discussed in more detail.

Inside the breaker zone, however, especially near the water line, the asymmetry will become so strong that an orbital velocity, as described by any existing theory, will be practically non-existent. Under the breaking wave crest an extremely non-linear mass-transport of water will flow in landward direction near the surface, while in the lower regions (near the bed) a normal landward-directed orbital velocity might still exist. Under the wave trough the water will return in seaward direction over the full depth.
The form of the mass-transport velocity due to the breaking of the waves will be closely related to the breaker type p. In general it can be stated that:

$$v_{m1} = f\ (H,\ T,\ d/\lambda_0,\ z,\ p) \tag{2.2}$$

where v_{m1} = mass-transport velocity inside the breaker zone due to breaking waves

p = breaker type (plunging, spilling, etc.), which is partly determined by the profile characteristics.

Nakamura et al. [37] found experimentally that

$$\gamma = \frac{H}{d} = f(H/\lambda\ ,\ P(t),\ p) \tag{2.3}$$

where λ = wave length at water depth d

γ = breaker index.

With the aid of equation (2.3) it will be shown in Chapter 4 that

$$p = f(H/\lambda\ ,\ P(t),\ H/d) \qquad \text{(see Figure 29)} \tag{2.4}$$

It is thus obvious that it will be extremely difficult to obtain one analytical model to represent the water movement in the whole nearshore area (inside as well as outside the breaker zone).

However, it can be stated in general that at any time t the resultant velocity v_z at a height z above the bed, for any location in the nearshore region, can be written as:

$$v_z = v_y + v_m \tag{2.5}$$

where v_y = horizontal component of the orbital velocity at any time t, at a height z above the bed

$$= f(H,\ T,\ d/\lambda_o,\ \tau,\ z) \tag{2.6}$$

v_m = mass-transport velocity at time t, at a height z above the bed, which can be the result of either the wave asymmetry or of the breaking waves, or of both

v_z = resultant horizontal component of the velocity at time t, at a height z above the bed

τ = time: $0 < \tau \leq T$.

It follows from equation (2.1) ... (2.6) that:

$$v_z = f(H,\ T,\ d/\lambda_o,\ z,\ \tau,\ H/\lambda\ ,\ P(t),\ H/d) \tag{2.7}$$

where P(t) = a characteristic bottom profile quantity, which can be time-dependent.

For any specific set of wave conditions (H, T) and water depth d, equation (2.7) reduces to:

$$v_z = f(\tau, z, P(t)) \tag{2.8}$$

v_z will show both a short-term variation in time τ ($0 < \tau \leqslant T$) and a long-term variation in time t ($t \gg T$). The long-term variation in time t is related to the long-term variation in bottom profile P(t).
All water velocities are positive when directed in landward direction.
The form of the variation of these above-mentioned velocities in both time and space is left undefined, as it is not of importance for the following analysis.

2.3 Sediment concentration

The transport S_s of suspended material is built up of transport by convection, a diffusion transport, proportional to the gradient in the concentration and a transport due to the own motion of the suspended material. Thus:

$$S_{si} = Cv_i - \varepsilon \nabla_i C + Cw_i \tag{2.9}$$

where index i, being 1, 2 or 3, denotes the component in one of the three coordinate-directions

S_s = transport of suspended material/unit of area and time
C = sediment concentration
ε = diffusion coefficient
v = water velocity
w = sediment particle velocity with respect to the water velocity
∇_i = gradient in direction i
Cv_i = convection transport/unit of area and time
$\varepsilon \nabla_i C$ = diffusion transport/unit of area and time
Cw_i = transport due to own motion of material/unit area and time

The continuity equation for the sediment reads:

$$\frac{\partial C}{\partial t} + \nabla_i S_{si} = 0 \tag{2.10}$$

where subscript i denotes the component in <u>each</u> of the coordinate-directions, i = 1,2 and 3, according to the Einstein-convention, as long as i occurs twice in any term of the equation.

Substitution of equation (2.9) into equation (2.10) yields:

$$\frac{\partial C}{\partial t} + \nabla_i (Cv_i) - \nabla_i (\varepsilon \nabla_i C) + \nabla_i (Cw_i) = 0 \qquad (2.11)$$

By using the continuity equation for the water movement, viz.:

$$\nabla_i v_i = 0 \qquad (2.12)$$

equation (2.11) can be rewritten as:

$$\frac{\partial C}{\partial t} + v_i \nabla_i C - \nabla_i (\varepsilon \nabla_i C) + \nabla_i (Cw_i) = 0 \qquad (2.13)$$

The velocity v_i in any direction i in equation (2.13) is the resultant of all velocity components in direction i. In the two-dimensional case, where a wave propagates into shallower water, only the directions y (in the direction of wave propagation) and z (vertical coordinate) will remain. The velocity v_i will be time-dependent.
The solution of equation (2.13), the equation for the continuity of motion of suspended sediment, will yield the vertical distribution of the sediment concentration C_z.
Due to a lack of knowledge regarding both the mechanism of sediment entrainment under wave action and the diffusion coefficient ε, the solution of equation (2.13) is unknown. Various researchers, such as Shinohara et al. [46], Hom-ma and Horikawa [19], Hattori [18] and Bhattacharya [5], making different assumptions, arrived to expressions regarding the vertical distribution of the suspended sediment. Summarizing their results, it can be stated that all the relationships for the vertical distribution of suspended sediment are of the form:

$$C_z = \overline{C}_0 f(z) \qquad (2.14)$$

where C_z = sediment concentration at any time t, at a height z above the bed

$\overline{C}_0$ = time-average (over one wave period) of the sediment concentration at time t, at a reference level at a small height z_0 above the bed

= $\overline{C}_0(t)$ ($t >> T$). For $t \leqslant T$ it will be assumed that $\overline{C}_0$ is independent of time. This long-term time-dependence of the sediment concentration is a result of a variation in time of the bottom profile characteristics, and consequently $\overline{C}_0 = \overline{C}_0 (P(t))$.

$f(z)$ = a function which has to account for the short-term time-variation of the sediment concentration ($\tau \leqslant T$). $f(z)$ is

dependent of the height z above the bed, as well as of the local profile, wave and sediment characteristics, i.e.

$$f(z) = F(H, T, d, z, w, \tau, P(t)) \qquad (2.15)$$

where $0 < \tau \leqslant T$

$t >> T$

w = sediment particle fall velocity

For fixed wave conditions (H, T) and bed material (D_{50}, w) and for a specific water depth d, equation (2.15) reduces to:

$$f(z) = F(z, \tau, P(t)) \qquad (2.16)$$

Physically equation (2.14) means that at any time t the sediment concentration at any height z above the bed can be expressed in terms of the sediment concentration at a reference level close to the bed. The precise form of the expression f(z), relating these concentrations to each other, will be dependent of the mechanism of sediment entrainment, as has been stated earlier. For the analysis in this chapter the form of f(z) need not be explicity known.

2.4 Sediment transport

Qualitatively the sediment transport, as described by equation (2.9), can be schematized as shown in Figure 1. It has been shown in the introductory remarks in Chapter 2.1 that the sediment transport can be subdivided into different classes. In the upper layer the gradients (in both time and space) of the water velocity and sediment concentration are low, and it is sufficiently accurate to describe the sediment transport as being purely convection transport, i.e.

$$\overline{S}_s = \frac{-1}{T} \int_{z_0}^{d+\eta} \int_{0}^{T} v_z \, C_z \, d\tau \, dz \qquad (2.17)$$

where $\overline{S}_s$ = time-average of the sediment transport in the upper layer, averaged over one wave period. $\overline{S}_s$ will be called suspended load in the rest of this evaluation and is positive when directed in seaward direction. The minus-sign is the result of the fact that the sediment particle and water velocities are positive when directed in different directions ($\overline{S}_s$ positive seawards, v_z positive landwards)

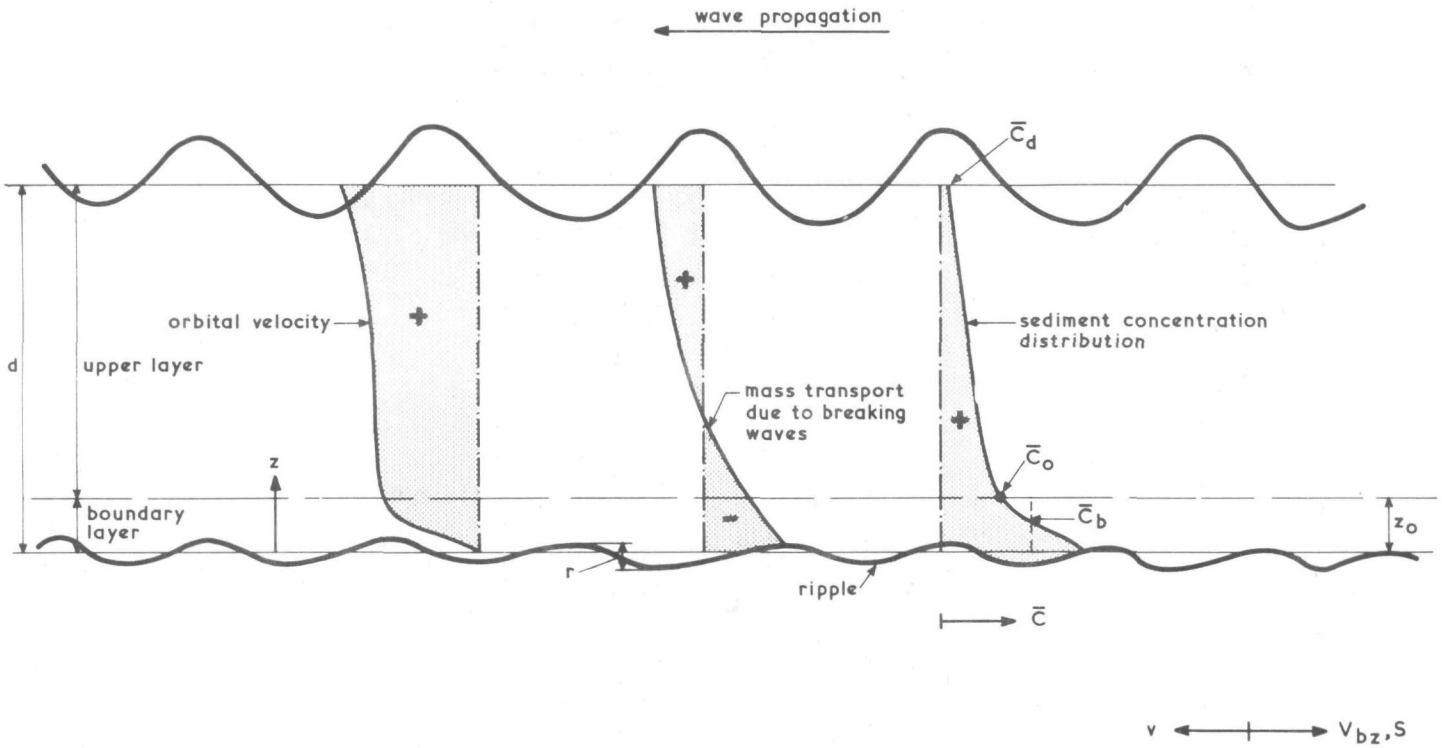

SCHEMATIZATION OF TRANSPORT

FIGURE 1

T = wave period

$d+\eta$ = water surface, measured relative to the bed.

Substitution into equation (2.17) of the value of v_z from equation (2.8) and of the value of C_z from equations (2.14) and (2.16) respectively, yields:

$$\overline{S}_s = - \int_{z_0}^{d+\eta} \int_{0}^{T} \frac{\bar{C}_0 (P(t))}{T} v_z (z, \tau, P(t)) F(z, \tau, P(t)) \, d\tau dz \qquad (2.18)$$

If the precise forms of v_z and F are known, equation (2.18) can be integrated, the variables z and τ will then be eliminated. For a specific bed material, wave condition and location in the profile, the integral will then have the following form:

$$\overline{S}_s = - \overline{C}_0 (P(t)) \Psi_s (P(t)) \qquad (2.19)$$

where $\Psi_s (P(t))$ = a function which is defined for a specific bed material, wave condition and location in the profile.

In the boundary layer, on the other hand, where the sediment entrainment takes place, and which is as such the origin of the sediment concentration in the vertical, the gradients in both the water velocity and the sediment concentration are large. The interaction between the complicated turbulent water movement and the sediment transport is accordingly quite strong. The onshore-offshore component of the bed load/unit of height will have to be expressed as the product of a sediment particle velocity V_{bz} and a sediment concentration. The total bed load then becomes:

$$\overline{S}_b = \frac{1}{T} \int_{0}^{z_0} \int_{0}^{T} V_{bz} C_z \, d\tau dz \qquad (2.20)$$

where V_{bz} = sediment particle velocity in the boundary layer. V_{bz} is positive when in seaward direction.

The sediment particle velocity V_{bz} in the boundary layer will at any moment be related to the local water velocity.

$$V_{bz} = K_v (\tau, P(t))\, v_z (z, \tau, P(t)) \qquad (2.21)$$

where $K_v (\tau, P(t))$ = a function defining the relationship between the instantaneous sediment particle velocity and the local water velocity. K_v can show both a short-term ($0 < \tau \leqslant T$) and a long-term ($t >> T$) variation in time.

Substitution of the value of V_{bz} from equation (2.21) and of the value of C_z from equations (2.14) and (2.16) into equation (2.20) yields:

$$\overline{S}_b = \int_0^{z_0} \int_0^{T} \frac{\overline{C}_0 (P(t))}{T} K_v (\tau, P(t))\, v_z (z, \tau, P(t))\, F (z, \tau, P(t))\, d\tau dz \qquad (2.22)$$

As soon as the precise forms of K_v, v_z and F are known, equation (2.22) can be integrated and the variables z and τ will be eliminated. For a specific bed material, wave condition and location in the profile, the integral will then have the following form:

$$\overline{S}_b = \overline{C}_0 (P(t))\, \Psi_b (P(t)) \qquad (2.23)$$

where $\Psi_b (P(t))$ = a function which is defined for a specific bed material, wave condition and location in the profile.

At any moment the total sediment load can be found by addition of the bed load and the suspended load:

$$\begin{aligned} \overline{S(d)} &= \overline{S}_s + \overline{S}_b \\ &= \overline{C}_0 (P(t)) \left[\Psi_b (P(t)) - \Psi_s (P(t)) \right] \\ &= f (P(t)) \end{aligned} \qquad (2.24)$$

where $\overline{S(d)}$ = the total sediment transport (suspended load plus bed load) through a section with actual water depth d

$f(P(t))$ = an analytical function of the profile characteristic P(t), which is defined for any specific bed material, wave condition and water depth.

If $f(P(t))$ is continuous in time, which seems to be a realistic assumption, it can be rewritten in terms of an infinite Taylor-series, viz.:

$$\overline{S(d)} = f(P(t)) = \sum_{n=0}^{\infty} \frac{(P(t) - P(t_0))^n}{n!} f^{(n)}(P(t_0)) \tag{2.25}$$

$$= f(P(t_0)) + \sum_{n=1}^{\infty} \frac{(P(t) - P(t_0))^n}{n!} f^{(n)}(P(t_0)) \tag{2.26}$$

$$= f(P(t_0)) + \Phi(P(t), P(t_0)) \tag{2.27}$$

where $\Phi(P(t), P(t_0)) = \sum_{n=1}^{\infty} \frac{(P(t) - P(t_0))^n}{n!} f^{(n)}(P(t_0))$ (2.28)

$P(t_0)$ = a constant, which is dependent of the bed material, wave characteristics and the water depth

$f^{(n)}(P(t))$ = the n^{th} derivative of $f(P(t))$

$f(P(t_0))$ = a constant, which is dependent of the bed material, wave characteristics and the water depth. $f(P(t_0))$ is a function of the constant characteristic $P(t_0)$.

The constant $f(P(t_0))$ can be determined if at any time t the values of both $\overline{S(d)}$ and $\Phi(P(t), P(t_0))$ are known. In the following it will be shown that at $t = \infty$ the boundary conditions $\overline{S(d)}$ and $\Phi(P(t), P(t_0))$ are known. Due to the variation of the water velocity in time and space the resultant transport through any section in the profile at any time t can consist of both a landward and a seaward component. Addition of these two components will yield the total sediment transport through a section. The transport determined in this manner will be the same as that found in equation (2.27) by the addition of the bed load and the suspended load. Due to this resultant transport bottom changes will occur in the profile. The bottom profile is thus a function of time, as has already been assumed from equation (2.1) onwards. However, as has been shown in equation (2.7), the velocity field in the profile is in turn a function of the profile characteristics. Consequently the sediment concentration, which is a function of the turbulent diffusion and is as such related to the velocity field, will also be a function of the profile characteristics. This implies that both

the landward - and the seaward - directed components of the sediment transport will vary over a longer period of time ($t >> T$). Thus the possibility exists that the transport $\overline{S(d)}$ through any arbitrarily chosen section in the profile will become equal to zero. In long-duration model tests it has been shown that this phenomenon does indeed occur (see Chapter 4, Figures 37 ... 46). An equilibrium situation will thus be reached at such a section. It will be assumed that such an equilibrium situation will have been reached at all water depths in the region of active sediment transport after time t = infinity.
This implies that the profile has come into equilibrium, and that the water movement - and as such also the sediment concentration - will not change any more in time ($t >> T$).
Consequently it follows from equation (2.27) and the foregoing discussion that at time = ∞ :

$$\overline{S(d)}_{\infty} = 0 = f(P(\infty)) = f(P(t_0)) + \Phi(P(\infty), P(t_0)) \tag{2.29}$$

and thus $$f(P(t_0)) = -\Phi(P(\infty), P(t_0)) \tag{2.30}$$

where $$\Phi(P(\infty), P(t_0)) = \sum_{n=1}^{\infty} \frac{(P(\infty) - P(t_0))^n}{n!} f^{(n)}(P(t_0)) \tag{2.31}$$

(from equation (2.28))

= the value of $\Phi(P(t), P(t_0))$ at time t = infinity.

Substitution of equation (2.30) into equation (2.27) finally yields:

$$\overline{S(d)} = \Phi(P(t), P(t_0)) - \Phi(P(\infty), P(t_0))$$

$$= \Phi_t - \Phi_{\infty} \tag{2.32}$$

because $P(t_0)$ is a constant for a specific combination of wave characteristics, bed material and water depth.

where $$\Phi_t = \Phi(P(t), P(t_0)) \tag{2.33}$$

= a function of a characteristic profile quantity P(t), which is defined for a specific bed material, wave condition and location in the profile

$$\Phi_{\infty} = \Phi(P(\infty), P(t_0)) \tag{2.34}$$

= a function of a characteristic equilibrium profile quantity $P(\infty)$

$= (P(t), P(t_0))_{t=\infty}$, which is defined for a specific bed material, wave condition and location in the profile.

Physically equation (2.32) means that if the profile will eventually come into equilibrium (at time $t = \infty$), the transport of sediment at any location and at any time t will be related to the difference between the profile characteristics at time $t = \infty$ and time t. This is an interesting conclusion, as it is identically equal to the assumption made by Bakker [2] , regarding the variation in time of the onshore-offshore transport, viz.:

"Onshore-offshore transport at any time t is assumed to be proportional to the difference between the equilibrium profile form and the profile form at time t."

In making this assumption regarding the transport, Bakker implicitly assumed the existence of an equilibrium profile.
The profile quantity P(t) has been used to relate both the long-term variation in the water velocity and in the sediment concentration to the profile characteristics. It will have to be investigated within which limits in the profile P(t) is to be defined.
(1) P(t) was used in order to describe the long-term variation in the mass-transport velocity outside the breaker zone (equation (2.1)), which is a function of the bottom slope.
(2) In equation (2.3) P(t) was used to relate the breaker index ($\gamma = H/d$) to the breaker type p.
As the wave height H is partly determined by the amount of reflection from the beach, P(t) must be defined to at least the point of maximum wave run-up.
(3) The wave height as well as the orbital velocity at any water depth d is partly determined by the time-history of the wave, as it is shoaling on the sloping bottom, consequently P(t) must be defined to a depth where the bottom profile is not subject to time-variation (no sediment transport) any more.
(4) In equation (2.15) P(t) was used in the equation for f(z), which relates the actual sediment concentration at any elevation above the bed at any

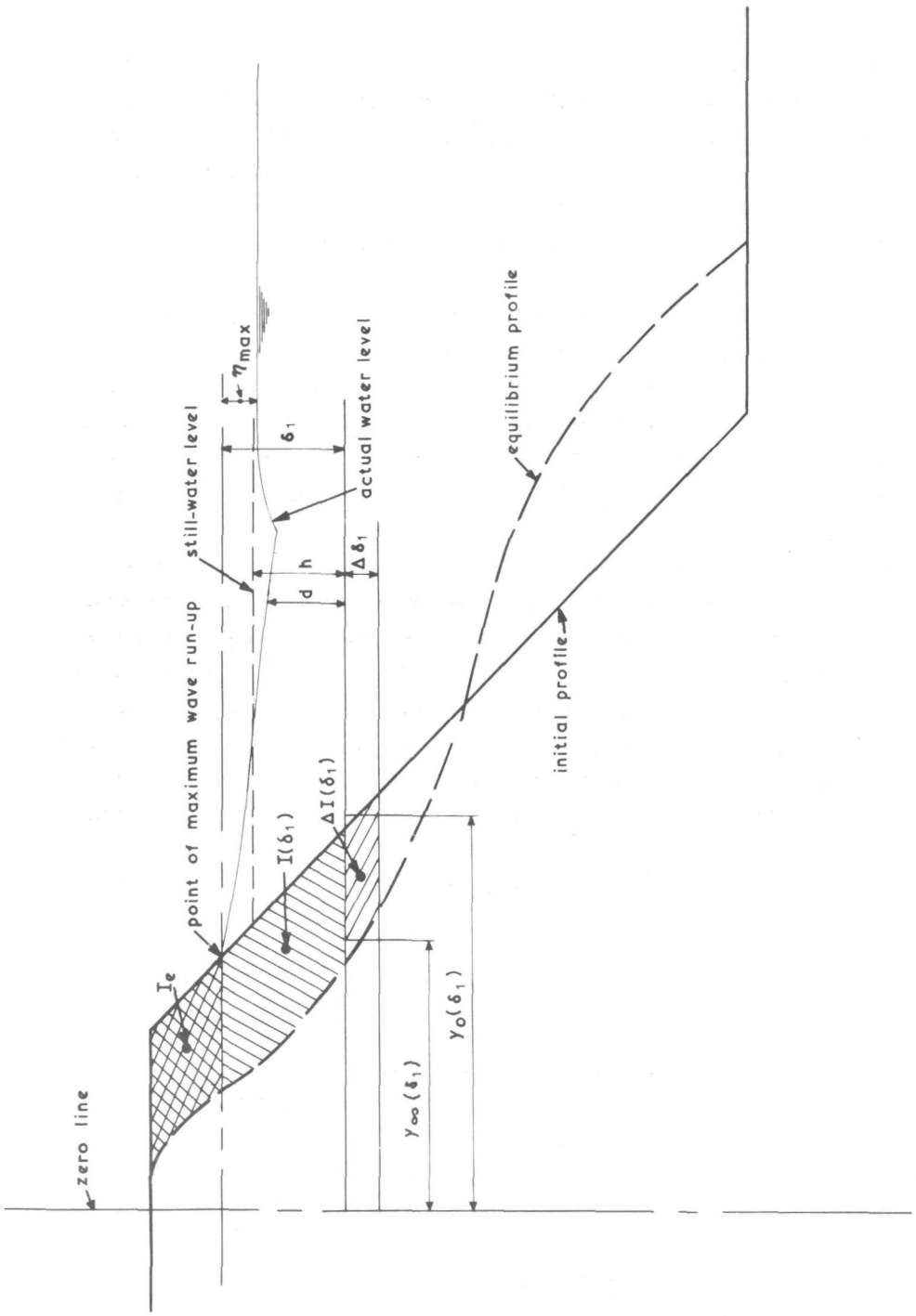

ANALYTICAL DETERMINATION OF EQUILIBRIUM PROFILE

FIGURE 2

time t to a mean sediment concentration at a small distance above the bed. The function f(z), and consequently also P(t), is not defined for the area above the point of maximum wave run-up. If the water depth becomes big enough, the function f(z) will become equal to zero. At depths greater than this limiting depth it will not be necessary to define P(t), although it is possible that some small resultant bed load transport might still occur.

The above-mentioned considerations lead to the conclusion that P(t) should be defined in an area bordered by the point of maximum wave run-up on its landward extremity and by some limiting depth for normal wave - induced sediment transport at its seaward extremity. In Chapter 4.5 the limits of the profile schematization will be related to the wave and bed material characteristics. The quantity P(t) must define the profile characteristics within these limits at time t.
A study of various different forms of the quantity P(t) led to the conclusion that if P(t) is in the form of a characteristic horizontal distance in the profile, measured perpendicular to the coastline, the best correlation is obtained with the physical process. In Chapter 3 the precise form of this characteristic length will be discussed in more detail and in Chapter 4 the schematization will be developed more fully in order to allow the evaluation of the above-mentioned two results, viz.:
(1) an equilibrium position of the bottom profile exists for any specific wave condition.
(2) the transport at any time t is proportional to the difference between the profile form at infinity and the profile form at time t.

2.5 The equilibrium profile

With the aid of equation (2.32), i.e., the relationship giving the seaward transport at any arbitrarily chosen section at any time t, and the initial profile, it becomes possible to determine the profile form at any time t, and consequently also the equilibrium profile at time t = infinity. The total sediment transport in seaward direction, passing the point with a water depth d in the profile, must equal the total amount of eroded material landwards of that point, i.e.

$$\int_0^{cs} \overline{S(d)}\, dt = I(\delta_1) + I_e \qquad (2.35)$$

where $\overline{S(d)}$ = sediment transport in seaward direction per unit of time and shoreline length, at a section with a water depth d

= $\Phi_t - \Phi_{cs}$ according to equation (2.32)

$I(\delta_1)$ = total volume of eroded material per unit of longshore length, landwards of the point where the water depth equals d, and seawards of the point of maximum wave run-up (see Figure 2)

δ_1 = $h + \eta_{max}$

= depth below the elevation of maximum wave run-up

h = still-water depth at that location

I_e = total volume of material eroded from above the point of maximum wave run-up per unit of longshore length (Figure 2).

When the water depth increases from d to $(d + \Delta\delta_1)$, the vertical distance δ_1 increases to $(\delta_1 + \Delta\delta_1)$ and the total volume of eroded material increases with $\Delta I(\delta_1)$, where:

$$\Delta I(\delta_1) = (y_0(\delta_1) - y_{cs}(\delta_1))\, \Delta\delta_1 \qquad (2.36)$$

where $\Delta I(\delta_1)$ = incremental increase in the total volume of material eroded between the initial and the final profile, when the location under consideration is taken $\Delta\delta_1$ lower than before

$y_0(\delta_1)$ = ordinate of the initial profile at a water depth of $d + (\Delta\delta_1/2)$, relative to some zero line

$y_{cs}(\delta_1)$ = ordinate of the equilibrium profile at a water depth of $d + (\Delta\delta_1/2)$, relative to the same zero line as that of $y_0(\delta_1)$.

Thus, in the limit, when $\Delta\delta_1 \longrightarrow 0$:

$$\frac{dI(\delta_1)}{d\delta_1} = y_0(\delta_1) - y_{cs}(\delta_1) \qquad (2.37)$$

and consequently

$$y_{cs}(\delta_1) = y_0(\delta_1) - \frac{dI(\delta_1)}{d\delta_1} \qquad (2.38)$$

Substitution of equation (2.32) into equation (2.35) yields:

$$I(\delta_1) = \int_0^{\infty} (\Phi_t - \Phi_{\infty}) \, dt - I_e \tag{2.39}$$

When equation (2.39) is substituted into equation (2.38), the form of the equilibrium profile can be found, viz.:

$$y_{\infty}(\delta_1) = y_0(\delta_1) - \frac{d}{d\delta_1} \left\{ \int_0^{\infty} (\Phi_t - \Phi_{\infty}) \, dt - I_e \right\}$$

$$= y_0(\delta_1) - \frac{d}{d\delta_1} \left\{ \int_0^{\infty} (\Phi_t - \Phi_{\infty}) \, dt \right\} \tag{2.40}$$

because $\frac{dI_e}{d\delta_1} = 0$, as long as $d \geqslant 0$, i.e. as long as a location at or below the water level is studied.

As soon as the form of the function $\Phi_t - \Phi_{\infty}$ is known in terms of the depth, it becomes possible to calculate the form and position of the equilibrium profile. In Chapters 3 and 4 expressions giving the form of the function $(\Phi_t - \Phi_{\infty})$ will be derived.

2.6 The effect of littoral current

In order to evaluate the effect of a littoral current due to oblique wave attack on the onshore-offshore transport, the hypothetical case of a littoral current without any longshore gradient in velocity and with flow lines parallel to a straight beach will be studied. This implies that the circulation pattern in the nearshore region is essentially a vertical one. As will be seen in Chapter 2.7, this is mostly not the case. However, in order to deepen the insight into the mechanism of onshore-offshore transport, it is interesting to study this case, before incorporating a horizontal circulation pattern.

If it is assumed that the angle of wave incidence is small in the nearshore region, the orbital velocity in the direction perpendicular to the beach will be approximately equal for the two- and three-dimensional cases. The wave set-up in the three-dimensional case will, in the case of a small angle of incidence, also be approximately equal to that in

the two-dimensional case (Bakker [3]).
Consequently, the resultant velocity components in the onshore-offshore direction will have approximately the same values as for the two-dimensional case.
The total resultant velocity, on the other hand, is clearly larger in the three-dimensional case than in the two-dimensional case, due to the vectoral addition of the longshore current and the velocity components in onshore-offshore direction. Consequently the resultant velocity at the bed will also be higher in the three-dimensional case, with as a result an increase in the bottom shear stress (Bijker [9]).
Various investigators have studied the movement of bed material under the influence of a stationary current, the most important of which are Meyer-Peter and Mueller [35], Einstein [13], Kalinske [29] and Frijlink [14]. All these studies revealed some relationship between the transport of bed material S_b and a critical bed shear τ_b.
Bijker [9] studied the longshore transport of bottom sediment under the combined action of waves and current. He found that in order to be able to predict the bed load, he had to incorporate an increased bed shear τ_{wc}, where:

$$\frac{\tau_{wc}}{\tau_c} = 1 + 1/2 \left(\xi \frac{u_0}{v}\right)^2 \qquad (2.41)$$

where τ_{wc} = resultant bed shear due to combined wave and current action, averaged over the wave period
τ_c = bed shear due to uniform flow, when it is assumed that the shear stress at the surface equals zero
u_0 = orbital velocity at the bed in the 1st order wave theory
v = longshore current velocity

$$\xi = \frac{p_B \mu C_h}{g^{1/2}} \qquad (2.42)$$

p_B = constant = 0.45 experimentally
μ = von Kármán constant = 0.4
C_h = Chezy roughness coefficient
g = gravitational acceleration.

It can thus be stated that an increase in the bed shear will lead to an

increased bed load transport.
Due to the increased resultant velocity at the bed the turbulence will also increase, consequently more sediment will be entrained at the bed. This implies that the sediment concentration at the bed will also increase. The vertical distribution of the sediment concentration will also change due to the change in the turbulence pattern. In general it can thus be concluded that both the sediment concentration and the water velocity at any depth in a section will be higher in the three- than in the two-dimensional case. As a result the functions Φ_t and Φ_{cs} (see equation (2.24)) and consequently also the difference $\Phi_t - \Phi_{cs}$ will show an increase, relative to the two-dimensional case. The total sediment transport per unit of time will thus be higher in the three-dimensional than in the two-dimensional case, if the comparison is made at corresponding times.
It is to be expected that the increase in the value of $\overline{S\ (d)}$ will be related to the increase in the resultant shear stress, i.e.

$$\overline{S\ (d)}_{3D} = \overline{S(d)}_{2D}\ f\ \left(\frac{\tau_{wc}}{\tau_w}\right) \tag{2.43}$$

where $\overline{S\ (d)}_{2D}$ and $\overline{S\ (d)}_{3D}$ are the values of $\overline{S\ (d)}$ in the two- and three-dimensional cases respectively

τ_w = bed shear in the two-dimensional case, i.e. due to the onshore-offshore velocity field only.

In the same manner it follows that

$$\left.\begin{aligned} \Phi_{t3D} &= \Phi_{t2D}\ f\ \left(\frac{\tau_{wc}}{\tau_w}\right) \\ \text{and } \Phi_{cs\,3D} &= \Phi_{cs2D}\ \ f\ \left(\frac{\tau_{wc}}{\tau_w}\right) \end{aligned}\right\} \tag{2.44}$$

where Φ_{t2D} (Φ_{cs2D}) and Φ_{t3D} (Φ_{cs3D}) are the values of Φ_t (Φ_{cs}) in the two- and three-dimensional cases respectively.

2.7 The effect of rip-currents

When oblique waves shoal on a coastline longshore currents are generated. Under the wave crests there is also a resultant landward flow of water.

The circulation in seaward direction can take place either in the vertical plane (two-dimensional case) or in the horizontal plane (three-dimensional case).

Bowen [7] showed that a horizontal circulation pattern will be formed for perpendicular wave attack when a longshore variation in radiation stress is existent along a coastline. As the radiation stress inside the breaker zone is proportional to H^2, the horizontal water circulation in the nearshore region will be directly dependent of the longshore variation in wave height. Bowen [7] showed that the flow inside the breaker zone will be directed from an area of larger wave height to an area of lower wave height. If it is assumed that the horizontal circulation will yield an additional transport, it means that in the area landwards of the higher waves sediment will be eroded, and that in the area of lower wave heights more sediment will arrive than at other locations at a similar distance from the water line.

Arthur [1] showed theoretically that the flow lines in a rip-current inside the breaker zone are convergent, as long as the depth is increasing in the flow direction. Outside the breaker zone, however, there is no forcing term available anymore, and the rip-current will disintegrate, i.e. the flow lines will diverge and the current velocity will decrease. Accordingly the transport capacity of the rip-current will decrease outside the breaker zone. Sediment will be deposited on the extremities of the rip-current head, with as a consequence an increase in the bottom elevation seawards of the breaker line, in the areas on both sides of the rip-current location. From this moment onwards the water movement in the breaker zone will be governed by the bottom configuration. Over the shoals waves will break as spilling breakers, dissipating more energy than the plunging breakers in the adjacent depressions. The resulting rip-current in the depression will lead to erosion of material that will be deposited on the shoals outside the breaker zone, where the rip-current disintegrates. In this manner the three-dimensional character of the bed will be increased. Eventually some equilibrium situation will be reached. This phenomenon has been observed frequently in both the model and the prototype. Due to the additional seaward-directed velocity v_{rip}, the absolute value in seaward direction of the mass-transport velocity at the bed will increase. Consequently the resultant bed shear will be even higher than in the idealized three-dimensional case, described in Chapter 2.6, and as result the resulting transport $\overline{S(d)}$ will increase. The additional

increase due to the rip-current will be some function of the rip-current velocity, i.e.

$$\overline{S(d)}_{rip} = \overline{S(d)}_{3D}\, f\,(v_{rip}) \tag{2.45}$$

where $\overline{S(d)}_{rip}$ = the value of $\overline{S(d)}$ in the vicinity of a rip-current

v_{rip} = seaward-directed rip-current velocity at the bed.

Substitution of equation (2.45) into equation (2.43) yields:

$$\overline{S(d)}_{rip} = \overline{S(d)}_{2D}\, f\,(\frac{\tau_{wc}}{\tau_w}, v_{rip}) \tag{2.46}$$

Due to the seaward-directed rip-current velocity an additional amount of bottom sediment will be transported in seaward direction, and the profile will change at the location of the rip-current, as has been stated earlier. This implies that the profile-dependent quantity Φ_t will also change. Consequently the equilibrium profile in the vicinity of the rip-current will differ from that in the ideal three-dimensional case, as discussed in Chapter 2.6.

$$\Phi_{t\ rip} = \Phi_{t\ 3D}\, f\,(v_{rip}) = \Phi_{t\ 2D}\, f\,(\frac{\tau_{wc}}{\tau_w}, v_{rip}) \tag{2.47}$$

where $\Phi_{t\ rip}$ is the value of Φ_t in an area where a rip-current occurs. In both the model and the prototype it has frequently been observed that rip-currents migrate in longshore direction, due to the vectoral addition of the rip-current and a longshore current generated by oblique wave attack. In this case the circulation pattern clearly takes place in a horizontal plane, rather than in a vertical plane. Most probably this horizontal circulation is initiated by the fact that the waves are random, and not regular. In this case the profile will be uniformly different from that in the ideal three-dimensional case over the full width of the area under consideration.

At the present insufficient knowledge regarding rip-currents is available, consequently this aspect of the problem will not be studied in more detail in this investigation. The increased transport in the three-dimensional case will be assumed to be purely a function of the increased bed shear, according to equation (2.43).

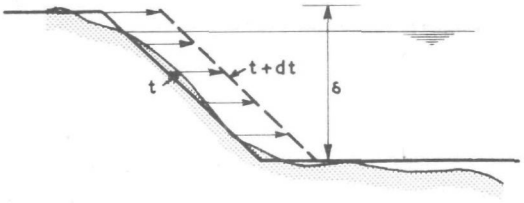

FIGURE 3 : ACCORDING TO PELNARD-CONSIDERE [39]

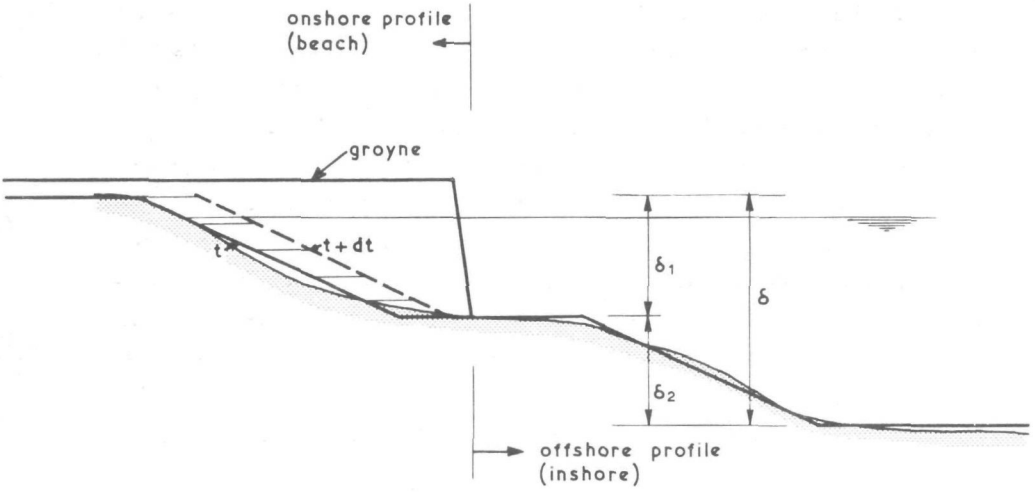

FIGURE 4 : ACCORDING TO BAKKER [2]

ACCRETION OF SCHEMATIZED BOTTOM PROFILE
FIGURES 3,4

Chapter 3: General profile schematization

3.1 General

In order to be able to determine analytically the successive shapes of a shoreline on which a structure has been built, due to oblique wave attack, Pelnard-Considère [39] assumed that the structure is so long that all littoral drift takes place landwards of its seaward extremity. Accordingly, he schematized the shoreline by one line, as is shown in Figure 3.

Bakker [2] extended the theory of Pelnard-Considère by dividing the profile into two zones, viz. (1) the beach, situated landwards of the seaward extremity of the structure, and (2) the inshore, seawards of it (Figure 4). He assumed that the bottom profile was in equilibrium before the building of the structure. Initially all littoral drift on the beach is intercepted by the structure, resulting into an updrift accretion and a downdrift erosion of the beach, which upsets the equilibrium. The steepening of the coastal profile on the updrift side of the structure will cause a seaward transport of sediment and the flattening of the profile on the downdrift side a landward transport of sediment. The above-mentioned onshore-offshore transports are at any time t assumed to be proportional to the difference between the profile at time t and the equilibrium profile (which existed initially, and will have been restored at time t = infinity).

This leads to a transport S_y through the division between the beach and inshore:

$$S_y = q_y (W - (L_2 - L_1)) \qquad (3.1)$$

(Bakker [2])

q_y = proportionality constant

$(L_2 - L_1)$ = schematized distance between beach and inshore at time t (Figure 5)

W = equilibrium distance between beach and inshore (Figure 5) = $(L_2 - L_1)_{t=\infty}$

S_y = positive in seaward direction

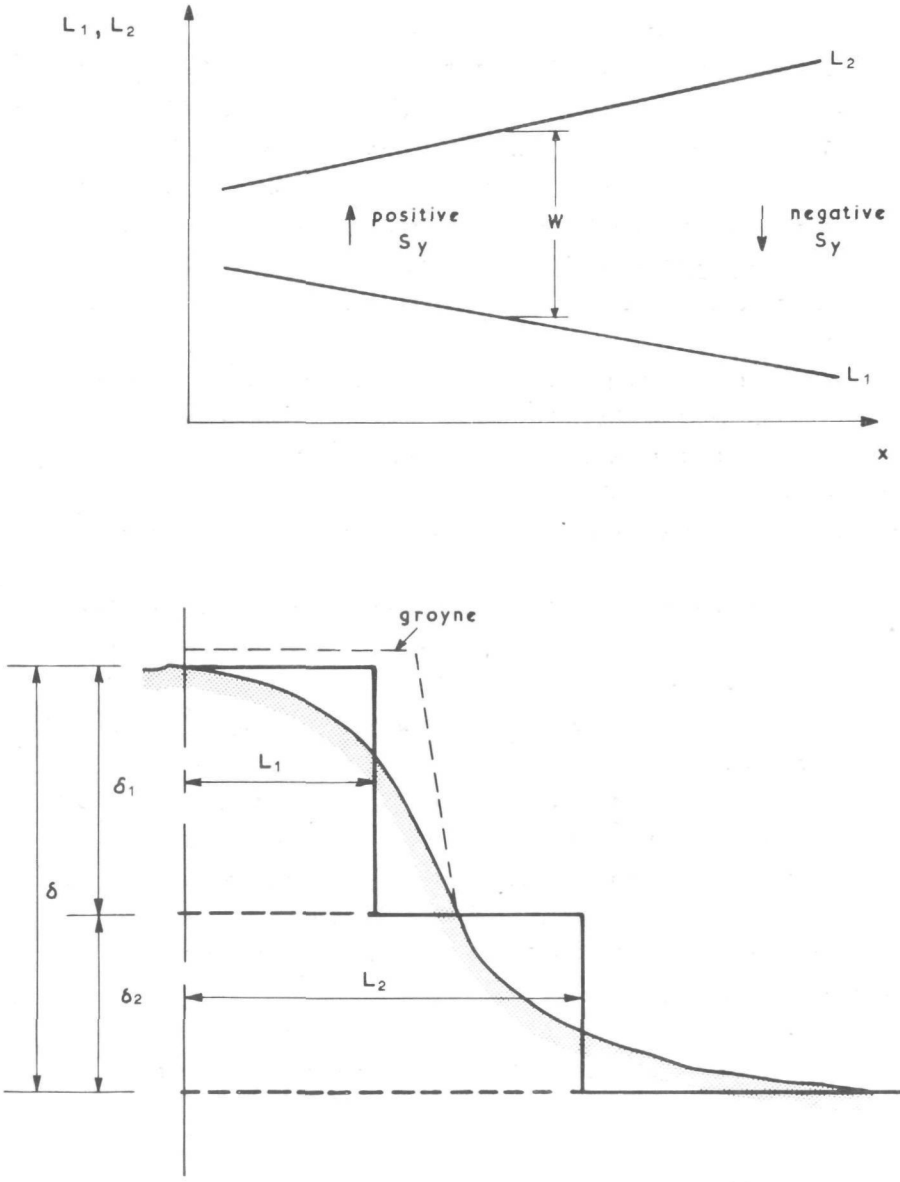

DEFINITION SKETCH FOR ONSHORE-OFFSHORE TRANSPORT (BAKKER [2])

FIGURE 5

It has been shown in Chapter 2 that an equation of the form of equation (3.1) is a reasonable assumption. It should be noted that the terms "beach" and "inshore", as defined by Bakker, are not the same beach and inshore, defined by the C.E.R.C. [50], which are in general use. Due to this inconsistency it was decided to choose other terms to describe the areas onshore and offshore of the point under consideration, viz. the onshore profile and the offshore profile. The term "onshore profile" corresponds with the "beach" of Bakker, while the "offshore profile" corresponds with Bakker's "inshore".

The Bakker-theory for computing shoreline changes is to a high degree dependent of the accuracy with which the onshore-offshore transport can be determined with the aid of equation (3.1). An investigation into the feasibility of (3.1) will actually consist of:

(1) an investigation into the characteristics of the constant of proportionality q_y.

(2) an investigation regarding the validity of the concept of an "equilibrium distance W".

If equation (3.1) is to be used generally, it is essential that it must be possible to determine W and q_y uniquely in terms of the wave, sediment and profile characteristics.

In order to determine such an unique relationship, equation (3.1) must be applied to numerous model (and prototype) cases, and the values of q_y and W determined. Such data must contain information regarding profile development, due to wave conditions which are constant in time.

In this chapter a method will be developed in order to allow the best possible use of equation (3.1), when determining values of q_y and W for different wave, sediment and profile characteristics. The division between the onshore and the offshore profile will be made arbitrarily, to allow the determination of q_y and W for every location in the profile.

3.2 Determination of $(L_2 - L_1)$

Usually profile data are available in the form of soundings of the bottom elevation z, relative to some reference level, for fixed points, which can either be at a constant or at a variable distance from each other. The data

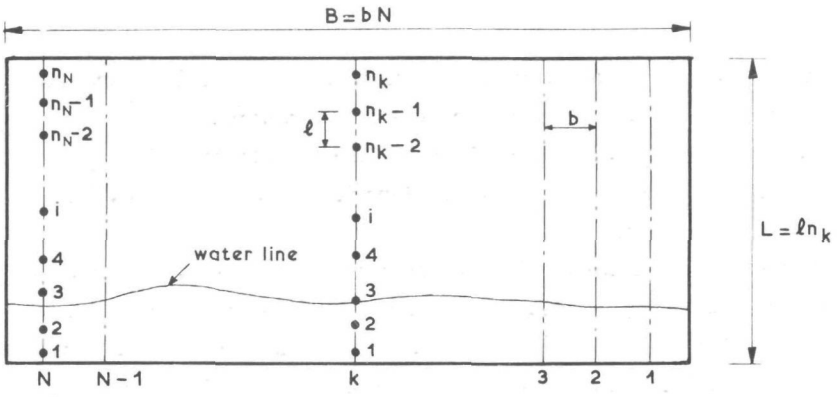

PLAN VIEW

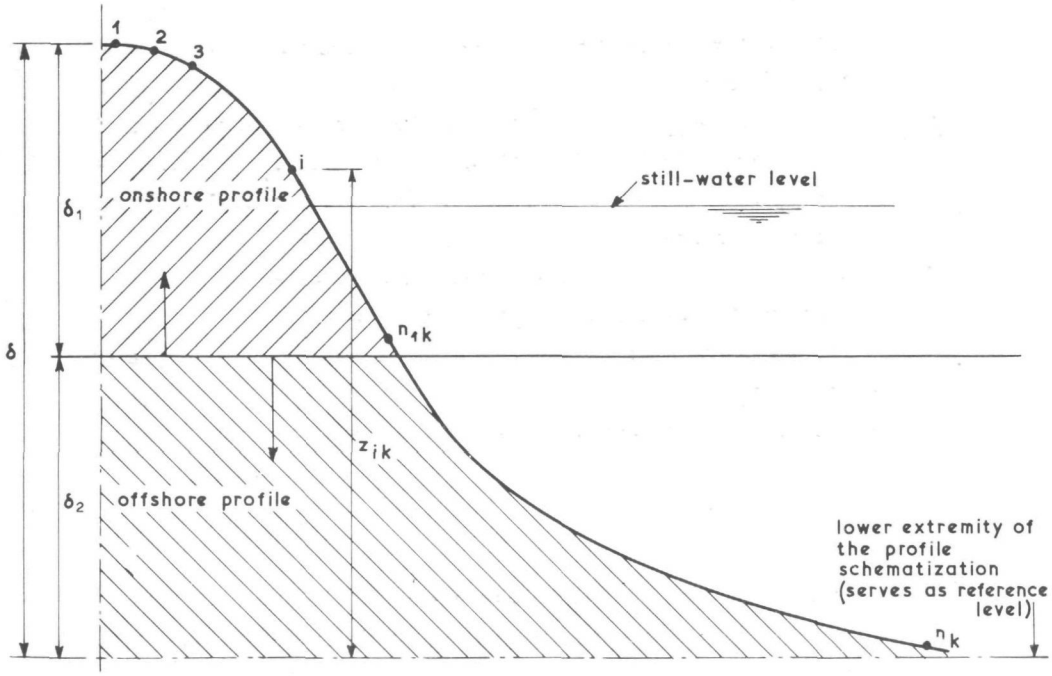

SECTION k

BEACH PROFILE AT SECTION k
FIGURE 6

to be studied in this report have all been reduced to a form where the distance between the measuring points, measured perpendicular to the coastline, was a constant, and equal to 1. In order to transform these bottom heights to schematized $(L_2 - L_1)$-lengths, a mass-conservation procedure will have to be used.

Assume that the coastal area under consideration is rectangular, as is shown in Figure 6, and that the bottom profile has been sounded in N sections. The distance between any two adjacent sections is constant and equal to b. The total width of the area B = Nb is a constant (see Figure 6). The volumes I, I_1 and I_2 can then be defined as follows:

$$I = lb \sum_{k=1}^{N} \sum_{i=1}^{n_k} z_{ik} \tag{3.2}$$

where I = total volume of sand in the area, relative to the reference level (Figure 6)

z_{ik} = height of the $\underline{i^{th}}$ measuring point from the landward extremity of the area, in the $\underline{k^{th}}$ section. z_{ik} is measured relative to the horizontal reference level at the lower extremity of the profile (Figure 6)

N = total number of measuring sections in the area

n_k = total number of measuring points in section k

l = distance perpendicular to the coast between measuring points = constant

b = distance between measuring sections = constant.

$$I_1 = lb \left(\sum_{k=1}^{N} \sum_{i=1}^{n_{1k}} z_{ik} - \delta_2 n_1 \right) \tag{3.3}$$

where I_1 = total volume of sand in the onshore profile area, i.e. above the horizontal division between the onshore and offshore profile at a height $z = \delta_2$

δ_2 = schematized offshore profile thickness

n_{1k} = total number of measuring points in the onshore profile in section k

n_1 = total number of measuring points in the onshore profile in the whole area

$$n_1 = \sum_{k=1}^{N} n_{1k}$$

$$I_2 = lb \left(\sum_{k=1}^{N} \sum_{i=n_{1k}+1}^{n_k} z_{ik} + \delta_2 \, n_1 \right) \qquad (3.4)$$

where l_2 = total volume of sand in the offshore profile area, i.e. below the horizontal division between onshore and offshore profile at height $z = \delta_2$.

The onshore and offshore profile volumes, I_1 and I_2 respectively, can also be related to the schematized onshore and offshore profile lengths, as defined initially by Bakker [2] .

$$\left.\begin{aligned} I_1 &= BL_1\delta_1 \\ I_2 &= BL_2\delta_2 \end{aligned}\right\} \qquad (3.5)$$

where B = total width of the coastal area (Figure 6)

L_1 = average length of the onshore profile volume, relative to the landward extremity of the coastal area (see Figure 5)

L_2 = average length of the offshore profile volume, relative to the landward extremity of the coastal area (Figure 5)

δ_1 = schematized onshore profile thickness.

$$\text{Thus } (L_2 - L_1) = \frac{I_2}{B\delta_2} - \frac{I_1}{B\delta_1}$$

$$= \frac{I_2\delta_1 - I_1\delta_2}{B\delta_1\delta_2}$$

$$= \frac{(I_1 + I_2)\,\delta_1 - (I_1\delta_1 + I_1\delta_2)}{B\delta_1\delta_2}$$

$$= \frac{I\delta_1 - I_1\delta}{B\delta_1\delta_2} \qquad (3.6)$$

because $I = I_1 + I_2$

and $\delta = \delta_1 + \delta_2$ (Figure 5)

The volumes I and I_1 are determined from soundings and are correspondingly subject to variation, due to possible measuring errors. In the following, the effect of measuring errors on the calculated length $(L_2 - L_1)$ will be studied.

As the variation of the $(L_2 - L_1)$-length in time has to be studied, it is not the absolute value of $(L_2 - L_1)$ which is of importance, but its value relative to the other $(L_2 - L_1)$- values in the time-series. Assume that no material enters or leaves the area shown in Figure 6. Accordingly I_t should be a constant, where I_t denotes the total volume of sand in the area, as measured at time t after the start of the test ($t \geqslant 0$). However, due to a measuring error Δz_{ik} per measuring point, it is possible that

$$\left(\sum_{k=1}^{N} \sum_{i=1}^{n_k} z_{ik} \right)_{\text{measured}} \neq \left(\sum_{k=1}^{N} \sum_{i=1}^{n_k} z_{ik} \right)_{\text{actual}}$$

Accordingly, $I_t \neq I_{t=0}$

Δz_{ik} can be different for every point i in any section k, and consequently:

$$\Delta z_1 = \frac{1}{n_1} \sum_{k=1}^{N} \sum_{i=1}^{n_{1k}} \Delta z_{ik} \tag{3.7}$$

where Δz_1 = average correction in height/point in the onshore profile area.

$$\Delta z_2 = \frac{1}{n_2} \sum_{k=1}^{N} \sum_{i=n_{1k}+1}^{n_k} \Delta z_{ik} \tag{3.8}$$

where Δz_2 = average correction in height/point in the offshore profile area

n_2 = number of measuring points in the offshore profile area

$$= \sum_{k=1}^{N} (n_k - n_{1k}).$$

$$\Delta z = \frac{1}{n} (n_1 \Delta z_1 + n_2 \Delta z_2)$$

$$\Delta z = \frac{1}{n} \sum_{k=1}^{N} \sum_{i=1}^{n_k} \Delta z_{ik} \tag{3.9}$$

where Δz = average correction in height/point in the whole area

n = total number of measuring points in the whole area = $\sum_{k=1}^{N} n_k$.

Furthermore

$$\text{bl} \sum_{k=1}^{N} \sum_{i=1}^{n_k} \Delta z_{ik} = I_{t = t_0} - I_{t = t_j} \tag{3.10}$$

where $I_{t = t_0} - I_{t = t_j}$ = volumetric error occurring in the sounding at time $t = t_j$ due to measuring errors.

This implies that:

$$I = I^{*} + \text{lb } n\Delta z \tag{3.11}$$

$$I_1 = I_1^{*} + \text{lb } n_1 \Delta z_1 \tag{3.12}$$

$$I_2 = I_2^{*} + \text{lb } n_2 \Delta z_2 \tag{3.13}$$

where I^{*}, I_1^{*} and I_2^{*} denote the uncorrected values of I, I_1 and I_2 respectively.

Accordingly, with the aid of equations (3.6), (3.11) and (3.12):

$$(L_2 - L_1) = \frac{(I^{*} + \text{lb } n\Delta z)\ \delta_1 - (I_1^{*} + \text{lb } n_1 \Delta z_1)\ \delta}{B\delta_1\delta_2}$$

$$= \frac{I^{*}\ \delta_1 - I_1^{*}\ \delta}{B\delta_1\delta_2} + \frac{\text{lb } (n\Delta z\delta_1 - n_1\Delta z_1\ \delta)}{B\delta_1\delta_2}$$

$$= (L_2 - L_1)^{*} + \frac{\text{lb}}{B\delta_1\delta_2} (n\Delta z\delta_1 - n_1\Delta z_1\ \delta)$$

$$= (L_2 - L_1)^{*} + \Delta\ (L_2 - L_1) \tag{3.14}$$

where $(L_2 - L_1)^*$ denotes the uncorrected value of $(L_2 - L_1)$ and $\Delta (L_2 - L_1)$ the correction that has to be applied, due to a measuring error at time $t=t_j$.

The transport of sediment S_y per unit of longshore length and per unit of time across the division between the onshore and offshore profile can either be calculated with the use of the variation of the onshore profile volume $\frac{dI_1}{dt}$, or by using the variation of the offshore profile volume $\frac{dI_2}{dt}$.

When using the onshore profile volume:

$$S_{y1} = \frac{I_{1t=t_0} - I_{1t=t_j}}{B\,(t_j - t_0)} \tag{3.15}$$

where S_{y1} = sediment transport across the division between onshore and offshore profile as calculated with the variation in the onshore profile volume. S_{y1} is positive in seaward direction.

With the aid of equation (3.12) it is possible to rewrite equation (3.15) as follows:

$$S_{y1} = \frac{I_{1t_0} - (I^*_{1t_j} + lb\, n_1 \Delta z_1)}{B\,(t_j - t_0)}$$

$$= S_{y1}^* - \frac{lb\, n_1 \Delta z_1}{B\,(t_j - t_0)}$$

$$= S_{y1}^* - \Delta S_{y1} \tag{3.16}$$

where S_{y1}^* denotes the uncorrected value of the transport S_{y1}, as calculated with the variation in onshore profile volume, and ΔS_{y1} the correction in S_{y1}.

When using the offshore profile volume:

$$S_{y2} = \frac{I_{2t_j} - I_{2t_0}}{B\,(t_j - t_0)} \tag{3.17}$$

where S_{y2} = sediment transport across the division between the onshore

and offshore profile, as calculated with the variation in offshore profile volume. S_{y2} is positive in seaward direction.

With the aid of equation (3.13), equation (3.17) can be rewritten as follows:

$$S_{y2} = \frac{(I^{*}_{2t_j} + lbn_2\Delta z_2) - I_{2t_0}}{B\,(t_j - t_0)}$$

$$= S_{y2}^{*} + \frac{lbn_2\Delta z_2}{B\,(t_j - t_0)}$$

$$= S_{y2}^{*} + \Delta S_{y2} \qquad (3.18)$$

where S_{y2}^{*} denotes the uncorrected value of the transport S_{y2}, calculated with the variation in offshore profile volume, and ΔS_{y2} the correction in S_{y2}.

If no measuring errors has been made, $\Delta z_1 = \Delta z_2 = 0$, and $S_{y1}^{*} = S_{y2}^{*} = S_y$. In this case the continuity equation must apply, i.e. the amount of sand eroded from the onshore profile, must equal the amount of sand deposited in the offshore profile.

$$\text{Thus } S_y = -\delta_1 \frac{dL_1}{dt} = +\delta_2 \frac{dL_2}{dt} \qquad (3.19)$$

$$= q_y\,(W - (L_2 - L_1)) \qquad (3.1)$$

Consequently

$$\frac{dL_1}{dt} = -\frac{q_y}{\delta_1}\,(W - (L_2 - L_1)) \qquad (3.20)$$

and

$$\frac{dL_2}{dt} = +\frac{q_y}{\delta_2}\,(W - (L_2 - L_1)) \qquad (3.21)$$

Accordingly

$$\frac{d\,(L_2 - L_1)}{dt} = \frac{q_y}{\delta_2}\,(W - (L_2 - L_1)) - \left(\frac{-q_y}{\delta_1}\,(W - (L_2 - L_1))\right)$$

$$= \left(\frac{q_y}{\delta_2} + \frac{q_y}{\delta_1}\right)\left(W - (L_2 - L_1)\right)$$

$$= \frac{(\delta_1 + \delta_2)q_y}{\delta_1\delta_2}\left(W - (L_2 - L_1)\right)$$

$$= \frac{\delta q_y}{\delta_1\delta_2}\left(W - (L_2 - L_1)\right) \qquad (3.22)$$

Equation (3.22) can be combined with equation (3.1) to yield:

$$S_y = \frac{\delta_1\delta_2}{\delta}\,\frac{d\,(L_2 - L_1)}{dt} \qquad (3.23)$$

It will be assumed that equation (3.23) stays valid, even if $S_{y1}^{*} \neq S_{y2}^{*}$. It will then be possible to calculate the transport across the division between the onshore and offshore profile by using the variation in time of $(L_2 - L_1)$, viz.:

$$S_y = \frac{\delta_1\delta_2}{\delta}\left\{\frac{(L_2 - L_1)_{t = t_j} - (L_2 - L_1)_{t = t_0}}{t_j - t_0}\right\} \qquad (3.24)$$

Equation (3.24) can be rewritten with the aid of equation (3.14):

$$S_y = \frac{\delta_1\delta_2}{\delta(t_j - t_0)}\left[\left\{(L_2 - L_1)_{t_j}^{*} + \Delta\,(L_2 - L_1)\right\} - (L_2 - L_1)_{t_0}\right]$$

$$= S_y^{*} + \frac{\delta_1\delta_2\,\Delta(L_2 - L_1)}{\delta\,(t_j - t_0)}$$

$$= S_y^{*} + \frac{\delta_1\delta_2}{\delta\,(t_j - t_0)}\left(\frac{lb}{B\delta_1\delta_2}\left(n\Delta z\delta_1 - n_1\Delta z_1\delta\right)\right)$$

(from equation (3.14))

$$= S_y^{*} + \frac{lb}{B\,(t_j - t_0)}\left(n\Delta z\,\frac{\delta_1}{\delta} - n_1\Delta z_1\right)$$

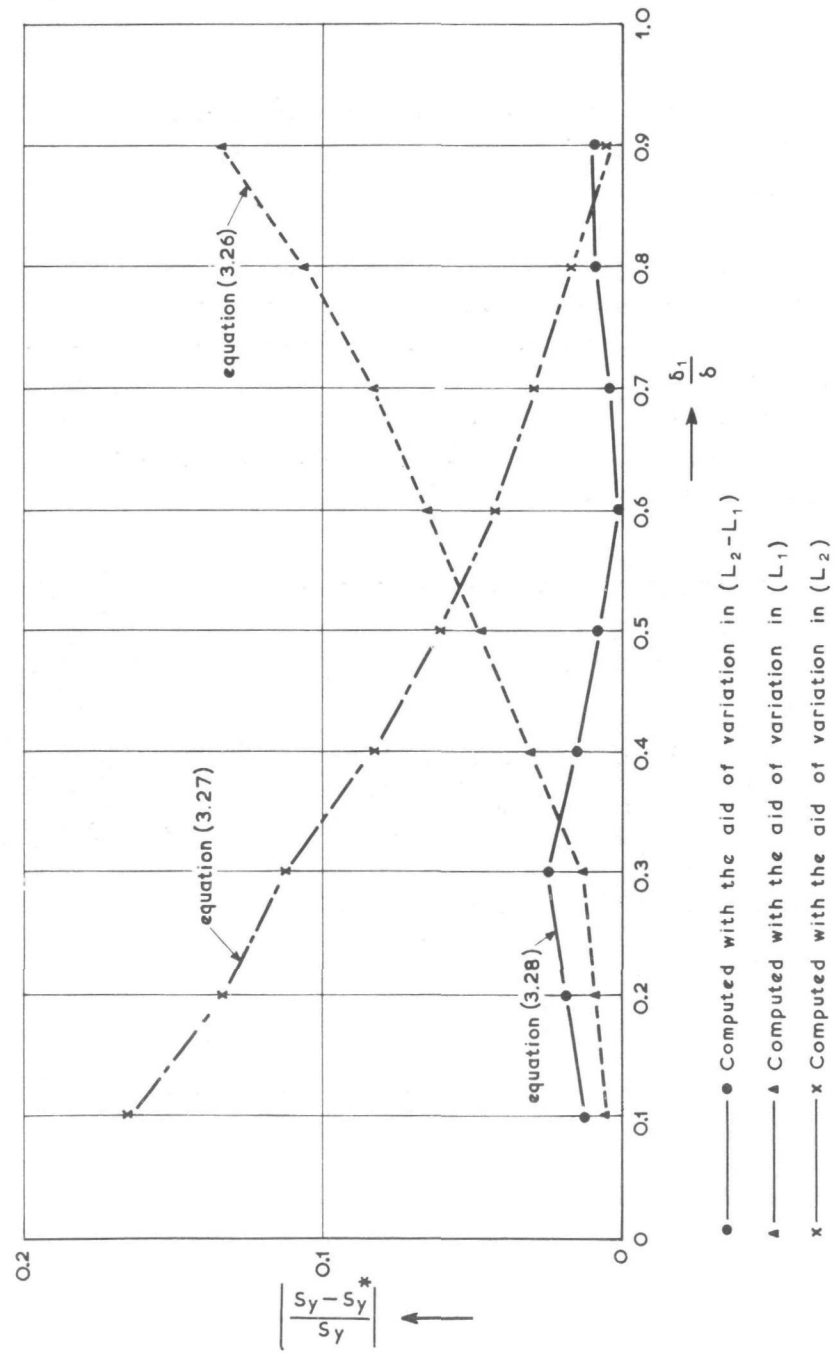

VARIATION OF $\left|\frac{S_y - S_y^*}{S_y}\right|$ WITH δ_1/δ

FIGURE 7

$$= S_y^{*} + \Delta S_y \qquad (3.25)$$

where S_y^{*} denotes the uncorrected value of the transport S_y, as calculated from the variation in $(L_2 - L_1)$, while ΔS_y is the correction that has to be applied.

Three methods have been described above, with which the transport S_y across the division between the onshore and offshore profile can be determined, viz. by using the variation in onshore profile volume, offshore profile volume and $(L_2 - L_1)$ respectively. When a series of soundings is to be used to determine the best possible values of W and q_y respectively, the method to determine S_y to be used, will be the one that will introduce the smallest relative error $(S_y - S_y^{*})/S_y$.

The relative errors for the three alternatives are:

(1) When using the onshore profile volume: -

$$\left| \frac{S_{y1} - S_{y1}^{*}}{S_{y1}} \right| = \left| \frac{\Delta S_{y1}}{S_{y1}} \right| = \left| \frac{lb}{B\, S_{y1}\, (t_j - t_0)} (n_1 \Delta z_1) \right| \qquad (3.26)$$

(with the aid of equation (3.16))

(2) When using the offshore profile volume: -

$$\left| \frac{S_{y2} - S_{y2}^{*}}{S_{y2}} \right| = \left| \frac{\Delta S_{y2}}{S_{y2}} \right| = \left| \frac{lb}{B\, S_{y2}\, (t_j - t_0)} (n_2 \Delta z_2) \right| \qquad (3.27)$$

(with the aid of equation (3.18))

(3) When using $(L_2 - L_1)$: -

$$\left| \frac{S_y - S_y^*}{S_y} \right| = \left| \frac{\Delta S_y}{S_y} \right| = \left| \frac{1b}{B\, S_y\, (t_j - t_0)} \left(n\Delta z\, \frac{\delta_1}{\delta} - n_1 \Delta z_1 \right) \right| \qquad (3.28)$$

(with the aid of equation (3.25))

As S_{y1}, S_{y2} and S_y denote the corrected values of the transport across the division between the onshore and offshore profile, it follows that:

$$S_{y1} = S_{y2} = S_y$$

Consequently it becomes evident from equations (3.26) ... (3.28) that the relative errors will be proportional to $(n_1 \Delta z_1)$, $(n_2 \Delta z_2)$ and $(n\Delta z\, \frac{\delta 1}{\delta} - n_1 \Delta z_1)$ respectively, for the three alternatives. Of these three, the third alternative (equation (3.28))will on the average give the smallest relative error in the calculated transport. This is illustrated for a specific two-dimensional model case in Figure 7.

This implies that if the values of q_y and W have to be determined as a function of δ_1/δ, i.e. for various different locations in the profile, it will yield the best results if the variation in time of $(L_2 - L_1)$ is used. In the rest of this report this approach will also be used.

3.3 Relationship between $(L_2 - L_1)$ and time t

In Chapter 3.2 it has become clear that, when a systematic study of the characteristics of q_y and W has to be carried out, the transport S_y should be calculated from the variation of $(L_2 - L_1)$ in time. When the two-dimensional case is studied, equation (3.22) can be rewritten for this purpose, viz.:

$$\frac{d\,(L_2 - L_1)}{dt} - \frac{\delta q_y}{\delta_1 \delta_2} \left(W - (L_2 - L_1) \right) = 0$$

$$\text{or } \frac{d\,(L_2 - L_1)}{dt} + \frac{\delta q_y}{\delta_1 \delta_2} (L_2 - L_1) - \frac{\delta q_y W}{\delta_1 \delta_2} = 0 \qquad (3.29)$$

However, in the most prototype cases the situation is three-dimensional, i.e. in addition to an onshore-offshore transport, a longshore gradient in longshore transport is also existent in the coastal area under consideration. Assume that the situation as sketched in Figure 8 applies. In the coastal area with a width B the volumes I_1 of the onshore profile and I_2 of the offshore profile will change as follows during a time $\Delta t = t_j - t_0$:

$$I_{1t_j} - I_{1t_0} = (S_{11} - S_{12})\,\Delta t - B\,S_y \Delta t \tag{3.30}$$

$$I_{2t_j} - I_{2t_0} = (S_{21} - S_{22})\,\Delta t + B\,S_y \Delta t \tag{3.31}$$

where S_{11}, S_{12}, S_{21} and S_{22} are the longshore transport capacities in L^3T^{-1} at the locations as shown in Figure 8.

I_{1t_j} and I_{2t_j} denote the values of I_1 and I_2 respectively at time $t = t_j$. In terms of the profile schematization, however:

$$I_{1t_j} - I_{1t_0} = B\,\delta_1\,(L_{1t_j} - L_{1t_0}) = B\,\delta_1 \Delta L_1 \tag{3.32}$$

and $$I_{2t_j} - I_{2t_0} = B\,\delta_2\,(L_{2t_j} - L_{2t_0}) = B\,\delta_2 \Delta L_2 \tag{3.33}$$

where ΔL_1 and ΔL_2 are the variations in L_1 and L_2 respectively, due to onshore-offshore and longshore transport in the time Δt. From (3.30) ... (3.33) it follows that:

$$B\,\delta_1\,\left(\frac{\Delta L_1}{\Delta t}\right) = (S_{11} - S_{12}) - B\,S_y \tag{3.34}$$

and $$B\,\delta_2\,\left(\frac{\Delta L_2}{\Delta t}\right) = (S_{21} - S_{22}) + B\,S_y \tag{3.35}$$

$\left(\frac{1}{B\delta_2}\right)$ x equation (3.35) - $\left(\frac{1}{B\delta_1}\right)$ x equation (3.34) yields:

$$\frac{\Delta L_2}{\Delta t} - \frac{\Delta L_1}{\Delta t} = \frac{\Delta\,(L_2 - L_1)}{\Delta t} = \left(\frac{S_{21} - S_{22}}{B\,\delta_2} + \frac{S_y}{\delta_2}\right) - \left(\frac{S_{11} - S_{12}}{B\,\delta_1} - \frac{S_y}{\delta_1}\right)$$

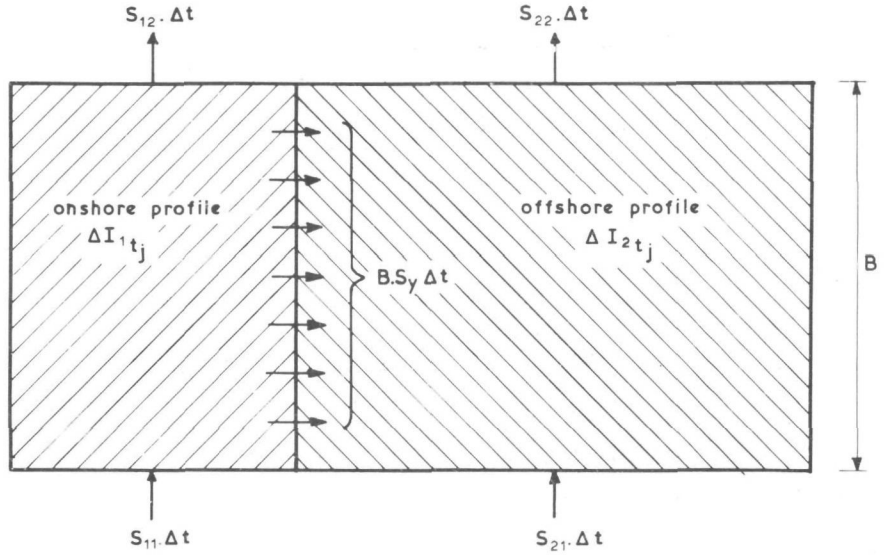

$\Delta t = t_j - t_o : \Delta I_{1t_j} = I_{1t_j} - I_{1t_o} : \Delta I_{2t_j} = I_{2t_j} - I_{2t_o}$

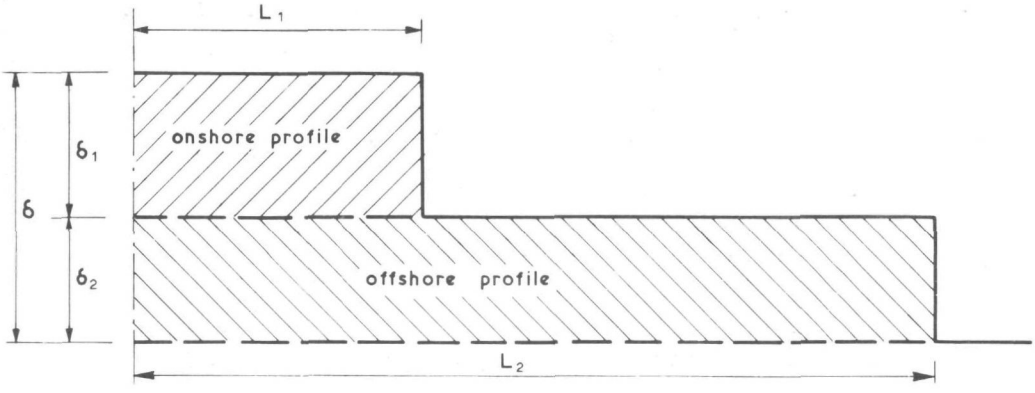

DEFINITION SKETCH : SAND BALANCE
FIGURE 8

$$= \left(\frac{S_{21} - S_{22}}{B\,\delta_2} - \frac{S_{11} - S_{12}}{B\,\delta_1}\right) + \left(\frac{1}{\delta_2} + \frac{1}{\delta_1}\right) S_y$$

$$= \left(\frac{S_{21} - S_{22}}{B\,\delta_2} - \frac{S_{11} - S_{12}}{B\,\delta_1}\right) + \frac{\delta}{\delta_1\delta_2} S_y \qquad (3.36)$$

where $\delta = \delta_1 + \delta_2$

Substitution of S_y from equation (3.1) yields:

$$\frac{\Delta(L_2 - L_1)}{\Delta t} = \left(\frac{S_{21} - S_{22}}{B\,\delta_2} - \frac{S_{11} - S_{12}}{B\,\delta_1}\right) + \frac{\delta q_y}{\delta_1\delta_2}\left(W - (L_2 - L_1)\right) \qquad (3.37)$$

When equation (3.37) is written in its differential form, the following differential equation is obtained:

$$\frac{d\,(L_2 - L_1)}{dt} + \frac{\delta q_y}{\delta_1\delta_2}(L_2 - L_1) - \frac{\delta q_y W}{\delta_1\delta_2} + \left[\left(\frac{S_{11} - S_{12}}{B\,\delta_1}\right) - \left(\frac{S_{21} - S_{22}}{B\,\delta_2}\right)\right] = 0$$

$$\text{or } \frac{d\,(L_2 - L_1)}{dt} + \frac{\delta q_y}{\delta_1\delta_2}(L_2 - L_1) - \frac{\delta q_y W}{\delta_1\delta_2} + \left[\frac{(S_{11} - S_{12})\delta_2 - (S_{21} - S_{22})\delta_1}{B\,\delta_1\delta_2}\right] = 0$$

$$\text{or } \frac{d\,(L_2 - L_1)}{dt} + \frac{\delta q_y}{\delta_1\delta_2}(L_2 - L_1) - \frac{\delta}{\delta_1\delta_2}(q_y W - \Delta S) = 0 \qquad (3.38)$$

$$\text{where } \Delta S = \frac{(S_{11} - S_{12})\,\delta_2 - (S_{21} - S_{22})\,\delta_1}{B\,\delta}$$

If there is no longshore gradient in the longshore transport, i.e. if $S_{11} = S_{12}$ and $S_{21} = S_{22}$, $\Delta S = 0$ and equation (3.38) reduces to equation (3.29).

The solution of the first order differential equation (3.38), is:

$$(L_2 - L_1) = \left\{W - (y_1 - y_2)_{t_0} \exp\left(\frac{-q_y\,\delta t}{\delta_1\delta_2}\right)\right\} + \left\{\frac{\Delta S}{q_y}\left(\exp\left(\frac{-q_y\,\delta t}{\delta_1\delta_2}\right) - 1\right)\right\} \qquad (3.39)$$

$$= (L_2 - L_1)_y + (L_2 - L_1)_x \tag{3.40}$$

where $(L_2 - L_1)_y = W - (y_1 - y_2)_{t_0} \exp\left(\frac{-q_y \delta t}{\delta_1 \delta_2}\right)$ (3.41)

and $(L_2 - L_1)_x = \frac{\Delta S}{q_y}\left(\exp\left(\frac{-q_y \delta t}{\delta_1 \delta_2}\right) - 1\right)$ (3.42)

$$(y_1 - y_2)_{t_0} = W - (L_2 - L_1)_{t_0} \tag{3.43}$$

$(L_2 - L_1)_y$ represents the effect of the onshore-offshore transport on the variation in $(L_2 - L_1)$, and is also the solution of equation (3.29). $(L_2 - L_1)_x$ represents the effect of a longshore gradient in the longshore transport on the variation in $(L_2 - L_1)$. It equals zero if there is no longshore gradient in longshore transport.

The fact that the solution of equation (3.38) reduces to the solution of equation (3.29) if no longshore gradient in longshore transport exists, does not mean that in that case the values of q_y and W will be the same. Even if there is no longshore gradient in the longshore transport, q_y for the three-dimensional case (q_{y3D}) will not equal q_y for the two-dimensional case (q_{y2D}). Due to the longshore current the shear stress at the bottom will be higher in the three-dimensional than in the two-dimensional case (Bijker [9]), with as consequence that q_{y3D} will most probably be larger than q_{y2D}.

In Chapter 6 this aspect of the problem will be studied in more detail.

3.4 The equilibrium profile

With the aid of equation (3.39) it becomes possible to determine the values of q_y and W for different divisions between the onshore and offshore profile. A relationship will result between q_y (and W) and the height z above the reference level:

$$q_y = q_y(z) \tag{3.44}$$

$$W = W(z) \tag{3.45}$$

The theoretical equilibrium profile can be determined with the aid of the relationship between W and z. If the relationship is in the form of finite differences, as is mostly the case, the equilibrium profile can e calculated numerically. However, if W can be expressed as an analytical function of z, the possibility exists to calculate the equilibrium profile by means of a differential equation, as will be shown below.

Numerical approach

Assume that the reference level lies at a lower level than the lower extremity of the profile, such that:

$$Z_{ik} = z_{ik} + Z_m \tag{3.46}$$

where Z_{ik} = the height of the i^{th} point in the k^{th} section, relative to the reference level

z_{ik} = the height of the i^{th} point in the k^{th} section, relative to the lower extremity of the profile schematization

Z_m = height of the lower extremity of the profile schematization, relative to the reference level (see Figure 9).

The total volume of sand in the equilibrium profile can be determined with the aid of the lengths in the two-layer schematization (Figure 9).

$$\text{area (aefj)} = \text{area (abj)} \tag{3.47}$$

$$\text{area (jghd)} = \text{area (jbcd)} \tag{3.48}$$

where area (aefj) = schematized onshore profile area

area (abj) = actual onshore profile area

area (jghd) = schematized offshore profile area

area (jbcd) = actual offshore profile area.

Consequently

$$\text{area (aekd)} + \text{area (fghk)} = \text{area (abcd)} \tag{3.49}$$

or, written in symbols:

$$L'_{1k} (Z_0 - Z_m) + W_k (Z_k - Z_m) = I_0/B \tag{3.50}$$

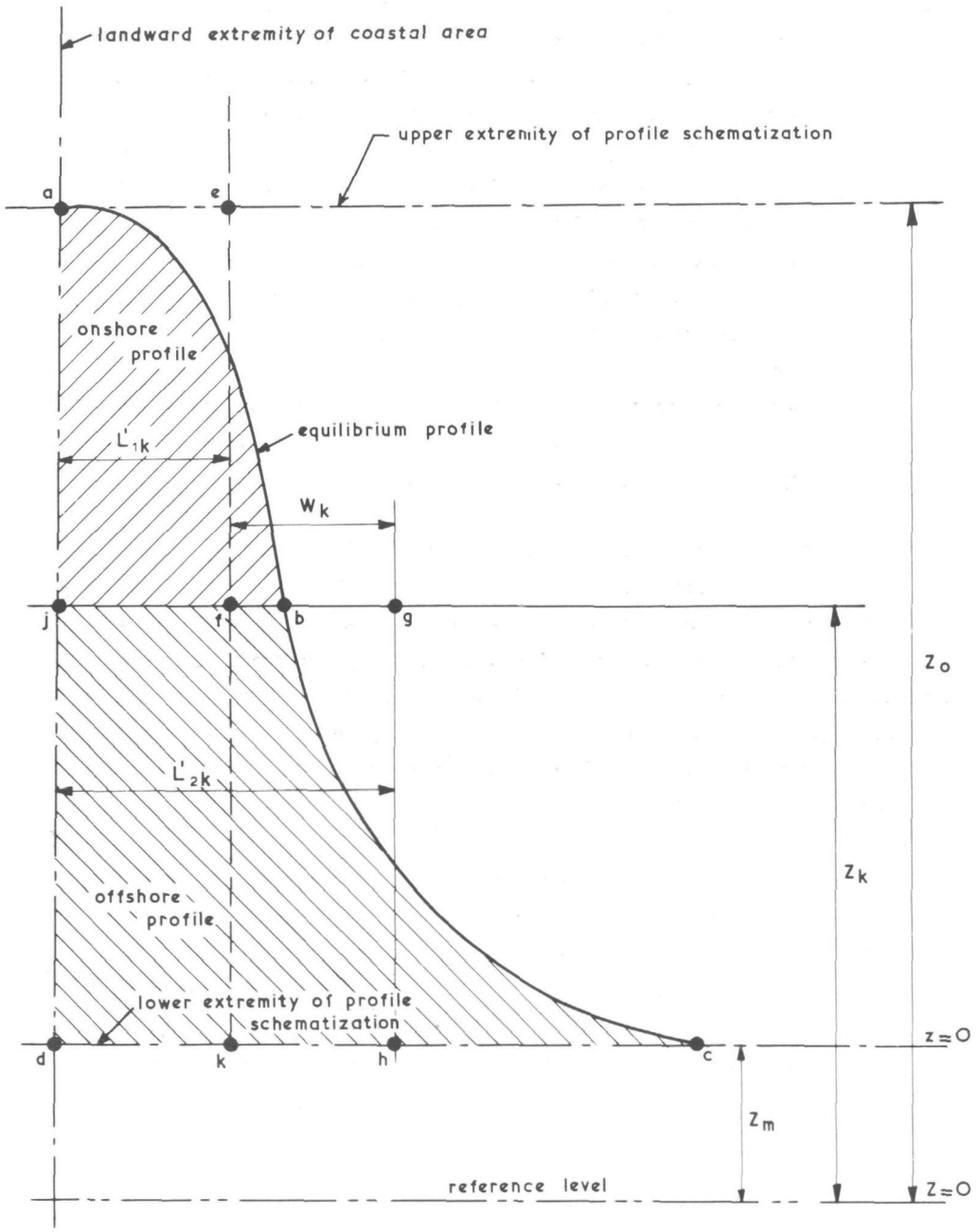

DETERMINATION OF EQUILIBRIUM PROFILE (1)
FIGURE 9

where L'_{1k} = equilibrium length of the onshore profile, relative to the landward extremity of the coastal area, with the division between the onshore and offshore profile at height Z_k above the reference level. The onshore profile is defined by $Z_0 \geqslant Z \geqslant Z_k$

Z_0 = elevation of upper extremity of the profile schematization, relative to the reference level

W_k = equilibrium distance between the schematized onshore profile and offshore profile, when the division between the onshore and offshore profile lies at a height Z_k above the reference level

I_0 = total volume of sand in the equilibrium profile, relative to the landward extremity of the area and the lower extremity of the profile schematization.

When making the two-layer schematization, as described in the previous sections, the zero line for the determination of L_1 and L_2 was chosen at the landward extremity of the coastal area. This landward extremity was chosen arbitrarily, and is mostly determined by the particular model dimensions. When calculating the ordinates of the equilibrium profile, it will be more consistent if a zero line is chosen, which is fixed for any equilibrium profile, and is independent of the model dimensions, such as for instance the water line.

In Chapter 6, when the model data are processed, a choice will be made regarding the position of the zero line. This choice will be dependent of the form of the results of the model investigation. In this section it will be assumed in general that the zero line lies at a distance L'_{1r} seawards of the landward extremity of the coastal area, where L'_{1r} is the equilibrium onshore length of the area of the profile defined by $Z_0 \geqslant Z \geqslant Z_r$. Consequently, it follows from equation (3.50) that:

$$L'_{1r}(Z_0 - Z_m) + W_r(Z_r - Z_m) = I_0/B \qquad (3.51)$$

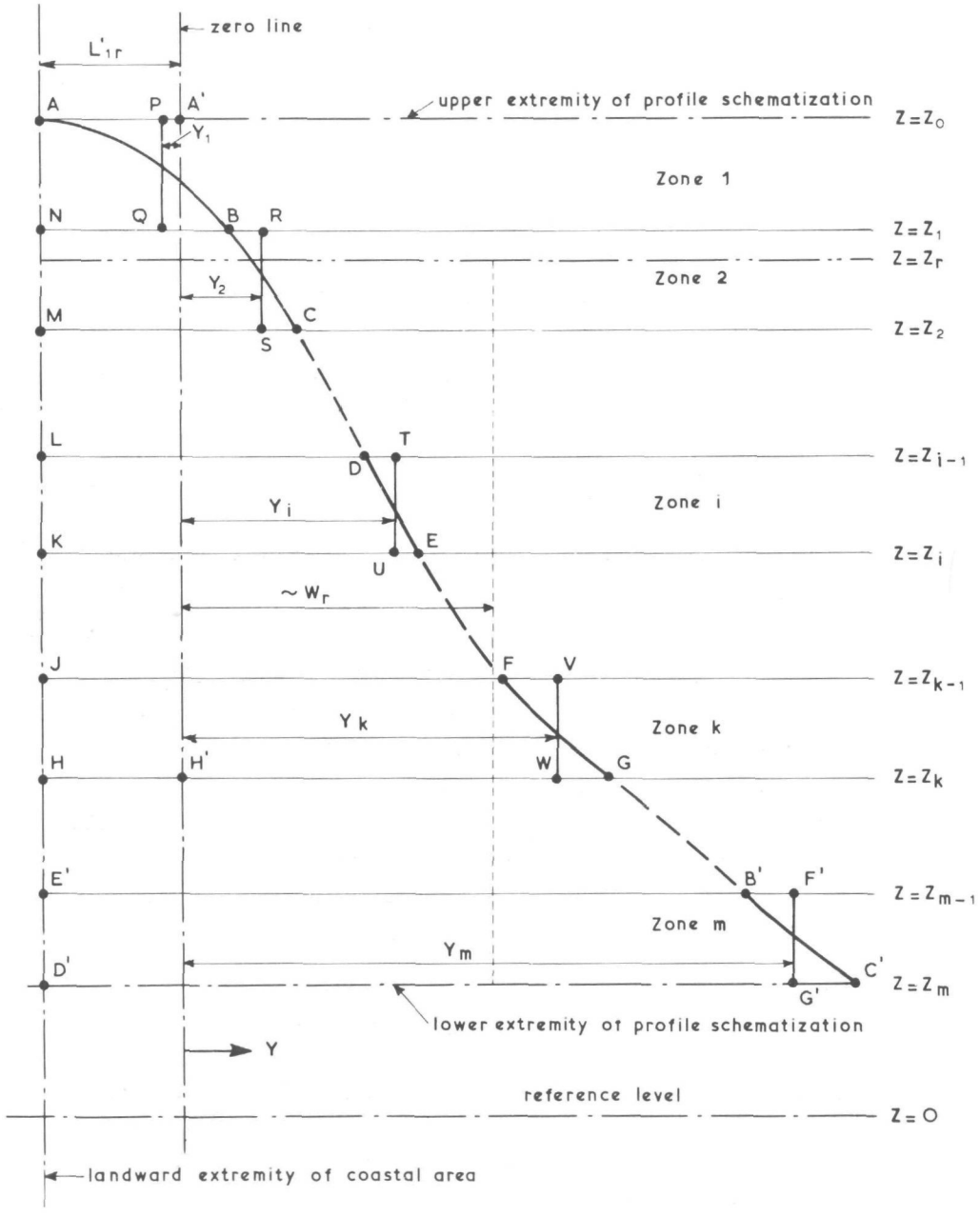

DETERMINATION OF EQUILIBRIUM PROFILE (2)
FIGURE 10

where L'_{1r} and W_r have the same definitions as L'_{1k} and W_k, except that the division between the onshore and the offshore profile lies at an elevation $Z = Z_r$ above the reference level.
Subtraction of equation (3.51) from equation (3.50) and division by $(Z_0 - Z_m)$ yields:

$$(L'_{1k} - L'_{1r}) = W_r \left(\frac{Z_r - Z_m}{Z_0 - Z_m}\right) - W_k \left(\frac{Z_k - Z_m}{Z_0 - Z_m}\right) \tag{3.52}$$

The difference $(L'_{1k} - L'_{1r})$ equals the equilibrium length of the onshore profile relative to the zero line when the division between the onshore and offshore profile lies at an elevation Z_k above the reference level. It will be called L_{1k}.

$$\text{Thus } L_{1k} = W_r \left(\frac{Z_r - Z_m}{Z_0 - Z_m}\right) - W_k \left(\frac{Z_k - Z_m}{Z_0 - Z_m}\right) \tag{3.53}$$

The equilibrium volume of sand in the onshore profile area can be determined from:

$$I_{1k} = L_{1k} (Z_0 - Z_k) B \tag{3.54}$$

where I_{1k} = the equilibrium volume of sand in the onshore profile area, relative to the zero line, when the division between the onshore and offshore profile lies at $Z = Z_k$ above the reference level. L_{1k} can be substituted from equation (3.53).

Instead of using the schematized onshore and offshore lengths to determine the equilibrium onshore profile volume, as was done to find equation (3.54), the ordinates of the equilibrium profile relative to the zero line, at fixed elevations, can also be used (see Figure 10), viz.:

$$\text{Equilibrium onshore profile volume } I_{1k} = \{ \text{area (ABC ... D E ...FGHA)} + \text{- area (AA}'\text{H}'\text{H)} \} B \tag{3.55}$$

Divide the onshore profile volume into k arbitrarily chosen horizontal zones, as is shown in Figure 10. The part of the profile in any zone i is assumed to be represented by a vertical line T U (Figure 10) with ordinate Y_i, which is such that

Y_i = average position of the actual equilibrium profile in zone i

$$= \left(\frac{1}{Z_{i-1} - Z_i}\right) \int_{Z_i}^{Z_{i-1}} Y \, dZ \qquad (3.56)$$

where Y = ordinate of the equilibrium profile at elevation $Z (Z_{i-1} \geq Z \geq Z_i)$.

This implies that the profile will be represented by the line (DTUE) in zone i instead of by the curve (DE). The volume of zone i stays the same. The total equilibrium volume of the onshore profile can then be found by addition of the areas of all k zones, viz.:

$$I_{1k} = \{\text{area (APQN)} + \text{area (NRSM)} + \ldots + \text{area (LTUK)} + \ldots\ldots + \ldots\ldots + \text{area (JVWH)} - \text{area (AA'H'H)}\} B \qquad (3.57)$$

$$= \{Y_1 (Z_0 - Z_1) + Y_2 (Z_1 - Z_2) + \ldots + Y_i (Z_{i-1} - Z_i) + \ldots\ldots + \ldots + Y_k (Z_{k-1} - Z_k)\} B$$

$$= \sum_{i=1}^{k} Y_i (Z_{i-1} - Z_i) B \qquad (3.58)$$

However, the values of I_{1k} as determined from equations (3.54), (3.55) and (3.58) are equal. Consequently

$$\sum_{i=1}^{k} Y_i (Z_{i-1} - Z_i) = L_{1k} (Z_0 - Z_k) \qquad (3.59)$$

L_{1k} can be substituted from equation (3.53):

$$\sum_{i=1}^{k} Y_i (Z_{i-1} - Z_i) = \left\{ W_r \left(\frac{Z_r - Z_m}{Z_0 - Z_m}\right) - W_k \left(\frac{Z_k - Z_m}{Z_0 - Z_m}\right) \right\} (Z_0 - Z_k) \qquad (3.60)$$

Equation (3.60) can be used to find the ordinates of the equilibrium profile, by varying i from 1 to the total number of zones in the complete profile. When k = 1, Y_1 can be found, when k = 2

$$\sum_{i=1}^{k} Y_i \, (Z_{i-1} - Z_i) = Y_1 \, (Z_0 - Z_1) + Y_2 \, (Z_1 - Z_2)$$

and as Y_1 is then already known, Y_2 can be found, etc.. Consequently it is possible to rewrite the left-hand side of equation (3.60) in the following way:

$$\sum_{i=1}^{k} Y_i \, (Z_{i-1} - Z_i) = \left\{ \sum_{i=1}^{k-1} Y_i \, (Z_{i-1} - Z_i) \right\} + Y_k \, (Z_{k-1} - Z_k) \qquad (3.61)$$

with the restriction that when k = 1

$$\sum_{i=1}^{k-1} Y_i \, (Z_{i-1} - Z_i) = 0 \qquad (3.62)$$

Combination of equations (3.60) and (3.61) leads to:

$$Y_k = \frac{\left\{ W_r \left(\frac{Z_r - Z_m}{Z_0 - Z_m}\right) - W_k \left(\frac{Z_k - Z_m}{Z_0 - Z_m}\right) \right\} (Z_0 - Z_k) - \sum_{i=1}^{k-1} Y_i \, (Z_{i-1} - Z_i)}{(Z_{k-1} - Z_k)} \qquad (3.63)$$

where Y_k = the ordinate in zone k of the equilibrium profile, at elevation $Z = 1/2 \, (Z_{k-1} + Z_k)$, i.e. at the average elevation of the k^{th} zone, as measured from the zero line.

Analytical approach

In case of an analytical relationship between W and Z, equations (3.53) and (3.59) have to be rewritten. In equation (3.53) L_{1k} is replaced by L_1, W_k by W and Z_k by Z.

Consequently equation (3.53) becomes:

$$L_1 = W_r \left(\frac{Z_r - Z_m}{Z_0 - Z_m}\right) - W \left(\frac{Z - Z_m}{Z_0 - Z_m}\right) \tag{3.64}$$

where L_1 = equilibrium length of the onshore profile relative to the zero line, with the division between the onshore and offshore profile at a height Z above the reference level

W = equilibrium distance between the schematized onshore and offshore profile, when the division between them lies at a height Z above the reference level.

The addition of the areas of the zones, as done in equation (3.59), has to be replaced by the integration of the area under the equilibrium profile:

$$L_1 (Z_0 - Z) = \int_Z^{Z_0} Y \, dZ \tag{3.65}$$

Y = ordinate in the equilibrium profile, relative to the zero line, at a height Z above the reference level.

Combination of equations (3.64) and (3.65) yields:

$$\int_Z^{Z_0} Y \, dZ = (Z_0 - Z) \left\{ W_r \left(\frac{Z_r - Z_m}{Z_0 - Z_m}\right) - W \left(\frac{Z - Z_m}{Z_0 - Z_m}\right) \right\}$$

$$= f(W, Z) \tag{3.66}$$

The ordinate Y in the equilibrium profile can be found from equation (3.66) by differentiation to Z, viz.:

$$Y = -\frac{\partial}{\partial Z} \left\{ f(W, Z) \right\} \tag{3.67}$$

$$= \left(\frac{1}{Z_0 - Z_m}\right) \frac{\partial}{\partial Z} \left\{ W (Z_0 - Z)(Z - Z_m) \right\} - \frac{W_r (Z_r - Z_m)}{(Z_0 - Z_m)} \frac{\partial}{\partial Z} (Z_0 - Z) \tag{3.68}$$

When grouping the terms in WZ^2, WZ, W and Z respectively together,

equation (3.68) becomes:

$$Y = \left(\frac{Z_r - Z_m}{Z_0 - Z_m}\right) W_r - \left(\frac{1}{Z_0 - Z_m}\right) \frac{\partial}{\partial Z} (WZ^2) + \left(\frac{Z_0 + Z_m}{Z_0 - Z_m}\right) \frac{\partial}{\partial Z} (WZ) + \\ - \left(\frac{Z_0 Z_m}{Z_0 - Z_m}\right) \frac{\partial W}{\partial Z} \qquad (3.69)$$

Equation (3.69) defines the equilibrium profile.

3.5 Application of the schematization

When applying the mathematical model, as described in the foregoing sections, in practice, it can be interpreted in various ways. In order to come to a consistent approach, it is thus necessary to standardize the different steps in the mathematical model. The steps that have to be followed to find the onshore-offshore transport and the equilibrium profile, are:

(1) determination of the upper and lower limits of the profile schematization
(2) determination of $(L_2 - L_1)$ from the soundings
(3) correction of $(L_2 - L_1)$-values to compensate for sounding errors
(4) determination of W and q_y as a function of z
(5) calculation of the equilibrium profile.

After the completion of steps (1) to (4) it becomes possible to determine the theoretical onshore-offshore transport at any time for any elevation z in the profile, with the aid of equation (3.1).

Upper and lower extremities of the profile schematization

Bakker [2] made the choice of the upper and lower limits of the profile schematization in such a way that no sediment movement will occur through

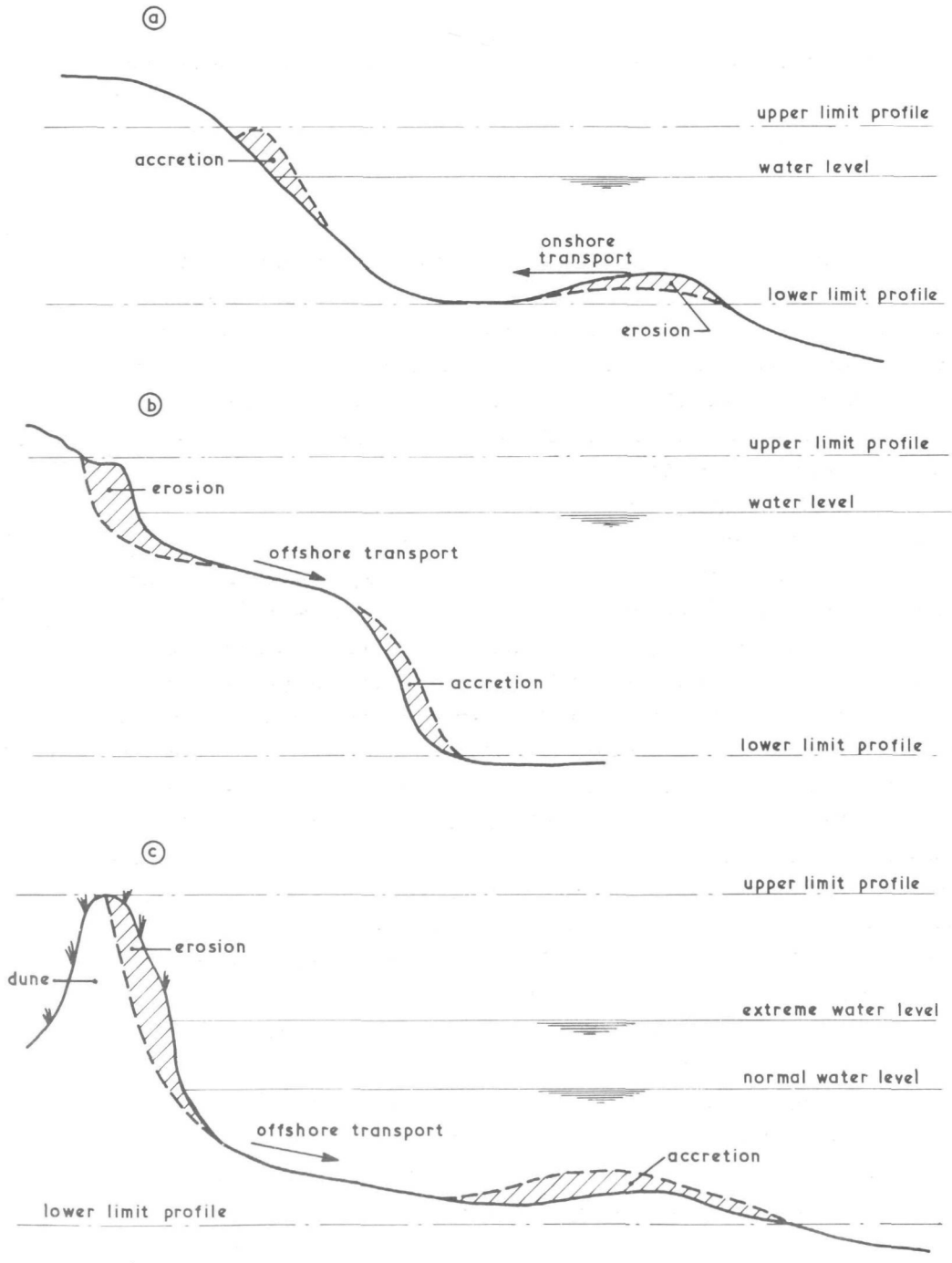

EFFECT OF PROFILE GEOMETRY ON PROFILE LIMITS
FIGURE 11

these two limits, as can be seen from his assumption regarding continuity, viz.:

$$\delta_1 \frac{dL_1}{dt} + \delta_2 \frac{dL_2}{dt} = 0 \qquad (3.70)$$

As long as equation (3.70) is only used in problems regarding coastline variations in the vicinity of for instance a groyne field, it is a reasonable assumption, because Bakker assumes that the profile had been in equilibrium before the construction of the groyne field. Profile changes will thus only take place in those areas of the profile where normal wave action can cause sediment transport (either longshore transport or onshore-offshore transport).

In this chapter, however, the possibility is studied to use equation (3.1) for the calculation of onshore-offshore transport in general. This includes cases in which the profile is not in equilibrium, and is developing (either eroding of accreting), as well as cases where extreme wave conditions, combined with high water levels, will cause large erosion from dune fields at the landward extremity of the profile (see Figure 11). In all these cases the extremities of the profile, through which no transport takes place, are largely determined by the profile geometry, and not only by the wave conditions and sediment characteristics. This applies even more for model tests, where the height of the sand package at the landward extremity of the profile and the water depth in front of the wave generator will mostly determine the layer thickness δ to be used. Accordingly, it will neither be possible to compare the results of model tests with different initial geometries, nor to compare prototype results of different locations along the coast.

Consequently, if no additional assumptions are made regarding the profile schematization, it will not be possible to determine the limits of the profile uniquely in terms of wave and sediment characteristics. In that case it is to be expected that it will be impossible to determine q_y and W uniquely for a specific wave condition and bed material. A solution will be to choose both the upper and lower limits of the profile to be

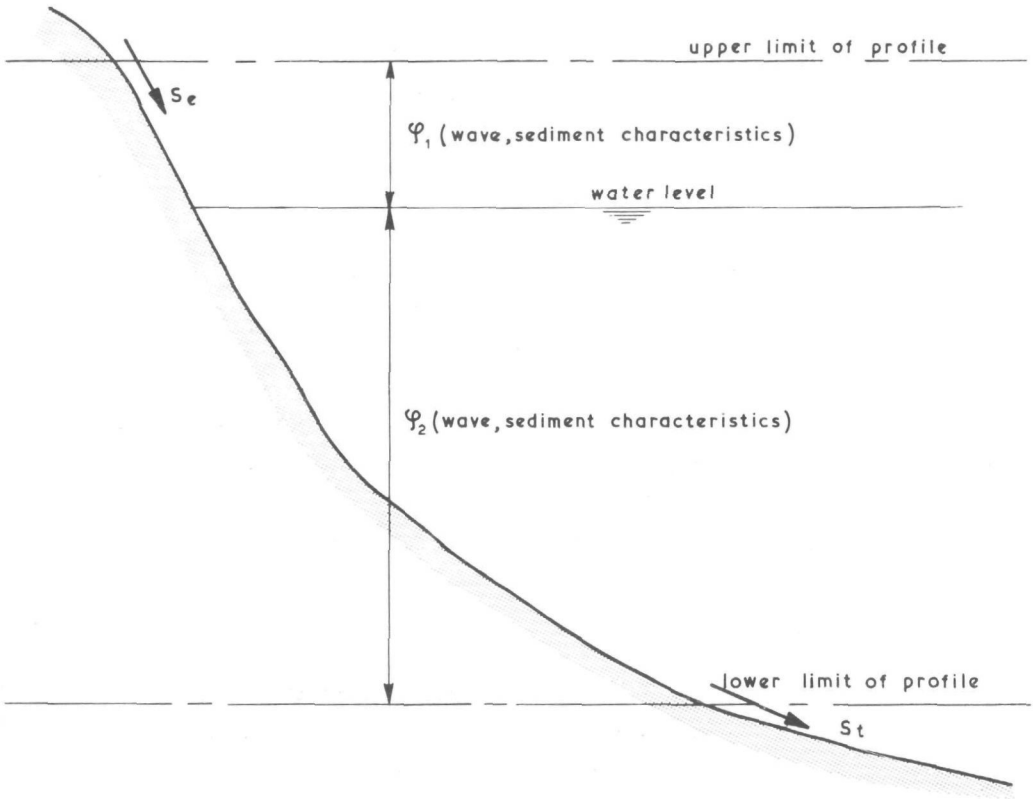

REMARK : φ = function

ADAPTED LIMITS OF PROFILE
FIGURE 12

equal to some function of the wave and sediment characteristics, and to alter the continuity equation (3.70) to include the transport of sediment through the chosen limits of the profile (Figure 12).

$$\delta_1 \frac{dL_1}{dt} + \delta_2 \frac{dL_2}{dt} + S_t - S_e = 0 \qquad (3.71)$$

The transports S_e and S_t respectively, will then serve as boundary conditions at the upper and lower boundaries of the profile schematization. These transports S_e and S_t must be known as a function of time, to enable the calculation of q_y and W.
As the choice of the profile limits forms one of the major problems in the application of the schematization, this aspect will be studied in more detail in Chapter 4.5. For the time being it will be assumed that the choice of the limits, as used by Bakker, applies, i.e. that $S_e = S_t = 0$.

Determination of $(L_2 - L_1)$

A clear distinction can be made between problems where the dynamics of a coastline, protected by a groyne field, are studied, and problems where the onshore-offshore transport is of primary importance. When problems regarding groynes are studied, the division between the onshore and offshore profile is actually defined vertically, i.e. a point Y is situated in the onshore profile if $Y < Y_d$ (see Figure 13). If $Y \geqslant Y_d$, the point lies in the offshore profile. When a profile is schematized according to the theory, this is also the criterion which is used to decide if a point lies in the onshore or offshore profile.
If, however, it is necessary to determine the onshore-offshore transport at any depth in a bottom profile, or if the equilibrium profile for any specific wave condition has to be found, more care has to be exercised. As long as the bottom profile has a form as is shown in Figure 6, the determination of $(L_2 - L_1)$ with the aid of equations (3.2) ... (3.6) would not give rise to any problem. The vertical division between the onshore and offshore profile, as used before, is still applicable.

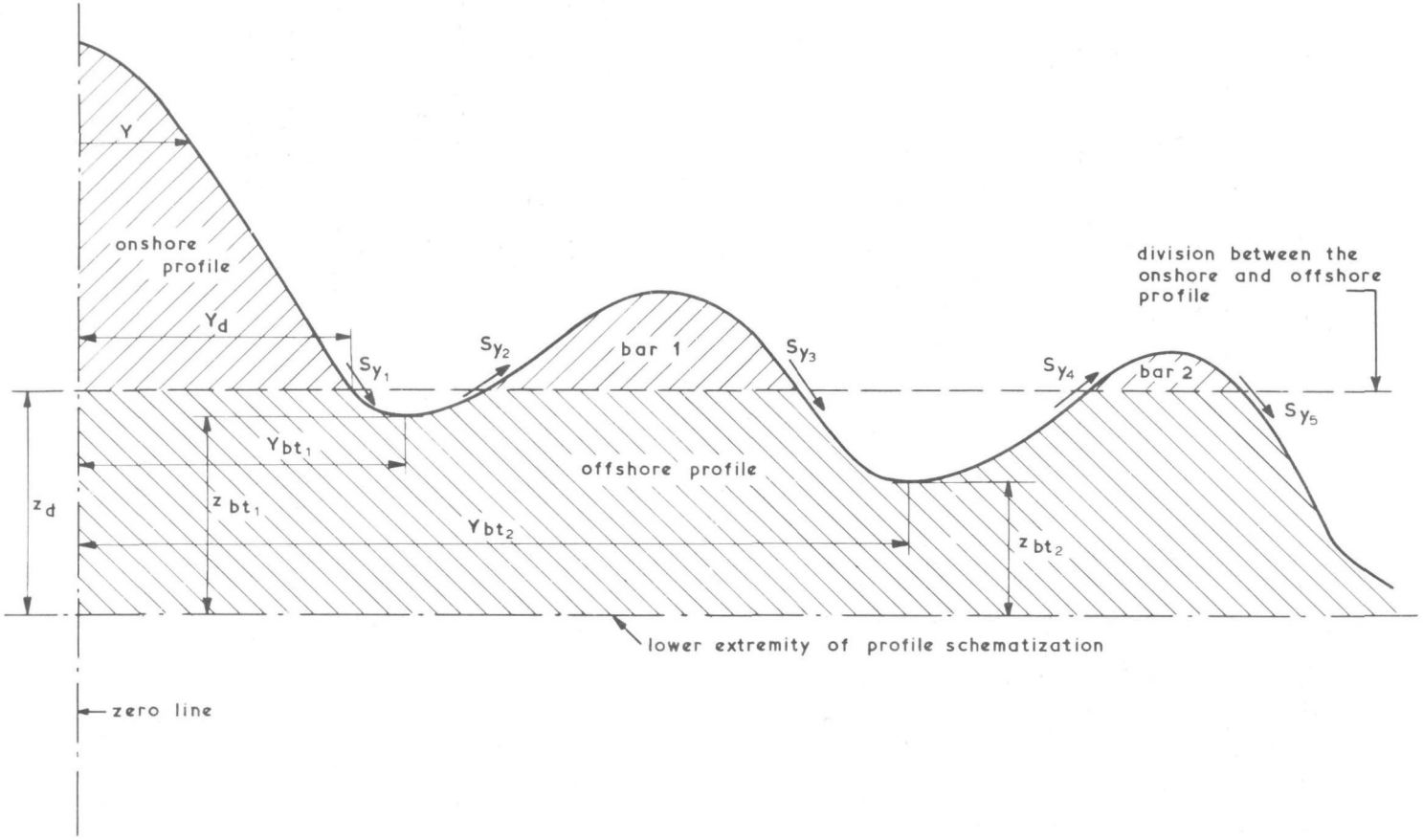

BEACH PROFILE WITH BARS

FIGURE 13

However, the profile mostly contains one or more breaker bars, as is shown in Figure 13.
As long as $z_d > z_{bt1}$ and $Y_d < Y_{bt1}$, the total volume of both bars belong to the offshore profile if the division between the onshore and offshore profile is assumed to be a vertical one. When $z_{bt1} > z_d > z_{bt2}$ and $Y_d < Y_{bt2}$, the total volume of bar 1 is part of the onshore profile, while the total volume of bar 2 still belongs to the offshore profile. As soon as $z_d < z_{bt2}$ and $Y_d > Y_{bt2}$, bar 2 also becomes part of the onshore profile. The relationship between $(L_2 - L_1)$ and z will thus exhibit as many discontinuities as there are different bar troughs in the profile. If the time-variation in $(L_2 - L_1)$ is then used to determine W in the form of equation (3.45) for every elevation z in the profile, W (z) will also be subject to discontinuities. The determination of the equilibrium profile as discussed in Chapter 3.4 is then impossible.
In such cases it is better to determine the onshore and offshore profile volumes by means of another criterion, viz.:
(1) A point is situated in the onshore profile if $z > z_d$
(2) A point is situated in the offshore profile if $z \leqslant z_d$.

The areas of the bars in Figure 13 above the line $z = z_d$ will then belong to the onshore profile, the rest of the bar volumes will be added to the offshore profile. The onshore-offshore transport S_y, calculated with the aid of equation (3.1), with $(L_2 - L_1)$ and W determined by using the criterion as suggested above, is then the mean value of all transports across the horizontal division between the onshore and offshore profile.

$$S_y = q_y\,(W - (L_2 - L_1)) = (S_{y1} + S_{y3} + S_{y5}) - (S_{y2} + S_{y4})$$
(for an explanation of S_{yi} $(i = 1 \ldots 5)$ see Figure 13) (3.72)

It can be shown that no discontinuity will occur in the relationship between W and z if the division between the onshore and offshore profile changes from z_{d1} to z_{d2} (see Figure 14), where:

$$z_{d2} < z_{bt} < z_{d1} \tag{3.73a}$$

$$z_{d2} \rightarrow \bar{z}_{bt} \tag{3.73b}$$

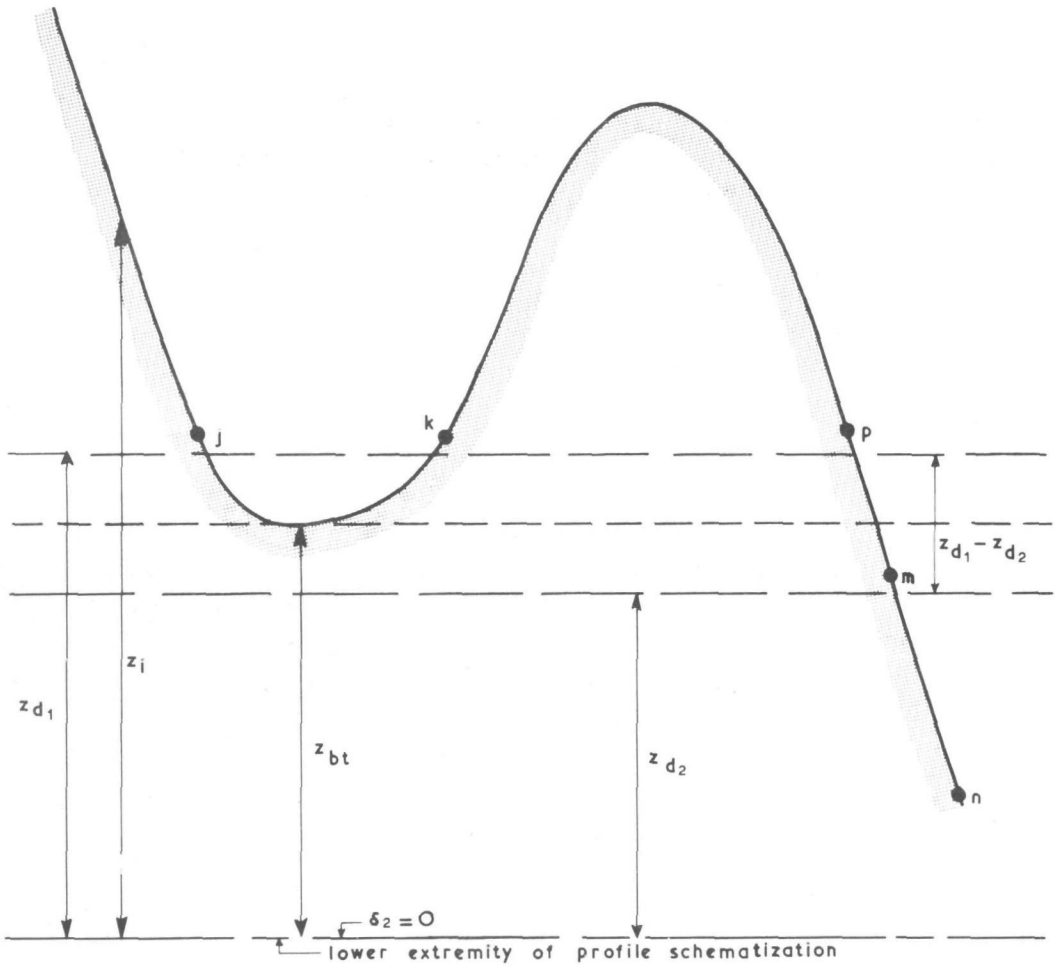

EFFECT OF BARS ON TRANSPORT
FIGURE 14

$$z_{d1} \rightarrow z_{bt}^{+} \tag{3.73c}$$

$$z_{d1} - z_{d2} \rightarrow 0 \tag{3.73d}$$

where z_{bt} = elevation of the bar trough above the lower extremity of the profile. If the division between the onshore and offshore profile lies at height z_{d2}, $(L_2 - L_1)$ can be computed as follows:

$$I_1 = bl \left(\sum_{i=1}^{m} z_i - mz_{d2} \right) \tag{3.74}$$

$$I_2 = bl \left(\sum_{i=m+1}^{n} z_i + mz_{d2} \right) \tag{3.75}$$

where I_1 = volume of sand in the onshore profile area of a characteristic profile with a longshore width b (two-dimensional case)

I_2 = volume of sand in the offshore profile area of a characteristic profile with a longshore width b (two-dimensional case)

m = number of measuring points in the onshore profile area when the division between onshore and offshore profile lies at elevation $z = z_{d2}$ (see Figure 14)

n = total number of measuring points in the characteristic profile.

With the aid of equation (3.6) it can be shown that:

$$(L_2 - L_1) = \frac{I_2}{B\delta_2} - \frac{I_1}{B\delta_1} \tag{3.6}$$

$$= l \left\{ \frac{\delta_1 \sum_{i=m+1}^{n} z_i - \delta_2 \sum_{i=1}^{m} z_i}{\delta_1 \delta_2} + \frac{m\delta}{\delta_1} \right\} \tag{3.76}$$

where $\delta_2 = z_{d2}$

$B = b$

When the division between the onshore and offshore profile lies at height z_{d1}:

$$I_1 = bl \left(\sum_{i=1}^{j} z_i + \sum_{i=k}^{p} z_i - (j + p - k + 1)\, z_{d1} \right) \tag{3.77}$$

$$I_2 = bl \left(\sum_{i=j+1}^{k-1} z_i + \sum_{i=p+1}^{n} z_i + (j + p - k + 1)\, z_{d1} \right) \tag{3.78}$$

where j = the most seaward measuring point landwards of the bar trough, for which $z > z_{d1}$. Point j consequently belongs to the onshore profile area

k = the most landward point on the bar for which $z > z_{d1}$. Point k belongs to the onshore profile area

p = the most seaward point on the bar for which $z > z_{d1}$, i.e. the most seaward point in the whole profile which still belongs to the onshore profile area.

$$\sum_{i=j+1}^{k-1} z_i = 0 \text{ if } k = j + 1 \tag{3.79}$$

Consequently, with the aid of equation (3.6):

$$(L_2 - L_1) = l \left\{ \frac{\delta_1 \left(\sum_{i=j+1}^{k-1} z_i + \sum_{i=p+1}^{n} z_i \right) - \delta_2 \left(\sum_{i=1}^{j} z_i + \sum_{i=k}^{p} z_i \right)}{\delta_1 \delta_2} + \right.$$

$$\left. + \frac{(j + p - k + 1)\delta}{\delta_1} \right\} \tag{3.80}$$

where $\delta_2 = z_{d1}$

When $z_{d2} \longrightarrow z_{bt}^{-}$ and $z_{d1} \longrightarrow z_{bt}^{+}$, until there is no measuring point left between the k^{th} and j^{th} measuring points and the p^{th} and m^{th} points coincide, k = j + 1 and p = m. Equation (3.80) will then reduce to equation (3.76). Consequently no discontinuities will result from the existence of

the bar. In the rest of this report the division between the onshore and offshore profile will thus be defined as a horizontal line, dividing the onshore profile from the offshore profile.

Correction of $(L_2 - L_1)$

The calculated volume I_t in the profile at any time t can differ from the initial volume $I_{t=0}$, as a result of errors of any of three general types:

(1) errors which are inherent to the method of measuring of the bottom elevations,

(2) errors which are inherent to the variation in time of the soil mechanical properties of the bed material, and

(3) errors which are inherent to the form of the bottom profile.

re(1). In all model tests under consideration in this report, the bottom elevation was measured by means of a level and levelling rod. It is essential that the rod be kept in a vertical position when performing the measurements. If this is not the case, a seemingly too low depth will be measured, i.e. a consistent error in one direction. In Figure 15b the expected fault is shown which results from errors of this kind. Reading errors, made by the observer, can be either positive or negative. It will be assumed that these errors are normally distributed about their mean (Figure 15c). In this first general source of errors the effect of a wrong calibration of the level should actually also be included. It will, however, be assumed that no errors are made in the calibration.

re(2). When an initial profile is built into a model basin, the sand is normally not completely compacted. Accordingly, it is possible that the sediment will be subjected to compaction. This will lead to an apparent inconsistency in the sand balance. For the situation as sketched in Figure 15a, the bottom layer of the sand package in zone A will be subjected to a higher static pressure than in zone C. In zones B and C the effect of a dynamic pressure, due to wave action should, however, also be incorporated. This effect will most probably be the strongest in zone B, where an additional compaction is also to be expected as a result of sediment transport.

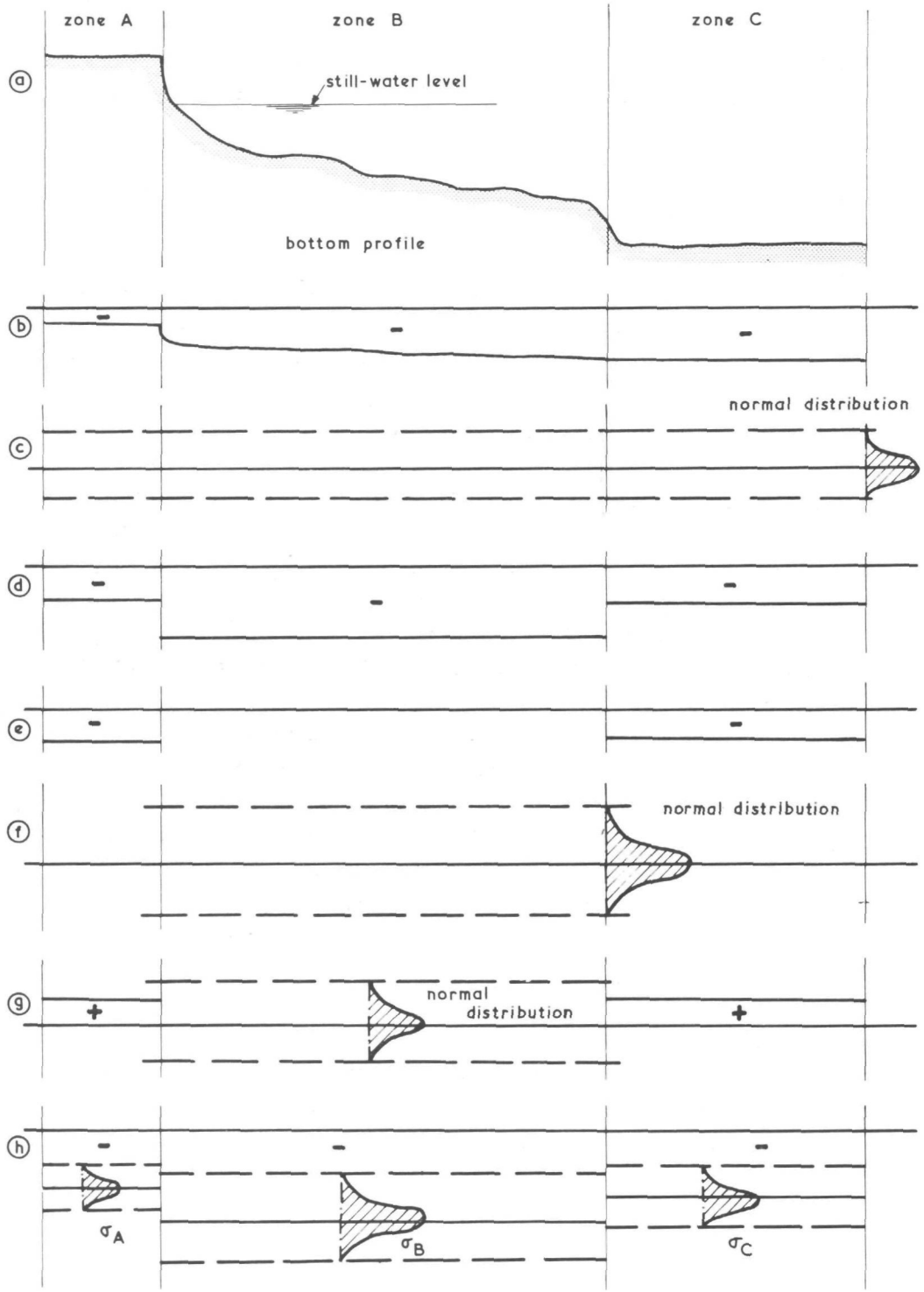

ERROR ANALYSIS
FIGURE 15

Accordingly, an error of the kind shown in Figure 15d will be the result. In tests of long duration ($t \geq 1000$ hours) the measuring points in zones A and C will show an additional compaction, due to the fact that the measuring rod has frequently been placed on the same spot (Figure 15e). In the active part of the profile (zone B) this will not be the case.

re(3). The height z_{ik} measured at any point i in any section k is assumed to resemble the bottom elevation in a rectangle, with its centre at point i in section k and with dimensions l times b, where b is measured in longshore direction. As long as the bottom slopes gently in all directions, this is a good approximation. Large variations in bottom slope in the onshore-offshore direction can lead to errors due to an incorrect volumetric schematization of the actual profile. This type of error will mostly occur in zone B, as well as at the transition between zone B and zones A and C respectively. As the chance of a bar trough passing through a measuring point is theoretically the same as that of a bar crest, this type of error will be assumed to be normally distributed about its mean (Figure 15f). Large longshore variations in bottom profile (three-dimensional effects) will lead to an error distribution analogous to that shown in Figure 15f. A simulation of the placing of the rod was performed under conditions which closely resemble the model conditions. It showed that the rod will be placed either too far landwards or too far seawards of the correct position, in such a way that the different places where the rod is placed, will be distributed with a normal distribution around the correct position. If the measuring rod is not placed in the correct position (the distance l between the measuring points being a constant) when the point falls in either zone A or zone C, a seemingly too high bottom elevation, relative to the compacted bottom height at the measuring point itself (Figure 15e), will be measured. In zone B the relative error can be either positive or negative, depending on the local bottom configuration. It will be assumed to be normally distributed about its mean (see Figure 15g).
The relative values of the possible errors, shown schematically in Figure

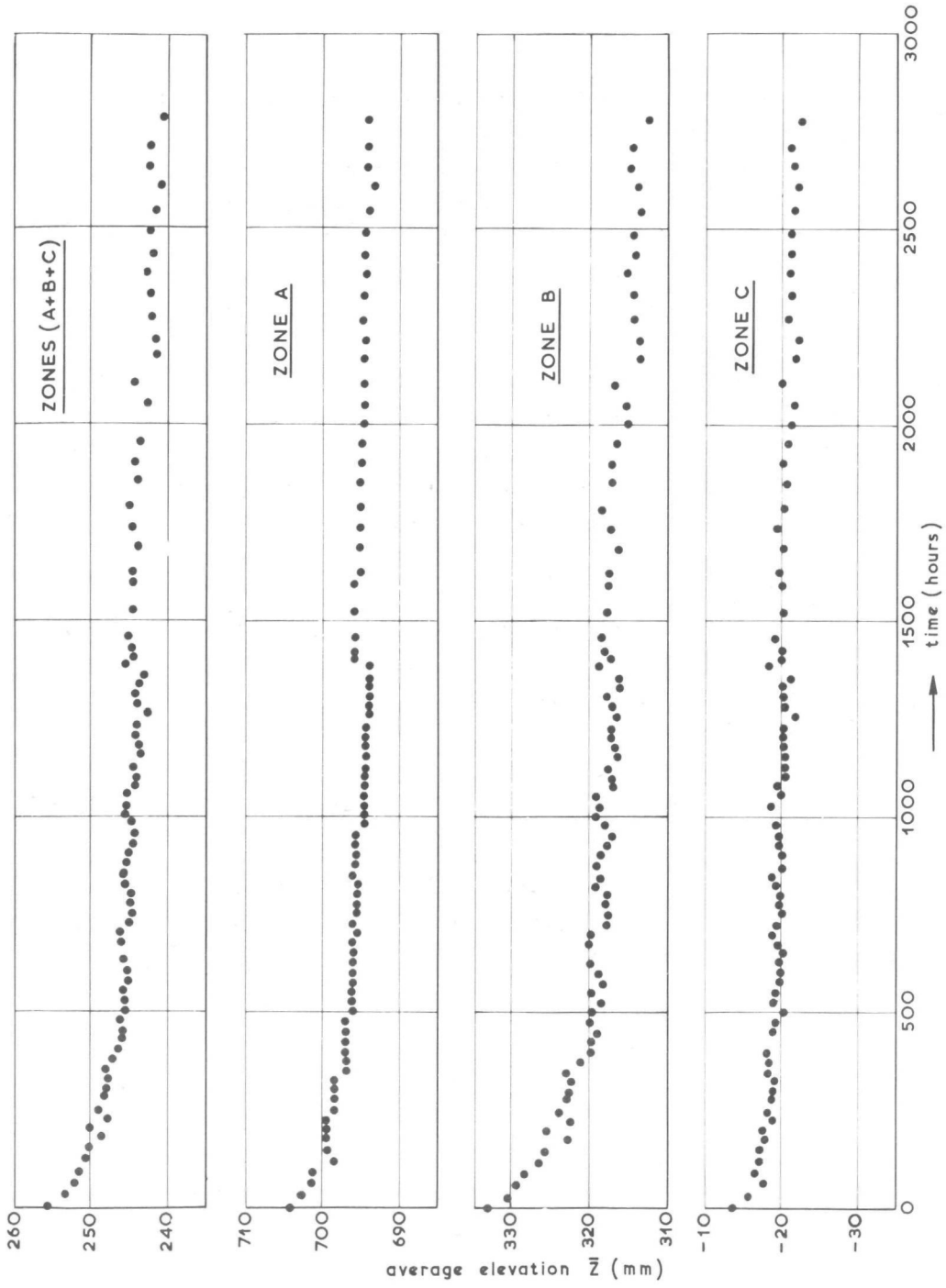

REMARKS: 1) for definition of the zones, see Figure 15

2) bed material was sand with D_{50}= 0.17mm

3) no transport occurred across the divisions between zones A→B, B→C respectively.

APPARENT VOLUMES

FIGURE 16

15b - 15g, are variable in time and unknown. However, it is to be expected that a possible error as is shown in Figure 15h will result. In Figure 16 the variation in time of the apparent volumes in zones A, B and C is given for a specific long-duration two-dimensional test. It is evident that $\sigma_B >> \sigma_A (= \sigma_C)$ (see Figure 15). This is a result of the larger variations in bottom slope in zone B than in zones A and C, due to a more active transport regimen. When the bottom profile is thus corrected, it will be the most logical to make the largest corrections at the points where the largest variations had occurred. As by definition no topographical bottom changes due to sediment transport occurred in zones A and C, it was decided to compensate the apparent volumetric changes in these zones fully, and to distribute the rest of the apparent loss $\Delta I_B = I_{Bt=t_0} - I_{Bt_j}$ in the following way in zone B:

$$\Delta z_{ik} = \left\{ \frac{\left| z_{ikt_0} - z^{*}_{ikt_j} \right|}{\sum_{k=1}^{N} \sum_{i=n_{B1k}}^{n_{Bk}} \left| z_{ikt_0} - z^{*}_{ikt_j} \right|} \right\} \left\{ \sum_{k=1}^{N} \sum_{i=n_{B1k}}^{n_{Bk}} (z_{ikt_0} - z^{*}_{ikt_j}) \right\} \qquad (3.81)$$

where $\Delta I_B = 1b \sum_{k=1}^{N} \sum_{i=1}^{n_k} \Delta z_{ik} - (\Delta I_A + \Delta I_C)$ (3.82)

Δz_{ik} = the correction applied to the bottom height in the i^{th} point of the k^{th} section, measured at time t_j, $= (z_{ik})_{t=t_j} - (z_{ik})^{*}_{t=t_j}$, where $z^{*}_{ikt_j}$ denotes the uncorrected value of z_{ikt_j}

$\left| z_{ikt_0} - z^{*}_{ikt_j} \right|$ = absolute value of the difference in the elevation of the i^{th} point in the k^{th} section at time $t=t_j$, measured relative to its value at time $t=t_0$

ΔI_A and ΔI_C = apparent losses in zones A and C respectively

n_{B1k} = the most landward measuring point in the k^{th} section which still falls in zone B

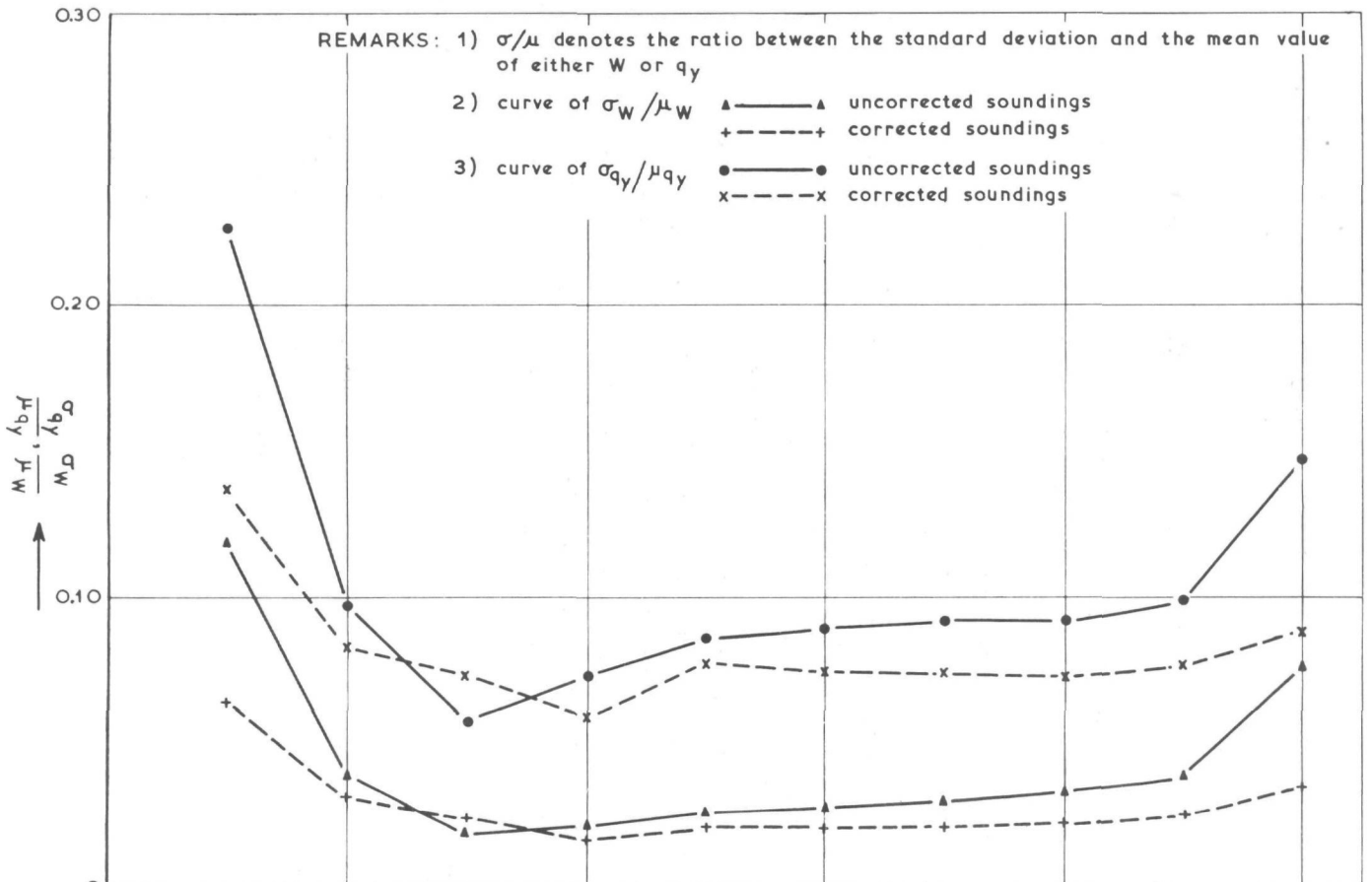

EFFECT OF SOUNDING CORRECTION

FIGURE 17

n_{Bk} = the most seaward measuring point in the k^{th} section which still falls in zone B.

The term $\sum_{k=1}^{N} \sum_{i=n_{B1k}}^{n_{Bk}} (z_{ikt_0} - z^{*}_{ikt_j})$ determines the algebraic amount that has to be compensated for. A negative sign implies that the sand volume in the area has increased, a positive sign that it has decreased.

The term $\dfrac{|z_{ikt_0} - z^{*}_{ikt_j}|}{\sum_{i=1}^{N} \sum_{i=n_{B1k}}^{n_{Bk}} |z_{ikt_0} - z^{*}_{ikt_j}|}$ determines which percentage of the total amount to be corrected will be attributed to the i^{th} point in the k^{th} section.

This implies that points where the largest variation in bottom height had occurred, will get the largest share of the correction.

If the corrected values of the bottom elevation, as determined with the aid of equation (3.81), are used to determine the values of $(L_2 - L_1)$, it is possible to make a more sound determination of W and q_y than if the uncorrected values of z_{ik} had been used, as can be seen in Figure 17. In the rest of this report the corrected values of z_{ik} (according to equation (3.81)) will be used for all calculations.

Determination of W and q_y

The only two unknown variables in equation (3.39) are q_y and W. It has been assumed in Chapter 3.1 that q_y is a constant in time. Consequently, it seems the most realistic to choose that value of the equilibrium distance W for which the coastal constant q_y shows the least variation in time.

Equation (3.39) can be rewritten as follows for $t = t_j$:

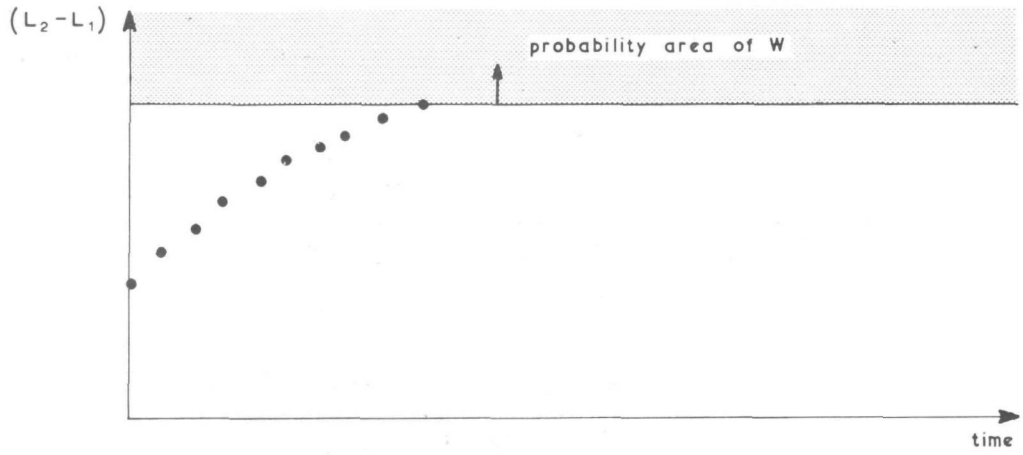

FIGURE 18(a)

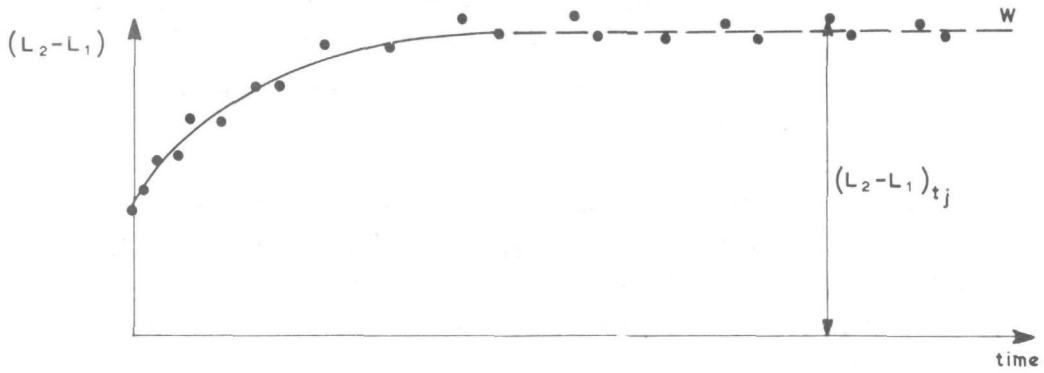

FIGURE 18(b)

DETERMINATION OF W
FIGURE 18

$$\left\{ (W - (L_2 - L_1)_{t_j}) - \frac{\Delta S}{q_{yt_j}} \right\} = \left\{ (W - (L_2 - L_1)_{t_0}) - \frac{\Delta S}{q_{yt_j}} \right\} \exp\left(\frac{-q_{yt_j}\,\delta(t_j - t_0)}{\delta_1 \delta_2} \right)$$

or:

$$\exp\left(+ \frac{q_{yt_j}\,\delta(t_j - t_0)}{\delta_1 \delta_2} \right) = \left\{ \frac{(W - (L_2 - L_1)_{t_0}) - \frac{\Delta S}{q_{yt_j}}}{(W - (L_2 - L_1)_{t_j}) - \frac{\Delta S}{q_{yt_j}}} \right\}$$

$$= \left\{ \frac{q_{yt_j}\,(W - (L_2 - L_1)_{t_0}) - \Delta S}{q_{yt_j}\,(W - (L_2 - L_1)_{t_j}) - \Delta S} \right\}$$

thus:

$$q_{yt_j} = \frac{\delta_1 \delta_2}{\delta(t_j - t_0)} \ln \left[\frac{q_{yt_j}\,(W - (L_2 - L_1)_{t_0}) - \Delta S}{q_{yt_j}\,(W - (L_2 - L_1)_{t_j}) - \Delta S} \right] \tag{3.83}$$

where q_{yt_j} = the coastal constant which is such, that the schematized distance $(L_2 - L_1)$ between the onshore and offshore profile varies from $(L_2 - L_1)_{t_0}$ at time $t = t_0$, via $(L_2 - L_1)_{t_j}$ at time $t = t_j$ to W at time $t = \infty$, according to equation (3.39).

It is possible to determine a probability area for W with the aid of the time-variation in the measured $(L_2 - L_1)$- values (see Figure 18a). By varying W systematically within this probability area, it is possible to find the optimal value of W, for which the relative standard deviation σ_{q_y}/μ_{q_y} is a minimum,

where: $$\mu_{q_y} = \frac{1}{m} \sum_{j=1}^{m} q_{yt_j} \tag{3.84}$$

$$\sigma^2_{q_y} = \frac{1}{m - 1} \sum_{j=1}^{m} (\mu_{q_y} - q_{yt_j})^2 \tag{3.85}$$

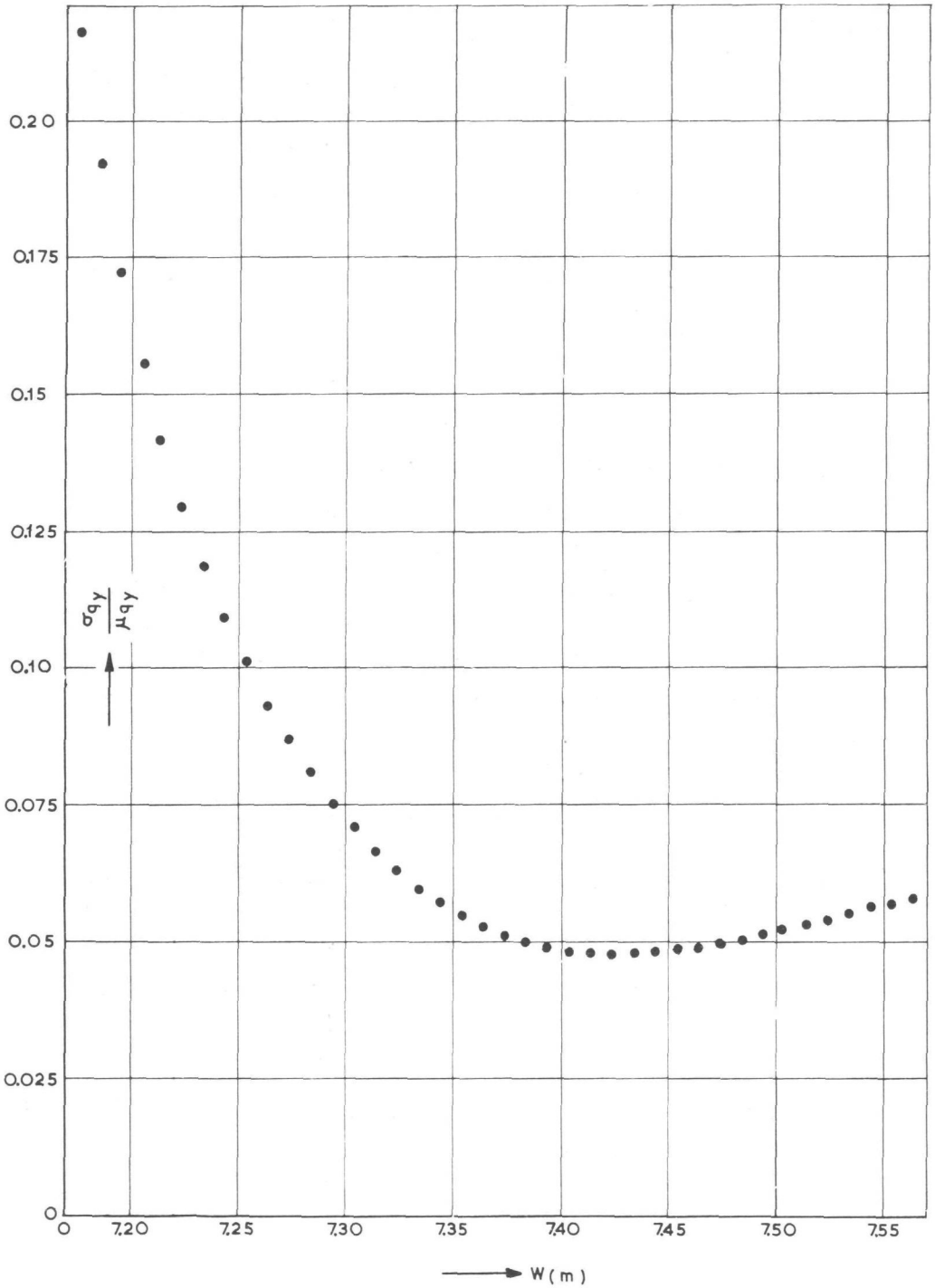

RELATION BETWEEN σ_{q_y}/μ_{q_y} AND W USED FOR THE CALCULATION OF W

FIGURE 19

$m + 1$ = number of measuring times (with the aid of only the first value of $(L_2 - L_1)$, at time $t = t_0$, it is not possible to determine a value of q_y, as up till then no transport has taken place)

μ_{q_y} = mean value of the m different values of q_{yt_j}

σ_{q_y} = standard deviation of the m different values of q_{yt_j}, relative to their mean.

For this optimal value of W the theory corresponds the best with the data, the corresponding value of μ_{q_y} gives the best average value of the coastal constant q_y. The optimal value of σ_{q_y}/μ_{q_y} gives an indication of the correlation between the theory and the data. In Figure 19 an example is given of the variation of σ_{q_y}/μ_{q_y} for varying W.

The above-mentioned method to determine q_y and W has been discussed as it represents the theoretical approach to the solution, which resembles the physical background of the original assumptions of Bakker [2] the closest. This approach cannot, however, be used to find W and q_y when there is such a scatter in the data, that any one (or more) of the values of $(L_2 - L_1)_{t_j} > W$ (see Figure 18b), as the natural logarithm on the right-hand side of equation (3.83) is then indeterminate, and the equation (3.83) cannot be solved. As experimental data always have some scatter, it will consequently be better to choose another approach to determine the values of W and q_y. In the rest of this report the method of least squares will thus be used to determine those values of W and q_y, for which the smallest deviation of the measured $(L_2 - L_1)$- values from the theoretical line will result, i.e.:

$$\sum_{j=0}^{m} \left[(L_2 - L_1)_{t_j \text{ measured}} - (L_2 - L_1)_{t_j \text{ theoretical}} \right]^2 = \text{minimum} \qquad (3.86)$$

Calculation of the equilibrium profile

When calculating the equilibrium profile with the aid of either of the two approaches described in Chapter 3.4, the choice of the elevation Z_r, which will be used to determine a reference volume for the rest of the profile, is of importance. The most logical choice seems to be to choose $Z_r = Z_0$. Equation (3.63) will then reduce to:

$$Y_k = \frac{(W_0 - \frac{Z_k - Z_m}{Z_0 - Z_m} W_k)(Z_0 - Z_k) - \sum_{i=1}^{k-1} (Z_{i-1} - Z_i) Y_i}{Z_{k-1} - Z_k} \qquad (3.87)$$

where W_0 = schematized length of the whole equilibrium profile, defined by $Z_0 \geqslant Z \geqslant Z_m$

$$= \frac{I_{t=\infty}}{(Z_0 - Z_m)B}$$

W_0 is measured relative to the landward extremity of the coastal area, because the zero line and the landward boundary of the area coincide in this case.

$I_{t=\infty}$ = total volume of sand in the equilibrium profile, in the area bordered by $Y = 0$ and $Z_0 \geqslant Z \geqslant Z_m$.

The choice of Z_r will be discussed in more detail in Chapter 6. The choice between the numerical and the analytical approach will be dealt with in the same chapter.

3.6 Summary

The procedure to be used to determine the values of q_y and W can be summarized as follows:

(1) Start a test with a profile which is not in equilibrium (profile P_j, bed material M_j).

(2) Let a wave condition (wave height H_i, wave period T_i, etc.) attack the profile during a time t (after which the profile need not be in equilibrium).

(3) Measure the profile changes frequently during this time t.
(4) If necessary, apply a correction to the bottom elevations of each sounding, to compensate for (apparent) losses (equation (3.81)).
(5) Calculate the schematized distance between the onshore and the offshore profile ($L_2 - L_1$) for a chosen division between onshore and offshore profile for every measuring time (equation (3.14)).
(6) Use the variation in time of the calculated ($L_2 - L_1$) values to predict the values of W and q_y by means of the method of least squares.
(7) Vary the division between the onshore and offshore profile systematically through the whole profile, and repeat steps (5) and (6).
(8) The variation of the equilibrium length W over the depth can be used to predict the equilibrium profile (equation (3.63) or equation (3.69) for the numerical or analytical approach respectively).
(9) For any specific depth the values of W and q_y can be used to calculate the onshore-offshore transport at any time with the aid of equation (3.1).

Some additional assumptions regarding the upper and lower extremities of the profile schematization will have to be made (see Chapter 4). It will then enable the unique determination of W and q_y in terms of the wave and bottom characteristics. Consequently, the application of the schematization in a more general sense will become possible, if the following steps are taken:
(1) Perform a large number of model tests as described in steps (1) - (3) above, and apply the processing procedure (steps (4) - (7) above) to each test, in order to gain an insight into the variation of q_y and W for different values of (P_j and M_j), (H_i and T_i), etc..
(2) Try to predict q_y and W as a function of (P_j and M_j), (H_i and T_i), etc. These functions can be determined either empirically or theoretically.
(3) Apply the method to prototype data, to check the applicability of the relationships, which were found in the model, under prototype conditions.
After making some additional assumptions regarding the profile schematization in Chapter 4, empirical relationships between q_y and W and the profile and wave characteristics will be developed in Chapter 6.

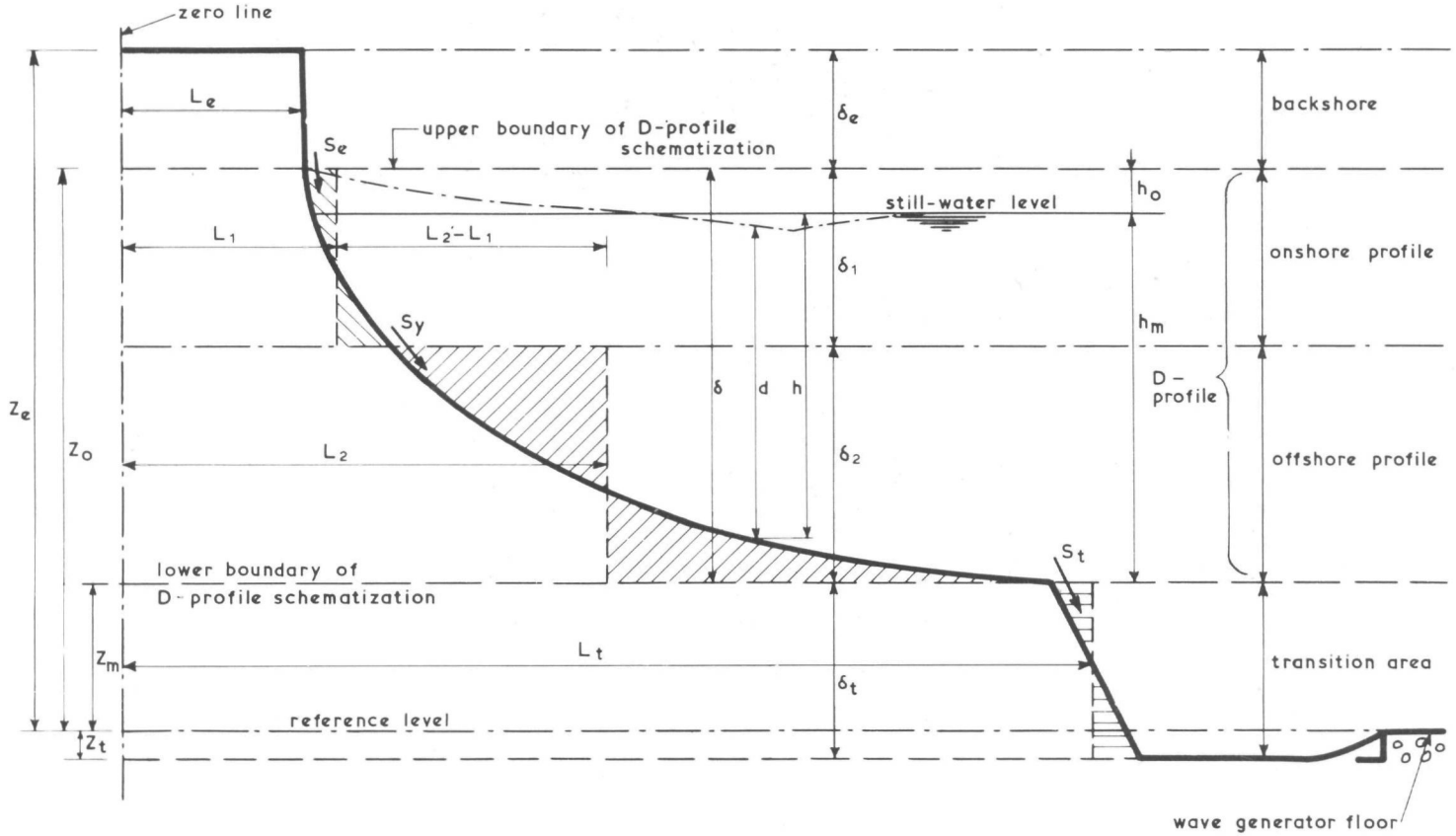

SCHEMATIZATION OF BEACH PROFILE
FIGURE 20

Chapter 4: D-profile assumptions

4.1 General

It was shown in Chapter 3 that some additional assumptions will have to be made, in order to enable a more general application of the schematization, as proposed originally by Bakker [2] . Bakker's original assumption regarding onshore-offshore transport, which led to the initiation of the present study, will in this chapter be expanded to a series of assumptions. The schematization which will then result, will be more general than that used by Bakker in his two-line theory.

The choice of the upper and lower boundaries of the two-layer schematization, as suggested by Bakker, should be done in such a way that a comparison of the results of tests in different models, as well as an eventual translation to prototype, becomes possible.

The profile development can be characterized into three definite zones, each with a different transport mechanism, viz. (1) the backshore, which is mostly eroded to above the wave run-up limit in model tests, (2) a transition area at the seaward extremity of the developing profile, which is formed due to the fact that the point of beginning of movement, landwards of which ripples and bars are formed on the model bed, normally does not coincide with the horizontal bed of the flume, and (3) the real developing (eroding) profile where transport under wave action takes place (Figure 20). In order to keep the schematization as close as possible to the physical process, but keeping the application in Bakker's theory for shoreline changes in mind, the onshore-offshore schematization was adapted as follows :

The total volume of sand in the flume is subdivided into four zones (Figure 20), viz. (1) the area above the wave run-up limit, (2) the onshore profile ("beach" in the terminology of Bakker [2]), (3) the offshore profile (Bakker's "inshore") and (4) the transition area. As has been stated in Chapter 3.1, the terms "beach" and "inshore", as used by Bakker, are not the same as the beach and inshore, defined by the C.E.R.C. [50] , which

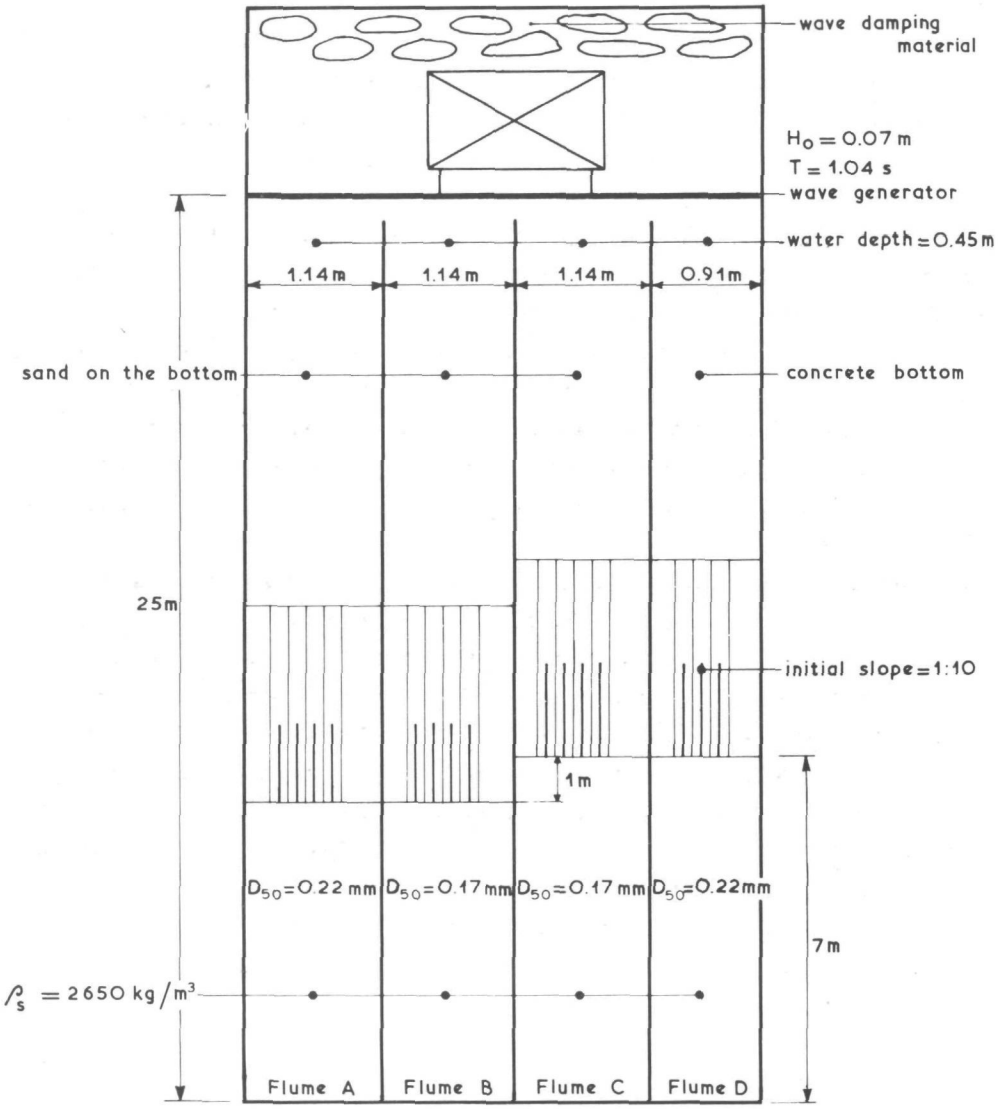

REMARK : sketch not to scale

BOUNDARY CONDITIONS FOR LONG-DURATION TEST 7301
FIGURE 21

are in general use. Consequently, Bakker's terminology will not be used in this report. The choice of the division between the onshore and offshore profile can be made arbitrarily, with the restriction that $0 \leqslant \delta_1 \leqslant \delta$ and $\delta_1 + \delta_2 = \delta$ (Figure 20). The onshore and offshore profiles together form the real developing profile (called the D-profile in the rest of this report).

Contrary to Bakker's schematization of onshore-offshore transport, the transport is now schematized separately for each of the three basic zones (backshore, D-profile, transition area).

The results of a two-dimensional test of long duration, performed in a model basin in the De Voorst Laboratory of the Delft Hydraulics Laboratory (Model II, test 7301; for an explanation of the test numbers and a description of the model, see Chapter 5) will be used to verify the assumptions regarding the transport mechanism in each different zone, as used in the theory.

The above-mentioned long-duration test was performed in a model basin, which was subdivided into four flumes (A to D), as is shown schematically in Figure 21. In flumes A and D sand with a D_{50} = .22 mm and in flumes B and C with a D_{50} = .17 mm was placed. The initial bottom slope in all four flumes was 1 : 10. The initial profiles in flumes C and D were placed 1 metre closer to the wave generator than those in flumes A and B, in order to see if the secondary waves, generated by the wave generator (Hulsbergen [21]), would have any influence on the final profile. This aspect will be discussed in Chapter 5.

The boundary conditions in test 7301, which were the same for all four flumes, are as follows:

H_0 = 0.07 m
T = 1.04 sec
h = 0.45 m (in front of the wave generator)
ρ_s = 2650 kg/m^3

The test lasted in total 3878 hours.

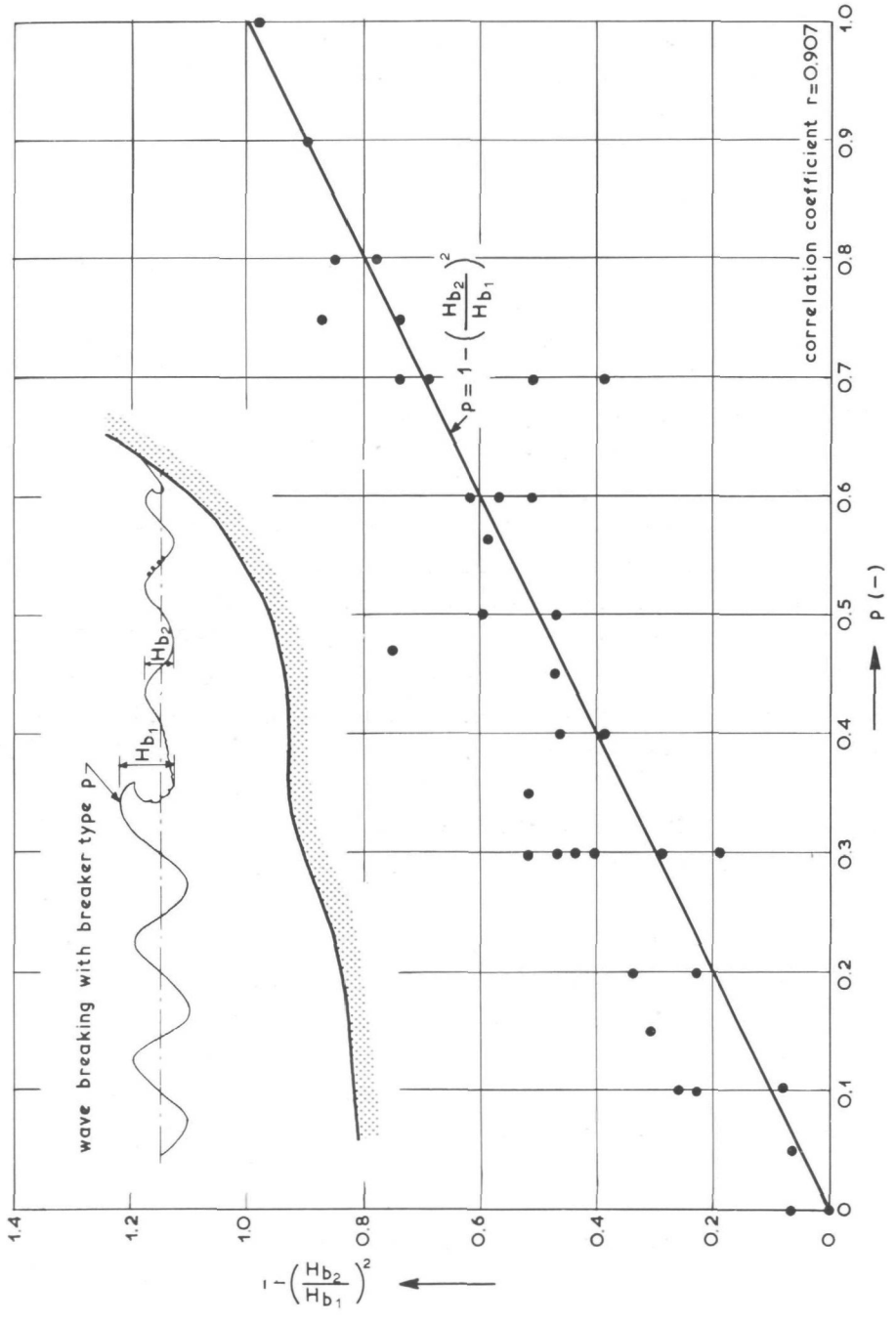

RELATION BETWEEN ESTIMATED p AND $1-(H_{b_2}/H_{b_1})^2$

FIGURE 22

A detailed description of the profile development, the water movement and the interaction between these two processes as it took place in the long-duration test 7301 will be given by the author in [49] .

4.2 The backshore

Backshore erosion is caused by the action of water against the backshore face. Thus it seems logical that the probability of erosion of the backshore is bigger with a higher than with a lower water level. In prototype variations in water level occur due to tidal action, wind effects, variation in wave breaker type (which leads to varying set-up) and changes in wave run-up due to changing wave conditions.
Under model conditions the still-water level is normally fixed, the only water level fluctuations taking place are those resulting from variations in the breaker phenomena. In the following the effect of variations in the breaker phenomena on the wave run-up and the wave set-up will be investigated, in order to be able to get an indication of the possible variations in water level that can be expected immediately in front of the backshore face. Thereafter it will be possible to make the necessary assumptions regarding the backshore erosion.

During the first 1000 hours of the long-duration test 7301 the breaker bar migration, as well as the corresponding breaker point and breaker type, was observed.
For this purpose a wave energy dissipation coefficient p was introduced. Plunging waves were classified by a value of p = 1 and completely spilling waves by a value of p = 0, while intermediate values were interpolated (see Photos 1 ... 11). The dissipation coefficient p was determined visually. Some simultaneous breaker wave height measurements and p-determinations were done, in order to gain an insight into the correlation between the coefficient p and the percentage of actually dissipated energy = $1 - (H_{b2}/H_{b1})^2$, where H_{b1} = wave height immediately before breaking, H_{b2} = the wave height immediately after the wave reformed itself landwards of the breaking point. Seeing that the determination of

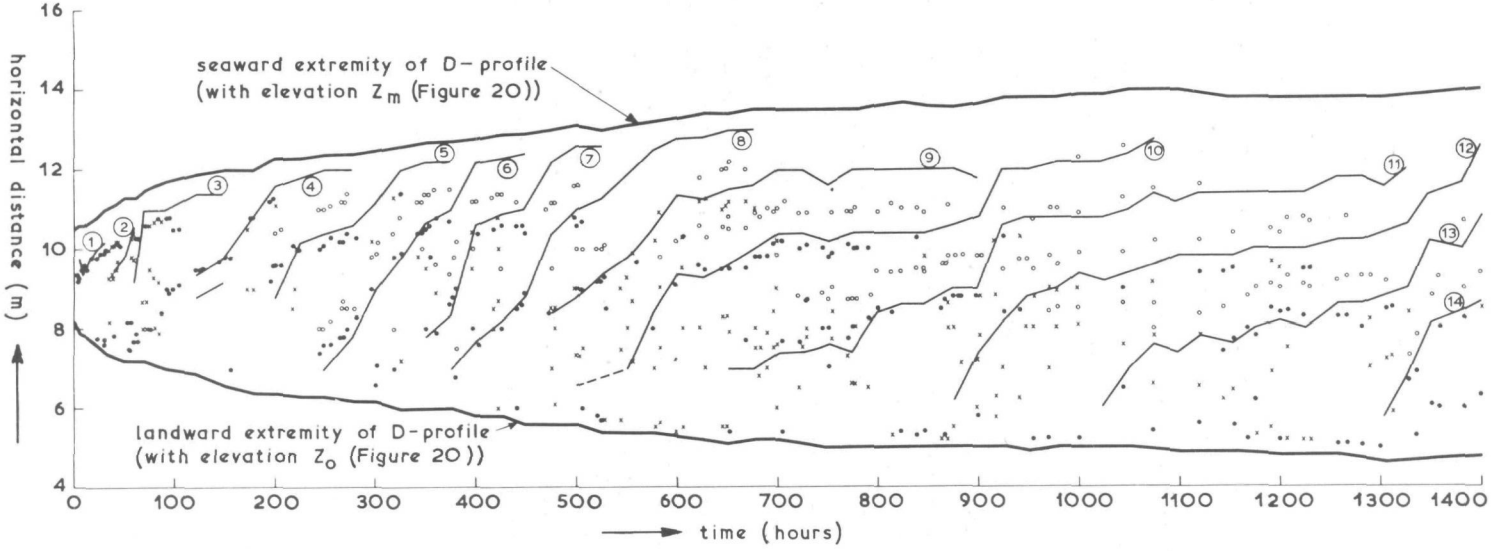

- • breaking waves
- x breaking waves over one half of the flume
- o double wave crests (secondary waves)
- ④ bar number

REMARK: shown is test 7301, flume B

MIGRATION OF BREAKER BARS

FIGURE 23

p is rather subjective, the correlation is quite good (Figure 22, correlation coefficient r = .907).
The data used for the determination of Figure 22 are given in Table I.
It has been observed in laboratory tests that waves breaking on an eroding profile form a breaker bar which moves slowly in seaward direction, due to the difference in transport capacity on the landward and seaward faces of the bar (Figure 23, 24a). Correspondingly the water depth over the bar increases (Figure 24b) and the wave energy-dissipation coefficient decreases (Figure 24c). As the bar moves seawards, the depth increases to such an extent, that a major portion of the wave energy is not dissipated at the breaker point, with the consequence that the wave, which reforms after breaking, will again break landwards of the first breaker point. Thus a new bar will be formed landwards of the first bar, and the same phenomenon will repeat itself (Figure 24).
In the following, the effect of the above-mentioned time-dependent variation in the breaking wave and breaker bar characteristics on the wave run-up and the wave set-up will be investigated.

Saville [42] did numerous experiments with regular waves on smooth impermeable slopes, in order to determine the wave run-up as a function of wave characteristics and bottom slope. His results are presented in Technical Report No. 4 of the C.E.R.C. [50] Hunt [22], restricting himself to breaking waves, used the above-mentioned data of Saville to come to a simplified relation between run-up and bottom characteristics. He found that

$$\frac{\eta}{H} = C_p \sqrt{\frac{\lambda_0}{H}} \tan\alpha \qquad (4.1)$$

where η = wave run-up relative to the still-water level
H = height of the breaking wave
C_p = porosity factor, which is approximately one for solid beaches and < 1 for permeable beach slopes
λ_0 = deepwater wave length
α = beach slope.

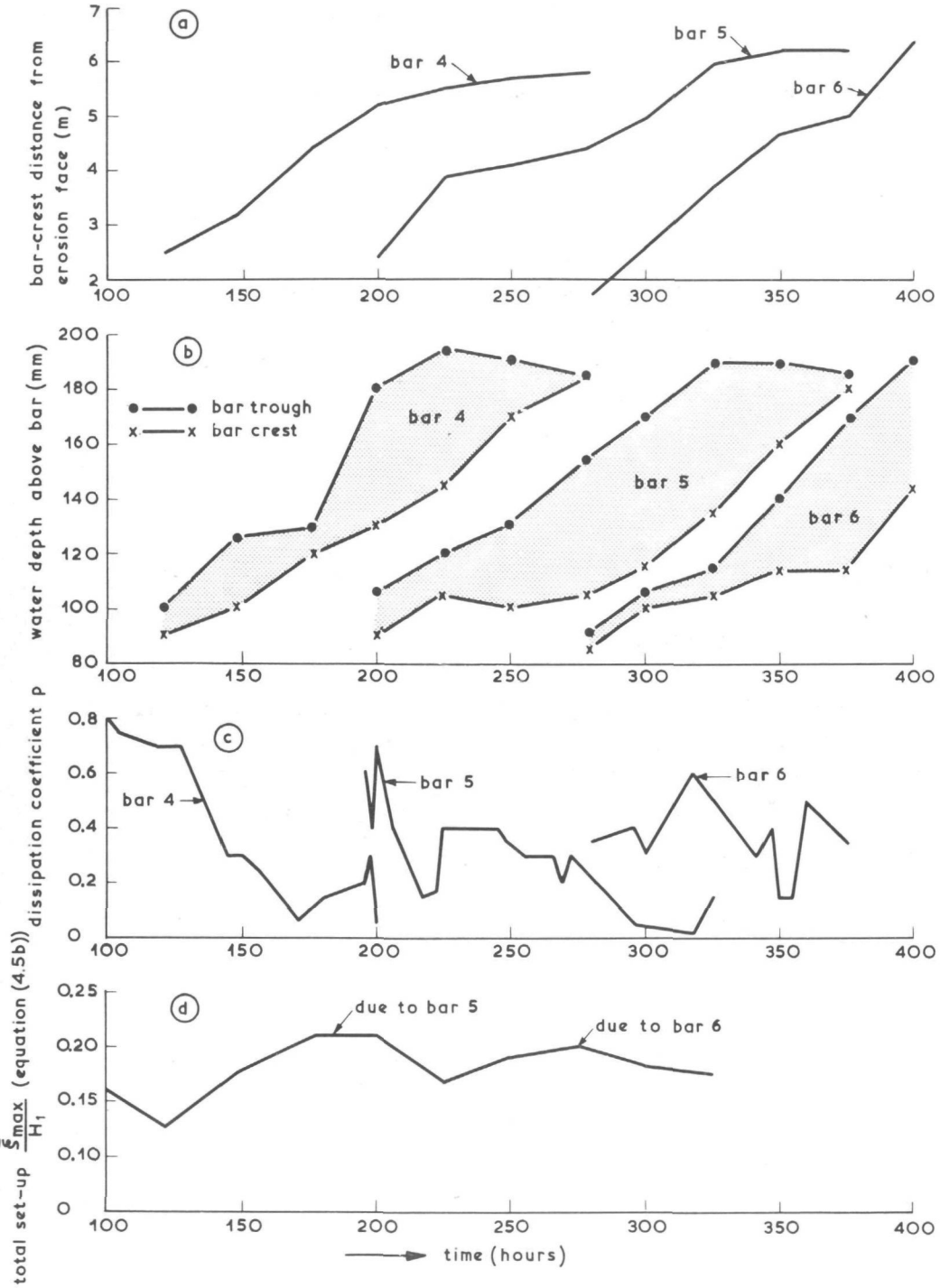

REMARK: measured in flume B, test 7301

EFFECT OF BREAKER BAR MIGRATION
FIGURE 24

As a first approximation, the wave run-up on a morphological beach slope will be written as:

$$\eta = \sqrt{H \lambda_0} \tan\alpha \tag{4.2}$$

where C_p has been put equal to unity.
For a specific bottom material tan α, i.e. the beach slope in front of the backshore face, is a constant (Wiegel [53]). That implies that the wave run-up is proportional to the square root of the height of the breaking wave, which breaks nearest to the shoreline, for any specific incident wave. The height of the wave breaking nearest to the shoreline can be written as:

$$H_3 = \gamma d_3 \tag{4.3}$$

where H_3 = wave height of the wave, breaking nearest to the shoreline
d_3 = the corresponding water depth
γ = breaker index.

In the long-duration test 7301, $\gamma = 0.79$ was found to apply rather well to the waves breaking nearest to the shoreline, while tan $\alpha = \frac{1}{6.7}$ and the deep-water wave length $\lambda_0 = 1.68$ m.
Thus, for test 7301, equation (4.2) can be rewritten to read:

$$\eta = (1.68)^{1/2} * \frac{1}{6.7} H_3^{1/2} \tag{4.4}$$

$$= 0.193 \, (0.79 \, d_3)^{1/2}$$

$$= 0.172 \, d_3^{1/2} \tag{4.5a}$$

In order to obtain a non-dimensional quantity, both sides of equation (4.5a) will be divided by H_1, the height of the most seaward breaker height, which stayed practically constant during the whole test.

$$\frac{\eta}{H_1} = 0.172 \frac{d_3^{1/2}}{H_1} \tag{4.5b}$$

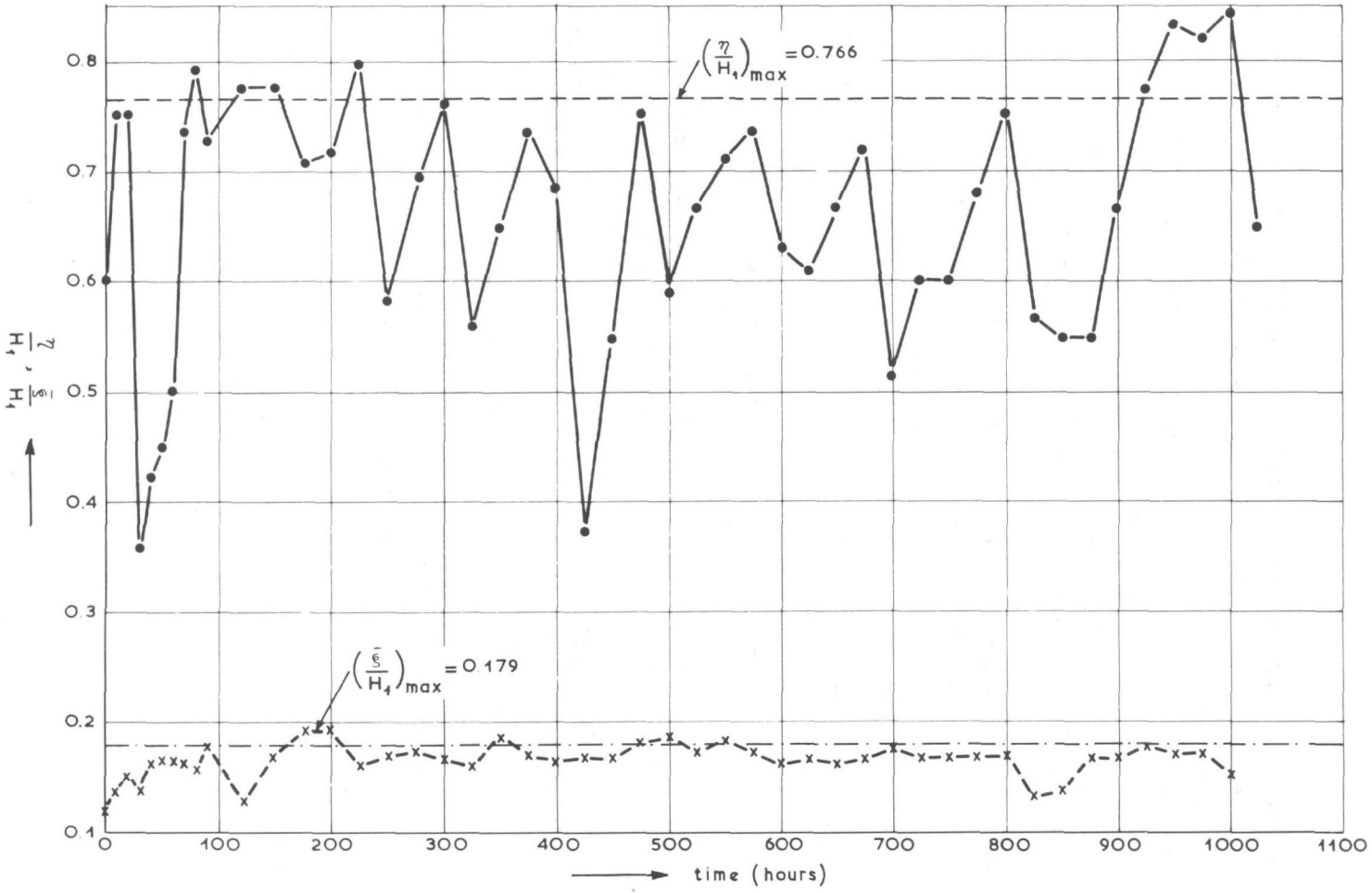

TIME-VARIATION IN η/H_1 AND $\bar{\xi}/H_1$

FIGURE 25

REMARKS: 1) $C_p=1$ in equation (4.1)
2) measured in flume B, test 7301

η/H_1 was calculated for the model data of test 7301 (flume B) for different times with the aid of equation (4.5b) and is plotted in Figure 25 as a function of time.

It should be pointed out that the wave run-up, as calculated with the aid of equation (4.5b), will most probably be higher than the actual wave run-up, due to the fact that the porosity factor C_p was taken to be equal to unity. It will be shown in Chapter 4.5 that $C_p = 0.69$.

As can be seen from Figure 25, the wave run-up varies in time, due to the migration of the breaker point. In the first 1000 hours of test 7301 (flume B), during which the breaker migration was observed, 11 peaks occurred in the wave run-up. The average height of these peaks, η_{max}, equals:

$$(\eta_{max})_{calculated} = 0.766\ H_1 \tag{4.6}$$

H_1 was chosen as reference to enable the comparison of the variations in wave run-up and wave set-up.

Using the concept of radiation stress, as introduced by Longuet-Higgins and Stewart [34], it can be shown for a smooth bottom profile that

$$\rho_w g\ (\bar{\zeta} + h)\ \frac{d\bar{\zeta}}{dy} + \frac{dR_{yy}}{dy} = 0 \tag{4.7}$$

where the y-coordinate is perpendicular to the water line

R_{yy} = radiation stress in y-direction

$\bar{\zeta}$ = set-up of the water level at location y due to wave action, measured positively upwards from the still-water line

h = still-water depth at location y

ρ_w = density of fluid.

According to Longuet-Higgins and Stewart [34]:

$$R_{yy} = E\ \left(\frac{2kh}{\sinh 2kh} + 1/2\right) \tag{4.8}$$

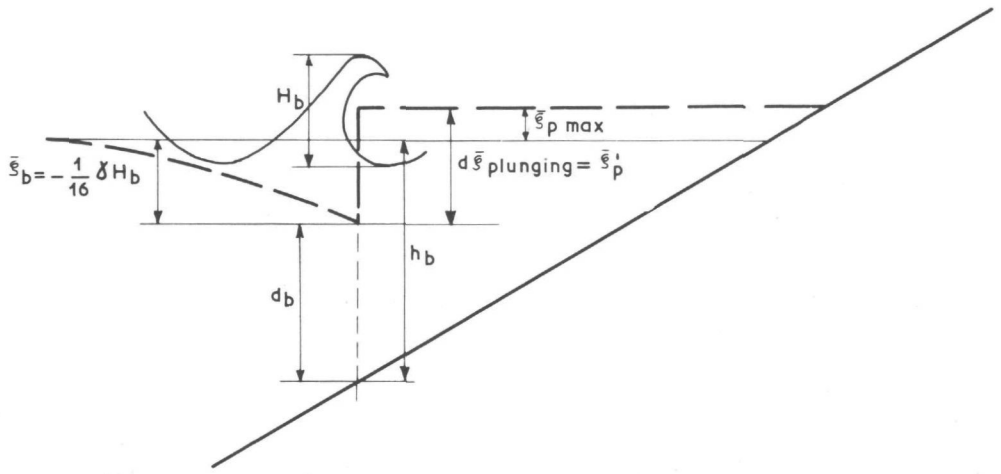

(a) Set-up due to plunging breakers

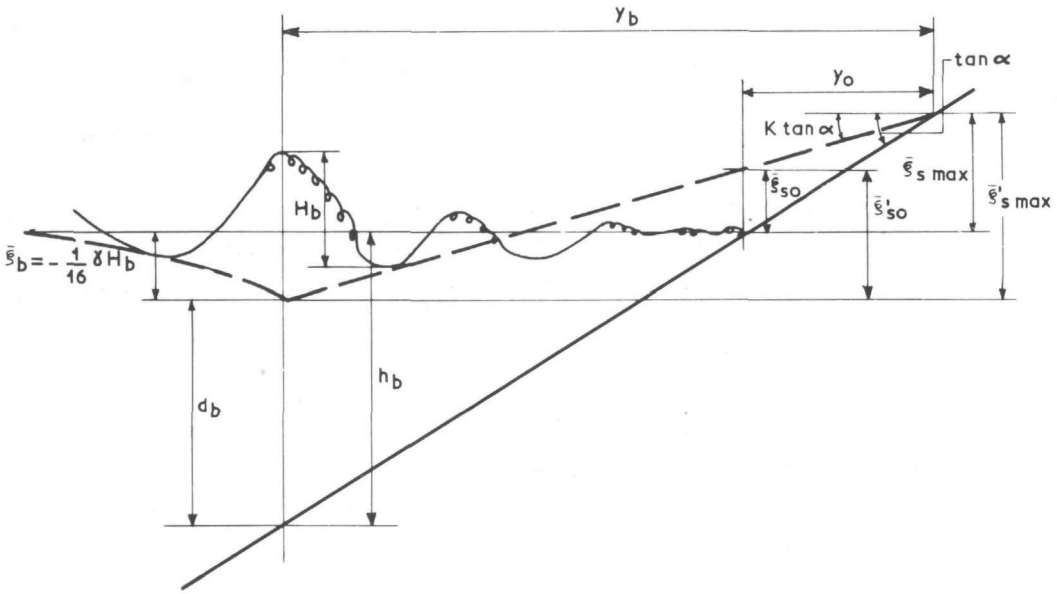

(b) Set-up due to spilling breakers

DEFINITION SKETCH OF SET-UP
FIGURE 26

where E = wave energy per unit surface area = $1/8\ \rho_w g H^2$

k = wave number = $2\pi/\lambda$

λ = wave length

H = wave height.

For shallow water $\dfrac{2kh}{\sinh 2kh} \longrightarrow 1$ and $R_{yy} \approx 3/2\ E$

and

$$R_{yy} = \frac{3}{16}\ \rho_w g H^2 \tag{4.9}$$

Consequently, if it is assumed that waves breaking as plunging breakers dissipate p of their energy instantaneously at the breaker point, equation (4.7) reduces to:

$$\begin{aligned} \rho_w g\ (\ \bar{\zeta}_b + h_b)\ d\ \bar{\zeta}_p &= -\ dR_{yy} \\ &= -\ 3/2\ dE \\ &= -\ 3/2\ \left\{\ (1 - p)\ (1/8\ \rho_w g H_b^{\,2}) - 1/8\ \rho_w g H_b^{\,2}\ \right\} \\ &= \frac{3}{16}\ p\ \rho_w g H_b^{\,2} \end{aligned} \tag{4.10}$$

where subscript b denotes breaking wave conditions

$d\ \bar{\zeta}_p$ = instantaneous variation in water depth at the breaker point, due to a wave losing a fraction p of its energy at breaking.

Furthermore $d_b = h_b + \bar{\zeta}_b$ (4.11)

where d_b = actual water depth at breaking

h_b = still-water depth at breaking

$\bar{\zeta}_b$ = set-up of the water level, relative to the still-water level, at breaking.

Consequently, when (4.11) is substituted into (4.10):

$$d\ \bar{\zeta}_p = \frac{3}{16}\ p\ \frac{H_b^{\,2}}{d_b}$$

$$= \frac{3}{16} p \gamma_p H_b = \bar{\xi}_p' \qquad (4.12)$$

(see Figure 26a)

because $H_b = \gamma_p d_b$

γ_p = breaker index for plunging breakers.

Assuming that no energy is lost due to friction and turbulence, Longuet-Higgins and Stewart [34] derived theoretically from equation (4.7) that for a shoaling wave

$$\bar{\xi} = - 1/2 \frac{a^2 k}{\sinh 2kd} \qquad (4.13)$$

where $\bar{\xi}$ = wave set-up in the area seawards of the breaking point. The minus-sign implies that $\bar{\xi}$ is actually a "set-down"

$a = H/2$.

In deep water $kd \longrightarrow \infty$ and $\bar{\xi} = 0$.

As has already been shown by Bakker [3], at the breaking point $\bar{\xi}$ equals:

$$\bar{\xi}_b = - 1/2 \left[\frac{a^2 k}{\sinh 2kd_b} \right]_{y = y_b}$$

$$= - 1/2 \frac{(1/2 \gamma d_b)^2}{2d_b} \left(\frac{2kd_b}{\sinh 2kd_b} \right)$$

$$\approx - \frac{1}{16} \gamma^2 d_b$$

$$= - \frac{1}{16} \gamma H_b \qquad (4.14)$$

Accordingly, the maximum wave set-up $\bar{\xi}_{pmax}$ relative to the still-water line, due to plunging breakers with $p = 1$, equals:

$$\bar{\zeta}_{pmax} = \frac{3}{16} \pm 1 \pm \gamma_p H_b - \frac{1}{16} \gamma_p H_b = 1/8 \gamma_p H_b \qquad (4.15)$$

(Figure 26a)

where subscript p denotes plunging breakers.

For spilling breakers a relationship can be found between the slope of the water level inside the breaker line ($\frac{d\bar{\zeta}}{dy}$) and the bottom slope $\frac{dh}{dy}$, by combining equations (4.7) and (4.9):

$$\frac{d\bar{\zeta}}{dy} = - \frac{1}{\rho_w g d} \left(\frac{dR_{yy}}{dy} \right)$$

$$= - \frac{1}{\rho_w g d} \frac{d}{dy} \left[\frac{3}{16} (\rho_w g H^2) \right]$$

$$= - \frac{1}{\rho_w g d} \frac{d}{dy} \left[\frac{3}{16} \rho_w g \gamma_s^2 d^2 \right] = - 3/8 \gamma_s^2 \frac{dd}{dy}$$

$$= - 3/8 \gamma_s^2 \left(\frac{d\bar{\zeta}}{dy} + \frac{dh}{dy} \right) \qquad (4.16)$$

because $d = h + \bar{\zeta}$.

Subscript s denotes spilling breakers.

In the above-mentioned approach it is assumed that $H = \gamma d$ for all locations inside the breaker zone. As long as the waves break as spilling breakers, i.e. as long as $p = 0$, this is a reasonable assumption.

From equation (4.16) it follows that:

$$\frac{d\bar{\zeta}}{dy} = \left[\frac{- 3/8 \gamma_s^2}{1 + 3/8 \gamma_s^2} \right] \frac{dh}{dy} \qquad (4.17)$$

$$= - K \tan \alpha \qquad (4.18)$$

(Bowen et al. [8])

where $K = \dfrac{3/8\ \gamma_s^2}{1 + 3/8\ \gamma_s^2}$ (4.19)

and $\tan\alpha = \dfrac{dh}{dy}$ = bed slope.

With the aid of Figure 26b the maximum wave set-up relative to the actual water level just after breaker ($\bar{\xi}'_{s\,max}$) can now be found with simple geometry.

$$(\bar{\xi}'_{s\,max} + d_b) = y_b \tan\alpha \tag{4.20}$$

And from equation (4.18):

$$\bar{\xi}'_{s\,max} = y_b\ K \tan\alpha \tag{4.21}$$

From (4.20) and (4.21) it follows that:

$$\bar{\xi}'_{s\,max} = \frac{K}{1 - K}\, d_b$$

$$= \left\{\frac{3/8\ \gamma_s^2}{1 + 3/8\ \gamma_s^2}\right\}\left\{\frac{1 + 3/8\ \gamma_s^2}{(1 + 3/8\ \gamma_s^2) - 3/8\ \gamma_s^2}\right\} d_b$$

$$= 3/8\ \gamma_s^2\, d_b \tag{4.22}$$

$$= 3/8\ \gamma_s\, H_b \tag{4.23}$$

where y_b = horizontal distance between the point of maximum wave set-up and the breaker point

$\bar{\xi}'_{s\,max}$ = maximum wave set-up relative to the actual water level just after breaking, for spilling breakers.

The maximum wave set-up relative to the still-water level is thus:

$$\bar{\xi}_{s\,max} = \bar{\xi}'_{s\,max} + \bar{\xi}_b$$

$$= \bar{\xi}'_{s\,max} - \frac{1}{16}\ \gamma_s^2\, d_b$$

$$= \left(\frac{3}{8} - \frac{1}{16}\right) \gamma_s^2 d_b$$

$$= \frac{5}{16} \gamma_s^2 d_b \qquad (4.24)$$

$$= \frac{5}{16} \gamma_s H_b \qquad (4.25)$$

where $\bar{\zeta}_{s\,max}$ = maximum wave set-up relative to the still-water level, for spilling breakers.

The wave set-up $\bar{\zeta}'_{s0}$ at the still-water line, relative to the actual water level at the point where spilling breakers start forming, can also be found from Figure 26b:

$$h_b = (y_b - y_0) \tan \alpha \qquad (4.26)$$

$$\bar{\zeta}'_{s0} = (y_b - y_0) K \tan \alpha \qquad (4.27)$$

From (4.26) and (4.27) it follows that:

$$\bar{\zeta}'_{s0} = K h_b$$

$$= K (d_b - \bar{\zeta}_b) \qquad \text{(from equation (4.11))}$$

$$= \left(1 + \frac{1}{16} \gamma_s^2\right) K d_b \qquad \text{(from equation (4.14))}$$

$$= \frac{3/8 \left(1 + \frac{1}{16} \gamma_s^2\right)}{1 + 3/8 \gamma_s^2} \gamma_s^2 d_b \qquad \text{(from equation (4.19))} \qquad (4.28)$$

where y_0 = horizontal distance between the point of maximum set-up and the still-water line

$\bar{\zeta}'_{s0}$ = wave set-up at the still-water line, relative to the actual water level just after breaking, for spilling breakers.

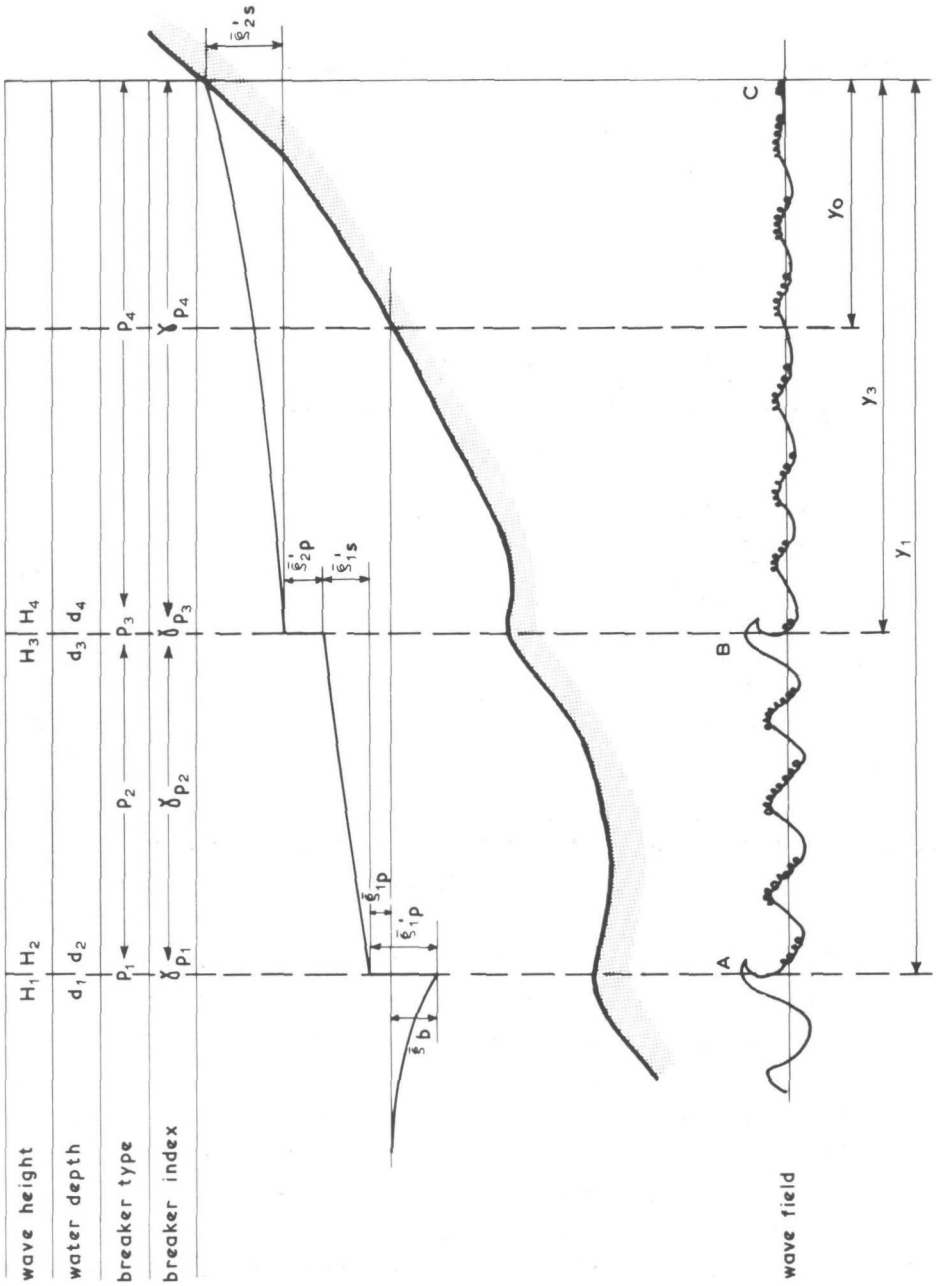

DEFINITION SKETCH OF WAVE FIELD IN MORPHOLOGICAL PROFILE

FIGURE 27

The wave set-up $\bar{\xi}_{s0}$ at the still-water line, relative to the still-water level is thus:

$$\bar{\xi}_{s0} = \bar{\xi}'_{s0} + \bar{\xi}_b$$

$$= \bar{\xi}'_{s0} - \frac{1}{16} \gamma_s^2 d_b$$

$$= \frac{3/8 \gamma_s^2 (1 + \frac{1}{16} \gamma_s^2) - \frac{1}{16} \gamma_s^2 (1 + 3/8 \gamma_s^2)}{1 + 3/8 \gamma_s^2} d_b$$

$$= \frac{\frac{5}{16} \gamma_s^2 d_b}{1 + 3/8 \gamma_s^2} \qquad (4.29)$$

$$= \frac{\frac{5}{16} \gamma_s H_b}{1 + 3/8 \gamma_s^2} \qquad (4.30)$$

where $\bar{\xi}_{s0}$ = wave set-up at the still-water line, relative to the still-water level, for spilling breakers.

In order to enable the prediction of the maximum wave set-up $\bar{\xi}_{max}$, relative to the still-water level, for the time-dependent situation described earlier in the paragraph, the following assumptions are made regarding the wave field inside the most seaward breaker point (see Figure 27):

(1) The incident wave always breaks twice in the profile; initially on a breaker bar (location A), for the second time either on a more landward breaker bar (location B) or near the still-water line (location C).

(2) At location A the wave breaks with loss p_1 of energy.

(3) q_1 of the remaining wave energy is dissipated between A and B (or C), while the wave is breaking with a breaker type p_2.

(4) At location B the wave loses a fraction p_3 of its remaining energy ($=(1 - p_1)(1 - q_1)$) while breaking. If location B is situated near the still-water line ($\longrightarrow$ location C), $p_3 \longrightarrow 1$.
(5) The rest of the wave energy is dissipated while the wave breaks with a breaker type p_4.
(6) The bottom slope is assumed to be mild and without a too large curvature or discontinuity, in order to allow the application of equations (4.17), (4.23), (4.25) and (4.28).

The maximum wave set-up $\bar{\zeta}_{max}$, relative to the still-water level, can accordingly be written as:

$$\bar{\zeta}_{max} = \bar{\zeta}'_{1p} + \bar{\zeta}'_{1s} + \bar{\zeta}'_{2p} + \bar{\zeta}'_{2s} + \bar{\zeta}_b$$

$$= \bar{\zeta}_{1p} + \bar{\zeta}'_{1s} + \bar{\zeta}'_{2p} + \bar{\zeta}'_{2s} \qquad (4.31)$$

(see Figure 27)

where $\bar{\zeta}'_{1p}$ = instantaneous set-up due to instantaneous dissipation p_1 of energy at location A, relative to the water level immediately before breaking of the wave at location A

$\bar{\zeta}_{1p}$ = set-up due to instantaneous dissipation p_1 of energy at location A, relative to the still-water level

$\bar{\zeta}'_{1s}$ = set-up at location B relative to that at location A, due to waves breaking with breaker type p_2

$\bar{\zeta}'_{2p}$ = instantaneous increase in set-up at location B, due to an instantaneous dissipation p_3 of energy

$\bar{\zeta}'_{2s}$ = set-up due to waves breaking with breaker type p_4, measured relative to the set-up at location B.

$\bar{\zeta}_{1p}$ can be found from equations (4.12) and (4.14), viz.:

$$\bar{\zeta}_{1p} = \bar{\zeta}'_{1p} + \bar{\zeta}_b$$

$$= \frac{3}{16} p_1 \gamma_{p1} H_1 - \frac{1}{16} \gamma_{p1} H_1$$

$$= \frac{1}{16} (3p_1 - 1) \gamma_{p1} H_1 \qquad (4.32)$$

where γ_{p1} = breaker index corresponding to a wave breaking with breaker type p_1

H_1 = breaking wave height at location A.

If the wave would have kept breaking with a breaker type p_2 in the area landwards of location A, until it reached the water line, the wave set-up at the still-water line, relative to the actual water level at location A, just after breaking, would have been:

$$\bar{\zeta}'_{1s0} = \frac{3/8 \, (1 + \frac{1}{16} \gamma^2_{p2}) \gamma^2_{p2} \, d_2}{1 + 3/8 \, \gamma^2_{p2}} \qquad \text{(from equation (4.28))}$$

$$\approx \frac{3/8 \, \gamma^2_{p2} \, d_2}{1 + 3/8 \, \gamma^2_{p2}} \qquad \because 1 + \frac{1}{16} \gamma^2_{p2} \longrightarrow 1$$

$$= \frac{3/8 \, \gamma_{p2} \, H_2}{1 + 3/8 \, \gamma^2_{p2}} \qquad (4.33)$$

where $\bar{\zeta}'_{1s0}$ = wave set-up at the still-water line relative to the actual water level just after breaking at location A, for a wave breaking with breaker type p_2 in the whole area landwards of A

d_2 = H_2 / γ_{p2}, water depth corresponding with a wave height of H_2, immediately landwards of point A (see Figure 27)

γ_{p_2} = breaker index corresponding to a wave breaking with breaker type p_2.

Assumption (2) implies that

$$E_2 = (1 - p_1) E_1 \qquad (4.34)$$

$$H_2 = (1 - p_1)^{1/2} H_1 \qquad (4.35)$$

where E_1 = wave energy at location A = $1/8\ \rho_w\ gH_1^2$

E_2 = wave energy which remains just landwards of location A
= $1/8\ \rho_w\ gH_2^2$.

It can be stated that the water depth does not change over the small distance, between the positions where the wave height changes from H_1 to H_2 (assumption (6)).

$$d_2 = \frac{H_2}{\gamma_{p_2}} = d_1 = \frac{H_1}{\gamma_{p_1}} \tag{4.36}$$

As long as the wave breaks as a completely spilling wave ($p = 0$), equation (4.36) is a reasonably good approximation. If, however, the wave loses an amount p of its energy instantaneously at the breaker point, the water level undergoes an instantaneous increase $\bar{\zeta}'_p$, which can be found from equation (4.12). Consequently, as assumption (6) implies that $h_1 = h_2$, it means at $d_1 \neq d_2$, due to the instantaneous increase in water level:

$$d_2 = d_1 + \bar{\zeta}'_p$$

$$= d_1 + \frac{3}{16}\ p_1\ \gamma_{p1}\ H_1 \qquad \text{(from equation (4.12))}$$

$$= d_1\ (1 + \frac{3}{16}\ p_1 \gamma^2_{p1}) \tag{4.36a}$$

For instance, for a breaking wave losing 50% ($p_1 = 0.5$) of its energy instantaneously at the breaker point, $\gamma_{p1} = 0.625$ (see Figure 28, which is based on model data, as will be shown later in this chapter).
Thus $d_2 = d_1\ (1 + \frac{3}{16} * 0.5 * (0.625)^2) = 1.037\ d_1$.
Consequently, it can be stated that equation (4.36) is a good approximation under normal model conditions.

Consequently, from (4.36) and (4.35):

$$\gamma_{p2} = \frac{H_2}{H_1} \gamma_{p1} = (1 - p_1)^{1/2} \gamma_{p1} \tag{4.37}$$

Substitution of (4.35) and (4.37) into equation (4.33) yields:

$$\bar{\xi}'_{1s0} = \frac{3/8 \gamma_{p1} (1 - p_1) H_1}{1 + 3/8 \gamma^2_{p1} (1 - p_1)} \tag{4.38}$$

Keeping in mind that $\bar{\xi}'_{1s0}$ is the total set-up at the still-water line due to waves breaking with breaker type p_2, and $\bar{\xi}'_{1s}$ the set-up at location B, when both set-ups are measured relative to the set-up at location A, just after breaking, it follows from assumption (3) and equation (4.38) that:

$$\bar{\xi}'_{1s} = q_1 \bar{\xi}'_{1s0}$$

$$= \frac{3/8 \gamma_{p1} q_1 (1 - p_1) H_1}{1 + 3/8 \gamma^2_{p1} (1 - p_1)} \tag{4.39}$$

q_1 can be approximated to be equal to the ratio between the distances $(y_1 - y_3)$ and $(y_1 - y_0)$ of B and C respectively from the initial breaker point A.

$$q_1 = \left(\frac{y_1 - y_3}{y_1 - y_0}\right) \tag{4.40}$$

From equation (4.12) it follows that the instantaneous wave set-up due to a wave losing p_3 of its energy instantaneously at location B, will be:

$$\bar{\xi}'_{2p} = \frac{3}{16} p_3 \gamma_{p3} H_3 \tag{4.41}$$

where H_3 = wave height just before breaking with breaker type p_3 occurs at location B

γ_{p3} = breaker index corresponding to a wave breaking with breaker type p_3.

As the wave loses q_1 of its remaining energy while breaking with breaker type p_2 in the area between locations A and B:

$$E_3 = (1 - q_1)\, E_2 \tag{4.42}$$

where E_3 = wave energy at location B, prior to the wave breaking with breaker type p_3; $E_3 = 1/8\ \rho_w g H_3^2$

Consequently

$$H_3 = (1 - q_1)^{1/2}\, H_2 \tag{4.43}$$

Thus it follows from equation (4.35) that

$$H_3 = (1 - q_1)^{1/2}\, (1 - p_1)^{1/2}\, H_1 \tag{4.44}$$

Substitution of (4.44) in (4.41) yields:

$$\bar{\zeta}'_{2p} = 3/16\ p_3\, \gamma_{p3}\, (1 - p_1)^{1/2}\, (1 - q_1)^{1/2}\, H_1 \tag{4.45}$$

It follows from equation (4.23) that the maximum wave set-up, relative to the water level immediately landwards of location B ($= h_4 + \bar{\zeta}_{1p} + \bar{\zeta}'_{1s} + \bar{\zeta}'_{2p}$, see Figure 27), for waves breaking with breaker type p_4, will be:

$$\bar{\zeta}'_{2s} = 3/8\ \gamma_{p4}\, H_4 \tag{4.46}$$

where H_4 = wave height just after breaking with breaker type p_3 occurred at location B

γ_{p4} = breaker index corresponding to a wave breaking with breaker type p_4.

As the wave lost p_3 of its remaining energy instantaneously at location B (assumption (4)):

$$E_4 = (1 - p_3)\, E_3 \tag{4.47}$$

where E_4 = wave energy which remains after breaking with breaker type p_3 occurred at location B = $1/8\ \rho_w g H_4^2$.

Consequently

$$H_4 = (1 - p_3)^{1/2}\, H_3 \tag{4.48}$$

$$= (1 - p_1)^{1/2}\, (1 - q_1)^{1/2}\, (1 - p_3)^{1/2}\, H_1 \tag{4.49}$$

(from equation (4.44))

As before it can be stated with the aid of assumption (6) that:

$$d_3 = \frac{H_3}{\gamma_{p_3}} = d_4 = \frac{H_4}{\gamma_{p_4}}$$

Thus $$\gamma_{p_4} = \frac{H_4}{H_3}\, \gamma_{p_3} \tag{4.50}$$

where d_3 and d_4 = actual water depths immediately before and after breaking with breaker type p_3 occurred at location B.

Substitution of equation (4.48) in (4.50) yields:

$$\gamma_{p_4} = (1 - p_3)^{1/2}\, \gamma_{p_3} \tag{4.51}$$

Substitute equations (4.49) and (4.51) in equation (4.46):

$$\bar{\xi}'_{2s} = 3/8\ \gamma_{p_3}\, (1 - p_1)^{1/2}\, (1 - q_1)^{1/2}\, (1 - p_3)\, H_1 \tag{4.52}$$

The maximum wave set-up, $\bar{\xi}_{max}$, relative to the still-water level, can now be found by addition of equations (4.32), (4.39), (4.45) and (4.52).

As the breaker index γ is closely related to the type of breaking p of the waves, it is to be expected that a relationship will exist between

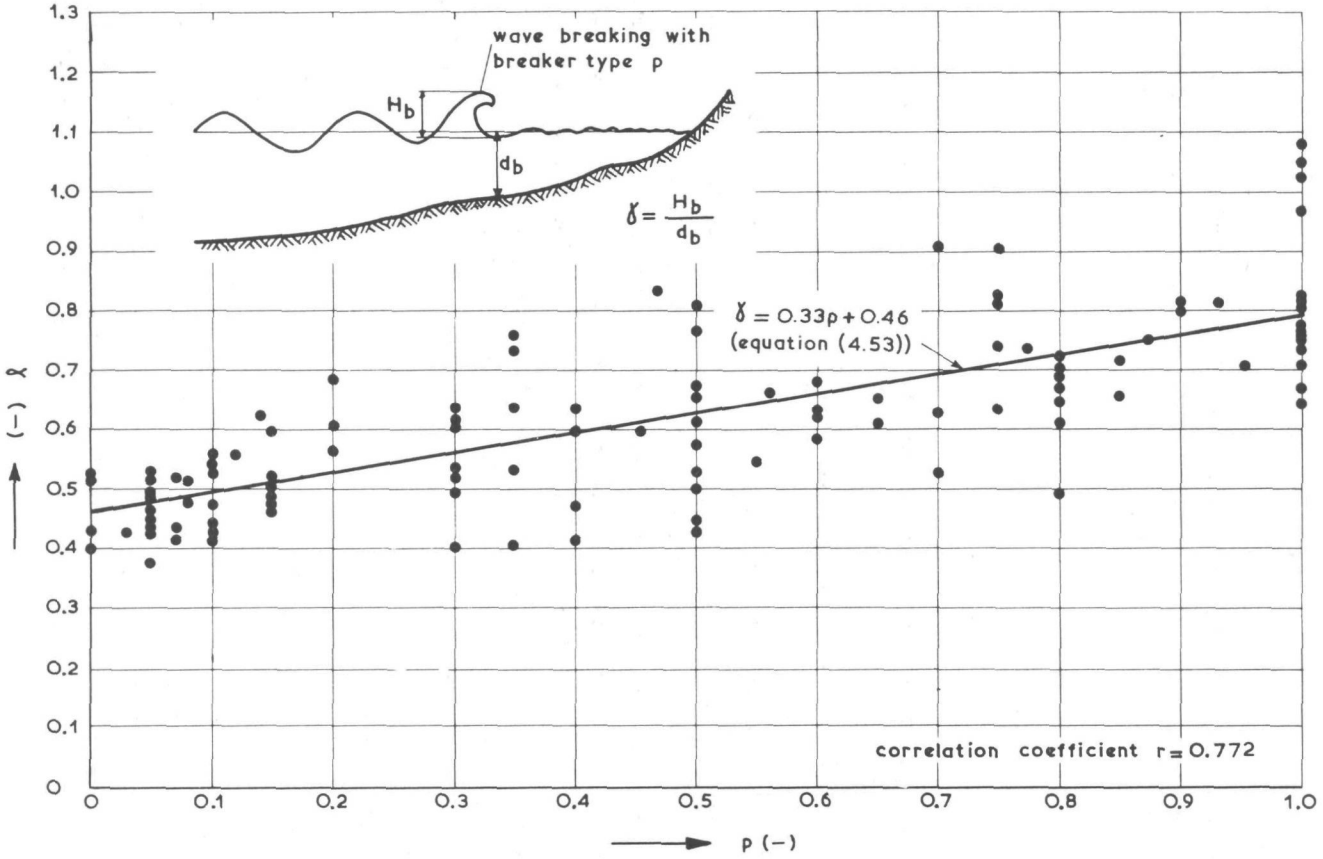

RELATION BETWEEN γ AND p

FIGURE 28

these two quantities. To test this hypothesis the breaker index was calculated for all data for which the breaker height and the dissipation coefficient p were determined simultaneously. The result, which can be seen in Figure 28, indicates that a linear relationship can be assumed to exist between p and γ, viz.:

$$\gamma = ap + b \tag{4.53}$$

$$\left.\begin{aligned} \text{where } a &= \gamma_p - \gamma_s = 0.33 \\ \text{and } \quad b &= \gamma_s \quad\quad = 0.46 \end{aligned}\right\} \tag{4.54}$$

The subscripts p and s denote plunging and spilling respectively.

The correlation coefficient r = 0.772; the data are listed in Table II.

Care must be exercised when interpreting Figure 28. As $0 \leqslant p \leqslant 1$, it would seem as if $0.46 \leqslant \gamma \leqslant 0.79$. This is, however, in contradiction with some available observations of wave heights which are of the same order of magnitude as the breaker depth, or even bigger (see Figure 28 at p = 1 and for instance Iversen [24]). These high breaker indices normally occur when the waves are breaking as plunging breakers on a breaker bar with a steep seaward slope. From Figure 28 it also becomes clear that values of $\gamma < 0.46$ can also occur. These low values of γ normally occur when the waves are breaking as spilling breakers on mild slopes.

However, it should be kept in mind that in order to arrive at a relationship of the form of equation (4.53), it was assumed that the breaker index is purely a function of the breaker type p. This is clearly not the case. This fact explains the scatter in the data, as well as the fact that $0.46 \leqslant \gamma \leqslant 0.79$, according to equations (4.53) and (4.54).

Although equations (4.53) and (4.54) will be sufficiently accurate to allow the elimination of γ_{p1} and γ_{p3} from equations (4.32), (4.39), (4.45) and (4.52), it does not conform to the physical boundary conditions. In the following the possibility will be investigated to find a relationship

that will allow a better prediction of γ than that given by equations (4.53) and (4.54).

Iversen [24] measured the transformation of wave height inside the breaker zone for a wide range of initial wave steepnesses on slopes varying between 1 : 10 and 1 : 50. From his results he deduced empirical relations for d_b/H_b in terms of H_0/λ_0 and tan α.

Experiments by Nakamura et al. [37] confirm the results of Iversen. They conclude that the effect of bottom slope can be used to estimate the wave characteristics at the breaker point.

In a study regarding wave transformation inside the surf zone, Horikawa and Kuo [20] made the following assumptions as basis for their analytical treatment of the problem:

(1) The second-order approximation of the solitary wave theory, introduced by Laitone [31], is used to express the features of the breaking wave progressing in the surf zone, i.e. the wave profile η_L, wave celerity C_L and the horizontal component U_L of the water particle velocity are given by the following equations respectively:

$$\eta_L = H_L \operatorname{sech}^2 \left[\left(\frac{3H_L}{4d^2 (H_L + d)} \right)^{1/2} (y - C_L t) \right] \tag{4.55}$$

$$C_L = \left[gd \left(1 + \frac{H_L}{d} \right) \right]^{1/2} \tag{4.56}$$

$$U_L = \sqrt{gd} \left[\frac{\eta_L}{d} \left\{ 1 - \frac{5H_L}{4d} - \frac{3H_L}{2d} \left(\frac{2z}{d} + \frac{z^2}{d^2} \right) \right\} + \left(\frac{\eta_L}{d} \right)^2 \left\{ \frac{5}{4} + \frac{9}{4} \left(\frac{2z}{d} + \frac{z^2}{d^2} \right) \right\} \right] \tag{4.57}$$

where η_L = surface elevation, measured vertically upwards from the still-water level

H_L = wave height, according to their theory

d = actual water depth

C_L = wave celerity
z = vertical axis measuring upwards from the still-water level
y = horizontal axis, taken along the still-water level, being positive in the direction of wave propagation
U_L = horizontal component of the water particle velocity at an elevation z above the bed.

Laitone's nomenclature has been used for the above-mentioned equations, after adding a subscript L to the wave properties.

(2) Wave energy is dissipated due to the effect of turbulence and bottom friction. The effect of percolation is negligible.

(3) The turbulence is isotropic and decreases exponentially with the distance from the breaker point, as long as $p \neq 0$.
Using the above-mentioned assumptions, they find a differential equation relating $\partial d/d$ in terms of H_L/d and tan α. Finally they represent their results in the form:

$$\frac{H_L}{d} = \psi \left(\frac{H_0}{\lambda_0}, \frac{d}{d_b}, \tan \alpha\right) \qquad (4.58)$$

Their results indicate that:

(1) The breaker index $\gamma_L = H_{Lb}/d_b$ increases with increasing bed slope α.

(2) The effect of the deepwater wave steepness H_0/λ_0 on the breaker index is small relative to the effect of the bed slope.

(3) The relative wave height H_L/H_{Lb} for any specific location (d/d_b = constant) in the breaker zone decreases with decreasing bed slope α, where:

H_{Lb} = breaking wave height in their theory
d_b = actual water depth at the breaker point.

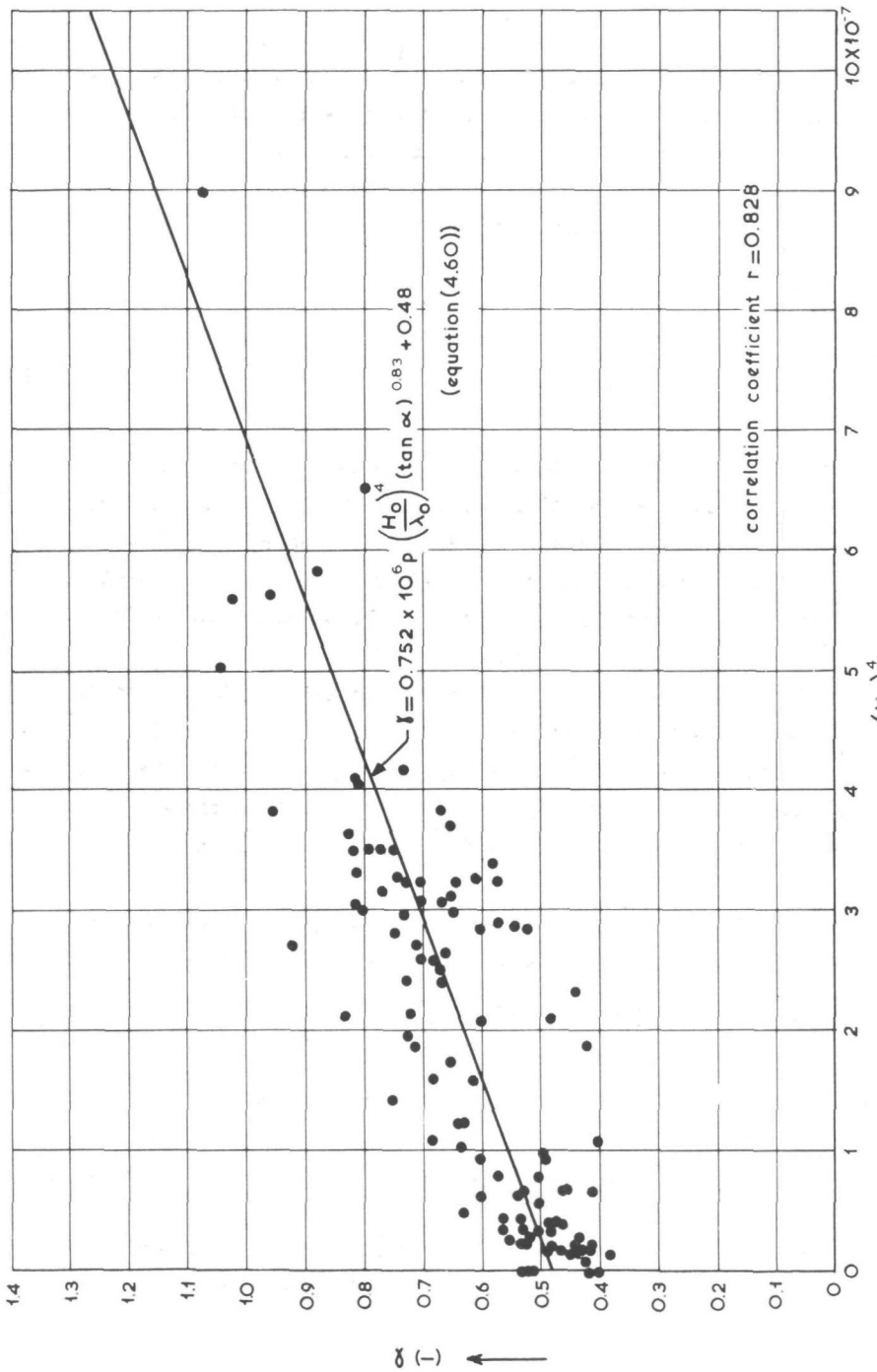

DETERMINATION OF BREAKER INDEX
FIGURE 29

Result (3) of Horikawa and Kuo is attributed to the fact that the decay distance from the breaker point is larger on a gentle slope than on a steep slope. The decay distance is in fact a function of the breaker type; a plunging breaker, for instance, loses its energy over a shorter horizontal distance than a spilling breaker.

Accordingly, equation (4.58) can be rewritten to read:

$$\frac{H_L}{d} = \gamma_L = \varphi \left(\frac{H_0}{\lambda_0}, \tan\alpha, p\right) \tag{4.59}$$

The quantities H_0/λ_0 and p can be determined with reasonable accuracy. In a morphological profile the determination of tanα is, however, more difficult. It is evident that some bottom slope seawards of the breaker point has to be used, as the history of the wave over the sloping bottom is of importance when determining its breaker characteristics. Which slope has to be used is, however, not clear.

For about 90% of the data used to determine the relationship in equation (4.53), measurements of the corresponding bottom profiles were also available. In order to test equation (4.59), the values of tanα were determined from these bottom profiles, by using the bed slope in the area immediately seawards of the breaker point, i.e. the seaward slope of the breaker bar itself.

A correlation of γ to all the available values of p, H_0/λ_0 and tanα by means of a least-squares fit then showed equation (4.59) to be:

$$\gamma = 0.752 \pm 10^6\, p \left(\frac{H_0}{\lambda_0}\right)^4 (\tan\alpha)^{0.83} + 0.48 \tag{4.60}$$

The correlation coefficient r = 0.828 (Figure 29). The data are listed in Table II. The correlation is only slightly better than that of equation (4.53), as is to be expected, due to the uncertainty in the determination of tanα.

However, when problems regarding wave deformation are studied, equation (4.60) must be preferred, due to its better physical background. On the

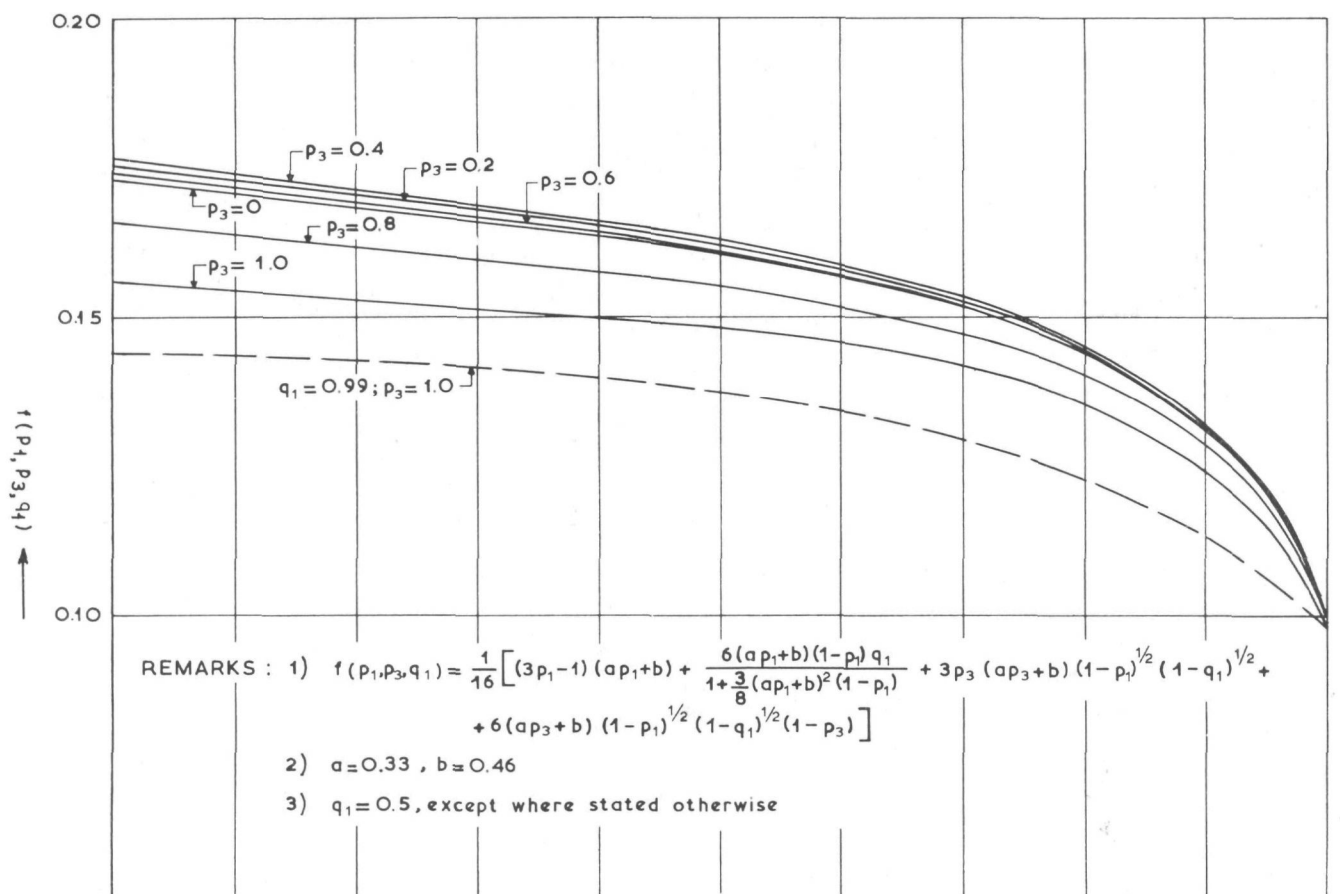

SET-UP FUNCTION $f(p_1, p_3, q_1)$ FOR $q_1 = 0.5$

FIGURE 30

other hand, when the values of γ_{p1} and γ_{p3} are to be eliminated from equations (4.32), (4.39), (4.45) and (4.52), to allow an easier application of these formulae, it will be sufficiently accurate to replace γ by a linear function of p, according to equations (4.53) and (4.54). This implies that the total maximum set-up $\bar{\zeta}_{max}$ (equation (4.31)) is purely a function of the breaker types p_1 and p_3, the dissipation coefficient q_1 and the initial breaker height H_1, viz.:

$$\bar{\zeta}_{max} = H_1 \, f\,(p_1, p_3, q_1) \tag{4.61}$$

where $f\,(p_1, p_3, q_1)$ can be found from equations (4.32), (4.39), (4.45) and (4.52) by the substitution $\gamma = a\,p + b$.

$$\text{Thus } f\,(p_1, p_3, q_1) = \frac{1}{16}\Big[(3p_1 - 1)(ap_1 + b) + \frac{6\,(ap_1 + b)\,(1 - p_1)q_1}{1 + 3/8\,(ap_1 + b)^2(1 - p_1)} +$$

$$+ 3p_3\,(ap_3 + b)\,(1 - p_1)^{1/2}\,(1 - q_1)^{1/2} +$$

$$+ 6\,(ap_3 + b)\,(1 - p_1)^{1/2}\,(1 - q_1)^{1/2}\,(1 - p_3)\Big] \tag{4.62}$$

where $a = 0.33$

$b = 0.46$

While the most landward breaker bar is migrating in seaward direction the value of q_1 changes from 0.9 (bar formed at the shoreline) to approximately 0.3 when the wave ceases breaking on the bar. For any fixed combination of p_1 and p_3, the value of the total relative set-up $\bar{\zeta}_{max}/H_1$ varies by only $\pm$ 3% relative to its mean value, when q_1 varies between 0.9 and 0.3. In Figure 30 equation (4.62) has been plotted for $q_1 = 0.5$. With the aid of Figure 30 it is possible to determine the variation in time of the relative set-up $\bar{\zeta}_{max}/H_1$ for the first thousand hours of the long-duration test 7301 (flume B). In Figure 25 the variation in re-

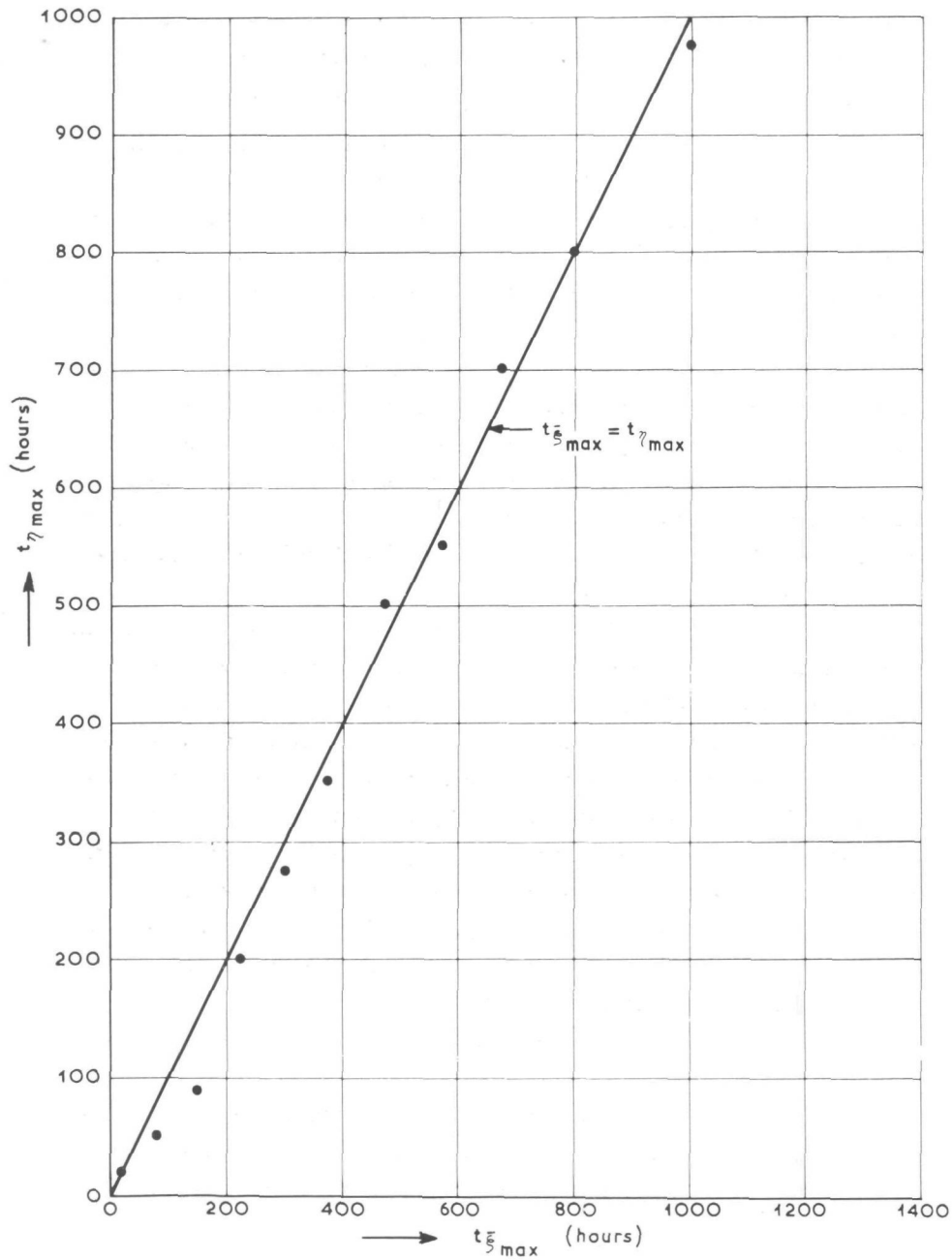

RELATION BETWEEN $t_{\bar{\xi}\,max}$ AND $t_{\eta\,max}$

FIGURE 31

lative set-up has been plotted together with the variation in relative wave run-up. In Figure 31 the times of occurrence of a peak in the curves of the relative run-up and set-up ($t_{\eta_{max}}$ and $t_{\bar{\zeta}_{max}}$ respectively) have been set out against each other. As can be seen from Figure 31, the times of occurrence of a peak in the curves of relative run-up and set-up (as plotted in Figure 25) show a reasonable resemblance to each other. The periodic increase in $\bar{\zeta}/H_1$ corresponds with the formation of a new breaker bar, landwards of the initial breaker, as can be seen in Figure 24.

Summarizing, it can be stated that the wave run-up and set-up both show the same time-dependent variation, due to the breaker bar migration. It is to be expected that the periodic increases in the water level in front of the backshore face will lead to periodic increases in the probability of backshore erosion. Accordingly, the recurrence interval of the highest water levels in front of the backshore face is of importance when determining the time-dependent variation in the backshore erosion.

In Figure 32 the number of periods with increased water level n (i.e. the number of formations of a new breaker bar) that had occurred up to any time t in the long-duration test 7301, has been plotted against time. From Figure 32 it becomes apparent that as the test duration increases the number of periods of increased water level n tends to become a constant n_∞, which represents the number of periods of increased water level when $t = \infty$. In Figure 33 the number of increased water levels that are still to occur at time t ($=n_\infty - n$) have been plotted against time. From Figure 33 it becomes apparent that the period of time that elapses between each two successive increases in the water level, i.e. the recurrence interval, increases with increasing test duration. In terms of the number of periods of increased water level the above-mentioned result can be reformulated as follows: the number of periodic increases in water level decreases exponentially in time. Thus, the average probability of backshore erosion per unit of time will also decrease exponentially in time. This result leads to the following assumptions regarding the erosion of the backshore:

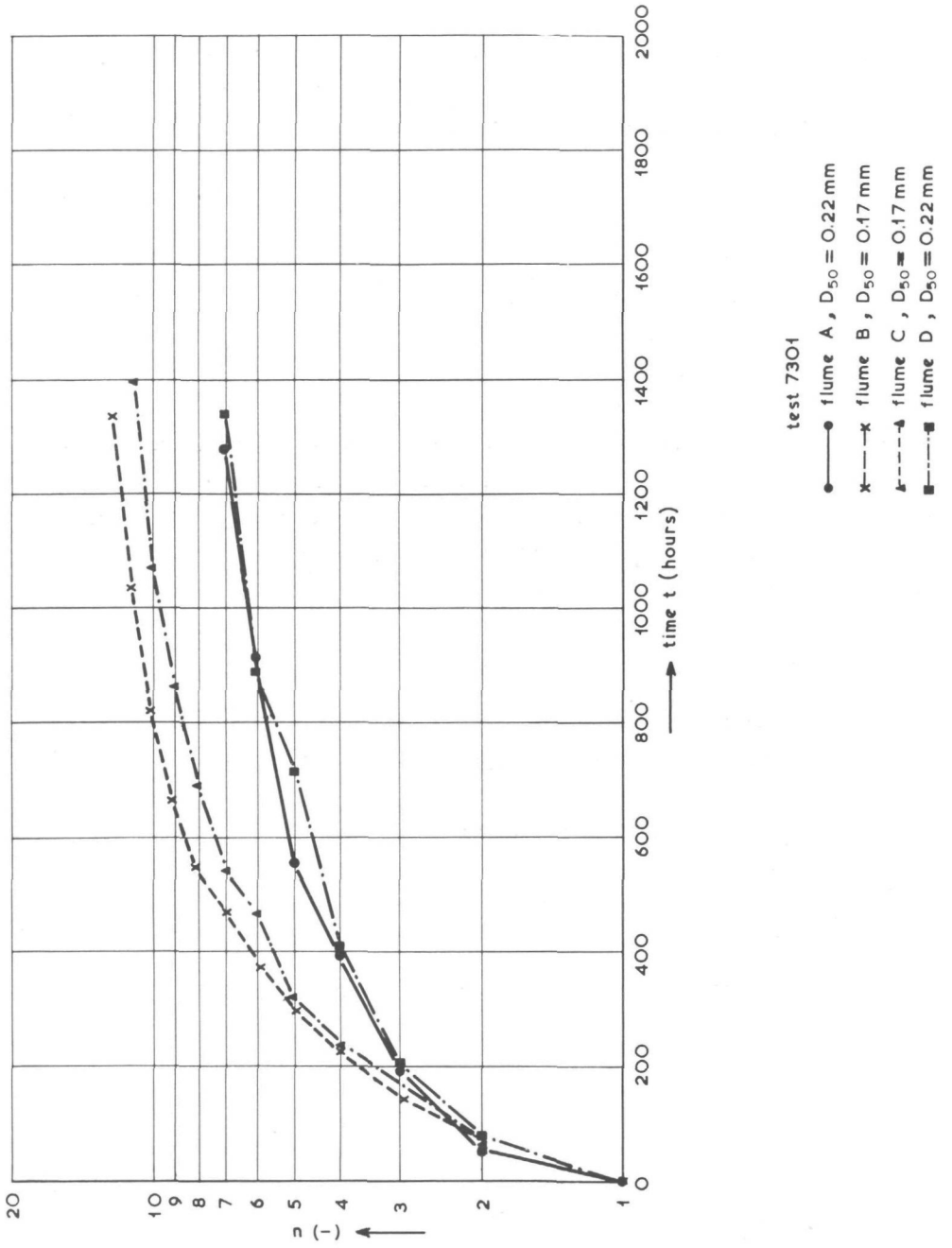

RELATION BETWEEN NUMBER OF INCREASED WATER LEVELS n AND TIME t

FIGURE 32

(1) As the recurrence time of the increased water level increases exponentially in time, it will be assumed that the erosion of the backshore per unit of time decreases exponentially in time, i.e.:

$$S_e = a_1 \exp(-a_e t) \tag{4.63}$$

where S_e = backshore erosion per unit of time and shoreline length, at time t, being positive when the backshore is being eroded (transport in seaward direction)

a_1 and a_e = constants which are to be determined.

(2) As it has been shown that the number of increased water levels becomes a constant when $t = \infty$, it means that the erosion of the backshore must stop if $t = \infty$. Consequently it will be assumed that for a specific wave condition and backshore geometry there exists an equilibrium position of the backshore erosion face, i.e.

$$(L_e)_{t=\infty} = L_{e\infty} \tag{4.64}$$

where L_e = schematized backshore length at any time t

$L_{e\infty}$ = schematized backshore length at time $t = \infty$.

Furthermore, from continuity considerations it follows that the erosion of the backshore:

$$S_e = -\delta_e \frac{dL_e}{dt} \tag{4.65}$$

Combination of equations (4.63) and (4.65) yields:

$$\delta_e \frac{dL_e}{dt} + a_1 \exp(-a_e t) = 0$$

Thus:

$$\int_{L_{e0}}^{L_e} dL_e = -\frac{a_1}{\delta_e} \int_0^t \exp(-a_e t)\, dt$$

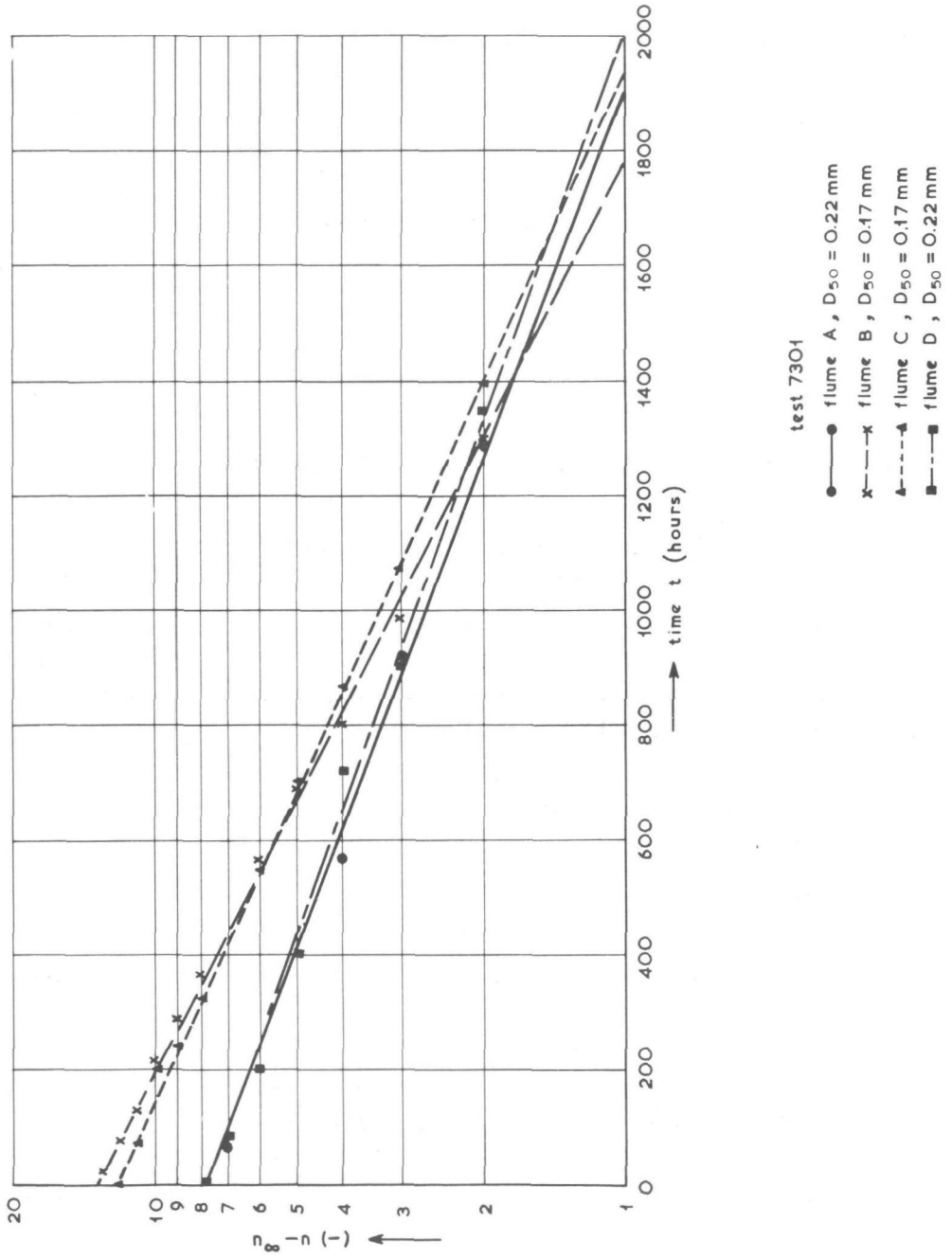

RELATION BETWEEN $(n_\infty - n)$ AND TIME t
FIGURE 33

where L_{e0} = schematized backshore length at time t = 0

$$\therefore L_e - L_{e0} = \frac{a_1}{\delta_e a_e} (\exp(-a_e t) - 1) \tag{4.66}$$

When $t = \infty$, $L_e = L_{e\infty}$, according to equation (4.64).

$$\therefore L_{e\infty} - L_{e0} = \frac{-a_1}{\delta_e a_e}$$

$$a_1 = \delta_e a_e (L_{e0} - L_{e\infty}) \tag{4.67}$$

Substitution of equation (4.67) in equation (4.66) yields:

$$L_e = L_{e0} + (L_{e0} - L_{e\infty}) \exp(-a_e t) - (L_{e0} - L_{e\infty})$$

$$= L_{e\infty} + (L_{e0} - L_{e\infty}) \exp(-a_e t) \tag{4.68}$$

Substitution of equation (4.67) into equation (4.63) yields the amount of backshore erosion per unit of time at any time t:

$$S_e = \delta_e a_e (L_{e0} - L_{e\infty}) \exp(-a_e t)$$

$$= \delta_e a_e \left\{ L_{e\infty} + (L_{e0} - L_{e\infty}) \exp(-a_e t) - L_{e\infty} \right\}$$

$$= \delta_e a_e (L_e - L_{e\infty}) \tag{4.69}$$

As $\delta_e a_e$ is a constant, equation (4.69) is of the same form as the equation for onshore-offshore transport in the D-profile, as used by Bakker (see equation (3.1)). Consequently ($\delta_e a_e$) will be called a "backshore constant", and will be denoted by the sign s_e i.e.:

$$s_e = \delta_e a_e \tag{4.70}$$

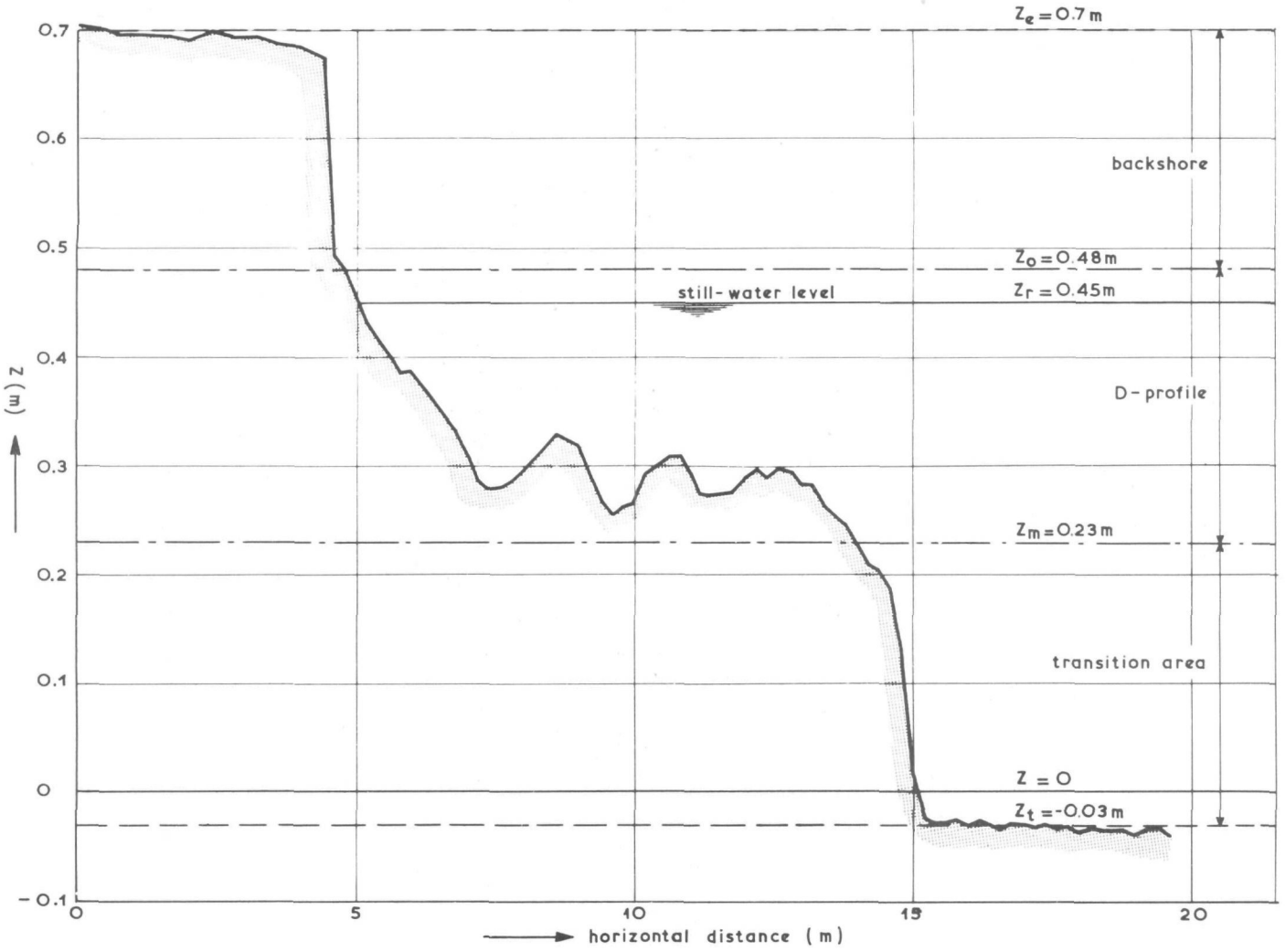

TEST 7301 B : BOTTOM PROFILE FOR t = 1400 hrs

FIGURE 34

With the aid of equation (4.70) it follows that

$$L_e = L_{e\infty} + (L_{e0} - L_{e\infty}) \exp\left(-\frac{s_e t}{\delta_e}\right) \tag{4.71}$$

and $$S_e = s_e (L_{e0} - L_{e\infty}) \exp\left(\frac{-s_e t}{\delta_e}\right)$$

$$= s_e W_e \exp\left(\frac{-s_e t}{\delta_e}\right) \tag{4.72}$$

where $W_e = L_{e0} - L_{e\infty}$ = the total schematized length of the recession of the backshore (W_e is positive when S_e is positive).

In Figure 34 a typical small-scale model profile is shown (test 7301, flume B, t = 1400 hours). The backshore area for this test is defined by $0.48 \text{ m} \leqslant Z \leqslant 0.70 \text{ m}$ (see Figure 34).
As can be seen in Figure 35, the theoretical recession of the backshore, calculated with the aid of equation (4.71), corresponds well with the actual recession measured in the two-dimensional small-scale model test (test 7301, flume B). The effect of the migration of the breaker bars on the backshore erosion can be seen in Figure 35, when the actual erosion rates are compared with the average rate of erosion.

4.3 The transition area

The D-profile, which is developing in seaward direction, is supplied by the erosion S_e of the backshore, according to equation (4.72). At any height Z above the reference level ($Z_0 \geqslant Z \geqslant Z_m$, Figure 20) the offshore transport S_y of sediment is given by:

$$S_y = -\frac{dI_1}{dt} + S_e \tag{4.73}$$

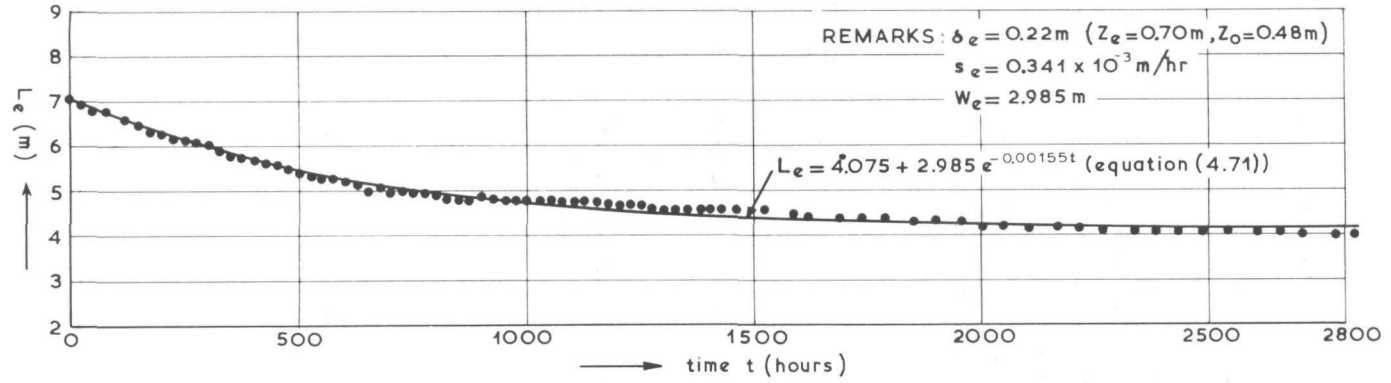

FIGURE 35 : TIME-VARIATION OF L_e

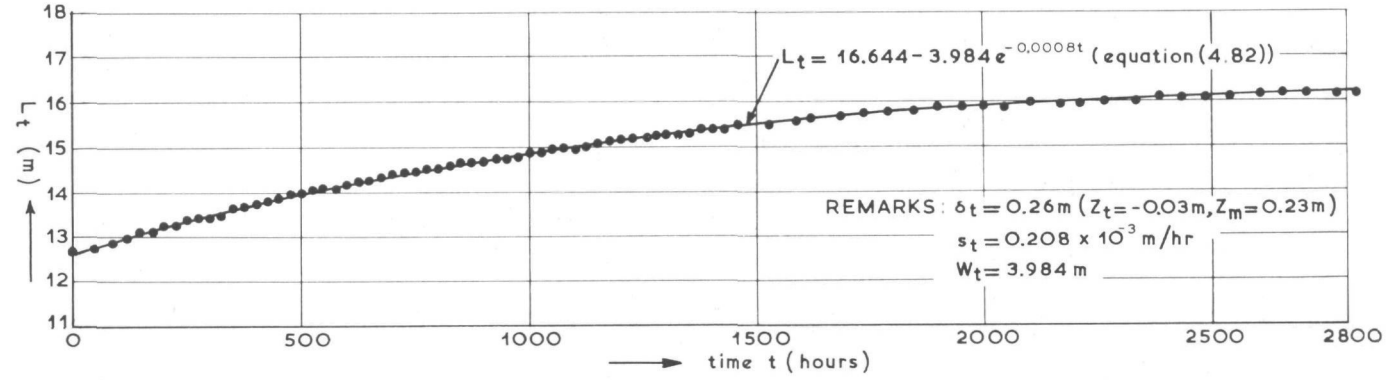

FIGURE 36 : TIME-VARIATION OF L_t

where I_1 = volume of sediment in the area between the elevations Z_0 and Z

S_y = offshore sediment transport at elevation Z.

If $Z = Z_m$, the offshore transport S_y will equal the transport of sediment S_t necessary to fill in the area between the lower boundary of the D-profile and the horizontal floor of the model. The volume I_1 will then represent the total volume of sediment in the D-profile ($Z_0 \geqslant Z \geqslant Z_m$). As it has been shown in Chapter 2 that it is realistic to assume that an equilibrium D-profile exists for any specific wave condition, it is evident that:

$$\frac{dI_1}{dt} \xrightarrow[\infty]{t} 0 \tag{4.74}$$

According to equation (4.72) S_e also decreases in time. Consequently, it seems realistic to make the following assumptions regarding the transition area:

(1) The growth per unit of time in the transition area will decrease exponentially in time, i.e.

$$S_t = a_2 \exp(-a_t t)$$

$$= a_2 \exp\left(-\frac{s_t}{\delta_t} t\right) \tag{4.75}$$

where S_t = growth of the transition area per unit of time and shoreline length at time t. S_t is positive in seaward direction

a_t = a constant, being put equal to s_t/δ_t, in analogy to equation (4.70)

s_t = transition area constant

δ_t = schematized thickness of the transition area

a_2 = a constant which is to be determined.

(2) For a specific water movement an equilibrium position of the transition area exists, i.e.:

$$(L_t)_{t=\infty} = L_{t\infty} \tag{4.76}$$

where L_t = schematized length of the transition area at time t
$L_{t\infty}$ = schematized length of the transition area at time $t = \infty$.

Furthermore, it follows from the continuity equation that the growth of the transition area

$$S_t = + \delta_t \frac{dL_t}{dt} \tag{4.77}$$

Combination of equations (4.75) and (4.77) leads to:

$$\delta_t \frac{dL_t}{dt} - a_2 \exp\left(\frac{-s_t t}{\delta_t}\right) = 0 \tag{4.78}$$

Thus

$$\int_{L_{t0}}^{L_t} dL_t = \frac{a_2}{\delta_t} \int_0^t \exp\left(\frac{-s_t t}{\delta_t}\right) dt$$

where L_{t0} = schematized transition area length at time t = 0.

$$L_t - L_{t0} = \frac{a_2}{\delta_t} \int_0^t \exp\left(\frac{-s_t t}{\delta_t}\right) dt \tag{4.79}$$

Thus

$$\begin{aligned} L_t - L_{t0} &= -\frac{a_2}{s_t}\left(\exp\left(\frac{-s_t t}{\delta_t}\right) - 1\right) \\ &= \frac{a_2}{s_t}\left(1 - \exp\left(\frac{-s_t t}{\delta_t}\right)\right) \end{aligned} \tag{4.80}$$

When $t = \infty$, $L_t = L_{t\infty}$ according to equation (4.76):

$$L_{t\infty} - L_{t0} = \frac{a_2}{s_t}$$

$$a_2 = s_t \, (L_{t\infty} - L_{t0}) \tag{4.81}$$

Substitution of equation (4.81) in equation (4.80) yields:

$$L_t = L_{t0} + (L_{t\infty} - L_{t0}) \, (1 - \exp \, (\frac{-s_t t}{\delta_t}))$$

$$= L_{t\infty} - (L_{t\infty} - L_{t0}) \exp \, (\frac{-s_t t}{\delta_t}) \tag{4.82}$$

Substitution of equation (4.81) in equation (4.75) yields the growth of the transition area per unit of time at any time t:

$$S_t = s_t \, (L_{t\infty} - L_{t0}) \exp \, (\frac{-s_t t}{\delta_t})$$

$$= s_t \, W_t \exp \, (\frac{-s_t t}{\delta_t}) \tag{4.83}$$

where $W_t = L_{t\infty} - L_{t0}$ (4.84)

W_t is positive when S_t is positive.
For the long-duration test 7301 B the transition area is defined by $-0.03 \text{ m} \leqslant Z \leqslant 0.23 \text{ m}$ (see Figure 34).
As can be seen in Figure 36, the theoretical growth of the transition area, as calculated with the aid of equation (4.82), corresponds quite well with the growth, as measured in this test.

It has been observed in both the model and the prototype that the slope of the equilibrium bottom profile decreases with increasing depth, as long as $Z_0 \geqslant Z \geqslant Z_m$, i.e. the average slope of the D-profile decreases with increasing distance from the water line. Thus it is to be expected

that the equilibrium position of the transition area lies at a great distance from the water line.
When the value of $s_t t/\delta_t$ is small relative to 1, $\exp(-s_t t/\delta_t) \longrightarrow 1$, and consequently the growth of the transition area will be approximately linear in time. Such a situation can arise when the test duration has been too short, for instance $t < 500$ hours.
In this case equation (4.83) becomes

$$S_t \approx c\, s_t\, W_t \tag{4.85}$$

where c is a constant, $c \longrightarrow 1^-$ (i.e. $c \longrightarrow 1$, $c < 1$), depending on the test duration. This implies that for small test durations the supply of sediment to the transition area will be nearly constant, and the growth of the transition area will still approximately be linear.
Combination of equations (4.77) and (4.85) will then lead to:

$$\delta_t \frac{dL_t}{dt} - c\, s_t\, W_t = 0 \tag{4.86}$$

Thus

$$L_t - L_{t0} = \frac{c\, s_t\, W_t}{\delta_t} \int_0^t dt$$

$$L_t = L_{t0} + \frac{c\, s_t\, W_t}{\delta_t}\, t$$

$$= L_{t0} + s_t^* t \tag{4.87}$$

$$\text{where } s_t^* = \frac{c\, s_t\, W_t}{\delta_t} = \text{constant} \tag{4.87a}$$

Equation (4.87) respresents an approximation of equation (4.82), and should only be used when $t << \infty$ (for instance $t < 500$ hrs) and $s_t t/\delta_t \longrightarrow 0$.

In that case the growth of the transition area is a linear function of time, which can be found by substitution of (4.87) in (4.77):

$$S_t = s_t^{*} \delta_t = c\, s_t\, W_t \tag{4.88}$$

Such a transformation from a negative exponential to a linear variation in time was not necessary for the backshore, as the time-variation in the transport capacity at the water line is normally much bigger than at the lower limit of the D-profile.

4.4 The D-profile

The D-profile is schematized by two lines, the onshore profile line L_1 and the offshore profile line L_2 (Figure 20). In Chapter 2 it has been shown that the assumptions made by Bakker [2] regarding the transport S_y through any arbitrarily chosen division between the onshore and offshore profile ($0 \leqslant \delta_1 \leqslant \delta$; $\delta_1 + \delta_2 = \delta$), are in agreement with the actual physical process which takes places in the developing profile. Consequently, these assumptions will be retained for the D-profile, viz.:
(1) For a specific division between the onshore and offshore profile, an equilibrium distance W can be found, i.e.:

$$(L_2 - L_1) \xrightarrow[\infty]{t} W \tag{4.89}$$

where $(L_2 - L_1)$ = distance between the schematized onshore and offshore layers, at any time t

W = equilibrium distance between the schematized onshore and offshore layers at time $t = \infty$.

(2) The onshore-offshore transport through the division between the onshore and offshore profile at time t is assumed to be proportional to the difference between the value of $(L_2 - L_1)$ at time t and at time $t = \infty$, i.e.

$$S_y = s_y \left[W - (L_2 - L_1) \right] \tag{4.90}$$

where S_y = transport through the division between the onshore and offshore profile, at a height $Z = Z_m + \delta_2$ above the reference level, per unit of time and shoreline length, at any time t. S_y is positive in seaward direction

s_y = coastal constant (q_y in the theory of Bakker). As the boundary conditions for the D-profile differ from those in the profile assumed by Bakker, the values of q_y and s_y will not be equal.

At any elevation $Z = Z_m + \delta_2$ $(0 \leqslant \delta_2 \leqslant \delta)$ the continuity equation has the following form:

$$\delta_1 \frac{dL_1}{dt} + \delta_2 \frac{dL_2}{dt} + S_t - S_e = 0 \tag{4.91}$$

or, in terms of the onshore-offshore transport S_y:

$$S_y = S_e - \delta_1 \frac{dL_1}{dt} \tag{4.92}$$

$$= \delta_2 \frac{dL_2}{dt} + S_t \tag{4.93}$$

Combination of equations (4.90) and (4.92), and of equations (4.90) and (4.93) respectively, yields:

$$\frac{dL_1}{dt} = \frac{S_e}{\delta_1} - \frac{s_y}{\delta_1} (W - (L_2 - L_1)) \tag{4.94}$$

$$\text{and } \frac{dL_2}{dt} = \frac{s_y}{\delta_2} (W - (L_2 - L_1)) - \frac{S_t}{\delta_2} \tag{4.95}$$

(4.95) - (4.94) gives:

$$\frac{dL_2}{dt} - \frac{dL_1}{dt} = \frac{d\,(L_2 - L_1)}{dt} = \left(\frac{s_y}{\delta_2} + \frac{s_y}{\delta_1} \right) (W - (L_2 - L_1)) - \left(\frac{S_t}{\delta_2} + \frac{S_e}{\delta_1} \right)$$

$$= \frac{(\delta_1 + \delta_2)s_y}{\delta_1\delta_2} (W - (L_2 - L_1)) - (\frac{S_t}{\delta_2} + \frac{S_e}{\delta_1})$$

$$= \frac{\delta s_y}{\delta_1\delta_2} (W - (L_2 - L_1)) - (\frac{S_t}{\delta_2} + \frac{S_e}{\delta_1}) \qquad (4.96)$$

$$\text{Thus } \frac{d\ (L_2 - L_1)}{dt} + \frac{\delta s_y}{\delta_1\delta_2} (L_2 - L_1) + (\frac{S_t}{\delta_2} + \frac{S_e}{\delta_1}) - \frac{W\delta s_y}{\delta_1\delta_2} = 0 \qquad (4.97)$$

Substitution of S_e and S_t from equations (4.72) and (4.83) respectively, yields:

$$\frac{d\ (L_2 - L_1)}{dt} + \frac{\delta s_y}{\delta_1\delta_2} (L_2 - L_1) + \frac{s_t W_t}{\delta_2} \exp\ (\frac{-s_t t}{\delta_t}) + \frac{s_e W_e}{\delta_1} \exp\ (\frac{-s_e t}{\delta_e}) +$$

$$- \frac{W\delta s_y}{\delta_1\delta_2} = 0 \qquad (4.98)$$

Equation (4.98) is a first order differential equation, with the solution:

$$(L_2 - L_1) = W - (W - (L_2 - L_1)_0) \exp\ (- \frac{\delta s_y t}{\delta_1\delta_2}) +$$

$$+ \frac{\delta_t s_t W_t \delta_1}{\delta_t\delta s_y - \delta_1\delta_2 s_t} (\exp\ (- \frac{\delta s_y t}{\delta_1\delta_2}) - \exp\ (\frac{-s_t t}{\delta_t})) +$$

$$+ \frac{\delta_e s_e W_e \delta_2}{\delta_e\delta s_y - \delta_1\delta_2 s_e} (\exp\ (- \frac{\delta s_y t}{\delta_1\delta_2}) - \exp\ (- \frac{s_e t}{\delta_e})) \qquad (4.99)$$

where $(L_2 - L_1)_0$ = schematized length between the onshore and offshore profiles at time t = 0.

When the test duration has not been very long ($t < 500$ hrs, for instance), and the transition area constant s_t is small, $s_t t/\delta_t \rightarrow 0$. In this case W_t cannot be determined easily, and $(L_2 - L_1)$ can rather be determined by substitution of equations (4.72) and (4.88) in equation (4.97), viz.:

$$\frac{d\,(L_2 - L_1)}{dt} + \frac{\delta s_y}{\delta_1 \delta_2}(L_2 - L_1) + \frac{s_t^{*}\delta_t}{\delta_2} + \frac{s_e W_e}{\delta_1} \exp\left(\frac{-s_e t}{\delta_e}\right) - \frac{W \delta s_y}{\delta_1 \delta_2} = 0 \quad (4.100)$$

The solution of equation (100) is:

$$(L_2 - L_1) = W - (W - (L_2 - L_1)_0) \exp\left(-\frac{\delta s_y t}{\delta_1 \delta_2}\right) +$$

$$+ \frac{\delta_t s_t^{*} \delta_1}{\delta s_y}\left(\exp\left(-\frac{\delta s_y t}{\delta_1 \delta_2}\right) - 1\right) +$$

$$+ \frac{\delta_e s_e W_e \delta_2}{\delta_e \delta s_y - \delta_1 \delta_2 s_e}\left(\exp\left(-\frac{\delta s_y t}{\delta_1 \delta_2}\right) - \exp\left(\frac{-s_e t}{\delta_e}\right)\right) \quad (4.101)$$

For any known profile development it is possible to determine s_y and W with the aid of either equation (4.99) or equation (4.101), by using the method of least squares to obtain the best fit of $(L_2 - L_1)$ against time t.

In the long-duration test 7301B the D-profile is defined by:
$0.23 \text{ m} \leqslant Z \leqslant 0.48 \text{ m}$ (see Figure 34).

In order to check the validity of the assumptions (equations (4.89) and (4.90)) which served as a basis for the preceding derivation, equation (4.99) was applied to 10 different locations in the D-profile (test 7301 B; $\delta_1/\delta = 0, 0.1, \ldots, 0.9$). When $\delta_1 = 0$, equation (4.99) cannot be applied. In this case it can be stated as a first approximation that $L_1 = L_e$ and instead of studying $(L_2 - L_1)$, $(L_2 - L_e)$ can be studied. Equation (4.99) can then still be applied to this special case ($\delta_1 = 0$) by substi-

tution into equation (4.99) of $\delta_1 = \delta_e$

$\delta_2 = \delta$

$\delta = \delta + \delta_e$

$\delta_e = 0$

This yields:

$$(L_2 - L_e) = W - (W - (L_2 - L_e)_0) \exp\left(-\frac{(\delta + \delta_e)\, s_y t}{\delta_e \delta}\right) +$$

$$+ \frac{\delta_t s_t W_t \delta_e}{\delta_t (\delta_e + \delta) s_y - \delta_e \delta s_t} \left(\exp\left(-\frac{(\delta + \delta_e) s_y t}{\delta_e \delta}\right) - \exp\left(-\frac{s_t t}{\delta_t}\right)\right) \qquad (4.99a)$$

The comparison between the measured $(L_2 - L_1)$- values and equation (4.99) can be seen in Figures 37 .. 46 for each of the 10 different divisions between the onshore and offshore profiles. From these figures it can be concluded that the concept of equilibrium applies to all elevations in the profile. Furthermore it follows that equation (4.99) applies with reasonable accuracy to the development of $(L_2 - L_1)$ in time. Consequently equation (4.99) (or in case of $s_t t/\delta_t \longrightarrow 0$, equation (4.101)) will be used to evaluate all available data.
In Figure 47 the values of s_y and W, as calculated with the aid of equation (4.99), are represented as a function of the dimensionless depth δ_1/δ. This is the general form in which the coastal constants W and s_y will be represented in Chapter 6.

4.5 Limits of the D-profile

If the proposed D-profile schematization is to be used generally, it is essential to make the choice of the limits of the D-profile in such a way that a comparison with other test results becomes possible. This implies that a relationship must be sought between the limits of the D-profile and the wave and sediment characteristics.

TIME-VARIATION OF $(L_2 - L_e)$ AND $(L_2 - L_1)$

FIGURE 37,38

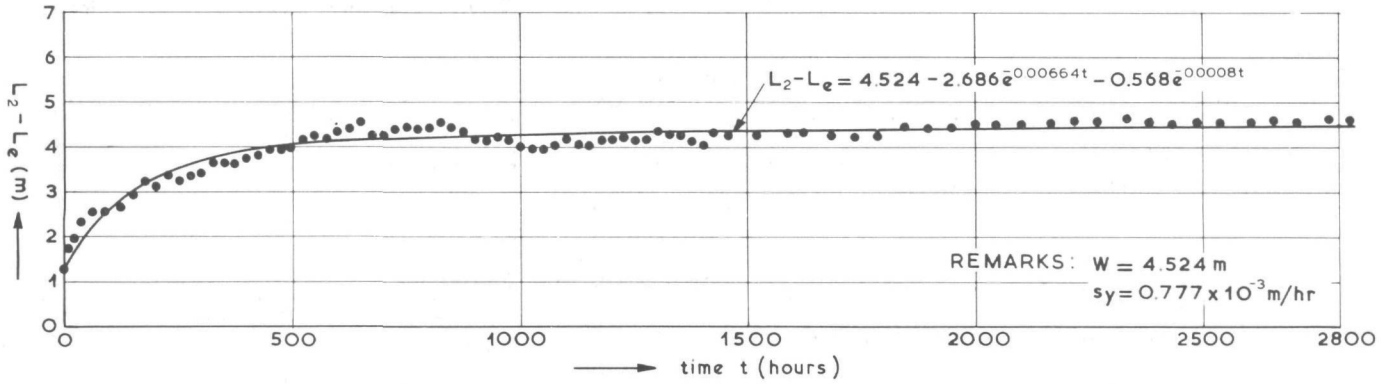

FIGURE 38 : $\delta_1 = 0.025$ m ; $\delta_2 = 0.225$ m

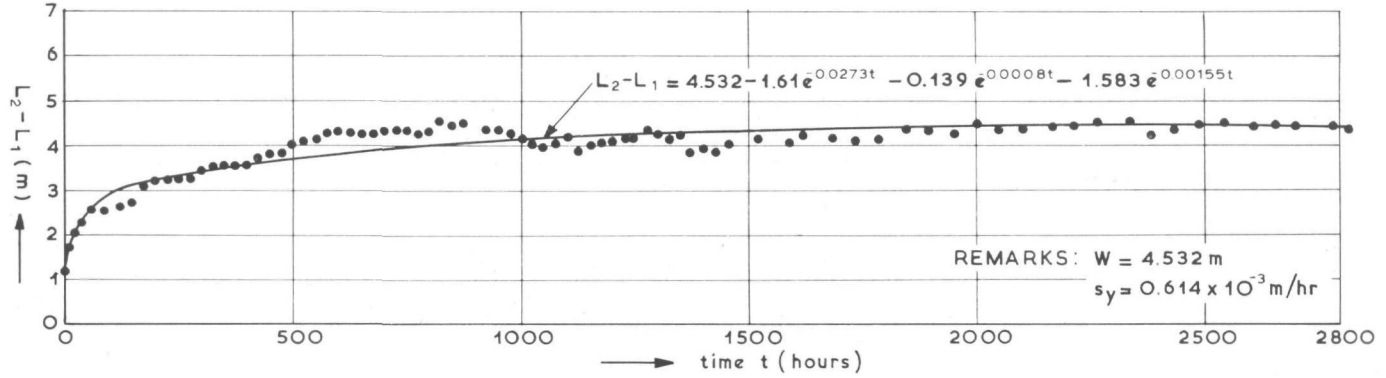

FIGURE 37 : $\delta_1 = \delta_e = 0.22$ m ; $\delta_2 = \delta = 0.25$ m

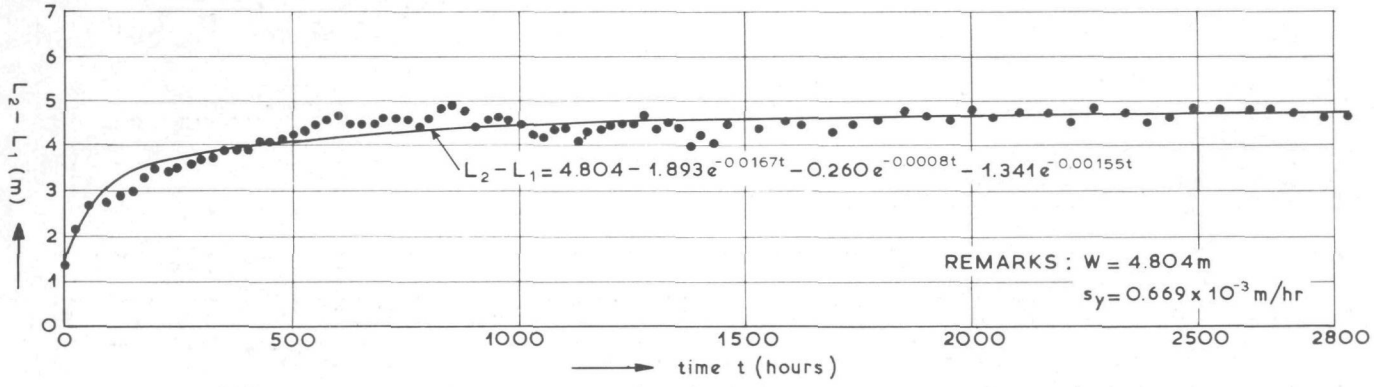

FIGURE 39 : $\delta_1 = 0.05$ m ; $\delta_2 = 0.20$ m

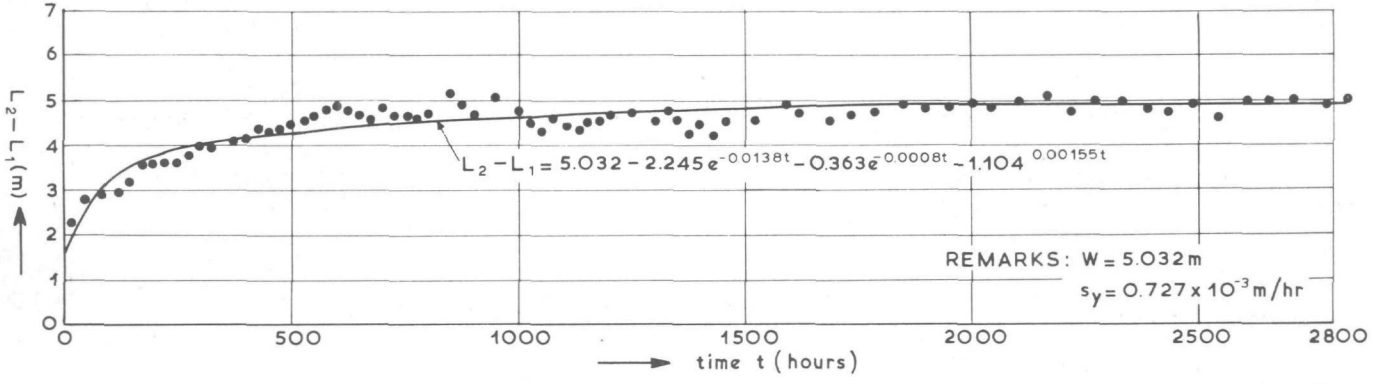

FIGURE 40 : $\delta_1 = 0.075$ m ; $\delta_2 = 0.175$ m

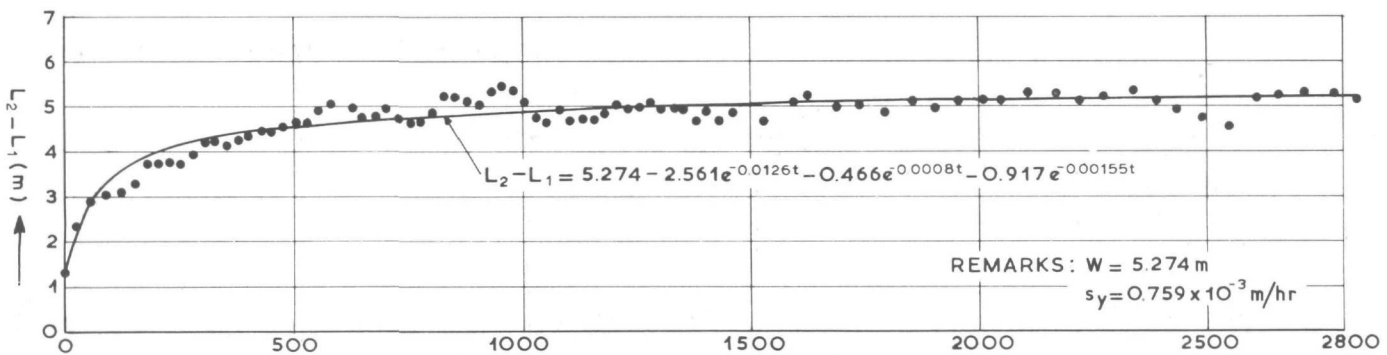

FIGURE 41 : $\delta_1 = 0.10$ m ; $\delta_2 = 0.150$m

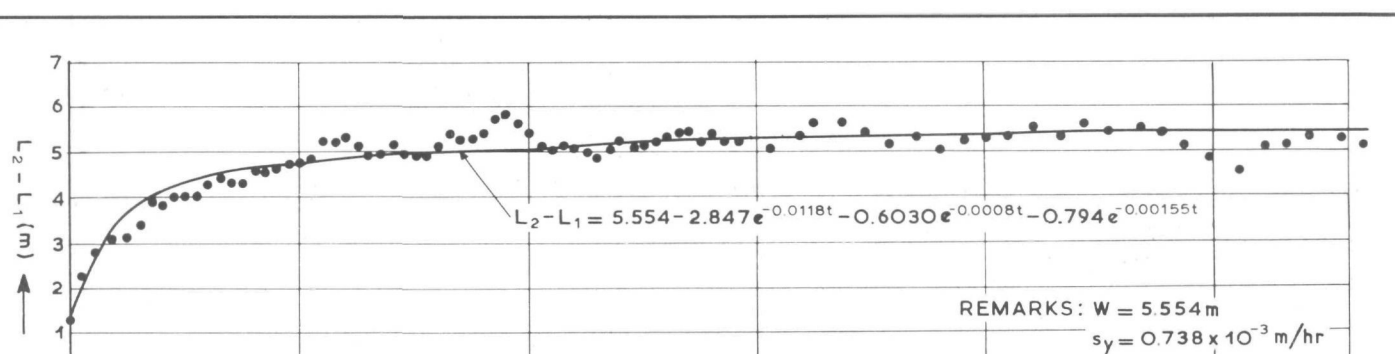

FIGURE 42 : $\delta_1 = 0.125$ m ; $\delta_2 = 0.125$ m

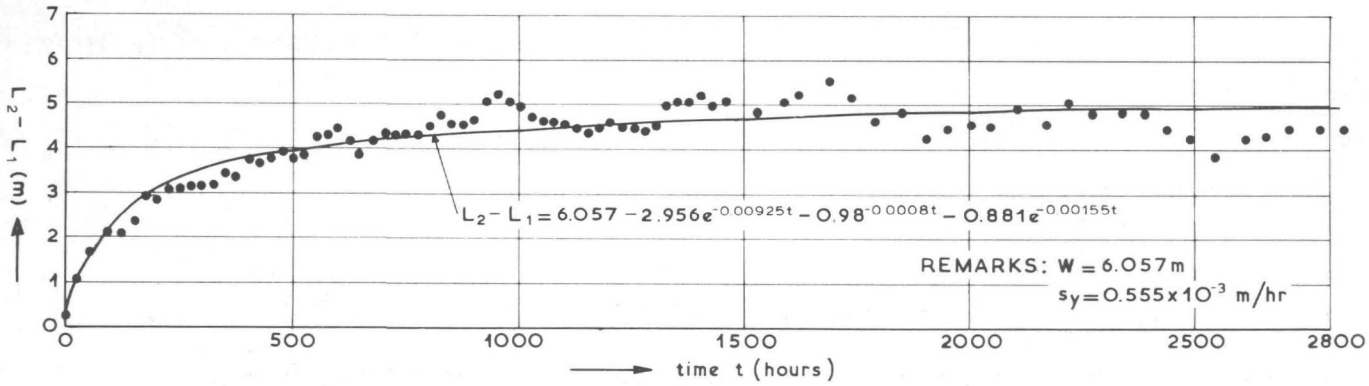

FIGURE 43 : $\delta_1 = 0.15$ m ; $\delta_2 = 0.10$ m

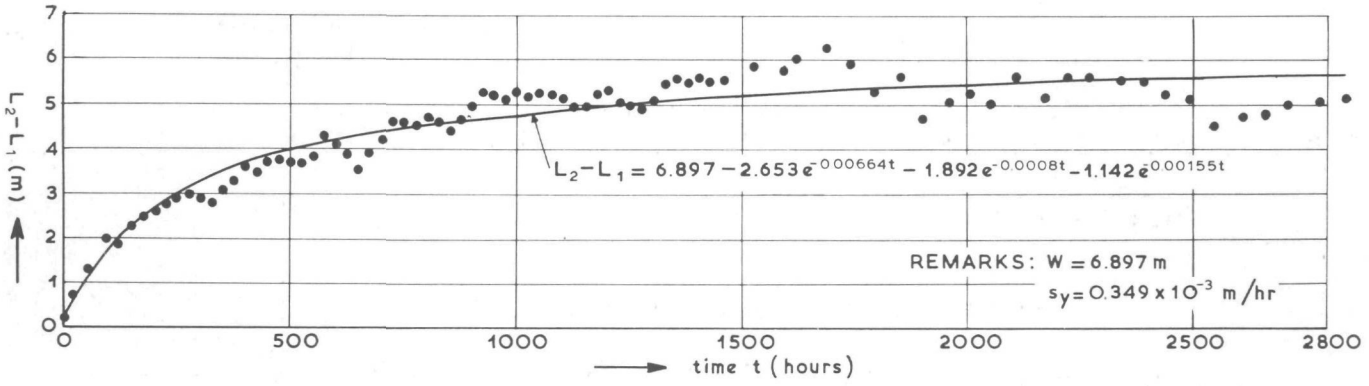

FIGURE 44 : $\delta_1 = 0.175$ m ; $\delta_2 = 0.075$ m.

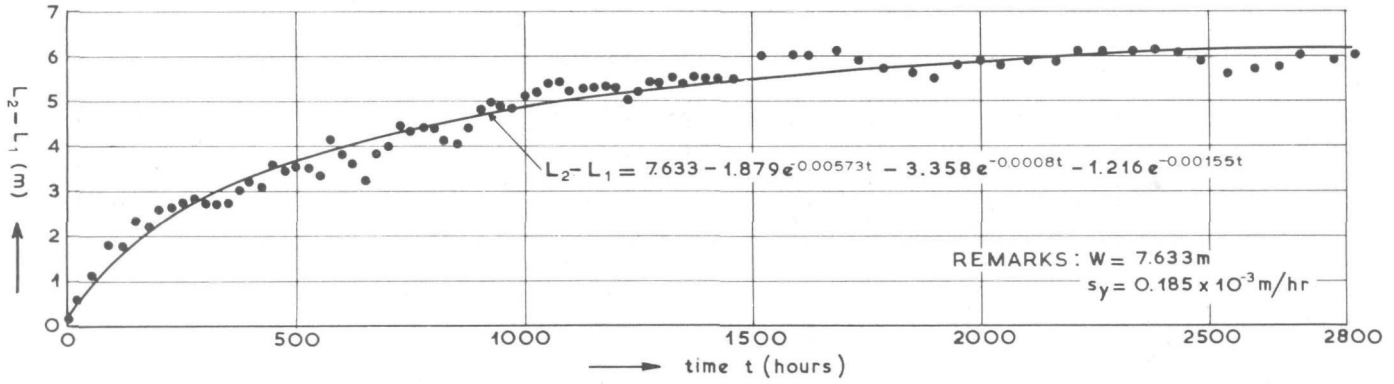

FIGURE 45 : $\delta_1 = 0.20$ m ; $\delta_2 = 0.05$ m

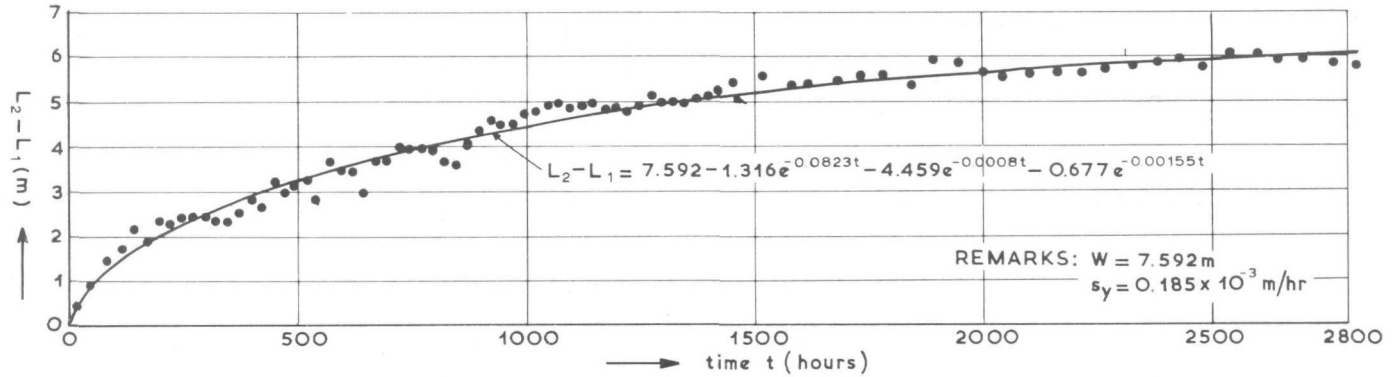

FIGURE 46 : $\delta_1 = 0.225$ m ; $\delta_2 = 0.025$ m

TIME-VARIATION OF (L_2-L_1)
FIGURE 45,46

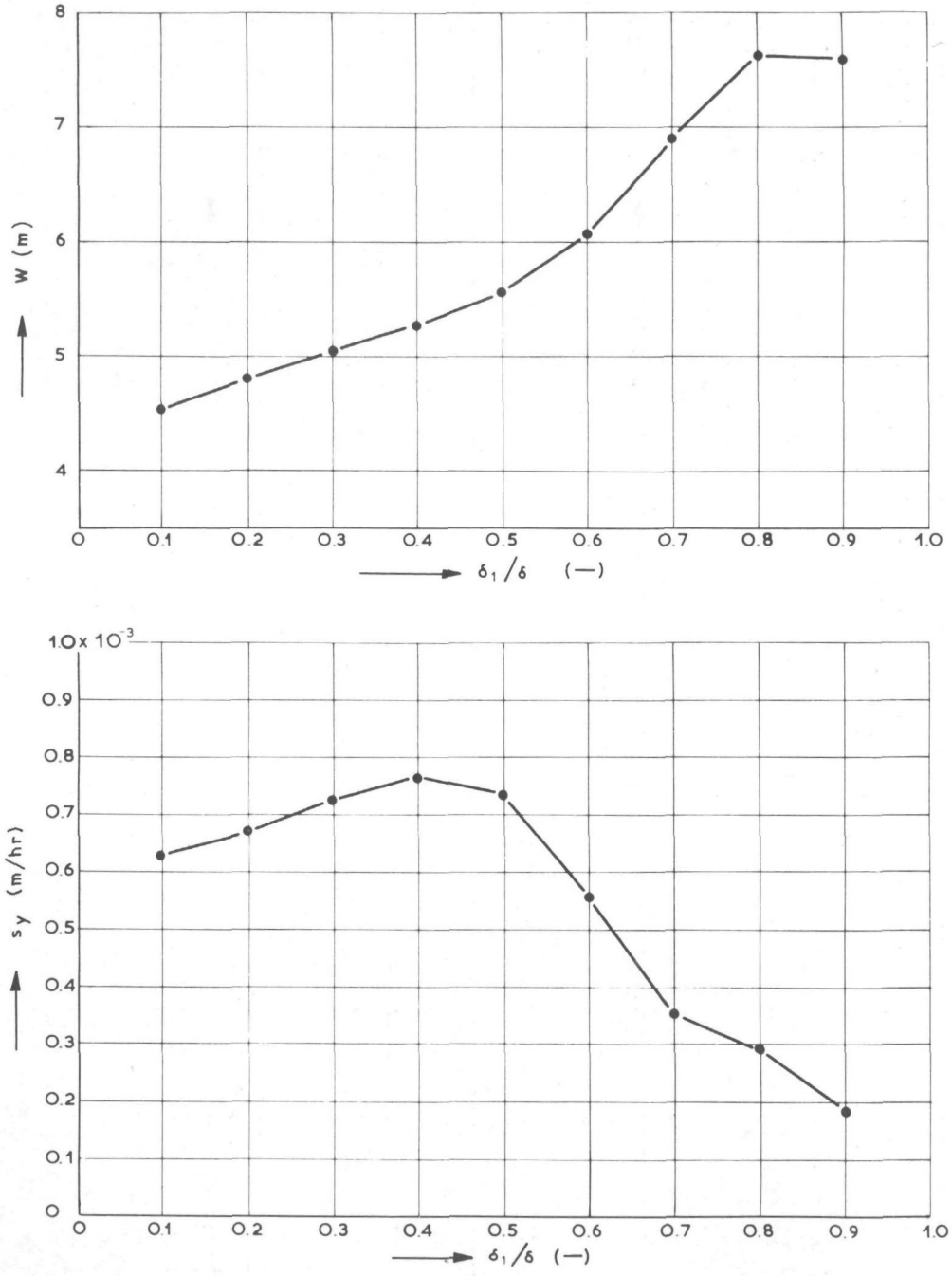

VARIATION OF COASTAL CONSTANTS W AND s_y
FIGURE 47

The upper boundary of the backshore (Z_e in Figure 20) and the lower boundary of the transition slope (Z_t in Figure 20) can be chosen arbitrarily, as long as no profile changes take place in any part of the profile, other than that defined by $Z_e \geqslant Z \geqslant Z_t$.

The division between the backshore and the D-profile, i.e. the upper limit of the D-profile (Z_0 in Figure 20) will be related to the maximum water level that can occur on the wetted beach, due to the definition of this division. As has been stated in Chapter 4.2, Hunt [22], restricting himself to breaking waves and using the laboratory data of Saville [42], found that

$$\frac{\eta}{H} = C_p \tan\alpha \left(\frac{H}{\lambda_0}\right)^{-1/2} \tag{4.1}$$

Battjes [4] compared the results of various authors (including that of Hunt). From his comparison of $\eta/(H\tan\alpha)$ with (H/λ_0) it can be concluded that equation (4.1) of Hunt is in reasonable resemblance with the data of the other authors (Djounkowski, 1940; Drogosz-Wawrzyniak, 1965; Karapetjan; Shankin, 1955; Kurlowitz, 1957; Sidorowa, 1957; Zukovec and Zajev, 1960; Maksimcuk, 1959 and Wagner, 1968).
The run-up can in general be written as:

$$\frac{\eta}{H \tan\alpha} = a_1 \left(\frac{H}{\lambda_0}\right)^{b_1} \tag{4.102}$$

where a_1 and b_1 are constants.

$$\text{Thus } \eta = a_1 H \tan\alpha \left(\frac{H}{\lambda_0}\right)^{b_1} \tag{4.103}$$

Wiegel [53] determined the relationship between the beach slope ($\tan\alpha$) and the median particle diameter (D_{50}) for protected, moderately protected and exposed beaches. He also states that all model beaches are "protected". For all three categories, however, the general relationship

$$\tan\alpha = a_2 \, (D_{50})^{c_2} \tag{4.104}$$

applies, where a_2 and c_2 are constants, depending on the type of beach under consideration.
Substitution of equation (4.104) into equation (4.103) gives:

$$\eta = a_3 \, H \, D_{50}^{c_2} \, (\frac{H}{\lambda_0})^{b_1} \tag{4.105}$$

where $a_3 = a_1 a_2$

When equation (4.105) is divided by D_{50}, a dimensionless value of the wave run-up (η/D_{50}) results:

$$\frac{\eta}{D_{50}} = a_3 \, H \, D_{50}^{c_3} \, (\frac{H}{\lambda_0})^{b_1} \tag{4.106}$$

where $c_3 = c_2 - 1$

Furthermore $\lambda_0 = 1.56 \, T^2 \quad (= \frac{g}{2\pi} T^2)$ (in metric units) (4.107)

and thus

$$\frac{\eta}{D_{50}} = a_4 \, H^{e_1} D_{50}^{c_3} \, T^{b_2} \tag{4.108}$$

where $e_1 = 1 + b_1$
$b_2 = -2b_1$
$a_4 = (1.56)^{-b_1} \, a_3$

If it is assumed that the upper limit of the D-profile at a height h_0 above the still-water level is proportional to η, h_0 can be found in general by equating:

$$\frac{h_0}{D_{50}} = f \, (H_0^{e} D_{50}^{c} \, T^{b}) \tag{4.109}$$

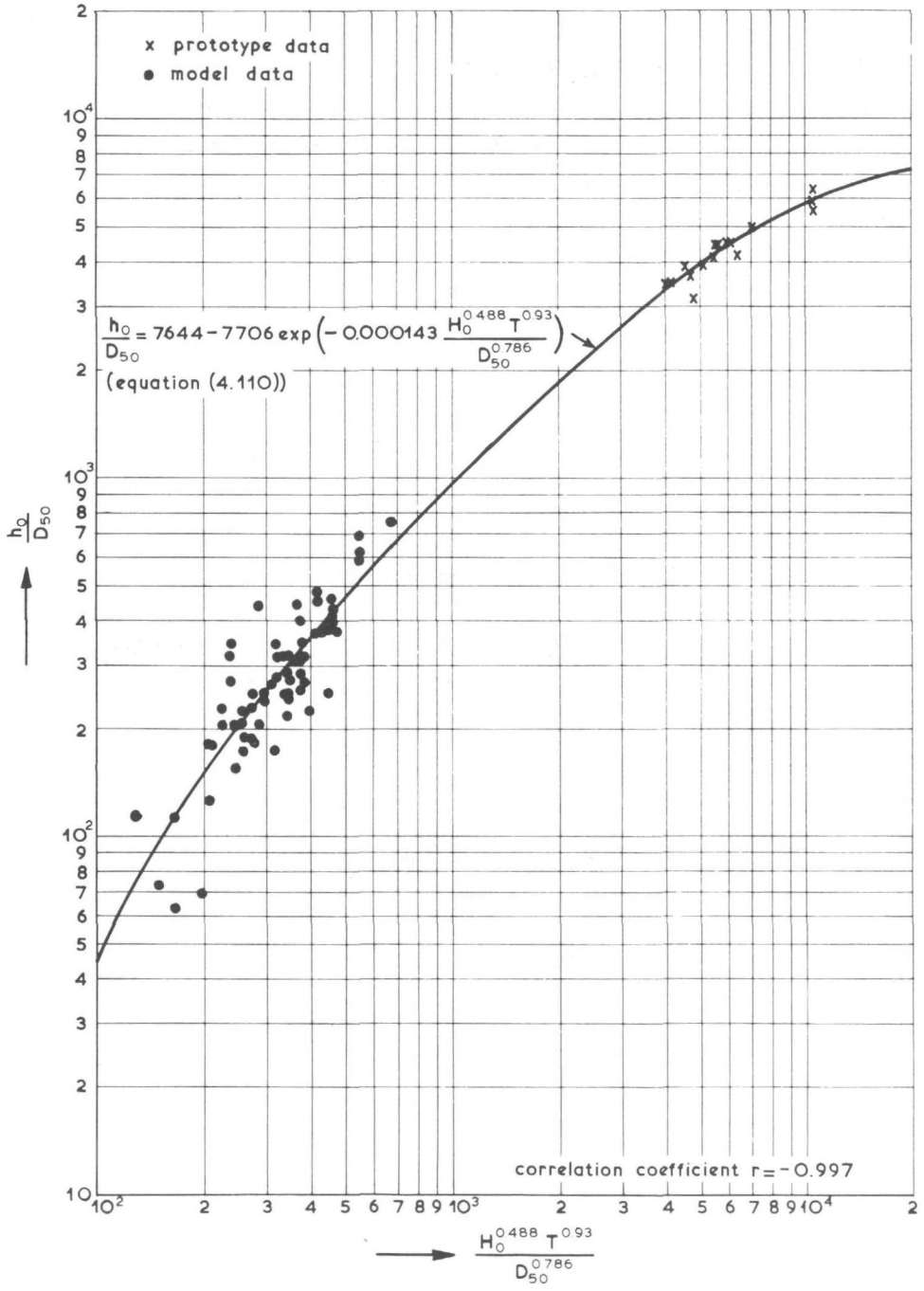

REMARKS: 1) h_0, H_0, D_{50} in m
2) T in sec

UPPER LIMIT OF D-PROFILE
FIGURE 48

where the deepwater wave height H_0 has been chosen instead of H for simplicity's sake, and e, c and b are constants of proportionality. It should be stressed that equation (4.109) has no theoretical background. In order to find the precise form of equation (4.109), the values of h_0, D_{50}, H_0 and T (as determined for 75 available model tests and 18 appropriate prototype situations) were correlated by means of the method of least squares.
The following relationship resulted:

$$\frac{h_0}{D_{50}} = 7644 - 7706 \exp\left(- 0.000143 \frac{H_0^{0.488}\, T^{0.93}}{D_{50}^{0.786}}\right) \qquad (4.110)$$

Equation (4.110) has been plotted in Figure 48, together with the data used for its determination. The data are listed in Table III.

From Figure 48 the value of (h_0/D_{50}) can be determined, which corresponds with the wave conditions in test 7301, flume B (D_{50} = 0.17 mm), viz.:

$$\frac{h_0}{D_{50}} = 218 \qquad (4.111)$$

As the value of the most seaward breaker height was H_1 = 0.07 m, this means that

$$\frac{h_0}{H_1} = 218 \frac{D_{50}}{H_1} = 0.530 \qquad (4.112)$$

As the upper limit of the D-profile corresponds with the maximum wave run-up, it means that

$$\frac{h_0}{H_1} = C_p \left(\frac{\eta_{max}}{H_1}\right)_{\text{calculated}} \qquad (4.113)$$

where C_p = porosity factor in Hunt's formula.

$\frac{\eta_{max}}{H_1}$ = determined from Figure 25

= 0.766 (equation (4.6))

Thus $C_p = (\frac{h_0}{H_1})/(\frac{\eta_{max}}{H_1})$ calculated

$= \frac{0.530}{0.766} = 0.69$ (for test 7301B) (4.114)

For any specific wave condition and bed material (either in the model or in the prototype), h_0, the upper limit of the D-profile, measured relative to the still-water level, can be determined from Figure 48 or equation (4.110).

The division between the lower boundary of the D-profile and the transition area is marked clearly by an abrupt change in the local slope of the profile. The slope of the transition area is normally much steeper than the average slope of the lower part of the D-profile.
It is to be expected that the division between the transition area and the D-profile, i.e. the lower limit of the D-profile, will be related in some way to the depth of beginning of movement of bed material. Bonnefille and Pernecker [6] found experimentally that beginning of movement is defined by the relationship:

$$D_{*} = 2.5\ R_{*}^{4/5} \qquad \text{for } R_{*} < 12 \tag{4.115}$$

$$\text{where } D_{*} = \left(\frac{\Delta_s g}{\nu^2}\right)^{1/3} D_{50} \tag{4.116}$$

$$\text{and } R_{*} = \frac{u_{*} D_{50}}{\nu} = 2.2 \left(\frac{H^2 \nu}{T^3 \sinh^2 \frac{2\pi d}{\lambda}}\right)^{1/4} \frac{D_{50}}{\nu} \tag{4.117}$$

Δ_s = relative density of bed material

$$= \frac{\rho_s - \rho_w}{\rho_w}$$

D_* and R_* = functions defined by Bonnefille and Pernecker according to equations (4.115) ... (4.117)

ρ_s = density of bed material

ρ_w = density of water

ν = kinematic viscosity

D_{50} = median particle diameter

u_* = bed shear stress velocity due to oscillatory wave action.

If only sand beaches are considered, $\Delta_s = 1.65$.
This implies that the restriction on the applicability of equation (4.115), viz. $R_* < 12$, can be rewritten to read $D_{50} < 0.721$ mm for a water temperature of 20° C.
From equations (4.115) ... (4.117) it follows that

$$\sinh \frac{2\pi d}{\lambda} = 48\, \nu^{1/6} D_{50}^{-1/2} H T^{-3/2} \Delta_s^{-5/6} g^{-5/6}$$

$$= \text{constant } (H D_{50}^{-1/2} T^{-3/2}) \qquad (4.118)$$

(for sand and water with a constant temperature)

For shoaling waves:

$$H = H_0 \sqrt{\frac{\sinh \frac{4\pi d}{\lambda} \coth \frac{2\pi d}{\lambda}}{\sinh \frac{4\pi d}{\lambda} + \frac{4\pi d}{\lambda}}} \qquad (4.119)$$

where H_0 is the deep-water wave height if no refraction occurs.
Thus, with the aid of equations (4.118) and (4.119) the depth of beginning of movement for a material with a specific density $\Delta_s = 1.65$, and a diameter $D_{50} < 0.721$ mm, is a function of $H_0/(D_{50}^{1/2} T^{3/2})$, i.e.:

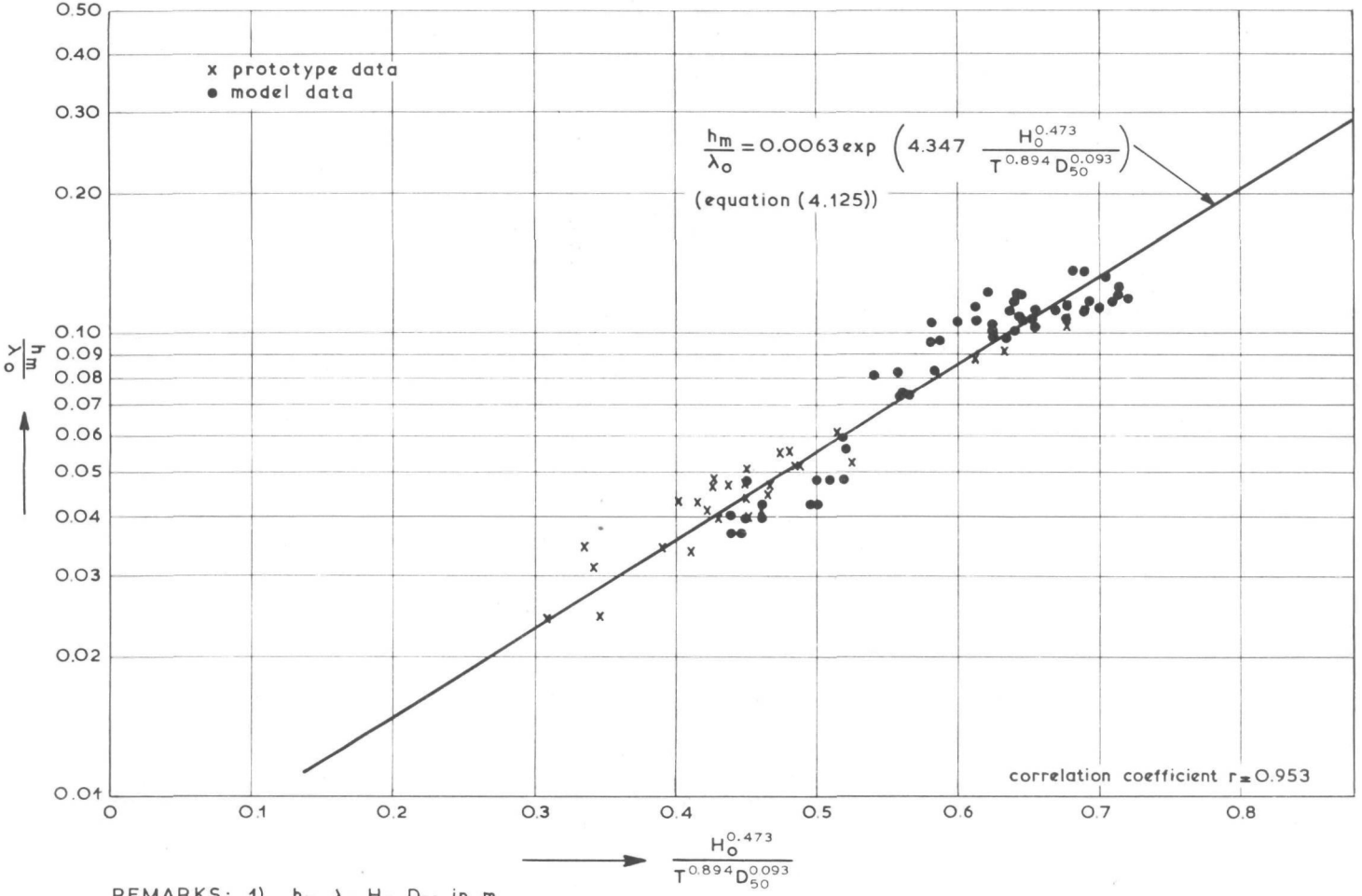

REMARKS: 1) $h_m, \lambda_o, H_o, D_{50}$ in m
2) T in sec

LOWER LIMIT OF D-PROFILE
FIGURE 49

$$\frac{d}{\lambda_0} = f\left(\frac{H_0}{D_{50}^{1/2}\, T^{3/2}}\right) \tag{4.120}$$

Goddet [15] found experimentally that the orbital velocity just outside the boundary layer which will induce beginning of movement of sand is given by:

$$u_0 = .00854\ (\rho')^{2/3}\ D_{50}^{1/4}\ T^{3/8} \quad \text{(m/s)} \tag{4.121}$$

(with the units in the International metric system)

where ρ' = apparent density of sand in water = $\rho_s - \rho_w$.

According to the first-order wave theory

$$u_0 = \frac{\pi H}{T \sinh \frac{2\pi d}{\lambda}} \tag{4.122}$$

where u_0 = orbital velocity at the bed.
Thus, according to Goddet, the depth of beginning of movement can be found with the aid of equations (4.119), (4.121) and (4.122) to be a function of $(H_0/(T^{11/8} D_{50}^{1/4}))$, i.e.:

$$\frac{d}{\lambda_0} = f\left(\frac{H_0}{T^{11/8} D_{50}^{1/4}}\right) \tag{4.123}$$

If it is consequently assumed that the lower limit of the D-profile (h_m relative to the still-water level) stands in some constant relationship to the depth d of beginning of movement of bed material, it can be stated in general that

$$\frac{h_m}{\lambda_0} = f\left(\frac{H_0^{\,a}}{T^b D_{50}^c}\right) \tag{4.124}$$

where a, b and c are constants.

By means of the method of least squares the precise form of equation (4.124) was determined by using 59 available model tests, which lasted long enough to enable the determination of the lower limit of the D-profile, as well as 31 appropriate prototype situations.

The following relationship resulted:

$$\frac{h_m}{\lambda_0} = 0.0063 \exp\left(4.347 \frac{H_0^{0.473}}{T^{0.894} D_{50}^{0.093}}\right) \qquad (4.125)$$

Equation (4.125) has been plotted in Figure 49 together with the data used for its determination. The data are listed in Table IV. For any specific wave condition and bed material (either in the model or in the prototype) the lower limit of the D-profile, h_m, measured relative to the still-water level, can be determined from equation (4.125) or Figure 49.

Chapter 5: Apparatus, data and analysing techniques

5.1 General

The classical way to develop an empirical predictive relationship for a process that cannot be solved purely analytically, due to a lack of knowledge regarding the internal mechanism of the process, such as for instance the problem of onshore-offshore transport, can be summarized as follows:

(1) Make some analytically-based assumptions regarding a schematization of the complicated process. Such a schematization will usually be based on external properties of the process, which are as such a result of the actual internal mechanism.

(2) Keeping the schematization in mind, tests can be done in a small-scale model to determine the relationships which will govern the process in the model. These small-scale tests should be done in a scale-range which is as large as possible, to allow the detection of scale effects, if these occur.

(3) Check the developed empirical relationship(s) against available prototype data. If necessary, the relationship(s) should be adjusted. This will especially be the case if scale-effects are present in the small-scale model.

The reliability of the final result and the possibility of application to prototype situations will be largely dependent of the validity of both the assumptions and the schematization. In Chapters 2 ... 4 the assumptions and the corresponding schematization were derived. However, of equal importance are the following aspects, viz. the type of model equipment and measuring techniques used, with their restrictions, the methods employed to use the unprocessed model data to come to an empirical relationship and the range in which the schematization has been tested.
In Chapter 3 a method of evaluation of model data was developed, in which the effect of measuring errors is reduced to a minimum. In this chapter

a description will be given of the model equipment, the data used to test the schematization and the analysing techniques employed to evaluate the data.

5.2 Model facilities

Laboratory tests regarding profile development can be classified generally into two categories, viz. two-dimensional and three-dimensional tests. The tests performed in the Delft Hydraulics Laboratory and used in the present study were performed in two different two-dimensional models (models I and II) and one three-dimensional model (model III).

Two-dimensional tests

Both two-dimensional models consisted of a wave basin, subdivided into four flumes each (flumes A to D). In model I the walls, separating the different flumes from each other, were made of plywood, in model II plastered brick walls were used.
Waves were generated simultaneously in all four flumes by means of a paddle-type wave generator, which is in normal use at the Delft Hydraulics Laboratory.
The wave board could be set in such a way that the rotational centre of the board lies anywhere between the bottom of the flume (pure rotation) and infinitely far below it (pure translation). In most of the tests a combination of rotation and translation was used to generate the waves, although in some tests waves were generated by means of a purely translating wave board. In both two-dimensional models the horizontal concrete floor on which the wave generator was fixed, extended to a distance of 2m in front of the central position of the wave board, except in flume D of model II, where the concrete floor extended over the whole length of the flume.
A water-level variation could be introduced in model II by means of a pump, installed behind the wave generator. Water was alternately pumped

into and out of the model. The flume widths and lengths as well as other general information are given in Table V.
In each flume two sections were set out in longitudinal direction, in which the bottom elevation was recorded at regular intervals (l = 0.20m). The water level was checked manually with a point gauge in a piezometer well outside the model. In order to facilitate a round-the-clock running of the model, a water-level sensoring device was installed and connected to the wave generator. As soon as the actual water level differed by more than 3 mm from the desired water level, the generator cut out automatically.

Three-dimensional tests

The three-dimensional model had a total beach length of 48m, while the distance from the landward extremity of the beach profile to the wave generator amounted to 16m. Waves were generated at the longer side of the model opposite to the beach, with an angle of wave incidence $\varphi = 10^{\circ}$, relative to the initial still-water line. The model had the same type of wave generator as the two-dimensional models. The horizontal concrete wave-generator floor extended to 1 m in front of the central position of the midpoint (in horizontal direction) of each wave board of 5m length (see Figure 50).
Due to the oblique wave attack a longshore current was generated inside the surf zone, with as a result a corresponding longshore transport of bed material. If the up- and downstream boundaries of the model were closed, sand would have been eroded from the upstream end of the model and deposited downstream. This rotation of the water line would have continued until it was parallel to the incoming wave crests. As the model beach was, however, thought to be part of an infinitely long straight beach, water as well as bed material was injected at the upstream end of the model. At the downstream end of the model water was drawn off and the sand which was transported across the downstream model boundary was caught in a sand trap. In order to diminish boundary effects to a minimum, a beach length of 5m at either end of the model was regarded as lying

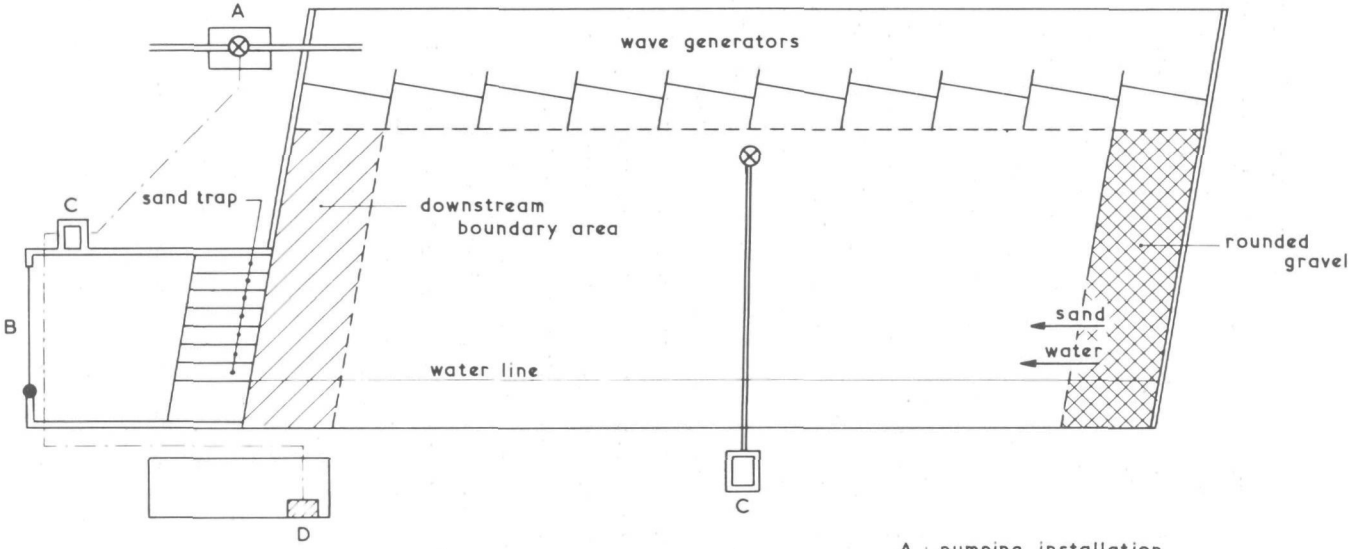

LAY-OUT : MODEL III
FIGURE 50

outside the actual model area and was used to eliminate boundary effects. Consequently the effective beach length was 38m. The bed material of the upstream boundary area consisted of a mixture of sand and rounded gravel. The profile in this area was continually altered to correspond with the actual sand profile in the model area directly adjacent to it. At the boundary between the actual model and the boundary area, where the longshore current pattern was already well-developed, sand was supplied.
At the downstream end of the model sand was caught in a deepened sand trap (see Figure 50). The sand trap was divided into different closed elements, each of 0.50m width in offshore direction, to enable the determination of the offshore distribution of longshore transport. Sand which did not reach the sand trap, but was deposited in the downstream boundary area, due to irregularities on account of the downstream model exit, was removed from the bed in the boundary area and added to the sand in the sand trap at regular intervals. From time to time the sand trap was emptied into specially-designed reservoirs, in which the volume of the trapped sand could be determined. A water-level variation could be introduced by means of a pumping installation behind the wave generators, which was in phase with a weir of adaptable height. While the weir was rising, water was pumped into the model, and vice versa. The water level was checked manually by means of a point gauge in a piezometer well outside the model. The model was covered by a measuring grid with a constant longshore distance b between the different sections perpendicular to the coastline(b=1m), and with a spacing l = 0.20 m between each two points in a section, measured perpendicular to the coastline. In all the measuring points in the grid the bottom elevation was recorded at regular intervals.

In all three models the bottom profile was measured by means of a measuring rod and a levelling instrument, with an accuracy of approximately one millimetre. All heights were measured relative to the horizontal concrete floor of the wave generator.
Wave heights were measured with a resistance-type wave gauge and the signal recorded on SANBORN-recording paper.

5.3 Data

The data used in this study can be subdivided into four groups, viz. (1) two-dimensional model data, (2) three-dimensional model data, (3) prototype data and (4) prototype-size two-dimensional model data. A large number of two-dimensional model tests have been performed to the present, both in the Delft Hydraulics Laboratory and elsewhere. The number of available three-dimensional tests is smaller, due to the bigger financial investment that is necessitated. Reliable prototype data, in which both the full profile development and the exact hydraulic boundary conditions are available, are practically non-existent. The data of the fourth type were supplied by the Coastal Engineering Research Center and are used in this report with the C.E.R.C.'s consent.

Model data

The factors which will determine if a specific model test can be used to test the schematization of onshore-offshore transport, as described in Chapter 4, are:

(1) test duration: - In order to determine with sufficient accuracy the values of s_y and W, it is essential that ample recordings of the bottom profile, made at regular time-intervals, are available. During the complete test duration the external boundary conditions (wave characteristics, water level, longshore current, longshore transport) should stay constant. Due to this restriction about 60% of the tests available in the Delft Hydraulics Laboratory could not be used.

(2) Completeness of the data: - As all tests were not performed with as primary objective a study of the profile development, the data of some of the tests were incomplete. These tests were not processed.

(3) Scale effects: - Scale effects occur if the process in a small-scale model and that in the full-scale prototype differ from each other in some aspects. As it has been shown in Chapter 2 that the effect of the

bed roughness on the sediment entrainment will vary with varying scale, it is to be expected that scale effects will occur. If the scale range of the available tests is large enough and some prototype data are available, the magnitude of these scale effects can be evaluated. Scale effects will accordingly not lead to the elimination of any data, on the contrary, it might lead to a need to perform additional tests to increase the rest range.

(4) Secondary effects: - Data which are affected by model effects caused by the geometry (or lay-out) of a particular model will have to be excluded. Hulsbergen [21] made a study regarding the origin of secondary waves and their effect on the sediment transport. He points out that secondary waves which are generated by the wave board for large Ursell-parameters (secondary waves are visually detectable for Ursell-parameters $U_r = H\lambda^2/d^3 > 14$) lead to an asymmetry in both the wave form and the orbital velocity at the model bed, which varies spatially along the flume. As the sediment transport is closely related to the velocity field at the bed, this implies a spatial variation in sediment transport, which results in the formation of a series of bars and troughs on the horizontal bed of the flume. These bars will influence the velocity field in the area landwards of them, and as such also the sediment transport. It is not known at which critical value of the Ursell-parameter the asymmetry in the wave form will become large enough to lead to a spatial variation in the transport. It is, however, to be expected that this critical value of the Ursell-parameter will be related to the orbital velocity at the horizontal bed, in front of the wave generator, at which sediment transport will be initiated. Secondary waves can also be generated by the profile geometry itself, as is shown in Figure 23 (Chapter 4). These secondary effects are, however, the same for all tests, as long as no secondary effects originating from the wave board are present. This phenomenon has also been observed in prototype (Larras [32]).

Goddet [15] found experimentally that the critical orbital velocity which will just lead to sediment entrainment (ripple formation) is:

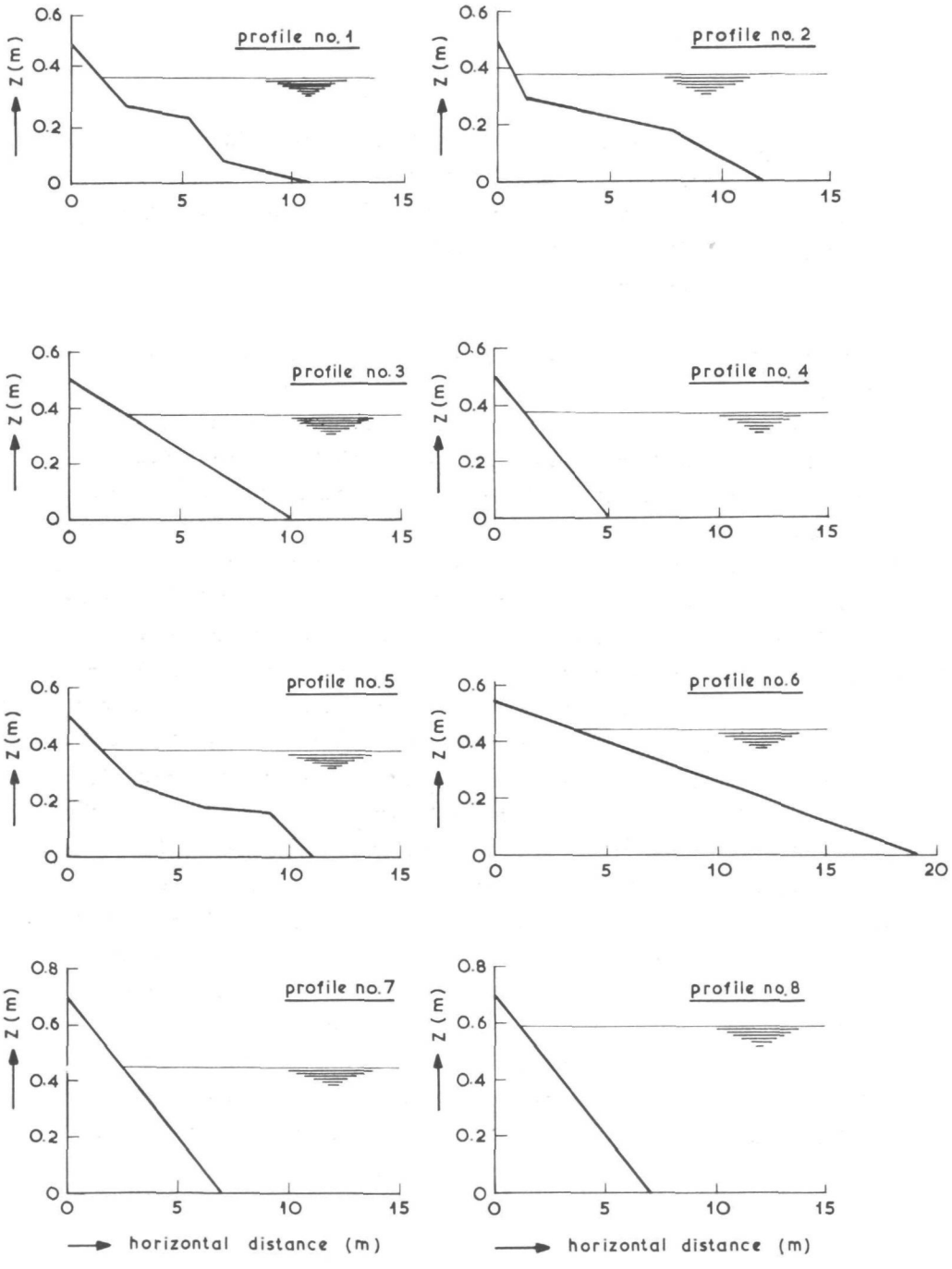

INITIAL PROFILES: TWO-DIMENSIONAL TESTS
FIGURE 51

$$(u_0)_{crit} = 0.0085\ (\rho')^{2/3}\ D_{50}^{1/4}\ T^{3/8} \quad (m/s) \qquad (5.1)$$

where $(u_0)_{crit}$ = critical orbital velocity just outside the boundary layer which will lead to sediment entrainment

ρ' = apparent density of bottom sediment in water = $\rho_s - \rho_w$

D_{50} = median particle diameter

T = wave period

The actual velocity at which sediment transport will be initiated will be higher than $(u_0)_{crit}$. If the orbital velocity at the horizontal bed in front of the wave generator exceeds this velocity at which sediment transport is initiated, the possibility exists that the lower limit of the D-profile schematization will lie below the horizontal wave-generator floor.

It is thus evident that in order to: (1) suppress secondary effects originating from the wave generator and (2) keep the D-profile schematization inside the normal flume dimensions, it will be necessary to choose the wave characteristics in such a way that both the Ursell-parameter and the orbital velocity at the bed stay below some critical value at the location of wave generation. When the Ursell-parameter is much smaller than its critical value, the magnitude of the orbital velocity on the horizontal bed will be of little importance, even with large orbital velocities the transport of bed material due to secondary effects will be negligible. On the other hand, for values of the Ursell-parameter in the vicinity of the critical value at which secondary effects will occur in the wave form, the magnitude of the orbital velocity on the horizontal bed is of great importance. Large orbital velocities might then lead to sediment transport due to secondary effects, while orbital velocities much lower than the critical velocity for sediment transport will not lead to secondary transport. Neither the exact values of these critical quantities, nor their relative importance is exactly known. Nevertheless, only those tests for which both $U_r > 14$ and $u_0 > 1.2(u_0)_{crit}$ were

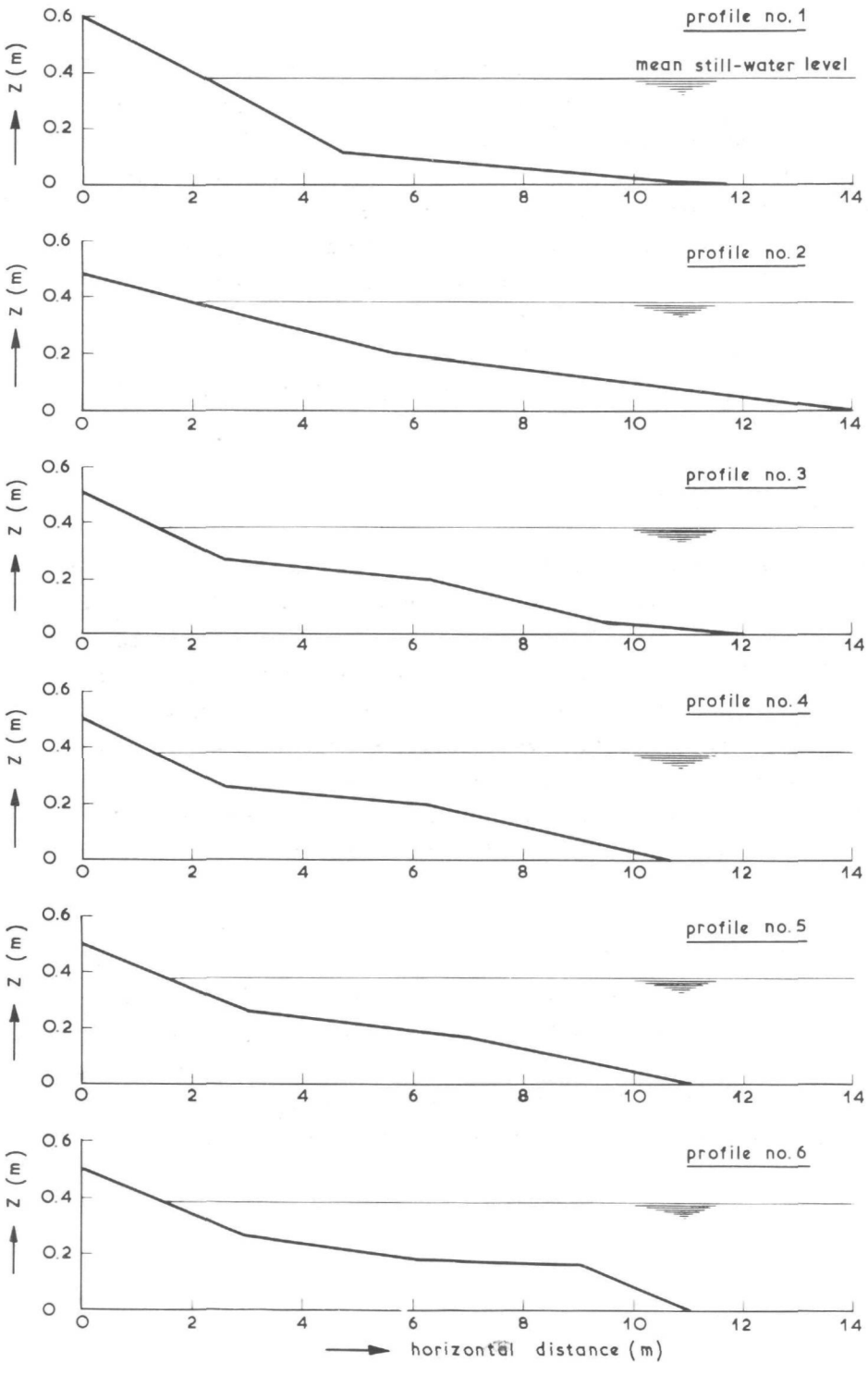

INITIAL PROFILES: THREE-DIMENSIONAL TESTS

FIGURE 52

used for the further evaluation, as it was evident from a visual study that secondary effects did play a role in the profile development when the U_r and u_0-values exceeded these critical values.
The boundary conditions for the remaining two-dimensional model tests are given in Table VI; the initial profiles are given in Figure 51.
In the three-dimensional model the longshore current velocity on the horizontal model bed in front of the wave generator was practically negligible. Consequently equation (5.1) can also be applied to the three-dimensional model tests. Only a few tests remained, to which the schematization could be applied. Their boundary conditions are listed in Table VII and Figure 52.

Prototype-size model data

The same criteria used to evaluate which small-scale model tests could be used also apply to the prototype-size data of the C.E.R.C.. The boundary conditions for the tests which were used in this report are listed in Table VIII. A study of the last-mentioned table reveals that except for one test (test 502), the Ursell-parameter exceeds by far the critical value. Furthermore, the orbital velocity on the horizontal bed in front of the wave generator exceeds the critical value at which sediment entrainment will take place in all the tests. This makes the value of the application of these tests to assist in the extrapolation of the small-scale model tests to prototype values dubious.

The amount of data available to determine the equilibrium profile characteristics under prototype conditions is sufficient (see Table IX), however, no data is available from which the behaviour of the coastal constant s_y under prototype conditions can be evaluated. For this reason the tests of the C.E.R.C. were used to assist in the evaluation of s_y in prototype, even though the Ursell-parameter exceeded the critical value in nearly all the tests.

Prototype data

The boundary conditions in prototype are extremely variable, the water level may vary strongly due to the tide while the wave characteristics (height, period, direction) also vary continually.
Mostly the available prototype data can be classified into two different types:
(1) type A: - Both coastal profiles which were measured during a period of persisting wave conditions and the significant wave characteristics are available. As will be shown in Chapter 6, such data can be used to gain some insight into the equilibrium profiles corresponding with these wave characteristics.
(2) type B: - Coastal profiles which were measured before and after a storm period, as well as the wind, wave and water-level variations which occurred during the storm are available. Mostly it is possible to determine with a fair amount of accuracy a representative set of boundary conditions, which led to the profile variations. If the equilibrium situation can be approximated (it will be shown in Chapter 6 that this is possible), it will be possible to determine the values of s_y representative for the specific storm conditions.
It was, however, felt that the uncertainties playing a role in the determination of the boundary conditions are too big to allow the determination of s_y-values with sufficient accuracy. Consequently no data of type B were used in this study.

In Table IX all available prototype data which could be used in the present study are listed, along with their corresponding boundary conditions.

5.4 Analysing techniques

In this paragraph a short summary will be given of the steps which are necessary to arrive to values of W and s_y, starting from unprocessed data.

Many of the formulae given in this paragraph were derived in Chapters 3 and 4. In such cases only the formulae will be given, for an explanation of the symbols reference will be made to the appropriate text in the foregoing chapters. The analysing techniques for model and prototype data differ from each other and will accordingly be discussed separately.

Model data

A schematic representation of the processing scheme is given in Figure 53.

(1) In a two-dimensional model all sediment has to remain in the model, consequently the cumulative bottom height for all points has to remain a constant. When this is not the case, a correction is applied to the height of each measuring point, as described in Chapter 3.5,

$$\Delta z_{ik} = \left\{ \frac{\left| z_{ikt_0} - z^{*}_{ikt_j} \right|}{\sum_{k=1}^{N} \sum_{i=n_{B1k}}^{n_{Bk}} \left| z_{ikt_0} - z^{*}_{ikt_j} \right|} \right\} \left\{ \sum_{k=1}^{N} \sum_{i=n_{B1k}}^{n_{Bk}} (z_{ikt_0} - z^{*}_{ikt_j}) \right\} \quad (5.2)$$

(equation (3.81))

$$\Delta I = \Delta I_A + \Delta I_B + \Delta I_C = 1b \sum_{k=1}^{N} \sum_{i=1}^{n_k} \Delta z_{ik} \quad (5.3)$$

(equation (3.82))

$$\Delta I_B = 1b \sum_{k=1}^{N} \sum_{i=n_{B1k}}^{n_{Bk}} \Delta z_{ik} \quad (5.4)$$

In a three-dimensional model, on the other hand, the amount of sand fed into the model on the upstream boundary and the sand trapped downstream have to be incorporated in the sand balance, viz.:

$$\Delta I_{3D} + (S_f - S_{tr}) = 0 \quad (5.5)$$

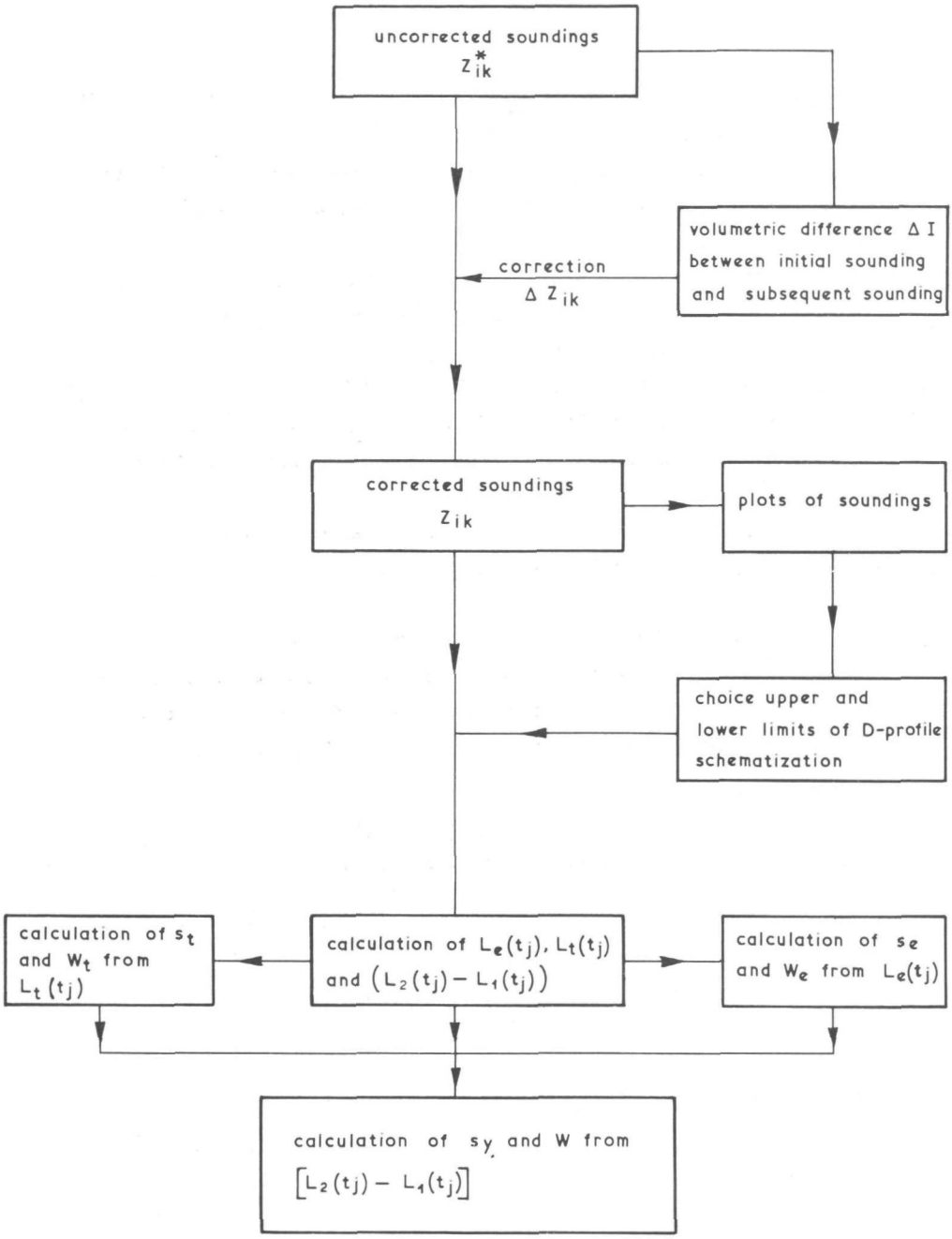

PROCESSING SCHEME: MODEL DATA
FIGURE 53

where $\Delta I_{3D} = lb \sum_{k=1}^{N} \sum_{i=1}^{n_k} (z_{ikt_0} - z_{ikt_j})$ (5.6)

= total volumetric change in the three-dimensional model between time $t = t_0$ and $t = t_j$, if no measuring errors had occurred

S_f = total amount of sand fed into the model in time $(t_j - t_0)$

S_{tr} = total amount of sand caught in the sand trap and downstream boundary area in time $(t_j - t_0)$.

Due to various errors, as described in Chapter 3.5, the volumetric change in the model will not amount to ΔI_{3D}, but to ΔI^*_{3D}, where ΔI^*_{3D} is the uncorrected value of ΔI_{3D}. A correction $\Delta I = (\Delta I^*_{3D} - \Delta I_{3D})$ will then be necessary to compensate for the errors.

In the same manner as for the two-dimensional case equations (5.2) ... (5.4) will now apply to the three-dimensional tests.

(2) Plots are made of the bottom profiles to detect possible large errors and to assist in the choice of the upper and lower boundaries of the D-profile. In Chapter 4.5 the choice of the limits of the D-profile was discussed. The upper boundary, which is determined by the point of maximum wave run-up, is given by:

$$\frac{h_0}{D_{50}} = 7644 - 7706 \exp\left(-0.000143 \frac{H_0^{0.488}\, T^{0.93}}{D_{50}^{0.786}}\right) \qquad (5.7)$$

(equation (4.110))

The lower boundary, which is related to the depth of beginning of movement of bottom sediment, is given by:

$$\frac{h_m}{\lambda_0} = 0.0063 \exp\left(4.347 \frac{H_0^{0.473}}{T^{0.894}\, D_{50}^{0.093}}\right) \qquad (5.8)$$

(equation (4.125))

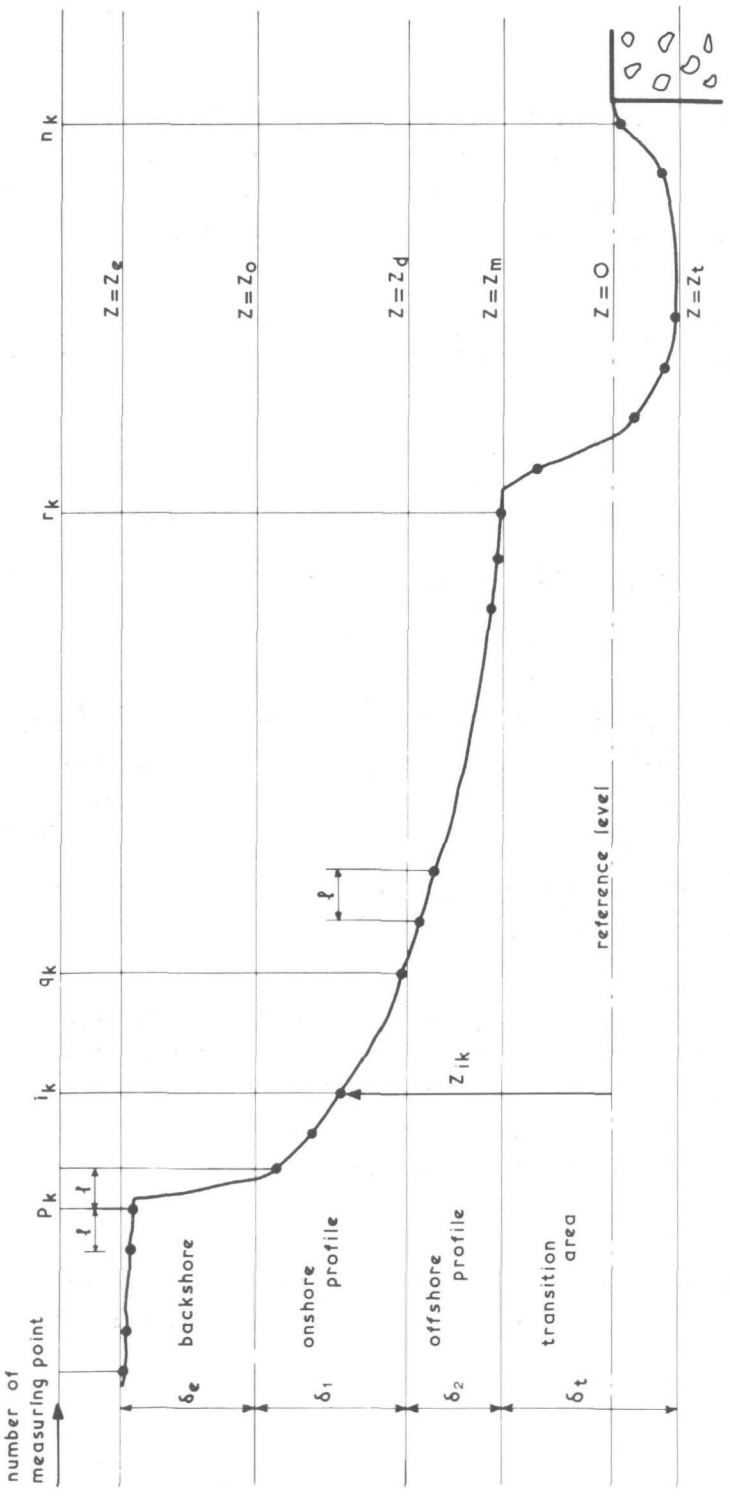

CROSS-SECTION : SECTION k

FIGURE 54

(3) The schematized lengths $L_e(t_j)$, $(L_2(t_j) - L_1(t_j))$ and $L_t(t_j)$ are calculated for each measuring section by computer from the corrected profiles, and are then averaged over all measuring sections.
From Figure 54 it can be seen for any time t_j that if the measuring sections are equally spaced:

$$L_e(t_j) = \frac{1}{N} \sum_{k=1}^{N} \left[\frac{1}{\delta_e} \sum_{i=1}^{p_k} (Z_{ik} - Z_0) \right] \tag{5.9}$$

$$L_1(t_j) = \frac{1}{N} \sum_{k=1}^{N} \left[\frac{1}{\delta_1} (\delta_1 p_k + \sum_{i=p_k+1}^{q_k} (Z_{ik} - Z_d)) \right] \tag{5.10}$$

$$L_2(t_j) = \frac{1}{N} \sum_{k=1}^{N} \left[\frac{1}{\delta_2} (\delta_2 q_k + \sum_{i=q_k+1}^{r_k} (Z_{ik} - Z_m)) \right] \tag{5.11}$$

$$L_2(t_j) - L_1(t_j) = \frac{1}{N} \sum_{k=1}^{N} \left[1(q_k - p_k) + \frac{1}{\delta_2} \sum_{i=q_k+1}^{r_k} (Z_{ik} - Z_m) - \frac{1}{\delta_1} \sum_{i=p_k+1}^{q_k} (Z_{ik} - Z_d) \right] \tag{5.12}$$

$$L_t(t_j) = \frac{1}{N} \sum_{k=1}^{N} \left[\frac{1}{\delta_t} (\delta_t r_k + \sum_{i=r_k+1}^{n_k} (Z_{ik} - Z_t)) \right] \tag{5.13}$$

where $L_e(t_j)$, $L_1(t_j)$, $L_2(t_j)$ and $L_t(t_j)$ are the mean values of L_e, L_1, L_2 and L_t respectively at any time t_j; p_k, q_k, r_k and n_k are the number of measuring points in the k^{th} section, from the landward extremity of the profile to the most seaward point in the backshore area, onshore profile, offshore profile and transition area respectively (see Figure 54). N is the number of measuring sections.

(4) With the aid of the method of least squares those values of s_e and W_e and of s_t and W_t respectively are chosen for which the values of

$(L_e(t_j)_{theor.} - L_e(t_j)_{measured})^2$ and $(L_t(t_j)_{theor.} - L_t(t_j)_{measured})^2$ are a minimum,

where: $L_e(t_j)_{theor.} = L_{e\infty} + W_e \exp\left(\frac{-s_e t_j}{\delta_e}\right)$ (5.14)

(equation (4.71))

$$L_t(t_j)_{theor.} = L_{t\infty} - W_t \exp\left(\frac{-s_t t_j}{\delta_t}\right) \quad (5.15)$$

(equation(4.82))

If $s_t t_j/\delta_t \longrightarrow 0$, $L_t(t_j)_{theor.}$ can be approximated as:

$$L_t(t_j)_{theor.} = L_{t0} + s_t^* t_j \quad (5.16)$$

(equation(4.87))

In the last-mentioned case s_t^* can be found by means of a regression analysis.

(5) Calculate the optimal values of s_y and W, for which $\left[(L_2(t_j) - L_1(t_j))_{theor.} - (L_2(t_j) - L_1(t_j))_{measured}\right]^2$ = minimum, with the method of least squares.

$$\left[L_2(t_j)-L_1(t_j)\right]_{theor.} = W-(W-(L_2-L_1)_0)\exp\left(\frac{-\delta s_y t_j}{\delta_1\delta_2}\right)+ \frac{\delta_t s_t W_t \delta_1}{\delta_t\delta s_y-\delta_1\delta_2 s_t}\left[\exp\left(\frac{-\delta s_y t_j}{\delta_1\delta_2}\right) + \right.$$

$$\left. - \exp\left(-\frac{s_t t_j}{\delta_t}\right)\right]+ \frac{\delta_e s_e W_e \delta_2}{\delta_e\delta s_y - \delta_1\delta_2 s_e}\left[\exp\left(\frac{-\delta s_y t_j}{\delta_1\delta_2}\right) - \exp\left(\frac{-s_e t_j}{\delta_e}\right)\right] \quad (5.17)$$

(equation (4.99))

If, however, $s_t t_j/\delta_t \longrightarrow 0$ (i.e. either $s_t/\delta_t \longrightarrow 0$, or t_j small, or both):

$$\left[L_2(t_j) - L_1(t_j)\right]_{theor.} = W - (W - (L_2 - L_1)_0)\exp\left(\frac{-\delta s_y t_j}{\delta_1 \delta_2}\right) + \frac{\delta_t s_t^* \delta_1}{\delta s_y} *$$

$$* \left[\exp\left(\frac{-\delta s_y t_j}{\delta_1 \delta_2}\right) - 1\right] + \frac{\delta_e s_e W_e \delta_2}{\delta_e \delta s_y - \delta_1 \delta_2 s_e}\left[\exp\left(\frac{-\delta s_y t_j}{\delta_1 \delta_2}\right) - \exp\left(\frac{-s_e t_j}{\delta_e}\right)\right] \quad (5.18)$$

(equation (4.101))

Steps (3) and (5) can be repeated for different values of Z_d, with the restriction that $Z_0 \geqslant Z_d \geqslant Z_m$. In such a way the variation of s_y and W over the D-profile can be found.

Prototype data

In Chapter 6 a method will be developed, with which the equilibrium profile can be determined with the aid of data of type A.
When data of type B are available, the relationship found with the aid of data of type A can be used to determine the equilibrium profiles corresponding with the different sets of data of type B.

(1) With the aid of the profile forms before and after the storm and the calculated equilibrium profile, values of $(L_2(t_0) - L_1(t_0)), (L_2(t_1) - L_1(t_1))$ and W can be calculated.

(2) The amount of backshore erosion during the storm can be calculated from the two available profiles (before and after the storm respectively), and introduced as boundary condition into equation (5.17), with W_t, $s_t \longrightarrow 0$. As s_y is the only unknown quantity in equation (5.17), it can be calculated.
This method was not used to assist in the derivation of the relationship for s_y. However, as soon as more reliable data of type B are available,

this procedure can be applied to determine with more accuracy s_y-values for prototype.

5.5 Statistical analysis of the data

As has been stated earlier, physically-based empirical relationships will be derived in Chapter 6 to enable the calculation of onshore-offshore transport. In order to enable the evaluation of the applicability of the relationships, the degree to which the relationships fit the data is of importance. Mostly the regression curve through the data is not a straight line. However, from the physical background of the process and a graphical analysis of the data, it will always be possible to find such transformation functions that the regression curve can be represented as a linear relationship between the transformed variables, i.e. if the original function is of the form

$$y = f(x) \tag{5.19}$$

where $f(x)$ is a non-linear function of x, the curve can be transformed to read:

$$Y = \overline{Y} + b\,(F(x) - \overline{F(x)}) \tag{5.20}$$

where $$\overline{Y} = \frac{1}{n} \sum_{i=1}^{n} Y_i \tag{5.21}$$

$\overline{Y}$ = the average value of all the Y_i-values

n = number of observations

$$\overline{F(x)} = \frac{1}{n} \sum_{i=1}^{n} F(x_i) \tag{5.22}$$

= the average value of all the $F(x_i)$-values

b = the slope of the regression line of Y against $F(x)$.

The theory of linear regression can now be applied to the transformed observations if it is assumed that the points (x, y), after having been transformed to (F (x), Y), are grouped around the straight line of equation (5.20) in such a manner that Y is normally distributed.
The correlation coefficient ρ (F (x), Y) can be used as a measure for the linearity of the transformed variables. An estimate of ρ is the correlation coefficient r (F (x), Y) of the data:

$$r\,(F\,(x),\,Y) = \frac{\sum_{i=1}^{n} (F\,(x_i) - \overline{F\,(x)})\,(Y_i - \overline{Y})}{\sqrt{\sum_{i=1}^{n} (F\,(x_i) - \overline{F\,(x)})^2 \sum_{i=1}^{n} (Y_i - \overline{Y})^2}} \qquad (5.23)$$

If F (x) and Y are stochastically independent, r = 0.
If $Y = \overline{Y} + b\,(F\,(x) - \overline{F\,(x)})$, $r = \pm 1$. The sign of r is the same as that of b. For all sets of data the appropriate value of the correlation coefficient r, calculated with the aid of equation (5.23), is given in the figure in which the data are represented. The value of b can be determined by choosing it in such a way that

$$S\,(b) = \sum_{i=1}^{n} \left[Y_i - \overline{Y} - b\,(F\,(x_i) - \overline{F\,(x)} \right]^2$$

is a minimum.
This can be done by differentiating S (b) to b and equating it to zero, with as a result:

$$b = \frac{\sum_{i=1}^{n} Y_i\,(F\,(x_i) - \overline{F\,(x)})}{\sum_{i=1}^{n} (F\,(x_i) - \overline{F\,(x)})^2} \qquad (5.24)$$

When two sets of data, which have each formed the basis of a regression analysis in the manner as described above, are to be compared with each other, the following approximate method can be used.
Let the equations of the two regression lines be:

$$Y^{(1)} = \overline{Y}_1 + b_1 \left(F(x) - \overline{F(x)}\right) \tag{5.25}$$

$$Y^{(2)} = \overline{Y}_2 + b_2 \left(F(x) - \overline{F(x)}\right) \tag{5.26}$$

From each set of observations three quantities have been determined, viz. the mean value $\overline{Y}$ of Y, the slope b of the line and the variance s^2. The values $(\overline{Y}_1, b_1, s_1^2; \overline{Y}_2, b_2, s_2^2)$ are estimates of the corresponding values $(\alpha_1, \beta_1, \sigma_1^2; \alpha_2, \beta_2, \sigma_2^2)$ for the two populations. The two populations can be compared with each other by comparing the estimates of the above-mentioned three parameters. In the following a summary of the steps that will have to be followed are given; for a more detailed analysis reference is made to Hald [16].

(1) Firstly the hypothesis that $\sigma_1^2 = \sigma_2^2$ is tested by means of the variance ratio $v^2 = s_1^2/s_2^2$. Values of v^2 can be found in the tables compiled by Hald [17]. If no significant difference exists between the variance, the slopes of the lines may be compared by means of the t-test. There is no exact test available for the comparison of the slopes if the variances do differ significantly (values of t are listed in Hald [17]).

(2) If, when the slopes are compared by means of the t-test, the value of t is not significant, the lines may be considered parallel.

(3) If the constant terms, i.e. the terms of the form $(\overline{Y} - b\,\overline{F(x)})$, are also equal, the two regression lines are identical.

(4) If the two regression lines are identical the quantity

$$u = \frac{\hat{b} - \bar{b}}{\sqrt{V\left\{\hat{b} - \bar{b}\right\}}} \qquad (5.27)$$

will be normally distributed.

$\hat{b}$ = the slope of the straight line which connects the points $(\overline{F(x_1)}, \overline{Y_1})$ and $(\overline{F(x_2)}, \overline{Y_2})$

$\bar{b}$ = the weighted mean of the slopes b_1 and b_2

$V(\hat{b}-\bar{b})$ = the variance of the quantity $(\hat{b} - \bar{b})$.

When u is calculated for the two available sets of data, it will have a t-distribution. The hypothesis that the constant terms are equal can accordingly be tested by applying the t-test. If the value of t is not significant, the constant terms do not differ significantly.
If both the v^2-test in (1) and the t-tests in (2) and (4) give values which are not significant, it can be concluded that the two regression lines do not differ significantly from each other.

The above-mentioned statistical methods are only approximations, however, as no more precise methods are available, they have been used to gain some insight into the reliability of the empirical relationships.

Chapter 6: Results and analysis of the data

6.1 General

The results of the extrapolation of the two- and three-dimensional model tests to an equilibrium situation are presented in the form as shown in Figure 47 (Chapter 4) for test 7301B. The graph of W against δ_1/δ defines the equilibrium profile. If this graph is used in conjunction with the graph of s_y against δ_1/δ, the offshore transport at any depth in the D-profile can be calculated.

In the case of the equilibrium profile characteristics the two-dimensional model results will be studied firstly, afterwards the effect of the three-dimensional model conditions on this result will be evaluated. Equilibrium situations in prototype can normally not be predicted in the same manner as for model tests. It will, however, be shown that the available prototype profiles are not in contradiction with the results obtained from the model tests.

Empirical relationships for the determination of s_y will be derived with the aid of the two-dimensional tests (model- as well as prototype-size). Afterwards the effect of three-dimensional model conditions on this result will be evaluated. Due to incompleteness of the available data it is not possible to determine with sufficient accuracy s_y-values for prototype. With the aid of a calculated example regarding the February, 1953 - storm on the Dutch coast it will, however, be shown that the empirical relationships, based on the available data, can be used with success to predict offshore transports in prototype.

6.2 Equilibrium profile characteristics

In Chapter 3 the total volume of sand in the equilibrium D-profile was related to a reference value of W, viz. W_r, if the division between onshore and offshore profile is made at an elevation Z_r above the reference level. The graph of W against δ_1/δ can be fully defined if this value of W_r is known, as well as the distribution of W/W_r in the rest of the

profile. The choice of the reference elevation Z_r must be made in such a way that the value of W_r can be correlated to the wave and sediment characteristics.

The author [48] did tests with various initial beach slopes m_0 to find a criterion for the division between eroding and accreting profiles. Eroding profiles were those in which sand was eroded from above the still-water level. He found that the neutral profile (no erosion or accretion relative to the water line) is defined by:

$$m_0 = f\left(\frac{\sqrt{g\,H_0}}{w}, \frac{H_0}{\lambda_0}\right) \qquad (6.1)$$

where m_0 = initial average beach slope at the still-water level
g = gravitational acceleration
w = sediment particle fall velocity
H_0 = deepwater wave height
λ_0 = deepwater wave length.

He represented his results in the form of a relationship between $m_0(H_0/\lambda_0)$ and $\sqrt{g\,H_0 m_0}/w$. The neutral profile for all investigated slopes could be represented by one line. It is evident that the neutral profile as defined in [48] corresponds with the situation where the profile is in equilibrium for a division between the onshore and offshore profile situated at the still-water line. In order to allow the application of this result in the present study, the definitions of erosion and accretion will be adapted as follows:

(1) erosion occurs if $(L_2 - L_1)_r$ increases
(2) accretion occurs if $(L_2 - L_1)_r$ decreases.

$(L_2 - L_1)_r$ is the value of $(L_2 - L_1)$ for a division between the onshore and offshore profile at the still-water level.

In equation (6.1) m_0 will then be replaced by a characteristic slope m_r:

$$m_r = \frac{\delta}{2W_r} = f\left(\frac{\sqrt{g\,H_0}}{w}, \frac{H_0}{\lambda_0}\right) \qquad (6.2)$$

m_r represents the average slope of the schematized equilibrium D-profile, for a division between the onshore and offshore profile at the still-water level. For this reason the choice of Z_r at the still-water level seems a realistic one, furthermore, the still-water line is an easily determinable location in the profile. The value of W_r will determine the horizontal scale of the equilibrium profile, while W/W_r will define the form of the dimensionless equilibrium profile.

Dimensionless form of the equilibrium D-profile

Wiegel [53] classified beaches into three groups, viz. protected beaches, moderately protected beaches and exposed beaches. The classification is based on the amount of energy which is dissipated by the waves on their way to the beach. For each of these types of beaches Wiegel gives a relationship between the particle diameter D_{50} and the beach slope α_1 in the area bordered by the limit of wave run-up and the low-water line (the wetted beach) of the form:

$$\alpha_1 = a_1 D_{50}^{b_1} \tag{6.3}$$

where D_{50} = particle diameter
α_1 = wetted beach slope
a_1, b_1 = constants dependent of the type of beach under consideration.

For all three types of beaches $b_1 > 0$. This means that larger particle diameters will lead to steeper wetted beach slopes. Eagleson et al. [11] studied the forces on a discrete spherical bed load particle outside the breaker zone under wave action. From the onshore-offshore bed load mechanics they found that for particles in oscillating equilibrium the bed slope is given by:

$$\sin\alpha_2 = \frac{K}{J} f_1 \left(\frac{d}{\lambda_0}\right) \tag{6.4}$$

where $\sin\alpha_2$ = bed slope in the area outside the breaker zone, where all transport takes place as bed load

$$K = 0.28\,\pi^2 \left(\frac{H_0}{\lambda_0}\right)^2 \frac{D_{50}}{\lambda_0} \left(\beta\, D_{50}\right)^{8/7} \quad \text{(in m/s)} \tag{6.5}$$

$$J = 2.12 \pm 10^{-2} \frac{D_{50}}{\nu} \sqrt{Tg} \left(\frac{D_{50}}{\lambda_0}\right)^2 \Delta_s \quad \text{(in m/s)} \tag{6.6}$$

$$f_1\left(\frac{d}{\lambda_0}\right) = \frac{\coth^2\left(\frac{2\pi d}{\lambda}\right)}{\sinh^2\left(\frac{2\pi d}{\lambda}\right) + \frac{2\pi d}{\lambda_0}} \tag{6.7}$$

$\Delta_s = \frac{\rho_s - \rho_w}{\rho_w}$ = relative density of bed material

ν = kinematic viscosity

T = wave period

$$\beta = \left(\frac{\pi}{\nu T}\right)^{1/2} \tag{6.8}$$

At a specific location in the profile (fixed depth) and for a given set of boundary conditions (H, T), the bed slope $\sin\alpha_2$ is proportional to K/J. From equations (6.5), (6.6) and (6.8) it follows that:

$$\frac{K}{J} = \left(\frac{250.7\,\lambda_0 \left(\frac{H_0}{\lambda_0}\right)^2 \nu^{3/7}}{\Delta_s\, T^{11/7}\, g}\right) D_{50}^{-6/7} \tag{6.9}$$

This implies that for a given set of wave conditions the bed slope in the area outside the breaker zone will be a function of the particle diameter. Increasing particle diameters will lead to decreasing slopes, i.e.

$$\alpha_2 = a_2\, D_{50}^{-6/7} \tag{6.10}$$

where: $\alpha_2 = \sin\alpha_2$ for small slopes

a_2 = a constant for a given set of boundary conditions, dependent of the location.

The above-mentioned results (equations (6.3) and (6.10)) imply that the equilibrium profile will become more concave upwards for increasing particle diameters. Consequently it can be stated that the form of the equilibrium profile will be a function of the particle diameter.

$$Y = A\, f\,(D_{50},\, Z) \tag{6.11}$$

where Y = ordinate in the equilibrium profile at elevation Z

A = a scale factor, which will be determined by the wave conditions.

However, the form of the equilibrium profile can also be found from equation (3.69), which reads:

$$Y = \left(\frac{Z_r - Z_m}{Z_0 - Z_m}\right) W_r - \left(\frac{1}{Z_0 - Z_m}\right)\frac{\partial}{\partial Z}\,(WZ^2) + \left(\frac{Z_0 + Z_m}{Z_0 - Z_m}\right)\frac{\partial}{\partial Z}\,(WZ) - \left(\frac{Z_0\, Z_m}{Z_0 - Z_m}\right)\frac{\partial W}{\partial Z} \tag{6.12}$$

Y is defined relative to the equilibrium position of the sediment in the area of the profile defined by $Z_0 \geqslant Z \geqslant Z_r$.

The reference level (Z = 0) for the elevations will be chosen at the lower extremity of the D-profile. Consequently:

$$\left.\begin{aligned} Z_m &= 0 \\ Z_0 - Z_m &= \delta \\ Z_r - Z_m &= h_m \end{aligned}\right\} \tag{6.13}$$

Substitution of the equations (6.13) into equation (6.12) and division by W_r yields:

$$\frac{Y}{W_r} = \frac{h_m}{\delta} + \frac{\partial}{\partial Z}\left[\frac{W}{W_r}\,(Z - Z^2/\delta)\right] \tag{6.14}$$

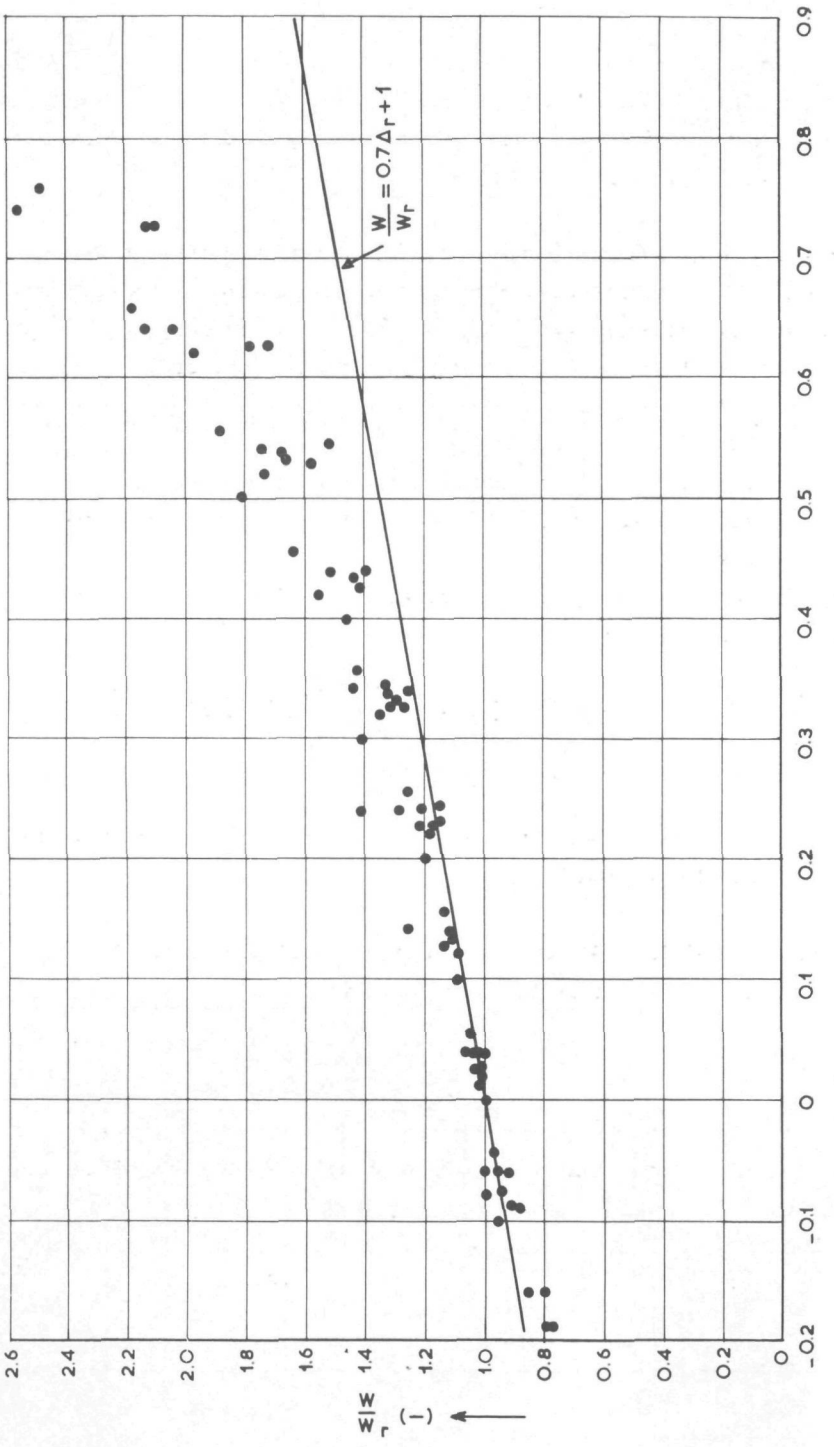

REMARK: $\Delta_r = \frac{h_m - \delta_2}{\delta}$

W/W_r-VALUES FOR $D_{50} = 0.22$ mm
FIGURE 55

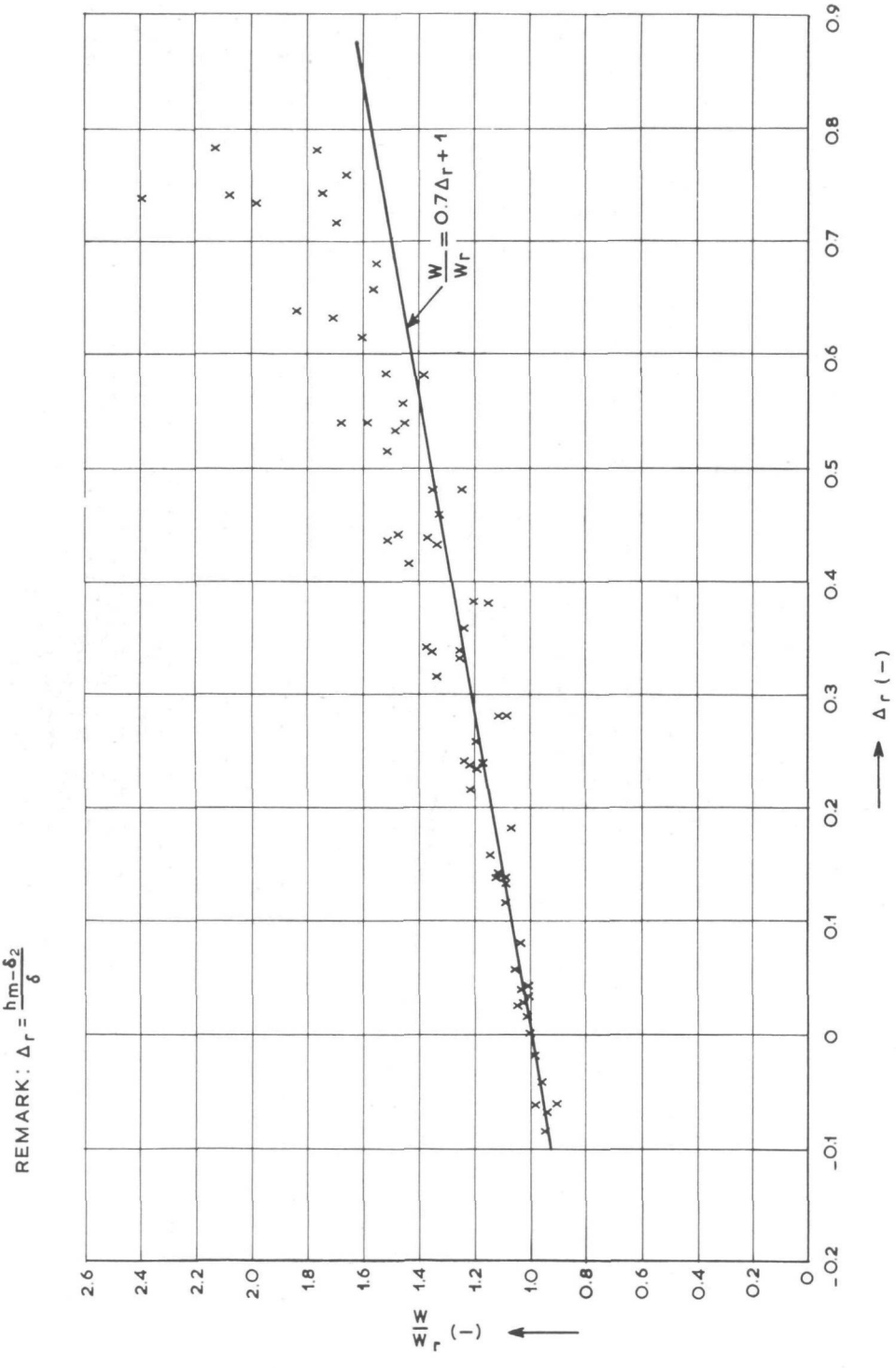

W/W_r – VALUES FOR $D_{50} = 0.165$mm

FIGURE 56

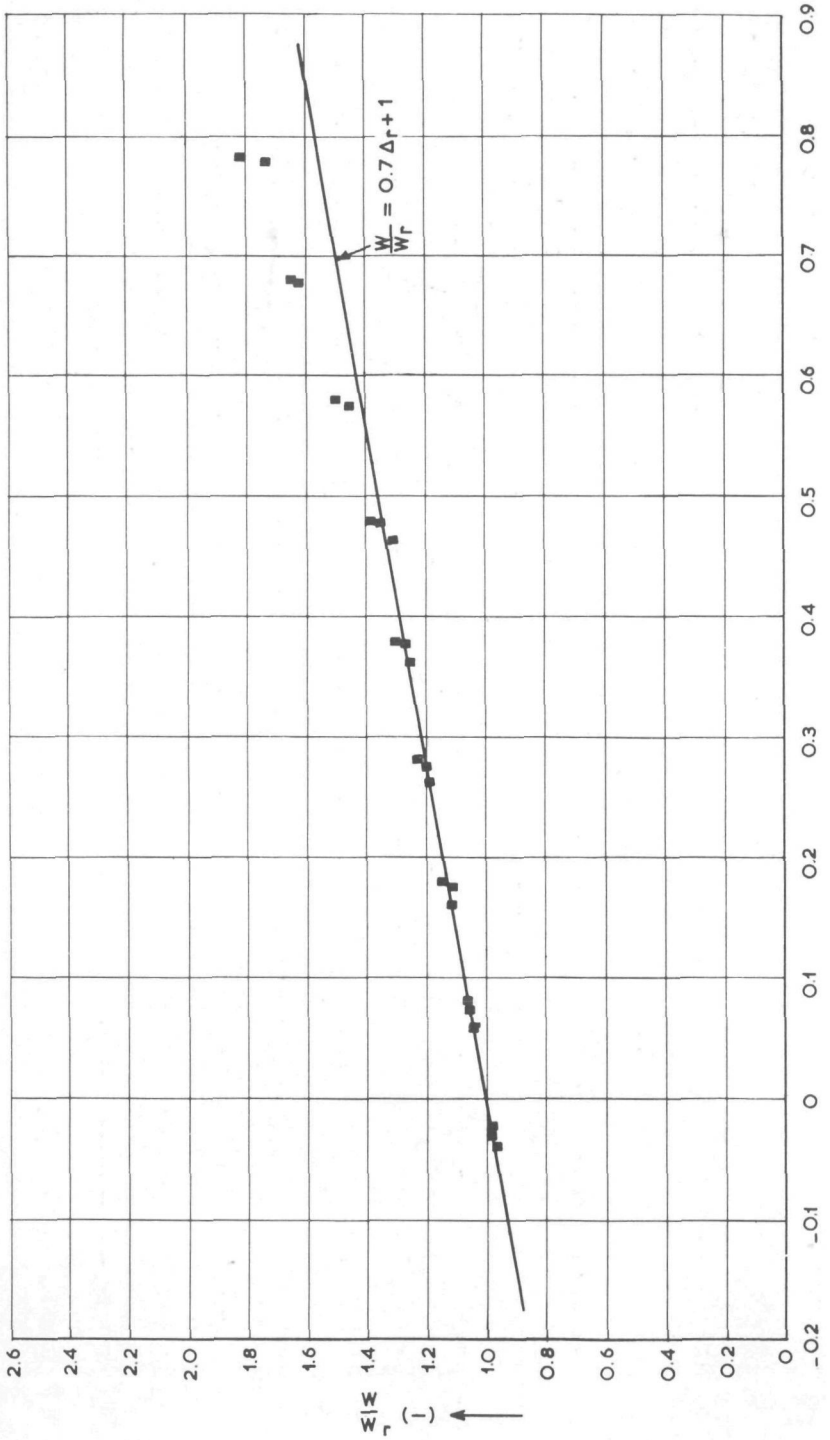

REMARK: $\Delta_r = \frac{h_m - \delta_2}{\delta}$

W/W_r – VALUES FOR $D_{50} = 0.11$ mm

FIGURE 57

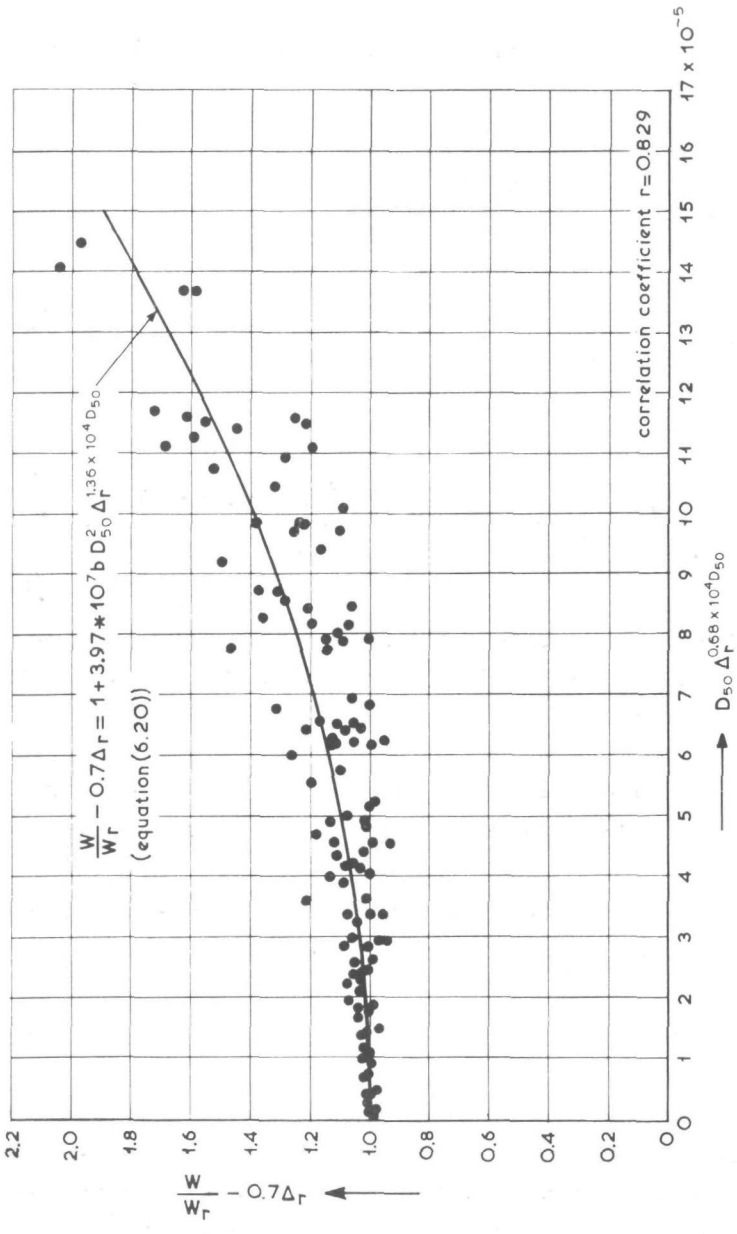

REMARK : D_{50} in m

GENERAL RELATIONSHIP FOR W/W_r
(TWO-DIMENSIONAL CASES)
FIGURE 58

If equation (6.14) is differentiated twice with respect to Z, the curvature of the dimensionless equilibrium profile Y/W_r can be found, viz.:

$$\frac{\partial^2(Y/W_r)}{\partial Z^2} = \frac{\partial^3}{\partial Z^3}\left(\frac{W}{W_r}(Z - Z^2/\delta)\right)$$

$$= (Z - Z^2/\delta)\frac{\partial^3}{\partial Z^3}\left(\frac{W}{W_r}\right) + 3\,(1 - 2Z/\delta)\frac{\partial^2}{\partial Z^2}\left(\frac{W}{W_r}\right) - (6/\delta)\frac{\partial}{\partial Z}\left(\frac{W}{W_r}\right)$$

$$= \left[(Z - Z^2/\delta)\frac{\partial^3}{\partial Z^3}\left(\frac{W}{W_r}\right) - (6/\delta)\frac{\partial}{\partial Z}\left(\frac{W}{W_r}\right)\right] + 3(1 - 2Z/\delta)\frac{\partial^2}{\partial Z^2}\left(\frac{W}{W_r}\right) \qquad (6.15)$$

It can be seen from equation (6.15) that the form of the Y/W_r-line, i.e. the form of the dimensionless equilibrium D-profile, is clearly related to the form of the W/W_r-line.

In Figures 55 ... 57 the W/W_r-values are given for the three different particle diameters used in the present study. A study of these three figures reveals:

(1) At the water line ($Z = Z_r$, $W = W_r$, $\Delta_r = 0$), the slopes of the three curves are the same, i.e. for all the investigated values of D_{50}:

$$\frac{\partial\,(W/W_r)}{\partial Z} = \text{constant} \qquad (6.16)$$

when $Z \longrightarrow Z_r$

(2) The curvature of the W/W_r-curve increases with increasing particle diameter. This is correspondence with the conclusion which was made earlier after studying the results of Wiegel [53] and Eagleson et al. [11] (equations 6.3) and (6.10) respectively). Seeing that such a clear

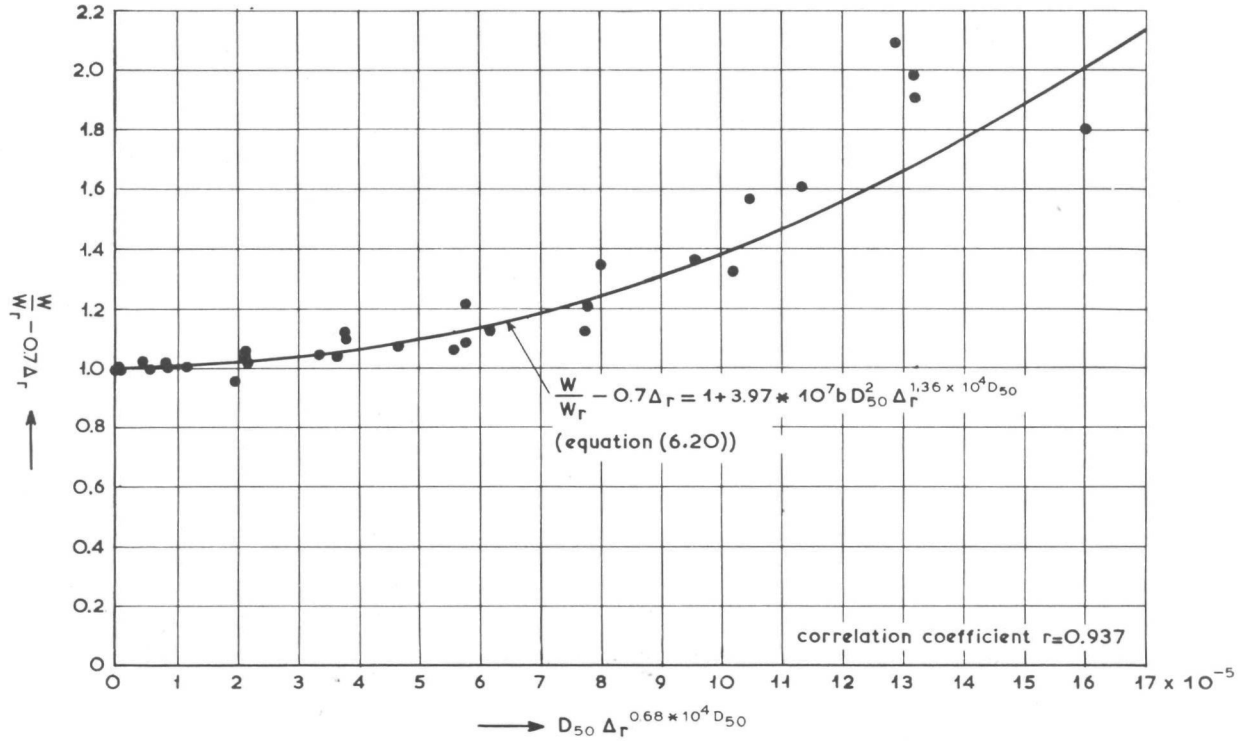

REMARK : D_{50} in m

W/W_r-VALUES FOR THREE-DIMENSIONAL MODEL TESTS

FIGURE 59

relationship exists between the form of the equilibrium profile and the form of the W/W_r-graph (equations (6.12) and (6.15)), it will be assumed that:

$$\frac{W}{W_r} = f\ (D_{50},\ \Delta_r) \tag{6.17}$$

$$\text{where } \Delta_r = \frac{h_m - \delta_2}{\delta} \tag{6.18}$$

Δ_r denotes the location in the profile, in vertical sense, relative to the still-water line. The results (1) and (2) above can be combined with equation (6.17) to yield an equation of the form:

$$\frac{W}{W_r} = a\Delta_r + \phi\ (D_{50},\ \Delta_r) \tag{6.19}$$

By using all the available two-dimensional data (Figures 55 ... 57) equation (6.19) was found to read:

$$\frac{W}{W_r} = 0.7\ \Delta_r + 1 + 3.97 \pm 10^7\ b\ D_{50}^2\ \Delta_r^{1.36 \pm 10^4\ D_{50}} \tag{6.20}$$

$$\text{where } b = \begin{cases} 1 \text{ for } \Delta_r > 0 \text{ (below still-water level)} \\ 0 \text{ for } \Delta_r \leqslant 0 \text{ (above still-water level).} \end{cases} \tag{6.21}$$

Equation (6.20) is plotted in Figure 58 together with the data used for its determination. The data are listed in Table X. It now remains to investigate the effect of three-dimensional model conditions on the form of W/W_r, as well as to evaluate the magnitude of possible scale effects when extrapolating to prototype conditions. The W/W_r-values as determined for the available three-dimensional model tests are listed in Table XI and are given in Figure 59 together with the curve of equation (6.20). When $Y = W/W_r - 0.7\ \Delta_r$ and $F(x) = b\ D_{50}^2\ \Delta_r^{1.36 \pm 10^4\ D_{50}}$ (see Chapter 5.5), a statistical analysis of the data in the manner as described in Chapter 5.5 leads to the conclusion that the three-dimensional model data do not differ significantly from the line predicted by equation (6.20). It will

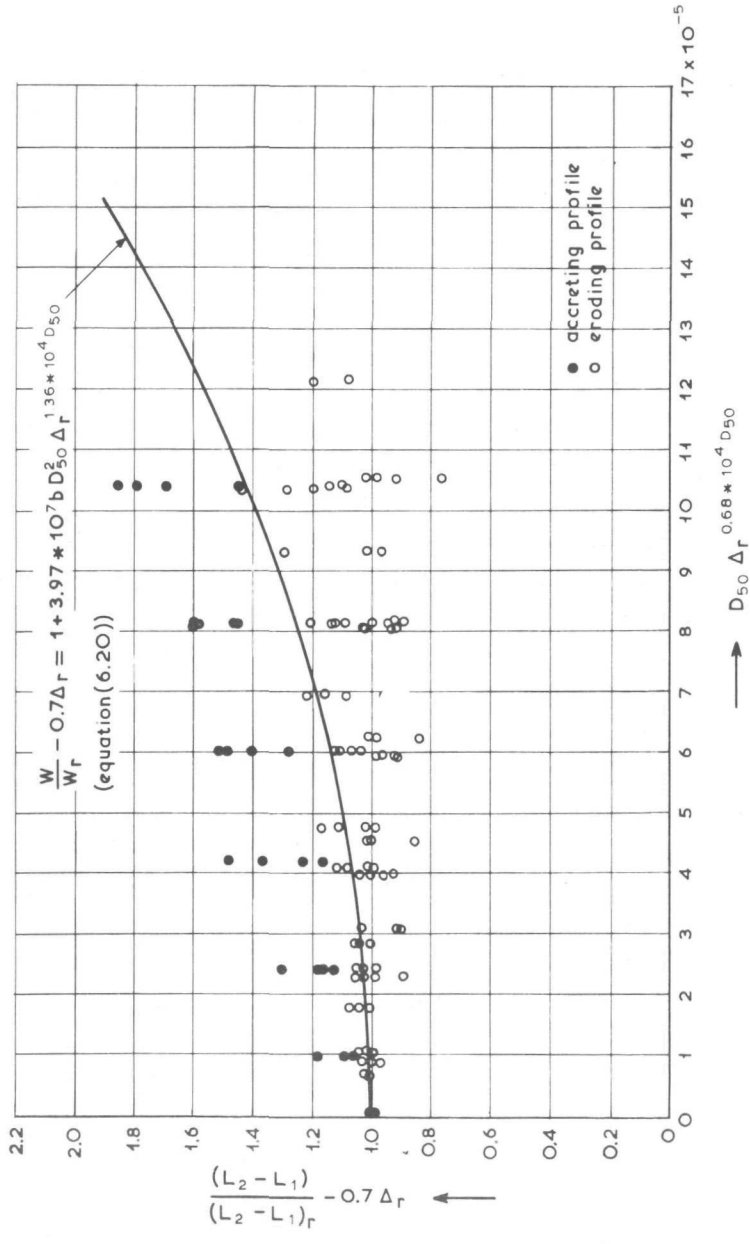

REMARK: D_{50} in m

$\frac{(L_2-L_1)}{(L_2-L_1)_r}$ - VALUES FOR PROTOTYPE CASES

FIGURE 60

consequently be assumed that equation (6.20) also applies to three-dimensional model conditions. It should be stressed that this does not necessarily mean that the two-dimensional and three-dimensional profiles are the same for corresponding wave conditions, it only means that the forms of the dimensionless profiles are the same. The effect of the three-dimensionality on the scale of the profile, i.e. on W_r, will be studied later in this section.

Due to the fact that the boundary conditions (i.e. wave height, period, direction; water level; wind direction, velocity) vary continuously in time, it is not possible to determine the resemblance of equation (6.20) with the form of prototype equilibrium profiles. However, it is possible to show that the result is not in contradiction with available prototype profile forms. If at any given location in the profile the resultant transport is in seaward direction, it is obvious that $(L_2 - L_1)$ must increase. On the other hand, if the resultant transport at a given location is in landward direction, $(L_2 - L_1)$ will decrease.
The model test results showed that in a developing profile the $(L_2 - L_1)$-values at any location in the D-profile, below the water line, showed a bigger rate of change than that of $(L_2 - L_1)_r$ at the water line. Consequently it can be stated that if the resultant transport at any given location in the profile is in seaward direction, $(L_2 - L_1)/(L_2 - L_1)_r$ will increase, while $(L_2 - L_1)/(L_2 - L_1)_r$ will decrease for a resulting transport in landward direction.
In Figure 60 the $(L_2-L_1)/(L_2-L_1)_r$-values for all available prototype profile data, for which the profiles were measured to a big enough water depth, are given together with the curve of equation (6.20). The data are listed in Table XII.
In Figure 61 the same data are plotted against the dimensionless depth in the profile. The curve of equation (6.20) clearly marks the division between eroding and accreting profiles fairly accurately over the full depth of the D-profile. Consequently it follows that the form of the dimensionless D-profile, as predicted with the aid of equation (6.20), can be applied to determine the three-dimensional prototype equilibrium

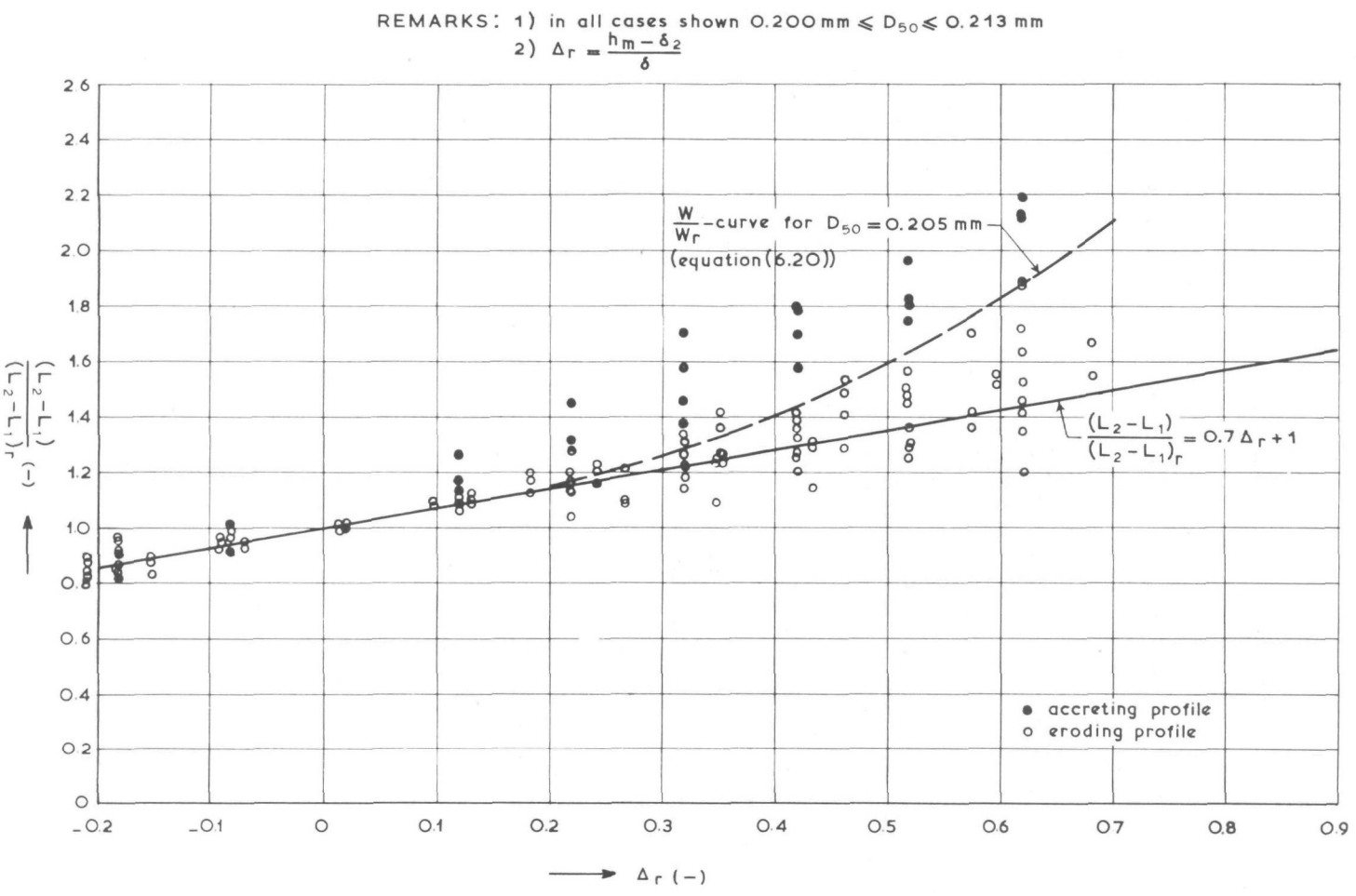

GENERAL PROTOTYPE PROFILE DATA

FIGURE 6.1

D-profile over the full depth of the D-profile.
Equation (6.20) will thus be used to determine the distribution of W/W_r for both model and prototype cases. The only restriction that will have to be made, is that no large gradients in longshore transport must exist, as such cases have not been incorporated in the present study.

Horizontal scale of the equilibrium profile

As stated earlier, the author [48] found the neutral slope (i.e. neither erosion nor accretion) at the water line to be determined by $f\ (\sqrt{gH_0}/w,\ H_0/\lambda_0)$. In terms of the definitions in the present study, this result can be used to find the schematized equilibrium slope at the water line, viz.:

$$m_r \frac{H_0}{\lambda_0} = f\ (\frac{\sqrt{g\ H_0}}{w}\ ,\ \frac{H_0}{\lambda_0}) \qquad (6.22)$$

The only bed material used in the present study was sand, consequently equation (6.22) can be rewritten as:

$$m_r \frac{H_0}{\lambda_0} = f\ (\frac{\sqrt{H_0}}{D_{50}^{b_2}}\ ,\ \frac{H_0}{\lambda_0})$$

where b_2 is a constant.
In general

$$m_r \frac{H_0}{\lambda_0} = f\ (H_0^a,\ D_{50}^b,\ (\frac{H_0}{\lambda_0})^c) \qquad (6.23)$$

where a, b and c are constants.

When the values of W_r, as determined for the two-dimensional model tests, were processed according to equation (6.23), it was found that:

$$m_r \frac{H_0}{\lambda_0} = f\left[H_0^{0.132}\ D_{50}^{-0.447}\ (\frac{H_0}{\lambda_0})^{-0.717}\right] \qquad (6.24)$$

REMARKS: 1) H_o, λ_o, D_{50} in m

2) $m_r = \frac{\delta}{2W_r}$

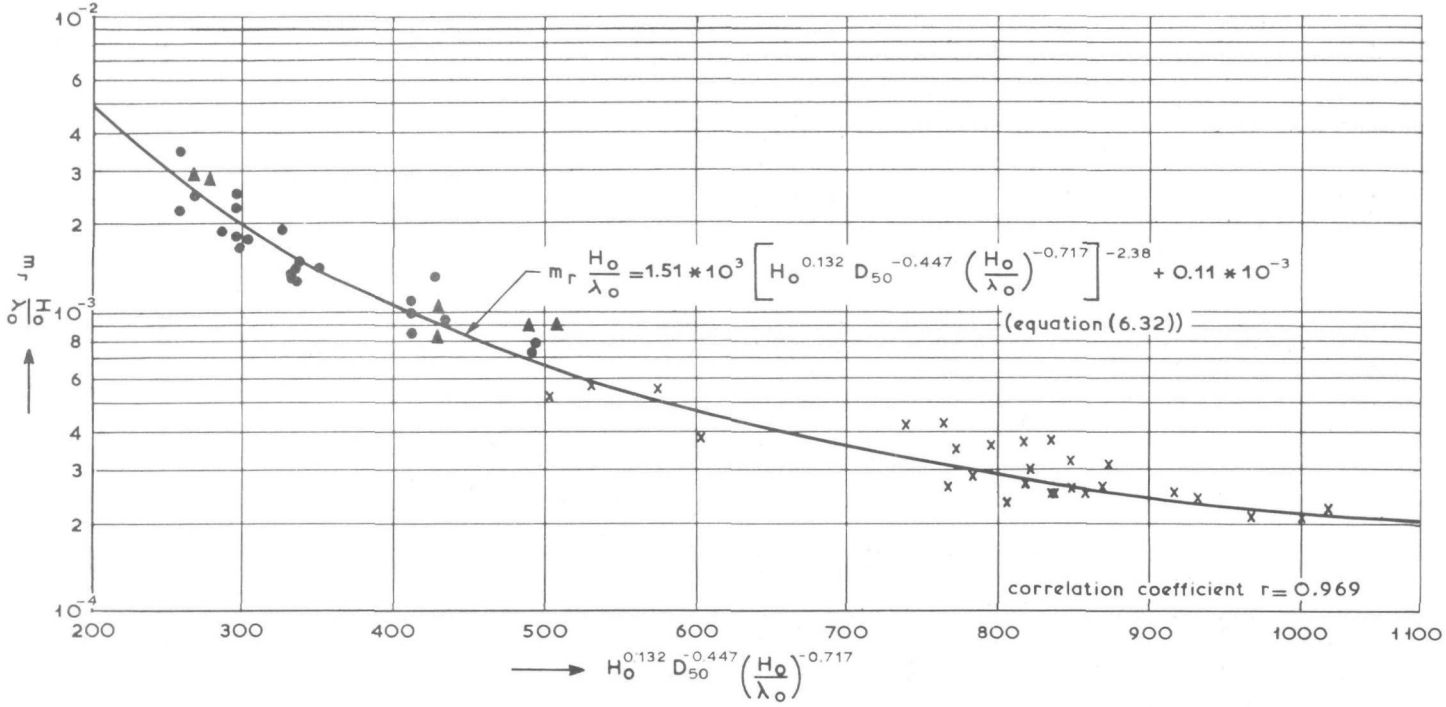

HORIZONTAL SCALE OF THE EQUILIBRIUM D-PROFILE

FIGURE 62

This result can be seen in Figure 62. The W_r-values as determined for the three-dimensional model tests are also included, it can be seen that although they represent slightly smaller W_r-values (i.e. slightly larger m_r-values, $m_r = \delta/2W_r$) than for corresponding two-dimensional cases, the difference is small with respect to the scatter in the two-dimensional model data. Both the two-dimensional and the three-dimensional model data are listed in Table XIII.

As can be seen from Figure 61, the forms of the prototype profiles, whether eroding or accreting, are in close resemblance with the predicted equilibrium profile forms in the vicinity of the water line. Furthermore, as stated earlier, equation (6.20) can be used to predict the equilibrium D-profile for prototype conditions. These two conclusions open the possibility to calculate the scale (W_r) of the equilibrium profile in the prototype in the following way:

The dimensionless profile Y/W_r can be calculated by substitution of the value of W/W_r (from equation (6.20))into the analytical equation for the equilibrium profile (equation(6.14)). For this purpose equation (6.20) will be written as:

$$\frac{W}{W_r} = 0.7\,\Delta_r + 1 + A_1 \Delta_r^{B_1} \tag{6.25}$$

where $A_1 = 3.97 \pm 10^7\, D_{50}^{2\,b}$ (6.26)

$B_1 = 1.36 \pm 10^4\, D_{50}$ (6.27)

Substitution of equation (6.18) into equation (6.25) yields:

$$\frac{W}{W_r} = (1 + 0.7\,\frac{h_m}{\delta}) - 0.7\,\frac{Z}{\delta} + A_1\,(\frac{h_m}{\delta} - \frac{Z}{\delta})^{B_1} \tag{6.28}$$

Equation (6.28) can now be substituted into equation (6.14):

$$\frac{Y}{W_r} = \frac{h_m}{\delta} + \frac{\partial}{\partial Z}\left[\left\{(1 + 0.7\,\frac{h_m}{\delta}) - 0.7\,\frac{Z}{\delta} + A_1\,(\frac{h_m}{\delta} - \frac{Z}{\delta})^{B_1}\right\}(Z - Z^2/\delta)\right]$$

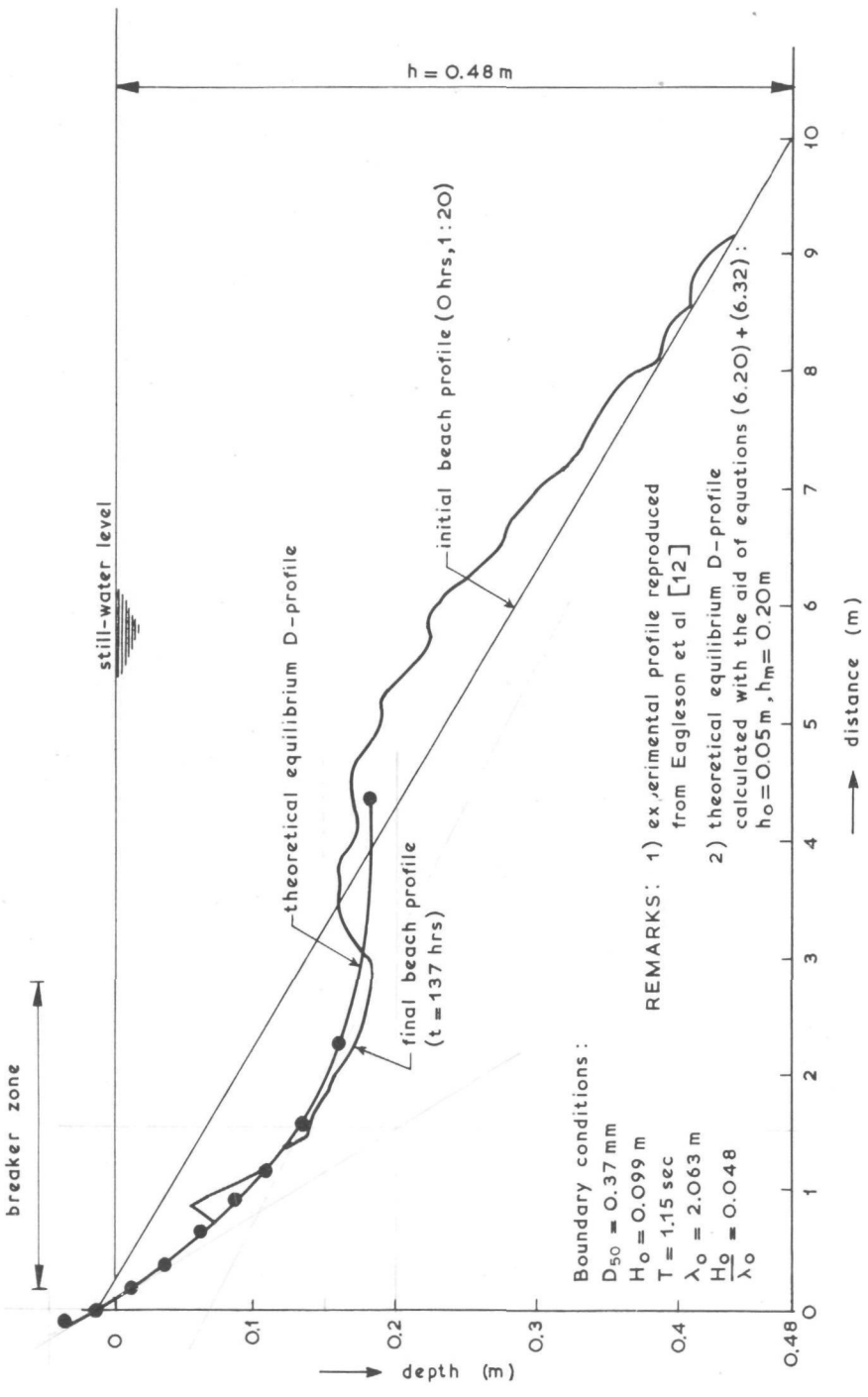

COMPARISON OF THEORETICAL AND EXPERIMENTAL EQUILIBRIUM PROFILES

FIGURE 63

$$= \frac{h_m}{\delta} + (1 + 0.7\frac{h_m}{\delta})(1 - \frac{2Z}{\delta}) - 0.7(\frac{2Z}{\delta}) + \frac{3 \pm 0.7Z^2}{\delta^2} +$$

$$- \frac{A_1 B_1}{\delta}(\frac{h_m}{\delta} - \frac{Z}{\delta})^{B_1 - 1} \pm (Z - Z^2/\delta) + A_1(\frac{h_m}{\delta} - \frac{Z}{\delta})^{B_1} \pm (1 - \frac{2Z}{\delta}) \qquad (6.29)$$

When the terms are regrouped and the substitution $z = \frac{Z}{\delta}$ is made, equation (6.29) becomes:

$$\frac{Y}{W_r} = (1 + 1.7\frac{h_m}{\delta}) - 2z(1.7 + 0.7\frac{h_m}{\delta}) + 2.1z^2 + A_1(\frac{h_m}{\delta} - z)^{B_1 - 1} \pm$$

$$\pm (\frac{h_m}{\delta} - (2\frac{h_m}{\delta} + 1 + B_1)z + (2 + B_1)z^2) \qquad (6.30)$$

Y is defined relative to the equilibrium position of the sediment in the area of the profile defined by $Z_0 \geqslant Z \geqslant Z_r$.
For a given set of boundary conditions (H_0, T, D_{50}) the values of h_m, δ, A_1 and B_1 can be calculated. By varying z from 1 (the upper limit of the D-profile) to 0 (the lower limit of the D-profile) the dimensionless form of the D-profile can be found. The value of W_r corresponding with the given boundary conditions is then that scale value which has to be applied to the dimensionless equilibrium D-profile (from equation (6.30)) to let the upper part of the predicted equilibrium D-profile coincide with the actual profile, in an area defined by:

$$-0.2 < \Delta_r < \approx 0.2 \qquad (6.31)$$

(see Figure 61)

For all available prototype data the value of W_r was determined in the above manner. These prototype data were added to the model data in Figure 62. The data are listed in Table XIII.

The curve giving the best fit through all the data is:

$$m_r \frac{H_0}{\lambda_c} = 1.51 \pm 10^3 \left[H_0^{0.132} \; D_{50}^{-0.447} \; \left(\frac{H_0}{\lambda_0}\right)^{-0.717} \right]^{-2.38} + 0.11 \pm 10^{-3} \quad (6.32)$$

For any given set of boundary conditions (incident wave height H_0, wave period T, bed material D_{50}) the value of W_r can be calculated with the aid of equation (6.32), where $W_r = \delta/(2m_r)$. The dimensionless form of the equilibrium profile can be calculated from equation (6.20). Combination of these two results yields the equilibrium profile for the given set of boundary conditions. In Figure 63 an equilibrium profile, calculated in the above manner, is compared with the actual equilibrium profile, formed after t = 137 hours (reproduced from Eagleson et al.[12]). As can be seen, the comparison is rather good.

6.3 Offshore transport: two-dimensional case

The result of the evaluation in the previous section can be used to calculate the offshore transport for a given set of boundary conditions, if the coastal constant s_y corresponding to the given boundary conditions is known. The curve defining s_y in terms of the dimensionless onshore profile thickness δ_1/δ can be fully described as soon as the following quantities are known:

(1) the magnitude of the maximum value of the coastal constant (s_{ym}) in the D-profile

(2) the location in the D-profile ($\delta_2 = \delta_{2m}$) where s_{ym} occurs

and (3) the dimensionless form (s_y/s_{ym}) of the distribution of the values of s_y in the D-profile.

In the analysis of Chapter 2 the momentary onshore-offshore transport was described as being the product of a momentary particle velocity and a momentary sediment concentration, i.e. by starting from the internal mechanism. The conclusion of the evaluation in Chapter 2 is that for a given set of boundary conditions the transport can be expressed in terms of an external time-dependent profile function P (t).

This means that by using the internal mechanism of the coastal process, a correlation was made between the onshore-offshore transport and the external beach profile characteristics. It follows from equations (2.14) ... (2.24) that the onshore-offshore transport can be written as:

$$\overline{S\,(d)} = S_y = f_1\,(P\,(t),\ H,\ T,\ h,\ D_{50}) \tag{6.33}$$

where $\overline{S\,(d)} = S_y$ = onshore-offshore transport at the location with an actual water depth d

$P\,(t)$ = a time-dependent characteristic bed profile quantity

H = local wave height

T = wave period

h = local still-water depth

D_{50} = particle diameter.

In equation (2.32) it is finally concluded that for a given set of boundary conditions:

$$\overline{S\,(d)} = \Phi\,(P\,(t),\ P\,(t_0)) - \Phi\,(P\,(\infty),\ P\,(t_0)) \tag{6.34}$$

where $P(\infty)$ is the value of $P(t)$ when time $t = \infty$. Consequently, the onshore-offshore transport $S_y (= \overline{S\,(d)})$ was written in the rest of this report as:

$$S_y = s_y\,(W - (L_2 - L_1)) \tag{6.35}$$

where $(L_2 - L_1)$ = schematized profile length, as discussed in detail in Chapters 3 and 4. $(L_2 - L_1) \xrightarrow{t \to \infty} W$

s_y = a coastal constant, assumed to be independent of the profile characteristics.

From equations (6.33) ... (6.35) it follows that:

$$s_y = f_2\,(H,\ T,\ h,\ D_{50}) \tag{6.36}$$

It has been shown in Chapter 6.2 that W is in turn also a function of the wave conditions.

In order to describe in more detail the form of the function f_2 in equation (6.36), a study was made of the available literature on onshore-offshore transport under wave action. Due to the lack of adequate sediment measurement techniques, measurements regarding the internal mechanism of sand transport are scarce, and when available, their reliability is unknown. The amount of available literature on the external characteristics of the coastal process (type of beach profile, direction of onshore-offshore transport,etc.) is, however, much larger.

Various investigators did tests to study the different types of beach profiles that can be formed. Beach profiles are classified into two categories, viz. storm profiles and normal profiles. Storm profiles are formed when sand is eroded from the beach, transported in seaward direction and deposited on a bar in the vicinity of the breaker point. Normal profiles are formed when material is transported in landward direction and deposited on the beach. A study of the type of beach profile which will be formed under a given set of boundary conditions will thus in fact show a strong resemblance with a study regarding the type of sediment transport (landward or seaward).

Waters [51] concluded that the type of beach profile which will be formed under two-dimensional conditions is governed by the deepwater wave steepness. Johnson [26] concluded from the results of the research of Waters that the type of coastal process (accretion, i.e. landward transport,or erosion, i.e. seaward transport) that will take place is governed solely by the deepwater wave steepness. The model tests of Waters [51], as well as those by Watts [52] and Scott [44] pointed to a critical wave steepness, which defines the transition from normal to storm profiles, which lies in the range $0.020 < H_0/\lambda_0 < 0.030$. Wave steepnesses lower than 0.020 will according to the above-mentioned result lead to normal profiles (accretion), while wave steepnesses higher than 0.030 will lead to storm profiles (erosion).

Saville [43] showed that the above-mentioned criterium for the determination of the type of profile, as derived under model conditions, does not apply to prototype conditions. Patrick and Wiegel [38] had earlier come to the same conclusion.
Motta [36], studying scale effects on the onshore-offshore coastal processes in models, found that the type of profile is governed by the type of material, the deepwater wave steepness H_0/λ_0 and the wave period T. Sitarz [47], measuring in prototype under ideal conditions (small tidal amplitude and practically no wind), found the critical deepwater wave height H_0 which will lead to a transition between erosion and accretion to be linearly related to the wave period T.
This implies that the coastal process is also a function of the absolute values of the wave height and period (i.e. of the scale). The critical deepwater wave steepness decreases with increasing wave height.

Rector [41] and Scott [44] found that larger particles move more readily in landward direction, while Motta [36] found that the critical deepwater wave steepness decreases for decreasing particle diameter. Iwagaki and Noda [25] found that the type of profile is determined by H_0/λ_0 and H_0/D_{50}, while Zwamborn and van Wyk [54], studying the effect of different bed materials, found the type of profile to be determined by H_0/λ_0 and $\sqrt{g\,H_0\,S_r}/w$, where H_0 is the deepwater wave height, w the bed material fall velocity and S_r the geometrical distortion of the model.

The author [48] concluded that the initial beach slope is of importance for the mode of transport (onshore or offshore). He presented his results in an adapted form of the criterium of Zwamborn and van Wyk, viz. in terms of m_0 (H_0/λ_0) and $\sqrt{g\,H_0 m_0}/w$, where m_0 is the initial beach slope at the water line.

Shinohara and Tsubaki [45] found that the equilibrium profile can be divided into two zones at the point where the waves break. The area landwards of the breaker point is determined only by the deepwater wave steepness H_0/λ_0, while the area seawards of it is determined by both H_0/λ_0

and the original profile. Kemp [30] suggested that the ratio between the wave run-up time and the wave period can be used to classify coastal profiles. The transition from eroding to accreting profiles will take place when the ratio is equal to unity.
Breaking waves can be classified mainly into two groups, viz. plunging breakers and spilling breakers (see Chapter 4). According to Kemp the transition from spilling to plunging breakers can also be defined by the wave run-up ratio. Thus it seems that some relationship exists between the mode of transport (onshore or offshore) and the breaker type. Although this last-mentioned criterion seems to be completely different from all the foregoing results, this is not the case. Plunging breakers normally arrive at the coastline under summer conditions, when normal profiles are formed, and have a low deepwater wave steepness. Spilling breakers, on the other hand, normally have a larger deepwater wave steepness.
The water movement under a spilling breaker differs from that under a plunging breaker (Iversen [23]), and by definition the rate of energy dissipation of the two types of breakers also differ. Kemp is thus actually working towards the internal mechanism which governs the processes.

Watts [52] studied the effect of tides and irregular wave trains on equilibrium profiles. He concluded that the profiles stay basically the same as under regular wave conditions. Wave trains with variable period lead to bars of diminished height.

In the present study, however, it is not only the direction of the transport (onshore or offshore) which is of importance, but also its magnitude. The available references in literature to this aspect of the problem are scarce. Rector [41] concluded that the tendency for particles to move in landward direction increases for decreasing deepwater wave steepness. Scott [44] found that the rate of change of the profile form increases if the difference between the actual deepwater wave steepness and the critical deepwater wave steepness increases.

A study of the data used in [48] reveals that the rate of change of the profiles increased for an increasing distance from the line defining the neutral conditions (neither erosion nor accretion). For a given set of wave conditions and bed material this result implies that the initial rate of change of the profile will be some difference function $F(m_0, m_{cs})$ of the initial slope m_0 and the final slope m_{cs}.

The foregoing discussion leads to the conclusion that the onshore-offshore sediment transport can be written as follows:

$$S_y = f_3(H_0/\lambda_0, H_0, T, D_{50}, p, F(m, m_{cs}), h) \tag{6.37}$$

where S_y = onshore-offshore transport per unit of time and beach width at any time t, at a location with actual water depth d
H_0/λ_0 = deepwater wave steepness
H_0 = absolute deepwater wave height
T = wave period
D_{50} = median particle diameter
p = breaker type
m_{cs} = final beach slope
m = beach slope at time t
h = still-water depth.

The difference function $F(m, m_{cs})$ can be compared with the characteristic quantity $P(t)$ of Chapter 2, as well as with the quantity $(W - (L_2 - L_1))$ of Chapters 3 and 4. Consequently, the available literature on the external characteristics of the onshore-offshore coastal process leads to the conclusion that:

$$s_y = f_4(H_0/\lambda_0, H_0, T, D_{50}, p, h) \tag{6.38}$$

This equation is of the same form as equation (6.36), which is the result of the basic evaluation of Chapter 2, with the difference that the local wave height at any location with a still-water depth h has been replaced by the deepwater wave height H_0 and the breaker type p. Furthermore, the

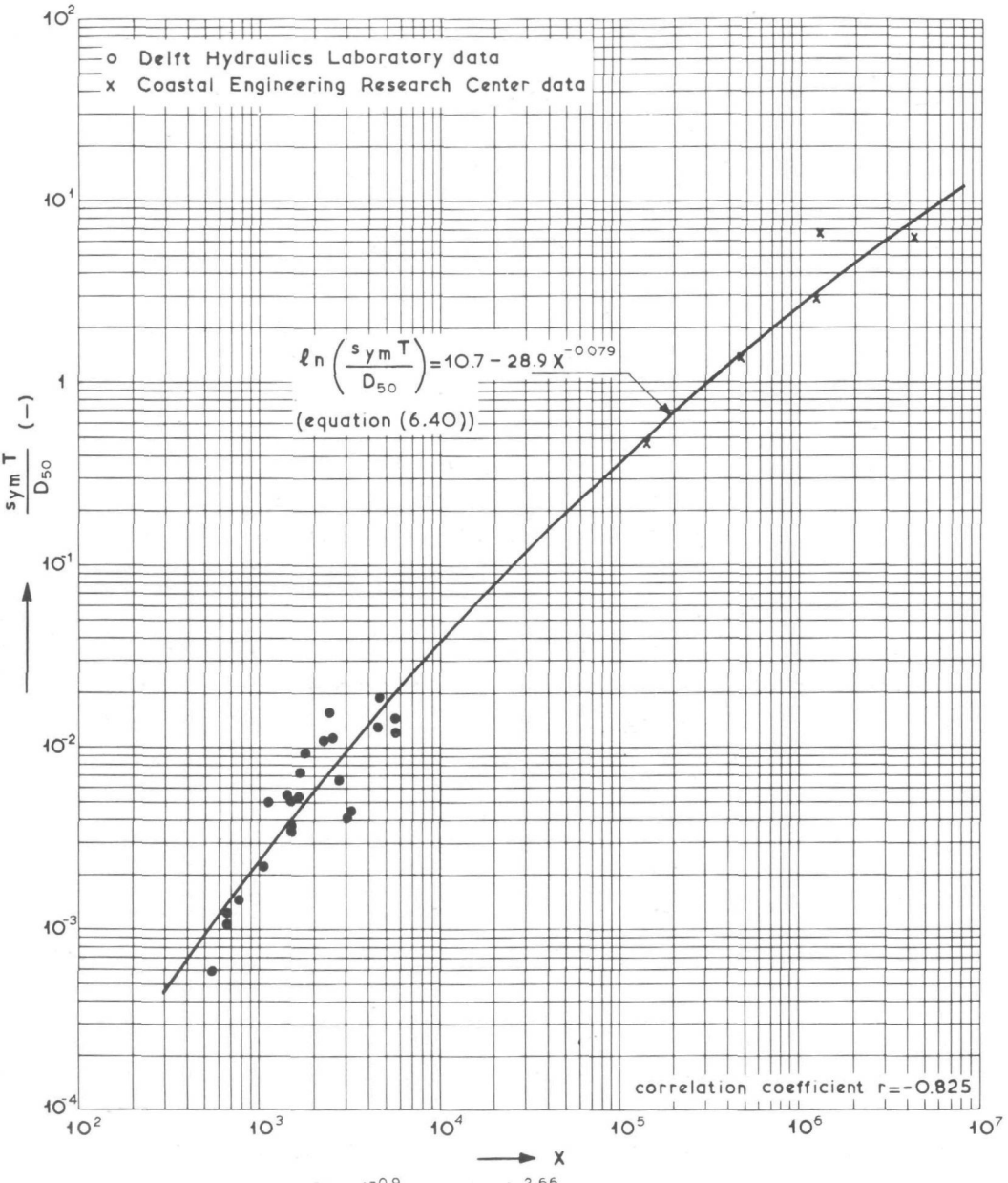

REMARKS: 1) $X=H_o^{1.68}\left(\frac{H_o}{\lambda_o}\right)^{-0.9}D_{50}^{-1.29}\left(\frac{H_o}{h_m}\right)^{2.66}$

2) $H_o, \lambda_o, h_m, D_{50}$ in m

3) T in sec

4) s_{ym} in m/sec

MAGNITUDE OF s_{ym}

FIGURE 64

terms H and T have been regrouped to include the deepwater wave steepness H_0/λ_0. The breaker type p is mostly not readily determinable in the prototype, consequently its presence will reduce the applicability of equation (6.38). However, it is possible to eliminate p. The breaker type p determines the breaker point and as such also the energy-dissipation pattern in the D-profile. From equation (4.53) it follows that p is a function of the breaker index γ. From equation (4.60) it can be seen that the bed slope α and the deepwater wave steepness H_0/λ_0 in turn play a role in the determination of the breaker index. In Chapter 6.2 it has been shown that the dimensionless form of the equilibrium profile is, for a given bed material, purely a function of the location in the D-profile. For a given set of boundary conditions (H_0, T, H_0/λ_0, D_{50}) the bed slope $\tan\alpha$ and consequently also the average breaker type p will thus be determined in general by the location of the breaker point in the D-profile. The location of the breaker point in the D-profile will to a large extent be determined by the ratio between the wave height H_0 and the still-water depth h_m at the seaward extremity of the D-profile. For values of $H_0/h_m < 0.4$, for instance, the waves will break more landwards than if for instance $H_0/h_m > 0.45$, with as a consequence that the average breaker type will be more plunging in the first case than in the second case.

Consequently the quantity p in equation (6.38) will be replaced by the ratio H_0/h_m. Equation (6.38) then reduces to:

$$s_y = f_5(H_0/\lambda_0,\ H_0,\ T,\ D_{50},\ H_0/h_m,\ h) \qquad (6.39)$$

where h_m = still-water depth at the seaward extremity of the D-profile (according to equation (4.125)).

The relationship of equation (6.39) will now be used to correlate the experimentally-determined distributions of s_y for the different two-dimensional model tests to the boundary conditions. In making this correlation the three characteristic elements of the s_y-curve, as mentioned earlier in this paragraph, viz. s_{ym}, δ_{2m} and s_y/s_{ym}, will be studied separately.

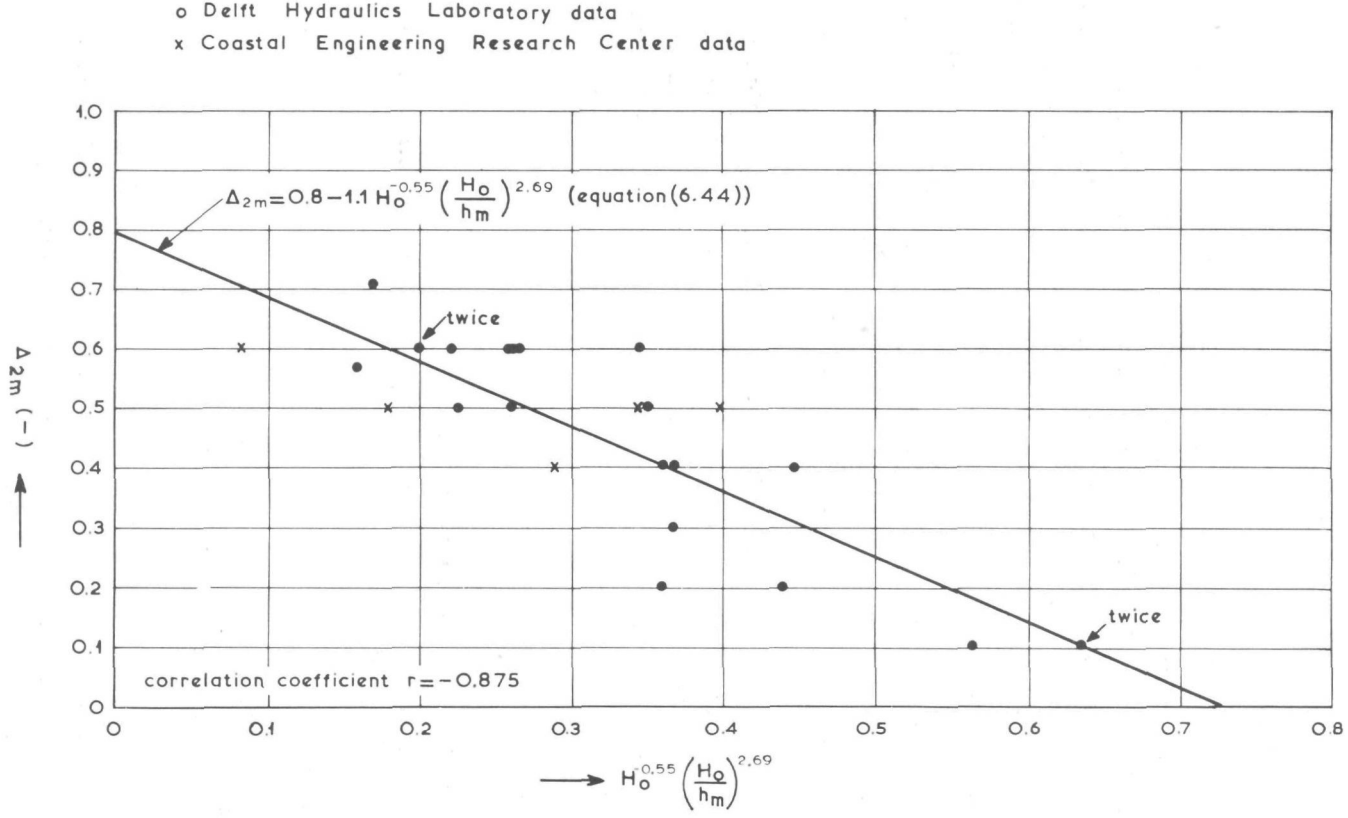

REMARK: H_o, h_m in m

FIGURE 65 POSITION OF s_{ym}

Magnitude of s_{ym}

The values of s_{ym}, i.e. the maximum value of s_y in the D-profile, as determined for the small-scale two-dimensional model tests and the prototype-size tests of the Coastal Engineering Research Center, were correlated to the wave and sediment characteristics according to equation (6.39). The correlation indicated that the value of s_{ym} is independent of the water depth at which s_{ym} occurs. Consequently, the following result was obtained:

$$\ln\left(\frac{s_{ym}T}{D_{50}}\right) = 10.7 - 28.9\left[H_0^{1.68}\left(\frac{H_0}{\lambda_0}\right)^{-0.9} D_{50}^{-1.29}\left(\frac{H_0}{h_m}\right)^{2.66}\right]^{-0.079} \qquad (6.40)$$

where s_{ym} = maximum value of s_y in the D-profile.

The left-hand side of equation (6.40) is dimensionless, whereas this is not the case on the right-hand size. This implies that a scale effect occurs when the size of the model varies. Equation (6.40) is plotted in Figure 64 together with the data used for its determination. The data are listed in Table XIV.

Position of s_{ym}

The location in the D-profile where the maximum value of s_y occurs is defined by the offshore profile thickness δ_{2m}, which will be made dimensionless by division by δ, i.e.:

$$\Delta_{2m} = \frac{\delta_{2m}}{\delta} \qquad (6.41)$$

where Δ_{2m} = position where the maximum value of s_y occurs
δ_{2m} = the offshore profile thickness at which the maximum value of s_y occurs.

The distribution of the offshore transport across the D-profile will be determined by the rate of energy-dissipation of the incoming waves, which is in turn a function of the breaker type. The breaker type is closely

related to the bed slope, which is on the average smaller in prototype cases than in model cases. Furthermore, Δ_{2m} can be written as follows:

$$\Delta_{2m} = \frac{\delta_{2m}}{\delta} = \frac{\delta_{2m}}{h_0 + h_m} \tag{6.42}$$

It can be seen from equations (4.110) and (4.125) that h_0 and h_m are reproduced according to different scales. Consequently it can be concluded that the ratio Δ_{2m} will vary with varying scale, i.e.:

$$\Delta_{2m} = f_6 (H_0, T, H_0/h_m) \tag{6.43}$$

A correlation of the available two-dimensional data (small-scale as well as prototype-size) according to equation (6.43) showed that Δ_{2m} is independent of the absolute value of the wave period and varies as follows with H_0 and H_0/h_m:

$$\Delta_{2m} = 0.8 - 1.1\, H_0^{-0.55} \left(\frac{H_0}{h_m}\right)^{2.69} \tag{6.44}$$

This result indicates that the location of the maximum value of s_y is determined solely by the breaker type (in the form of H_0/h_m) and the scale of the process (in the form of H_0). Equation (6.44), as well as the data used for its determination, is given in Figure 65. The data are listed in Table XV.

Distribution of s_y/s_{ym}

When the geometrical form of the equilibrium profile (W_r and W/W_r)is known, as well as the position and magnitude of s_{ym}, it is possible to determine the ratio s_y/s_{ym} at any location in the D-profile in terms of these quantities and the values of s_t, s_e, W_t and W_e. This method, however, involves the solution of a number of non-linear equations, which is a tedious procedure. This procedure will be described in Chapter 6.5. In order to gain an approximate value of the magnitude of s_y/s_{ym}, which will

be of sufficient accuracy to enable the determination of offshore transport, an approximate estimate of the ratio s_y/s_{ym} in terms of the known boundary conditions was made with the aid of the available test results. As stated above, the distribution of the offshore transport across the D-profile is determined by the incoming wave conditions. Consequently, it will be written in general that:

$$s_y/s_{ym} = f_7(H_o/\lambda_o,\ H_o/h_m,\ \Delta_m) \tag{6.45}$$

where $\Delta_m = \left| \frac{\delta_2 - \delta_{2m}}{\delta} \right|$ (6.46)

= dimensionless position in the D-profile relative to the location of s_{ym}.

Two areas can now be discerned, viz.:

Area 1: $\delta_2 - \delta_{2m} > 0$, i.e. the area landwards of the location where the maximum value of s_y occurs, and

Area 2: $\delta_2 - \delta_{2m} < 0$, i.e. the area seawards of the location of maximum s_y.

It is to be expected that the solution of equation (6.45) will be different in each of these two areas, due to the fact that area 1 falls primarily inside the breaker zone, while area 2 falls primarily outside the breaker zone. The data for these two areas should therefore be correlated separately to equation (6.45). When this was done, the following results were obtained:

Area 1 (i.e. onshore branch):

$$s_y/s_{ym} = \frac{0.93}{1 + 1.01\ X^{2.11}} + 0.07 \tag{6.47}$$

Area 2 (i.e. offshore branch):

$$s_y/s_{ym} = \frac{0.99}{1 + 1.14\ X^{2.11}} + 0.01 \tag{6.48}$$

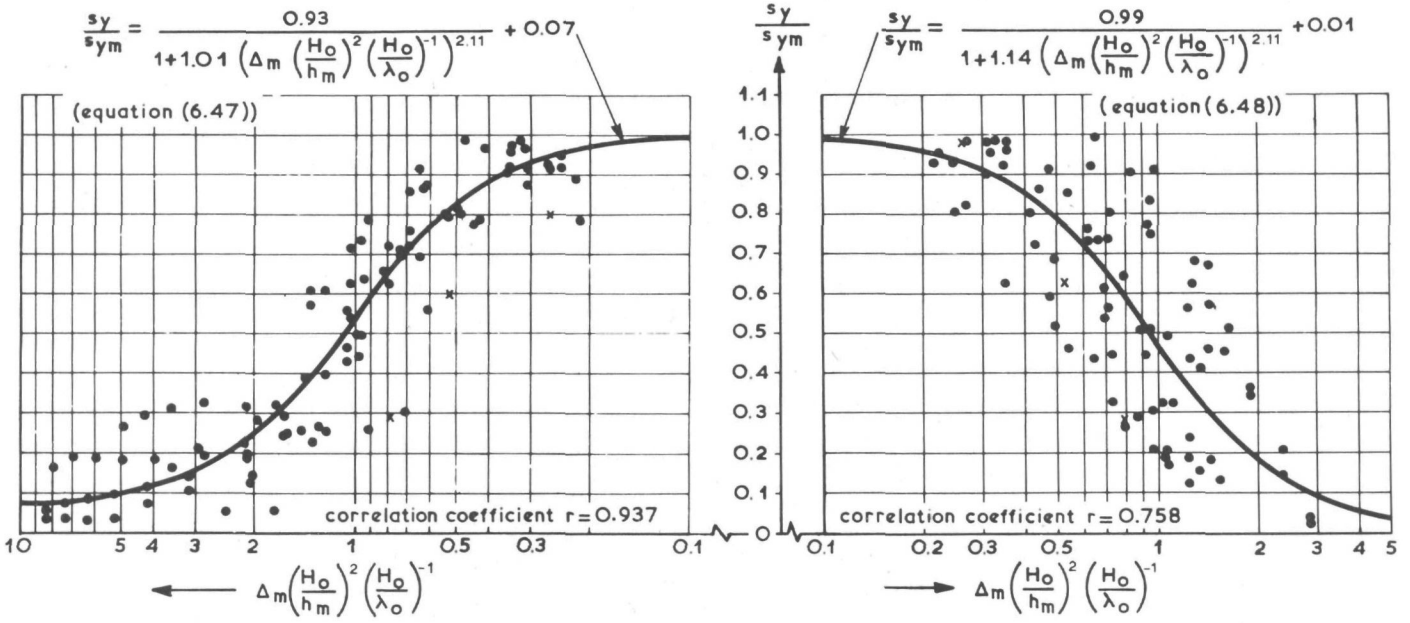

DISTRIBUTION OF s_y/s_{ym}

FIGURE 66

- Delft Hydraulics Laboratory data
- x Coastal Engineering Research Center data

REMARKS : 1) H_o, λ_o, h_m in m

2) $\Delta_m = \left|\frac{\delta_2 - \delta_{2m}}{\delta}\right|$

where in both cases

$$X = \Delta_m \left(\frac{H_o}{\lambda_o}\right)^{-1} \left(\frac{H_o}{h_m}\right)^2 \qquad (6.49)$$

Equations (6.47) and (6.48) are given in Figure 66, together with the data used for their determination. The data are listed in Tables XVI and XVII.

The data of the C.E.R.C. were not used to assist in the determination of equations (6.47)... (6.49), due to the presence of secondary effects (see Chapter 5 and Table VIII).The s_y/s_{ym}-values for the only C.E.R.C.-test in which the Ursell-parameter stayed below the critical value (test 502) have been plotted in Figure 66. It can be seen that these points fall inside the scatter of the small-scale test results. More prototype-size two-dimensional tests where secondary effects are kept to a minimum are necessary, in order to allow a more decisive evaluation of the application of equations (6.47) ... (6.49) to prototype-size. For the time being these equations will be used for both model- and prototype-size two-dimensional cases.

Offshore sediment transport can now be calculated with the aid of equation (6.35). In Figure 67 a comparison is given between the calculated transport rate and the measured transport rate, for a model test where too little data were available to allow the test to be used for the determination of the empirical equations in this chapter.
The steps that will have to be followed when the theory is used to calculate offshore transport will be summarized in Chapter 6.5.

6.4 Offshore transport: three-dimensional case

It has been shown in Chapter 2 that the onshore-offshore transport will increase under three-dimensional conditions, due to the increased shear stress at the bed. In Chapter 6.2, where the results of the profile

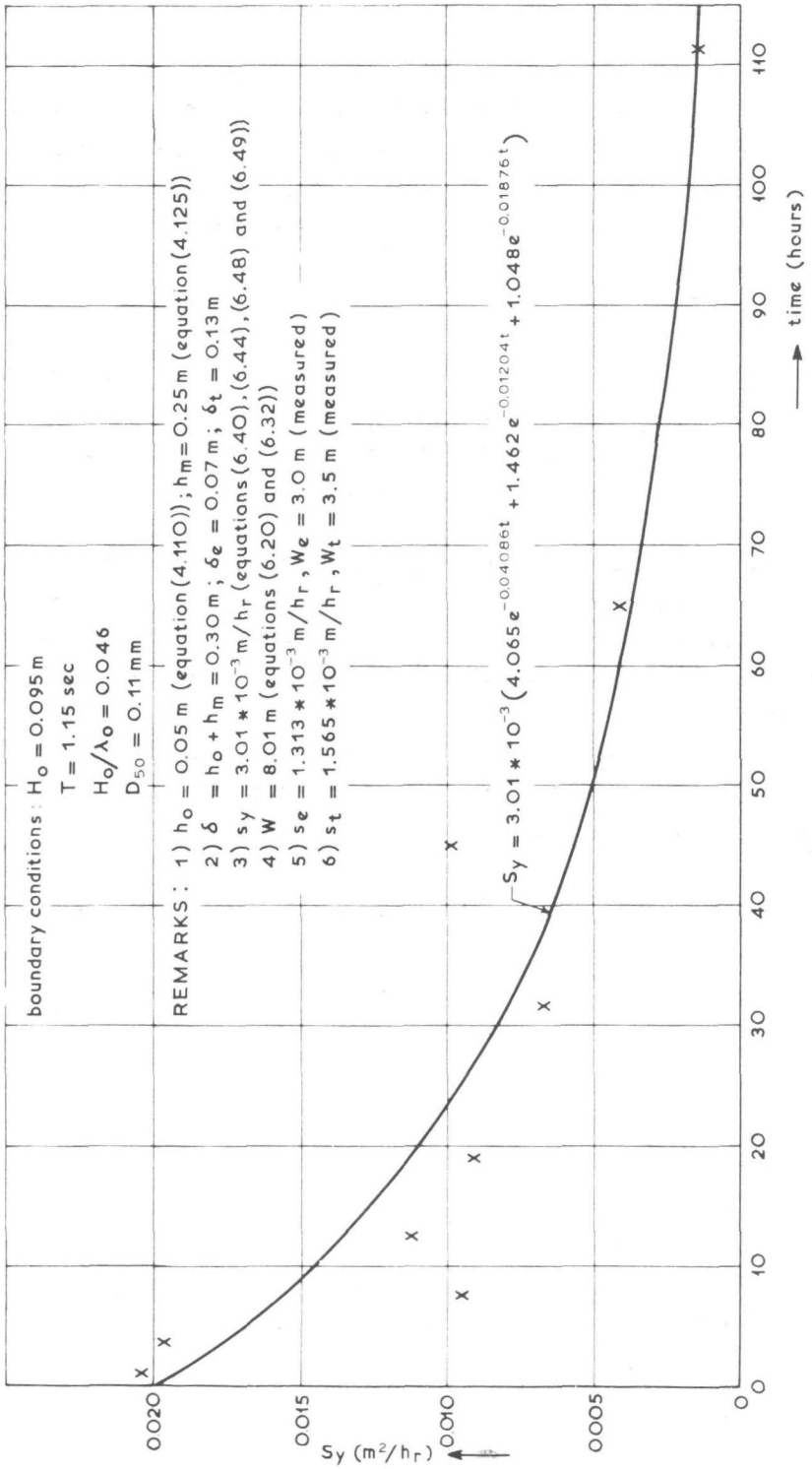

COMPARISON OF THEORETICAL AND MEASURED TRANSPORT RATES IN THE MODEL

FIGURE 67

characteristics were presented, it was concluded that the effect of three-dimensionality on the magnitude of W is negligible. The three-dimensional conditions will accordingly lead to an increase in the magnitude of s_y. With the aid of equation (2.43) it can thus be concluded that:

$$s_{y3D} = s_{y2D}\, f\left(\frac{\overline{\tau_{wc}}}{\tau_w}\right) \tag{6.50}$$

where s_{y2D} and s_{y3D} = the values of s_y in the two- and three-dimensional cases respectively

τ_{wc} = bed shear under combined wave and current action

τ_w = bed shear under wave action only.

Before the form of the function $f\left(\overline{\tau_{wc}/\tau_w}\right)$ can be studied, the magnitude of the ratio $\overline{\tau_{wc}/\tau_w}$ must be known. Bijker [9] studied the increase in the bed shear, if wave action is superimposed on an existing current pattern. In the present study the opposite is the case, viz. a current is added to an existing wave field.
It will be assumed that the increase in the absolute value of the bed shear, due to the addition of a current to the existing wave field, will determine the increase in the value of s_y.

Under turbulent conditions the bed shear can, according to Prandtl [40], be written as:

$$\tau = \rho_w l^2 \left(\frac{\partial v(z)}{\partial z}\right)_b^2 \tag{6.51}$$

where l = mixing length

$v(z)$ = velocity at a height z above the bed

ρ_w = fluid density

τ = bed shear

z = height above the bed.

Furthermore, according to Prandtl, l is related to the bed roughness and the height above the bed, viz.:

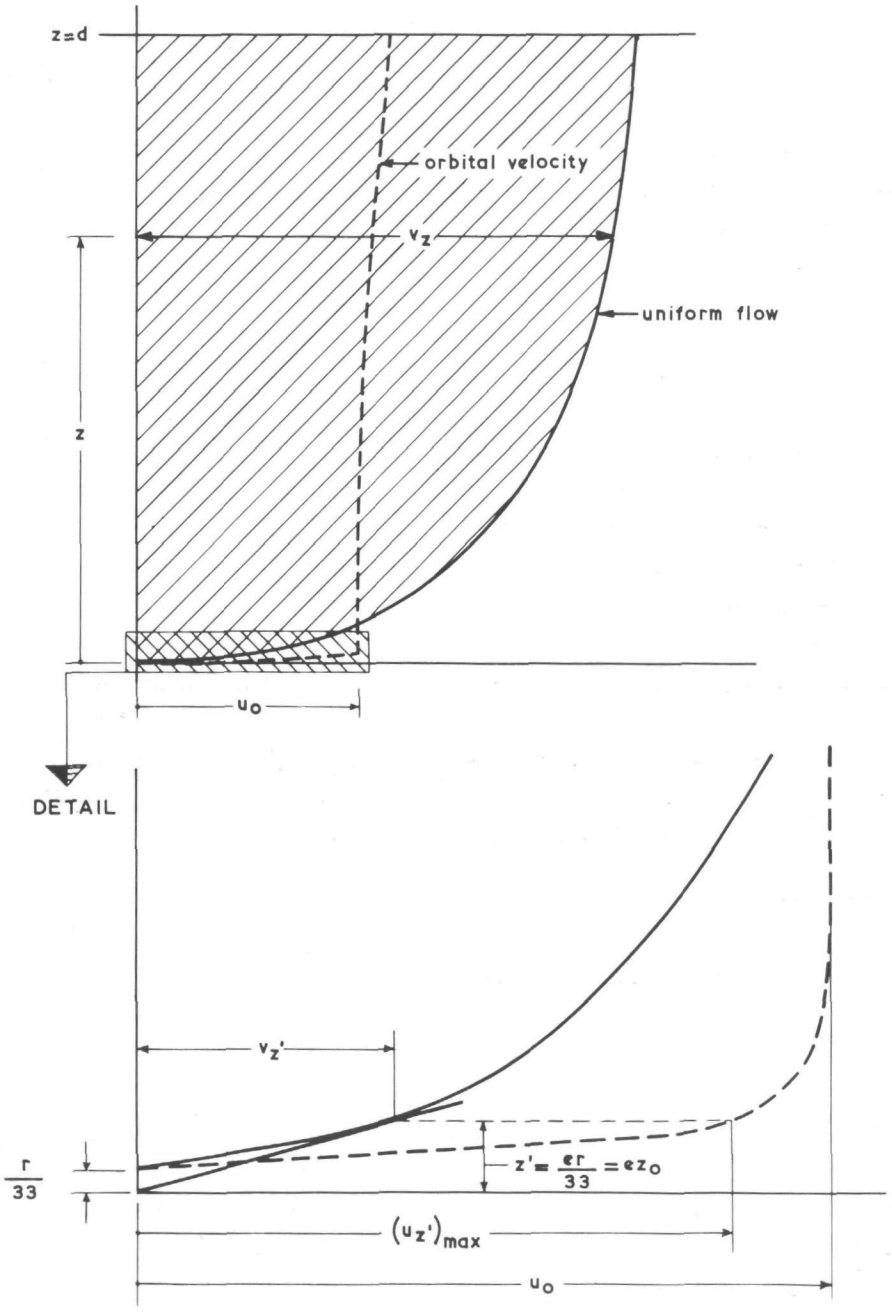

COMPARISON BETWEEN VELOCITY PROFILES
FIGURE 68

$$l = \kappa z \tag{6.52}$$

when z is small.

κ = von Kármán constant = 0.4.

The vertical velocity gradient for a normal fully turbulent current outside the laminar sublayer is given by:

$$\frac{\partial v(z)}{\partial z} = \frac{v_*}{\kappa z} \tag{6.53}$$

where $v_* = \left(\frac{\tau}{\rho_w}\right)^{1/2} = (gdI)^{1/2} = \frac{vg^{1/2}}{C_h}$ (6.54)

v_* = shear stress velocity

d = actual water depth

I = slope of energy gradient

v = mean velocity

C_h = Chezy-coefficient.

Integration of equation (6.53) yields a logarithmic distribution of the velocity over the vertical. The velocity equals zero at a small distance z_0 above the bed. According to experiments $z_0 = r/33$, where r is a value for the bed roughness. It will be assumed that the velocity gradient in the vicinity of the bed can be approximated by:

$$\frac{\partial v(z)}{\partial z} = \frac{\Delta v(z)}{\Delta z} \tag{6.55}$$

where $\Delta v(z)$ and Δz are finite differences.

Wave action only

For the evaluation of the velocity gradient according to equation (6.55), Δz will be put equal to z', where z' is the thickness of a hypothetical viscous sublayer. It can be shown that $z' = ez_0$ (e = base of natural logarithms). It then follows from equation (6.55) and Figure 68 that:

$$\frac{\partial v(z)}{\partial z} = \frac{u_{z'}}{z'} \tag{6.56}$$

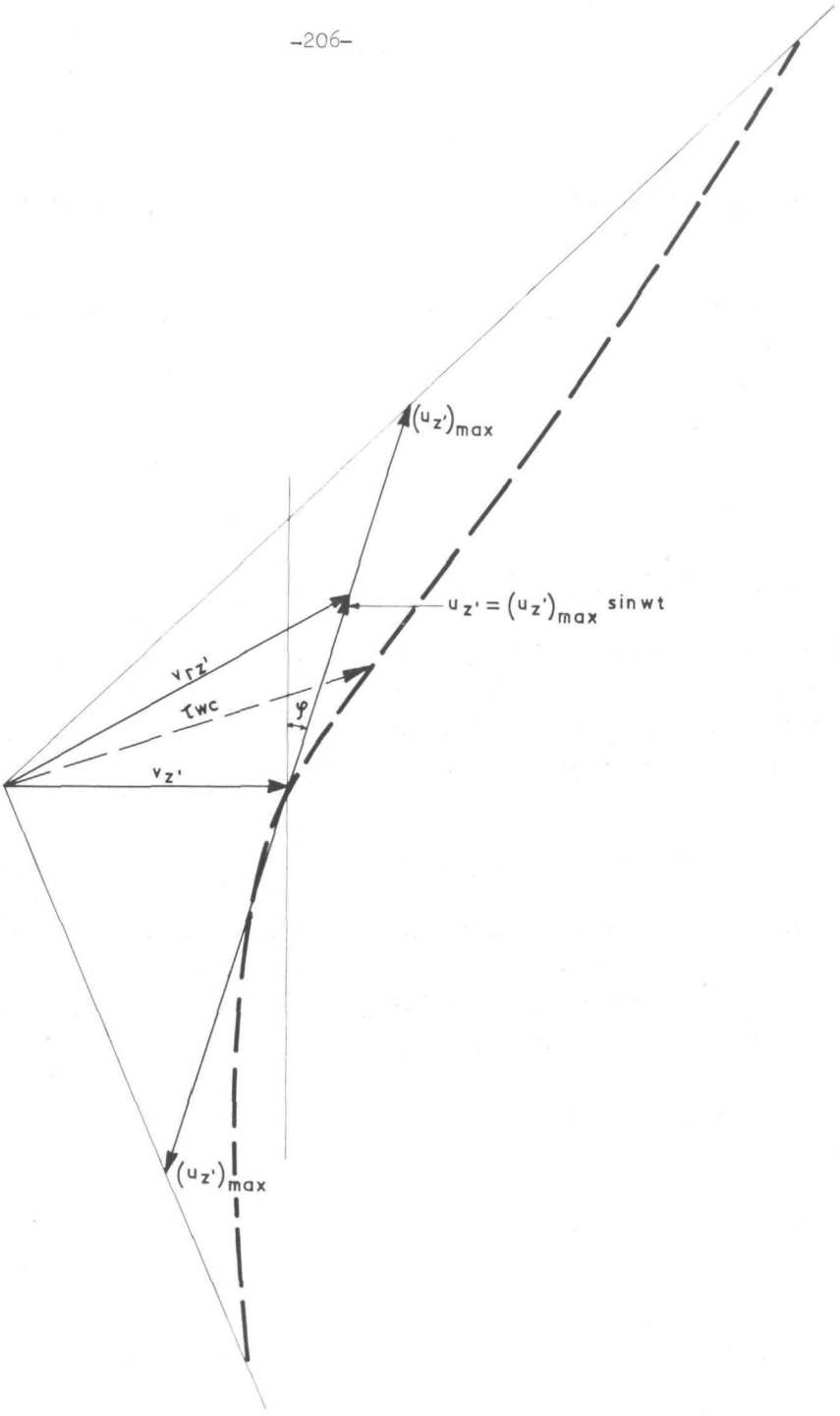

RESULTANT VELOCITY UNDER COMBINED CURRENT AND WAVE ACTION

FIGURE 69

where $u_{z'}$ = momentary value of the orbital velocity at a height z' above the bed.

Consequently, the bed shear can be found from equations (6.51), (6.52) and (6.56):

$$\tau_w = \rho_w (\mu z')^2 \left(\frac{u_{z'}}{z'}\right)^2$$

$$= \rho_w \mu^2 u_{z'}^2 \qquad (6.57)$$

Combined current and wave action

Under oblique wave attack (angle of wave incidence = φ) the resultant velocity at a height z' above the bed is a combination of the momentary orbital velocity $u_{z'}$ and the longshore current velocity $v_{z'}$. At a height z' above the bed the resultant velocity $v_{rz'}$ under the wave is then given by:

$$v_{rz'} = (v_{z'}^2 + u_{z'}^2 + 2v_{z'}u_{z'}\sin\varphi)^{1/2} \qquad (6.58)$$

(see Figure 69)

where $v_{rz'}$ = resultant velocity under the wave at a height z' above the bed, at time t

$v_{z'}$ = longshore current velocity at a height z' above the bed

φ = angle of wave incidence.

In the same manner as for wave action only, it now follows from Figure 68 and equations (6.51), (6.52) and (6.58) that:

$$\tau_{wc} = \rho_w (\mu z')^2 \left(\frac{v_{rz'}}{z'}\right)^2$$

$$= \rho_w \mu^2 v_{rz'}^2 \qquad (6.59)$$

Substitution of equation (6.58) into equation (6.59) yields:

$$\tau_{wc} = \rho_w \mu^2 (v_{z'}^2 + u_{z'}^2 + 2u_{z'}v_{z'}\sin\varphi) \qquad (6.60)$$

$$= \rho_w \mu^2 u_{z'}^2 \left[\left(\frac{v_{z'}}{u_{z'}}\right)^2 + 1 + 2 \left(\frac{v_{z'}}{u_{z'}}\right) \sin\varphi \right] \qquad (6.61)$$

Division of equation (6.61) by equation (6.57) yields the increase in the bed shear, viz.:

$$\frac{\tau_{wc}}{\tau_w} = 1 + \left(\frac{v_{z'}}{u_{z'}}\right)^2 + 2\left(\frac{v_{z'}}{u_{z'}}\right) \sin\varphi \qquad (6.62)$$

It now remains to determine the ratio $(v_{z'}/u_{z'})$ in terms of the mean velocity profiles.

If only current action is taken into account, equation (6.55) can be written as:

$$\frac{\partial v(z)}{\partial z} = \frac{v_{z'}}{z'} \qquad \text{(see Figure 68)} \qquad (6.63)$$

From equations (6.53) and (6.63) it can consequently be concluded that for $z = z'$:

$$v_{z'} = \frac{v_*}{\mu} \qquad (6.64)$$

Bijker [9] assumed that the orbital velocity $u_{z'}$ at a height z' above the bed is given by:

$$u_{z'} = p_B u_b \qquad (6.65)$$

where p_B = a constant according to Bijker [9]. In a study on the magnitude of p_B, Bijker found it to be equal to 0.39 (theoretically), while experiments yielded a value of $p_B = 0.45$

$$u_b = u_0 \sin wt \qquad (6.66)$$

$$u_0 = \pi H/(T \sinh \frac{2\pi d}{\lambda}) = 2\pi a_0/T \qquad (6.67)$$

$$w = \frac{2\pi}{T} \qquad (6.68)$$

T = wave period.

Application of Bijker's approximation of the increase in the bed shear due to the wave action, with the value of u_z, according to equation (6.65), yields good results in a wide range of boundary conditions. It is, however, to be expected that the effect of the wave motion on the shear stress will vary with a variation in the flow regime at the bed. Jonsson([27], [28]) defined the flow regime at the bed in terms of the ratio a_0/r, where a_0 = maximum wave particle amplitude at the bed and r = bed roughness (ripple height).
Furthermore, Jonsson([27],[28]) defined the maximum bed shear due to wave action in terms of a wave friction factor f_w:

$$\tau_{wm} = 1/2\ f_w \rho_w u_0^2 \tag{6.69}$$

where τ_{wm} = maximum value of τ_w
f_m = wave friction factor for τ_{wm}.
At any other time t the bed shear can be written as:

$$\tau_w = 1/2\ f_e \rho_w u_b^2 \tag{6.70}$$

where f_e = wave friction factor for τ_w.

The wave friction factors f_w and f_e in equations (6.69) and (6.70) are not necessarily the same. Jonsson [27] showed, however, that $f_w \approx f_e$ in the rough turbulent case, which occurs under morphological conditions (both in the model and the prototype). Consequently equation (6.70) can be rewritten as:

$$\tau_w = 1/2\ f_w \rho_w u_b^2 \tag{6.71}$$

The wave friction factor f_w is determined by the ratio a_0/r. Jonsson [27] found that in the rough turbulent case the wave friction factor f_w is defined by:

$$\frac{1}{4\sqrt{f_w}} + \log\left(\frac{1}{4\sqrt{f_w}}\right) = -0.08 + \log\left(\frac{a_0}{r}\right) \tag{6.72}$$

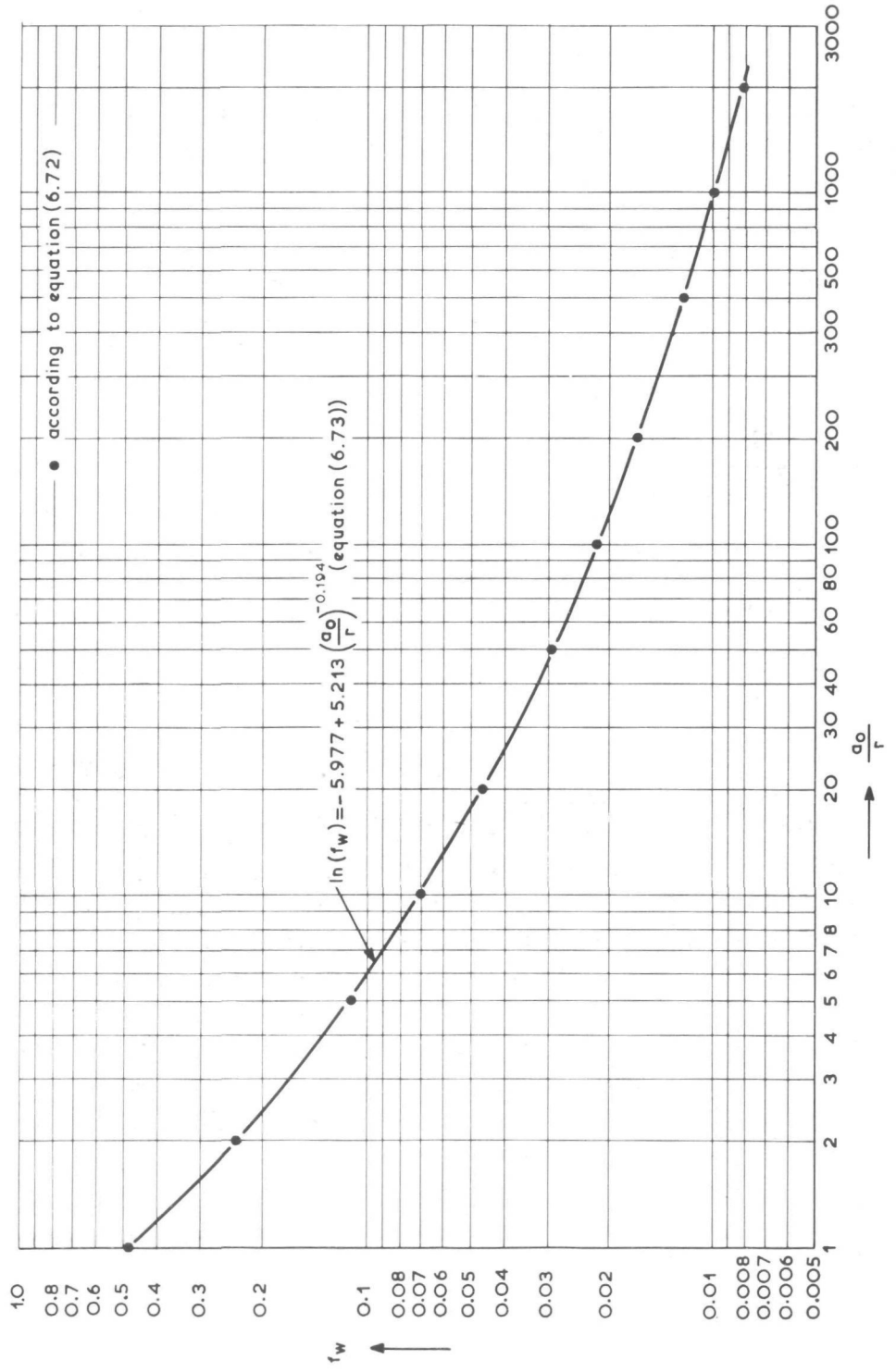

WAVE FRICTION FACTOR IN THE ROUGH TURBULENT REGIME
FIGURE 70

Equation (6.72) has been plotted in Figure 70. The determination of f_w from equation (6.72) has to done by means of a trial and error method. However, equation (6.72) can be closely approximated by the following equation:

$$\ln (f_w) = -5.977 + 5.213 \left(\frac{a_0}{r}\right)^{-0.194} \qquad \text{(see Figure 70)} \qquad (6.73)$$

A comparison of the equations for the determination of the bed shear under wave action only, as given by equations (6.57) and (6.71), leads to the conclusion that $u_{z'}$ can be written in terms of u_b:

$$u_{z'} = \left(\frac{1/2\ f_w}{\mathcal{H}^2}\right)^{1/2} u_b$$

$$= \sqrt{\frac{f_w}{2\mathcal{H}^2}}\ u_b$$

$$= p_J u_b \qquad (6.74)$$

where $p_J = \sqrt{\frac{f_w}{2\mathcal{H}^2}}$ (6.75)

p_J can be compared with the constant coefficient p_B of Bijker [9]. The coefficient p_J is a function of the relative roughness of the bed, according to equations (6.73) and (6.75). A 2.5m wave with a period of 10 sec will lead to a ratio of $a_0/r = 29.5$ in 4m water ($r = 0.1$m). The corresponding value of $p_J = 0.344$. Scaled down to model conditions, a wave of 0.1 m with a period of 2 sec will lead to a ratio of $a_0/r = 11.8$ in 0.16m water ($r = 0.01$m). The corresponding value of $p_J = 0.448$. In this report the use of p_J instead of p_B is preferred, due to the wide area of applicability of the eventual empirical relationships (model as well as prototype). With the use of equations (6.54), (6.64), (6.74) and (6.75) the ratio $v_{z'}/u_{z'}$ can be written as:

$$\frac{v_{z'}}{u_{z'}} = \left(\frac{v_*}{\mathcal{H}}\right) \pm \left(\frac{1}{p_J u_b}\right) \qquad (6.76)$$

$$= \frac{v_g^{1/2}}{C_h \mathcal{H} \sqrt{\frac{f_w}{2\mathcal{H}^2}}\, u_b}$$

$$= \frac{v}{u_b} \pm \frac{1}{C_h \sqrt{\frac{f_w}{2g}}}$$

$$= \frac{v}{\xi_J u_b} \tag{6.77}$$

where $\xi_J = C_h \sqrt{\frac{f_w}{2g}}$ (6.78)

Substitution of equations (6.77), (6.78) and (6.66) into equation (6.62) finally yields:

$$\frac{\tau_{wc}}{\tau_w} = 1 + \left(\frac{v}{\xi_J u_0}\right)^2 \operatorname{cosec}^2 wt + 2 \left(\frac{v}{\xi_J u_0}\right) \sin\varphi \operatorname{cosec} wt \tag{6.79}$$

where $\frac{\tau_{wc}}{\tau_w}$ = the time-dependent ratio between the bed shear under combined wave and current action and the bed shear under wave action only.

The mean value of this ratio can be found by integration over the time of passing of the wave:

$$\overline{\left(\frac{\tau_{wc}}{\tau_w}\right)} = \frac{2}{T} \int_{-T/4}^{T/4} \left(1 + \left(\frac{v}{\xi_J u_0}\right)^2 \operatorname{cosec}^2 wt + 2 \left(\frac{v}{\xi_J u_0}\right) \sin\varphi \operatorname{cosec} wt\right) dt \tag{6.80}$$

The integral has a singularity at its lower boundary (when $t = -T/4$). For this reason the mean value of the inverse ratio was evaluated, viz.:

$$\left(\frac{\overline{\tau_w}}{\tau_{wc}}\right) = \frac{2}{T}\int_{-T/4}^{T/4}\left(\frac{1}{1 + \left(\frac{v}{\xi_J u_0}\right)^2 \operatorname{cosec}^2 wt + 2\left(\frac{v}{\xi_J u_0}\right)\sin\varphi \operatorname{cosec} wt}\right) dt$$

$$= \frac{2}{T}\int_{-T/4}^{T/4}\left(\frac{\sin^2 wt}{\sin^2 wt + \left(\frac{v}{\xi_J u_0}\right)^2 + 2\left(\frac{v}{\xi_J u_0}\right)\sin\varphi \sin wt}\right) dt \qquad (6.81)$$

Equation (6.81) was integrated numerically for values of $\varphi = 0^\circ$, 5°, 10°, 15° and 20° respectively, the result is given in Figures 71 ... 75. With the aid of the method of least squares the results of the above-mentioned numerical integration was approximated by an equation of the form:

$$\left(\frac{\overline{\tau_w}}{\tau_{wc}}\right) = \frac{1}{1 + M\left(\frac{v}{\xi_J u_0}\right)^N} \qquad (6.82)$$

where $M = 1.91 - 1.32 \sin\varphi$ (6.83)

and $N = 1.24 - 0.08 \sin\varphi$ (6.84)

(under the whole wave)

Consequently it can be concluded that the increase in the bed shear can be written as a first approximation as:

$$\left(\frac{\overline{\tau_{wc}}}{\tau_w}\right) = 1 + M\left(\frac{v}{\xi_J u_0}\right)^N \qquad (6.85)$$

where M and N are given by equations (6.83) and (6.84) respectively. Inside the breaker zone, where the wave motion becomes extremely non-symmetrical, small vortices of sand are thrown up during the passing of the wave crest, during the passing of the wave trough these vortices are transported away. Thus it seems reasonable that somewhere inside the breaker zone the average value of τ_{wc}/τ_w under only the wave crest will be of importance

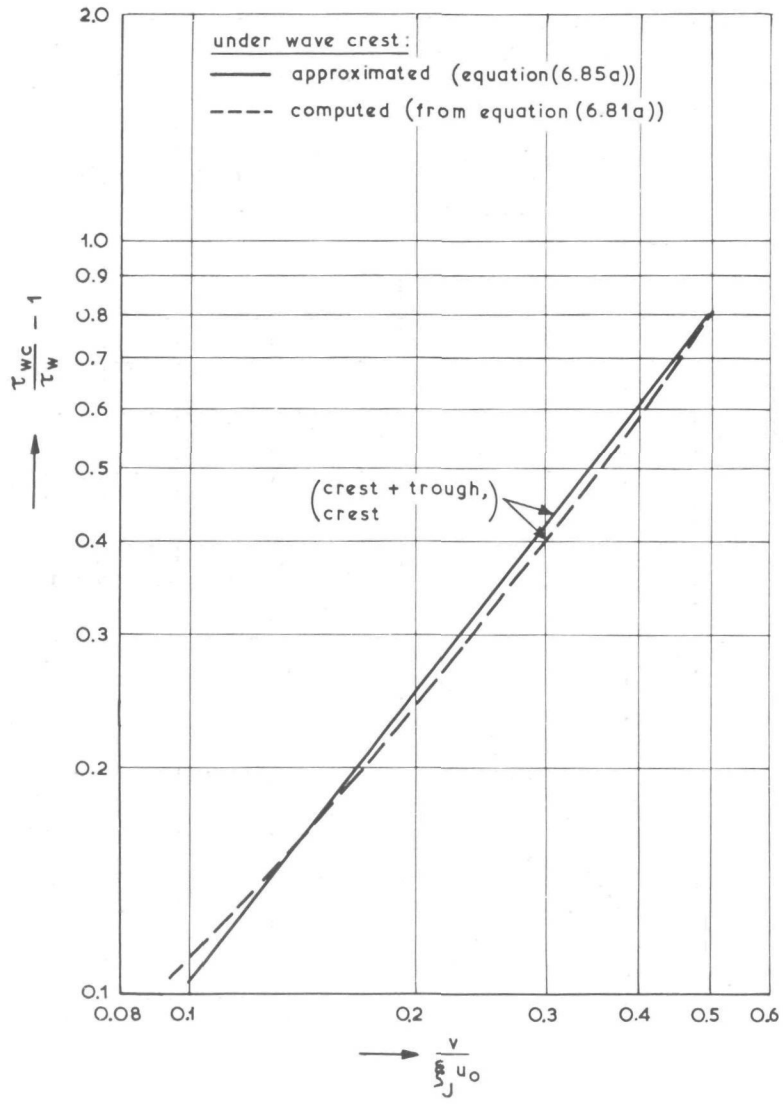

INCREASE IN BED SHEAR ($\varphi = 0°$)
FIGURE 71

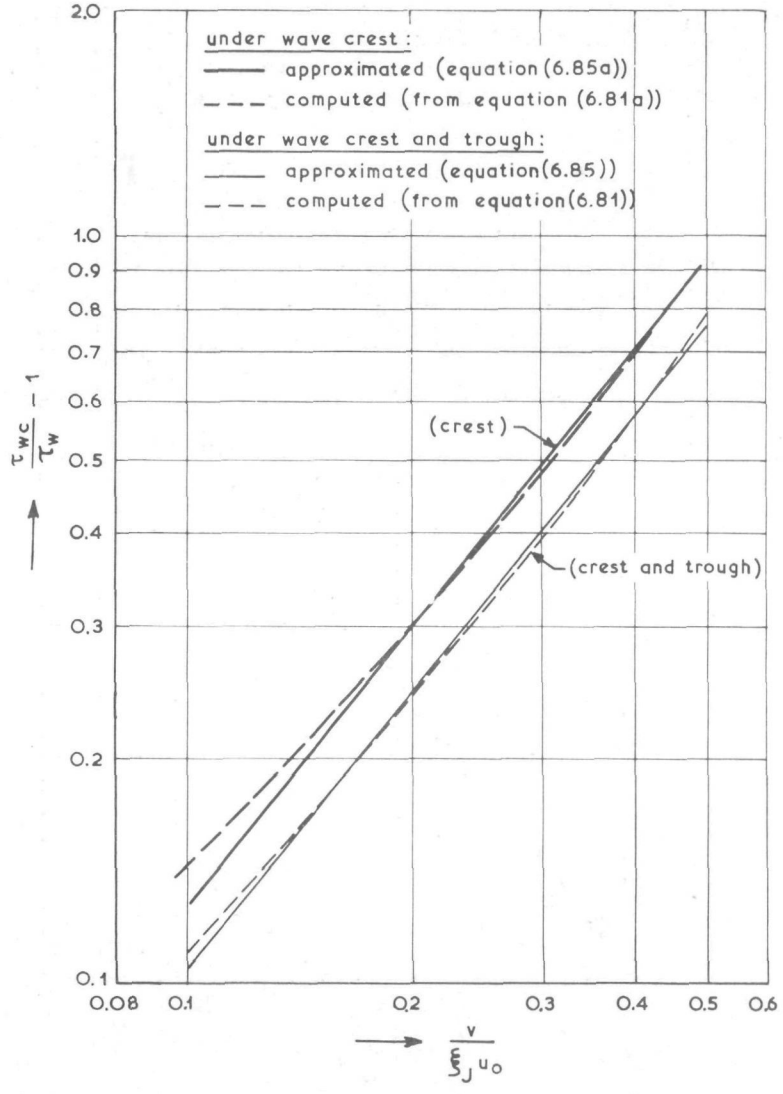

INCREASE IN BED SHEAR ($\varphi = 5°$)
FIGURE 72

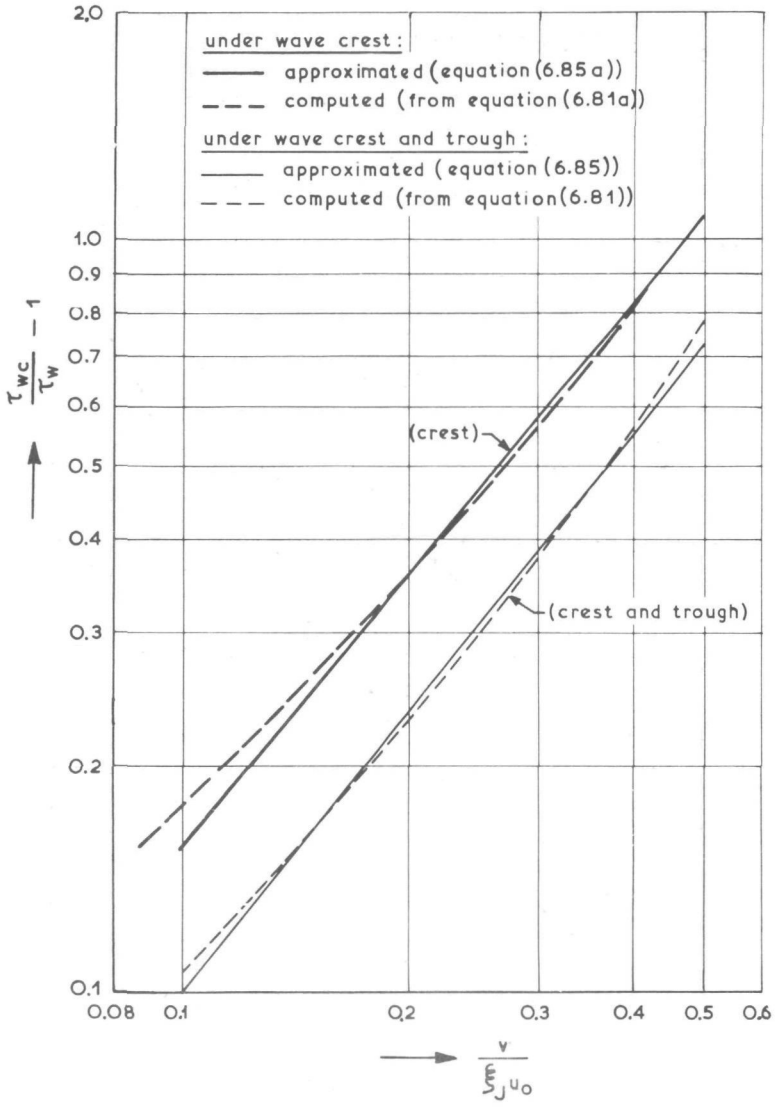

INCREASE IN BED SHEAR ($\varphi = 10^o$)
FIGURE 73

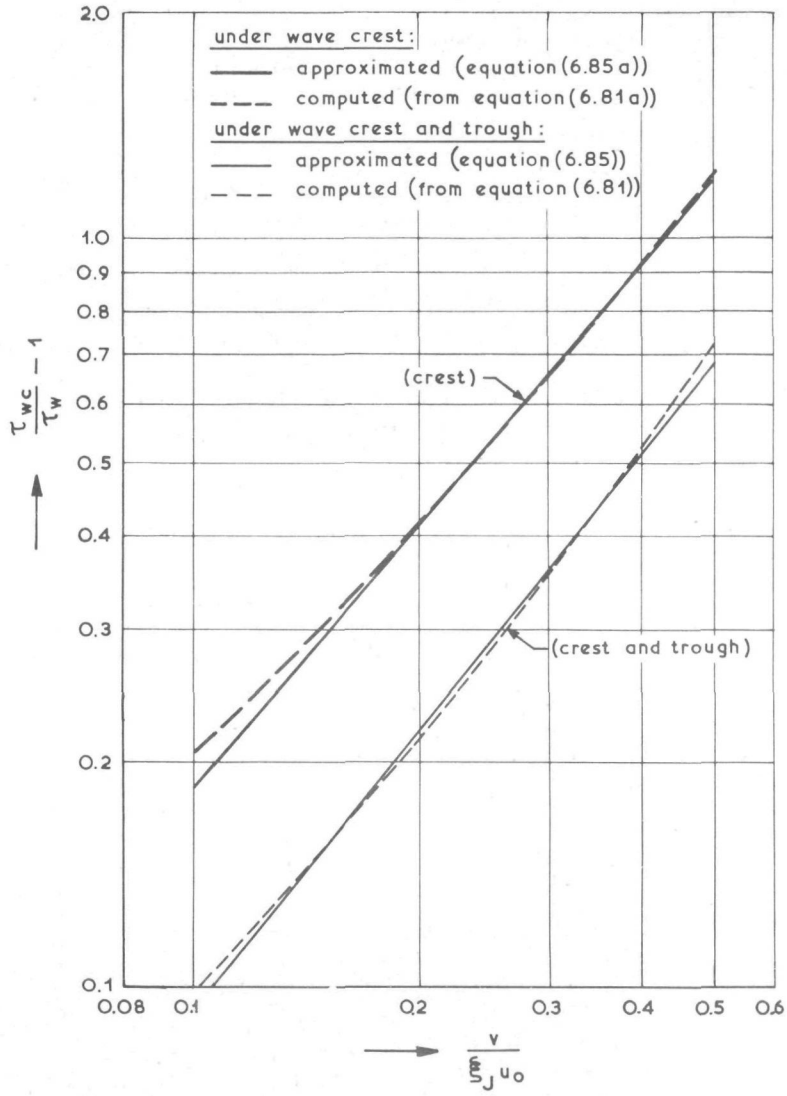

INCREASE IN BED SHEAR ($\varphi = 15°$)
FIGURE 74

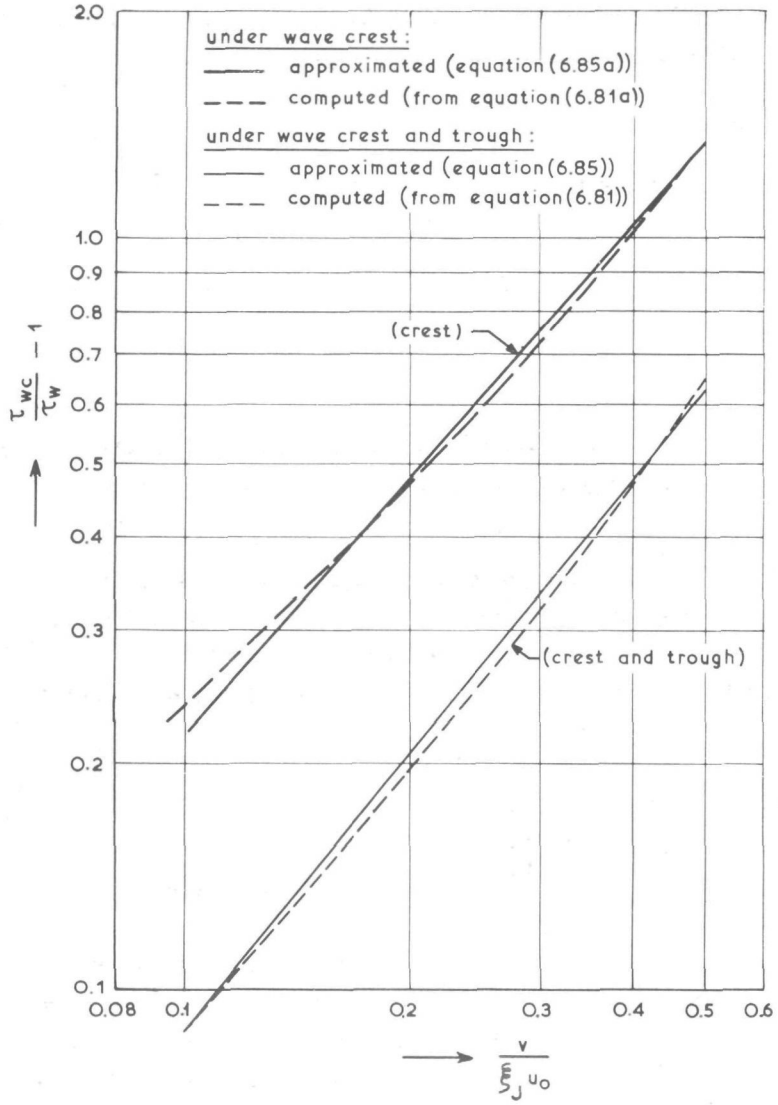

INCREASE IN BED SHEAR ($\varphi = 20°$)
FIGURE 75

when determining the increase of s_y. Equation (6.79) can then be integrated over the time of passing of the wave crest:

$$\left(\frac{\overline{\tau_{wc}}}{\tau_w}\right) = \frac{4}{T}\int_0^{T/4} \left(1 + \left(\frac{v}{\xi_J u_0}\right)^2 \operatorname{cosec}^2 wt + 2\left(\frac{v}{\xi_J u_0}\right) \sin\varphi \operatorname{cosec} wt\right) dt \tag{6.80a}$$

or, when the inverse value is taken in the same manner as in equation (6.81):

$$\left(\frac{\overline{\tau_w}}{\tau_{wc}}\right) = \frac{4}{T}\int_0^{T/4} \left(\frac{\sin^2 wt}{\left(\sin^2 wt + \left(\frac{v}{\xi_J u_0}\right)^2 + 2\left(\frac{v}{\xi_J u_0}\right) \sin\varphi \sin wt\right)}\right) dt \tag{6.81a}$$

Equation (6.81a) was also integrated numerically for values of $\varphi = 0^\circ$, 5°, 10°, 15° and 20° respectively. The results are also shown in Figures 71 ... 75. The results can, as has been done for the ratio under the whole wave, again be approximated by an equation of the form of equation (6.82).

In this case $M = 1.94 + 2.97 \sin\varphi$ (6.83a)

and $N = 1.27 - 0.39 \sin\varphi$ (6.84a)

(under the wave crest)

In Figures 71 ... 75 a comparison is given between the calculated and approximated values for the ratio of $\overline{\tau_{wc}/\tau_w}$, both under the whole wave and the wave crest respectively. Equation (6.85) can now be substituted into equation (6.50) and the result used to incorporate three-dimensional effects into the results of the previous section (Chapter 6.3), i.e.:

$$s_{y3D} = s_{y2D}\, f\left(1 + M\left(\frac{v}{\xi_J u_0}\right)^N\right) \tag{6.86}$$

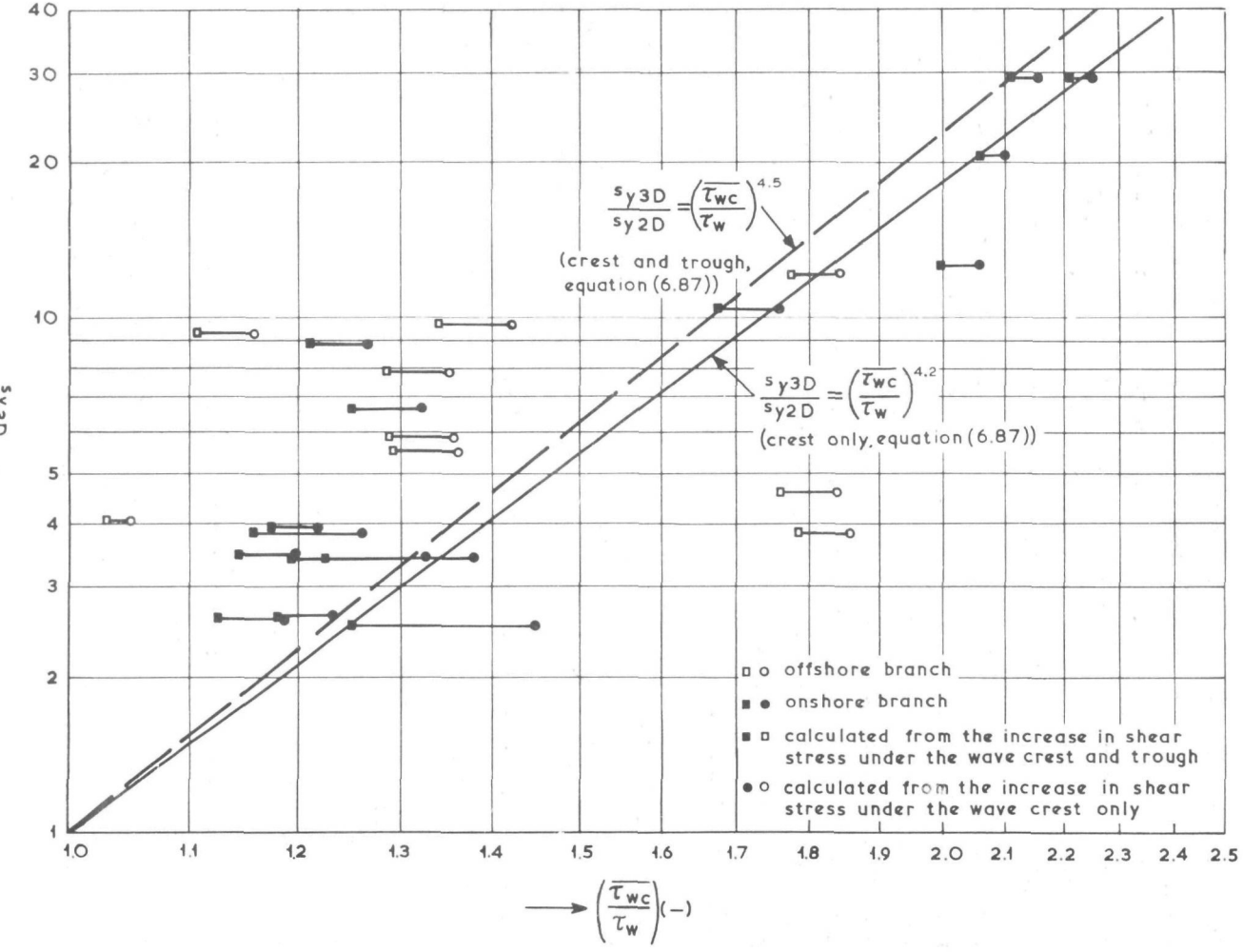

INCREASE IN COASTAL CONSTANT s_y

FIGURE 76

The number of three-dimensional cases that were available to determine the precise form of equation (6.86) is minimal. Due to the uncertainties regarding the boundary conditions, no prototype cases can be used. For the available three-dimensional model cases the s_y-values (s_{y3D}) were calculated in the normal way by the method of least squares from the time-variation in $(L_2 - L_1)$ (see Chapter 3). The coastal constants s_{y2D} for the corresponding two-dimensional cases (i.e. the same wave conditions and bed material, but with v = 0) were calculated with the aid of equations (6.40), (6.44), (6.47) ... (6.49). The ratio s_{y3D}/s_{y2D} was then determined for all available cases and correlated to the increase in the bed shear under the whole wave (crest and trough) and under the wave crest only as given by equations (6.83)... (6.85) and equations (6.83a), (6.84a) and (6.85) respectively, with as a result:

Under the whole wave:

$$s_{y3D}/s_{y2D} = (\overline{\tau_{wc}/\tau_w})^{4.5} \tag{6.87}$$

$$\text{i.e. } s_{y3D} = s_{y2D}\left(1 + M\left(\frac{v}{\xi_J u_0}\right)^N\right)^{4.5} \tag{6.88}$$

M and N are given by equations (6.83) and (6.84) respectively.

Under the wave crest:

$$s_{y3D}/s_{y2D} = (\overline{\tau_{wc}/\tau_w})^{4.2} \tag{6.87a}$$

$$\text{i.e. } s_{y3D} = s_{y2D}\left(1 + M\left(\frac{v}{\xi_J u_0}\right)^N\right)^{4.2} \tag{6.88a}$$

M and N are given by equations (6.83a) and (6.84a) respectively. The data are given in Table XVIII.

Equations (6.87) and (6.87a) are given in Figure 76, together with the data used for their determination. A better fit could have been obtained if more reliable data were available. The data used for the determination

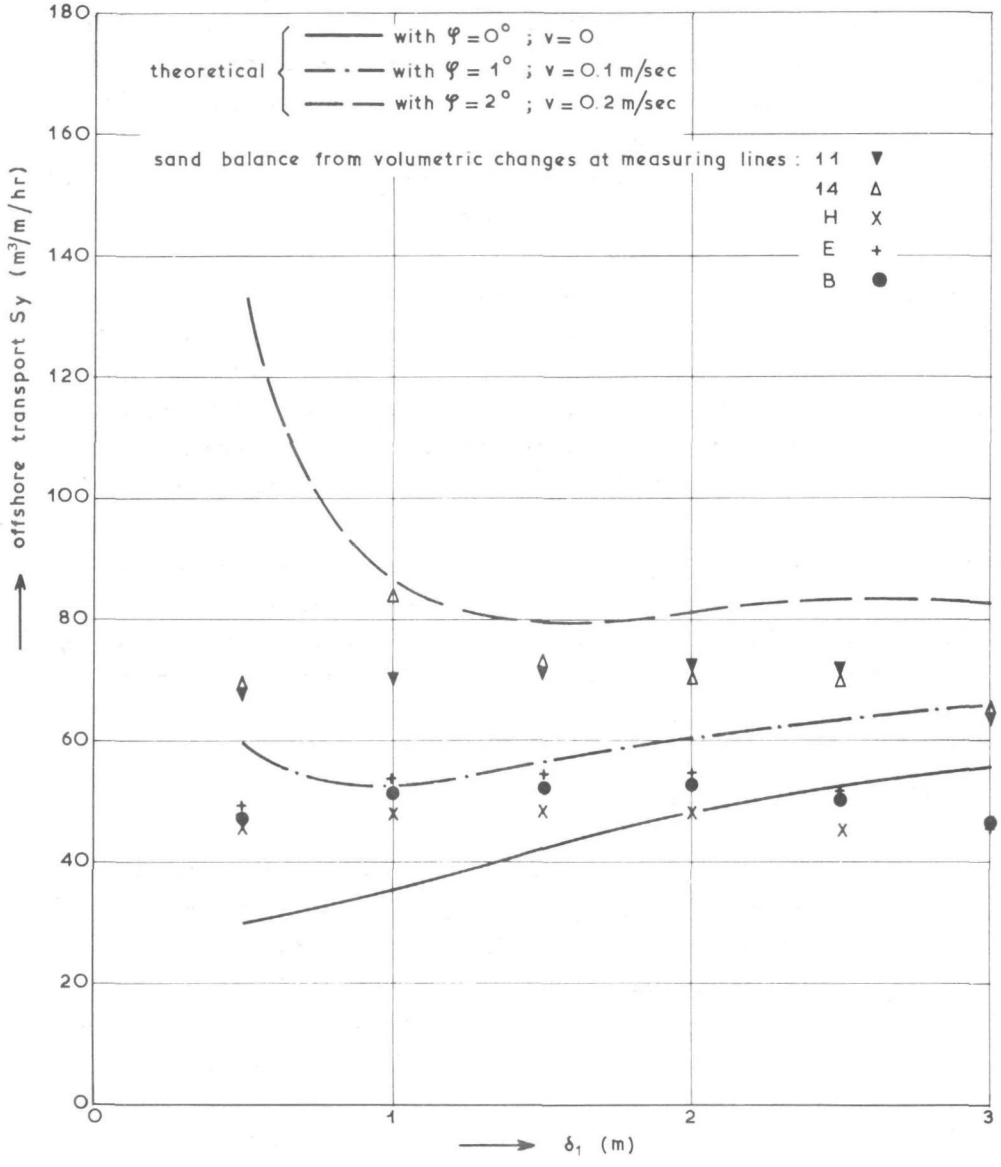

REMARKS : 1) H_o=4.5 m ; T=10 sec
2) date of storm : February, 1953
3) measuring lines situated at beach traverse no 6, North-Holland, the Netherlands

COMPARISON OF THEORETICAL AND MEASURED TRANSPORT RATES IN PROTOTYPE

FIGURE 77

of equations (6.87) and (6.87a) were in first instance not meant for this purpose, with a corresponding lack of complete information. It is, however, clear that equations (6.87) and (6.87a) (and thus also equations (6.88) and (6.88a)), are in correspondence with the tendency in the data. The available data are insufficient to help make a decision about which approach should be used for the increase in the shear stress. Eventually, when the insight into the problem of sediment entrainment is more advanced, the increase in shear stress, and as such also the increase in the coastal constant s_y, should be related to both the current field and the form of the wave profile. For the time being equation (6.88), i.e. the approach using the increase in bed shear under the whole wave to calculate the increase in the coastal constant s_y, will be used to determine the increase in the coastal constant due to three-dimensional effects, for both the model and the prototype.
When using this approach to compute the theoretical offshore transport rates at five selected sites on the North-Holland coastline in the Netherlands during a storm in February, 1953, a reasonably good correlation is obtained with the measured offshore sediment losses, as can be seen in Figure 77.

6.5 Application of the theory

The empirical results derived in the foregoing sections can be used to compute either time-dependent profile development or the magnitude of offshore transport, or both. The steps that will have to be followed to perform these computations will be listed systematically below, together with a summary of the appropriate empirical relationships. As these quantities can be computed for both small-scale model conditions and the full-scale prototype, the possibility also arises to use the empirical relationships to derive scale relationships for the transport phenomena occurring in a small-scale model in a direction perpendicular to the coastline. The procedure that has to be followed to derive these scale relationships will be mentioned briefly at the end of this chapter.

The different procedures will be dealt with under three headings, viz.:

A. Computation of offshore transport

B. Computation of time-dependent profiles

C. Derivation of scale relationships.

A. Computation of offshore transport

(1) Calculate the upper and lower limits of the D-profile, within which the actual profile development will take place.

Upper limit:

$$\frac{h_0}{D_{50}} = 7644 - 7706 \exp\left(-0.000143 \frac{H_0^{0.488} T^{0.93}}{D_{50}^{0.786}}\right) \qquad \text{(equation (4.110))} \tag{6.89}$$

Lower limit:

$$\frac{h_m}{\lambda_0} = 0.0063 \exp\left(4.347 \frac{H_0^{0.473}}{T^{0.894} D_{50}^{0.093}}\right) \qquad \text{(equation (4.125))} \tag{6.90}$$

The total D-profile thickness δ now equals: $\delta = h_0 + h_m$. (6.91)

(2) The maximum value s_{ym} of the coastal constant s_y can be calculated from:

$$\ln\left(\frac{s_{ym} T}{D_{50}}\right) = 10.7 - 28.9 \left[H_0^{1.68} \left(\frac{H_0}{\lambda_0}\right)^{-0.9} D_{50}^{-1.29} \left(\frac{H_0}{h_m}\right)^{2.66} \right]^{-0.079} \tag{6.40}$$

(3) The location of the maximum coastal constant s_{ym} in the D-profile is defined by the dimensionless offshore profile thickness Δ_{2m} ($= \delta_{2m}/\delta$) which can be determined as follows:

$$\Delta_{2m} = 0.8 - 1.1 H_0^{-0.55} \left(\frac{H_0}{h_m}\right)^{2.69} \tag{6.44}$$

(4) The distribution of the coastal constant s_y across the D-profile in the two-dimensional case is defined with the aid of the maximum value s_{ym},

its location Δ_{2m} and a dimensionaless distribution function s_y/s_{ym} of the form:

(i) for $\delta_2 > \delta_{2m}$ (i.e. landwards of the location of s_{ym}):

$$s_y/s_{ym} = \frac{0.93}{1 + 1.01\, X^{2.11}} + 0.07 \qquad (6.47)$$

(ii) for $\delta_2 < \delta_{2m}$ (i.e. seawards of the location of s_{ym}):

$$s_y/s_{ym} = \frac{0.99}{1 + 1.14\, X^{2.11}} + 0.01 \qquad (6.48)$$

In both the above cases

$$X = \Delta_m \left(\frac{H_0}{\lambda_0}\right)^{-1} \left(\frac{H_0}{h_m}\right)^2 \qquad (6.49)$$

where $\Delta_m = \left| \frac{\delta_{2m} - \delta_2}{\delta} \right|$ (6.46)

(5) If the situation under consideration is a three-dimensional case, i.e. if a longshore current with mean velocity v flows along the coastline, the shear stress at the bed will increase, with a corresponding increase in the value of s_{y2D} (as calculated from steps (2), (3) and (4)). At any given location in the profile the increase in the coastal constant can be written as:

$$s_{y3D} = s_{y2D} \left[1 + (1.91 - 1.32 \sin\varphi) \left(\frac{v}{\xi_J u_0}\right)^{(1.24 - 0.08 \sin\varphi)} \right]^{4.5} \qquad (6.88)$$

The steps (2) ... (5) yield the distribution of s_y across the D-profile in the three-dimensional case.

(6) The value of the equilibrium distance between the onshore and offshore profiles with the division between them at the water line (W_r) can be found from the following relationship:

$$\frac{\delta}{2W_r}\left(\frac{H_0}{\lambda_0}\right) = 1.51 \pm 10^3 \left[H_0^{0.132} D_{50}^{-0.447} \left(\frac{H_0}{\lambda_0}\right)^{-0.717} \right]^{-2.38} + 0.11 \pm 10^{-3} \tag{6.32}$$

(7) The distribution of the equilibrium length W across the D-profile is fully defined by the value of W_r and a dimensionless distribution function W/W_r:

$$\frac{W}{W_r} = 0.7\,\Delta_r + 1 + 3.97 \pm 10^7 b\, D_{50}^2\, \Delta_r^{1.36 \pm 10^4 D_{50}} \tag{6.20}$$

where $$\Delta_r = \frac{\delta_1 - h_0}{\delta} = \frac{h_m - \delta_2}{\delta} \tag{6.18}$$

and $$b = \begin{cases} 0; & \Delta_r \leq 0 \\ 1; & \Delta_r > 0 \end{cases} \tag{6.21}$$

The steps (6) and (7) yield the distribution of W across the D-profile. This distribution is as a first approximation independent of three-dimensional effects.

(8) The time-dependent length $(L_2 - L_1)_t$ between the onshore and offshore profiles can for any location inside the D-profile be calculated as follows:

$$\begin{aligned}(L_2 - L_1)_t = {} & W - (W - (L_2 - L_1)_0) \exp\left(-\frac{\delta s_y t}{\delta_1 \delta_2}\right) + \\ & + \frac{\delta_t s_t W_t \delta_1}{\delta_t \delta s_y - \delta_1 \delta_2 s_t}\left(\exp\left(-\frac{\delta s_y t}{\delta_1 \delta_2}\right) - \exp\left(-\frac{s_t t}{\delta_t}\right)\right) + \\ & + \frac{\delta_e s_e W_e \delta_2}{\delta_e \delta s_y - \delta_1 \delta_2 s_e}\left(\exp\left(-\frac{\delta s_y t}{\delta_1 \delta_2}\right) - \exp\left(-\frac{s_e t}{\delta_e}\right)\right)\end{aligned} \tag{6.92}$$

(equation (4.99))

The quantities s_e, W_e, s_t and W_t in equation (6.92) are unknown. In the most prototype cases under normal wave conditions, s_e and s_t will be small and the third and fourth terms in equation (6.92) (the terms

containing s_e and s_t) can be neglected. Under storm conditions, however, and in cases of steep initial slopes, s_e and s_t will be of considerable importance, and cannot be neglected. The values of these four unknown quantities (s_e, W_e, s_t and W_t) can be evaluated by making a study of the initial and equilibrium profile forms (i.e. at times $t = 0$ and $t = \infty$ respectively):

(i) Continuity at the upper limit of the initial D-profile

According to equation (4.72) the backshore erosion at time $t = 0$ can be written as:

$$\left[S_e\right]_{t = 0} = s_e W_e \tag{6.93}$$

The initial offshore transport (i.e. at time $t = 0$) when $\delta_1 = 0$, as calculated from equation (6.35), will as a first approximation be equal to $\left[S_e\right]_{t = 0}$, i.e.:

$$\left[S_e\right]_{t = 0} = \left[S_y\right]_{\delta_1 = 0,\ t = 0} \tag{6.94}$$

$$\text{or } s_e W_e = s_{y3}\left[W_3 - (L_2 - L_1)_{3,\, t = 0}\right] \tag{6.95}$$

where $(L_2 - L_1)_3$, W_3 and s_{y3} are the values of $(L_2 - L_1)$, W and s_y when $\delta_1 = 0$. W_3 and s_{y3} are known from steps (7) and (5) respectively, while $(L_2 - L_1)_{3,t=0}$ is known from the geometrical form of the initial D-profile. The right-hand side of equation (6.95) is thus known, with as a consequence that the product $s_e W_e$ is also known.

(ii) Continuity at the lower limit of the initial D-profile

In the same manner as at the upper limit of the initial D-profile, it can be shown that the initial offshore transport at the lower limit of the D-profile equals the initial growth of the transition area, i.e.

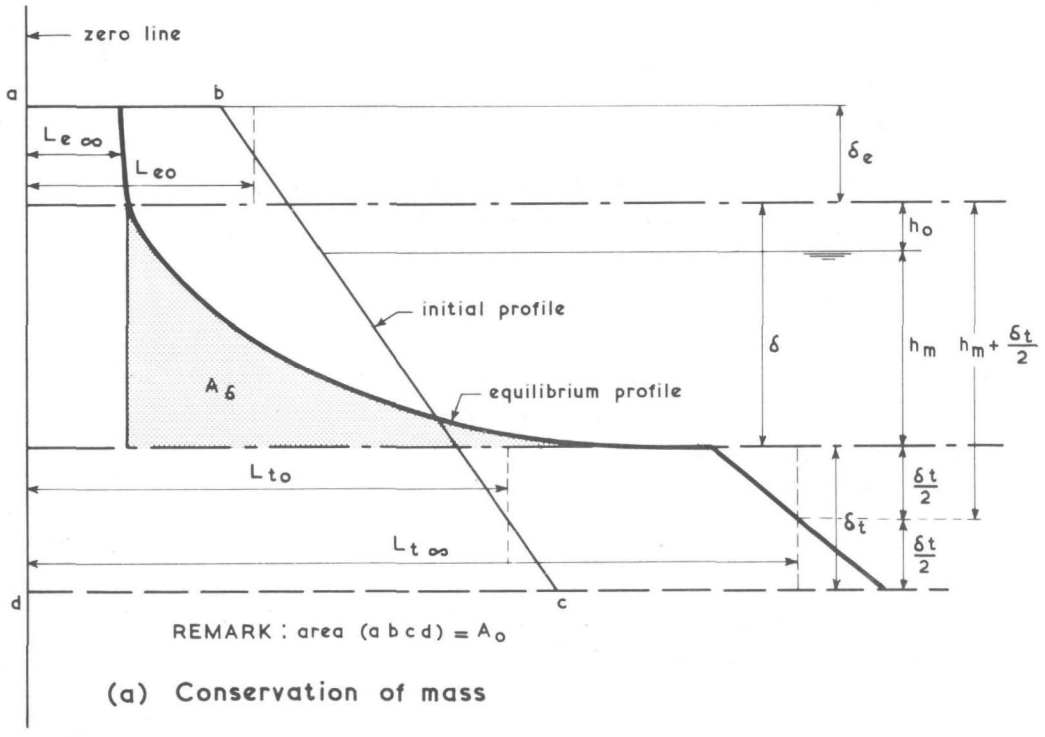

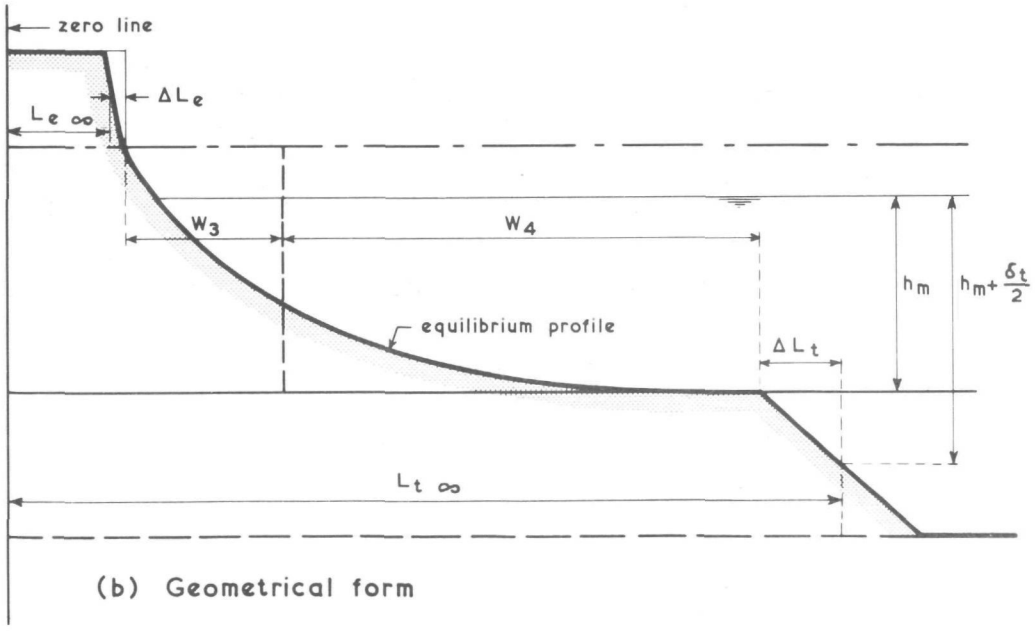

DEFINITION SKETCH : CALCULATION OF s_e, W_e, s_t AND W_t
FIGURE 78

$$\left[S_t \right]_{t=0} = \left[S_y \right]_{\delta_1 = \delta,\ t = 0} \tag{6.96}$$

$$\text{or } s_t W_t = s_{y4} \left[W_4 - (L_2 - L_1)_{4,t=0} \right] \tag{6.97}$$

where $(L_2 - L_1)_4$, s_{y4} and W_4 are the values of $(L_2 - L_1)$, s_y and W when $\delta_1 = \delta$. Consequently the product $s_t W_t$ is also known.

(iii) Conservation of mass

From the initial and equilibrium profile forms, as shown schematically in Figure 78a, the equation for the conservation of mass on the beach slope can be derived, for the case where no longshore gradient in longshore transport occurs, viz.:

$$L_{e\mathcal{S}} (\delta_e + \delta) + A_\delta + L_{t\mathcal{S}} \delta_t = A_0 \tag{6.98}$$

where A_δ = area under the equilibrium D-profile, in the area bordered by $0 \leqslant \delta_1 \leqslant \delta$ and $Y_{\delta_1=0}$

$$= -\int_0^\delta Y_{\mathcal{S}}\, dZ \tag{6.99}$$

$$Y_{\mathcal{S}} = \left(\frac{Z_r - Z_m}{Z_0 - Z_m}\right) W_r - \left(\frac{1}{Z_0 - Z_m}\right)\frac{\partial}{\partial Z}(WZ^2) + \left(\frac{Z_0 + Z_m}{Z_0 - Z_m}\right)\frac{\partial}{\partial Z}(WZ) + $$

$$- \frac{Z_0 Z_m}{Z_0 - Z_m}\frac{\partial W}{\partial Z} \qquad \text{(equation (3.69))} \tag{6.12}$$

= horizontal ordinate of the equilibrium D-profile at an elevation Z above the reference level

$Y_{\delta_1 = 0}$ = horizontal ordinate of the equilibrium D-profile when $\delta_1 = 0$

A_0 = total area in the initial profile, relative to the zero line.

As $L_{e\infty}$ and $L_{t\infty}$ are also unknown, equation (6.98) will be rewritten as follows:

$$(L_{e\infty} - L_{e0})\ (\delta_e + \delta) + L_{e0}\ (\delta_e + \delta) + A_\delta + (L_{t\infty} - L_{t0})\delta_t + L_{t0}\delta_t = A_0 \qquad (6.100)$$

When the terms in equation (6.100) are regrouped, it finally follows that:

$$W_t\delta_t - W_e\ (\delta_e + \delta) = (A_0 - A_\delta) - (L_{t0}\delta_t + L_{e0}\ (\delta_e + \delta)) \qquad (6.101)$$

$$\left.\begin{aligned} \text{because } W_e &= L_{e0} - L_{e\infty} \\ \text{and } W_t &= L_{t\infty} - L_{t0} \end{aligned}\right\} \qquad (6.102)$$

The terms on the right-hand side of equation (6.101) are all known in terms of the geometry of the initial and equilibrium profiles.

(iv) Geometrical form of the equilibrium profile

The geometrical form of the schematized equilibrium profile, as given in Figure 78b, yields the fourth equation:

$$L_{e\infty} + \Delta L_e + W_3 + W_4 + \Delta L_t = L_{t\infty} \qquad (6.103)$$

where ΔL_e = horizontal distance between the schematized position of the backshore and the landward extremity of D-profile in the equilibrium situation

ΔL_t = horizontal distance between the position of the schematized transition area and the seaward extremity of the D-profile in the equilibrium situation.

Substitution of equations (6.102) into equation (6.103) and regrouping of the terms yield:

$$W_t + W_e = (L_{e0} - L_{t0}) + (\Delta L_t + \Delta L_e) + (W_3 + W_4) \qquad (6.104)$$

In all cases the value of ΔL_e is negligible relative to that of ΔL_t and can be neglected, i.e.:

$$W_t + W_e = (L_{e0} - L_{t0}) + \Delta L_t + (W_3 + W_4) \tag{6.105}$$

ΔL_t can be approximated by means of the equation of Eagleson et al.[11], viz.:

$$\frac{\Delta L_t}{\lambda_0} = 42.73 \frac{J}{K} \left[\ln \left(0.01335 - 0.0161 \frac{h}{\lambda_0}\right) + 0.7271 \left(\frac{h}{\lambda_0}\right)^2 + 1.206 \frac{h}{\lambda_0} - 1.50 \right]_{(h_m + \delta_t/2)/\lambda_0}^{h_m/\lambda_0} \tag{6.106}$$

$$\text{where } \frac{J}{K} = \frac{T^{11/7} g \Delta_s D_{50}^{6/7}}{250.7 \lambda_0 \left(\frac{H_0}{\lambda_0}\right)^2 \nu^{3/7}} \qquad \text{(from equation (6.9))} \tag{6.107}$$

With the aid of the four equations (6.95), (6.97), (6.101) and (6.105) the four unknown quantities s_e, W_e, s_t and W_t can be found. The time-dependent length $(L_2 - L_1)_t$ can now be calculated for any location in the D-profile.

(9) The time-dependent offshore transport per unit of time and shoreline length at any location in the D-profile can now be calculated with the aid of equation (6.35), viz.:

$$S_{y_t} = s_y \left[W - (L_2 - L_1)_t \right] \tag{6.35}$$

(10) The cumulative transport across any depth contour in the D-profile can be found by integration in time of equation (6.35), i.e.:

$$V_{y_t} = \int_0^t S_{y_t} \, dt \tag{6.108}$$

where V_{y_t} = cumulative offshore transport across any given depth contour in the D-profile, up to time t.

B. Computation of time-dependent profiles

When the development of the D-profile in time is wanted, the steps (1) ... (8) above can be applied as described, except for steps (4) and (5), in which the variation in s_y is calculated. As stated in Chapter 6.3, the determination of s_y/s_{ym} with the aid of equations (6.47) ... (6.49) is an approximation. When the development of the profile in time is studied, this approximation is not good enough. The actual values of s_y can then be determined as shown below.

In the equations (6.95), (6.97), (6.101) and (6.105) the values of s_e, s_t, W_e and W_t are now not the only unknowns, the magnitude of the coastal constants s_{y3} and s_{y4} will also have to be determined. In order to determine these 6 quantities two more equations will be necessary. These equations can be found by considering the conditions at the time t_m when a known fraction f of the total transport had occurred through the section where the maximum value of s_y ($=s_{ym}$) occurs. This introduces one extra unknown, viz. t_m.

The total volume of sand that will pass the location of s_{ym} in time can be found from either the change in the volumes of the backshore and onshore profile areas, or from the change in the volumes of the transition area and offshore profile area, viz.:

$$V^{(1)}_{ym\infty} = W_e\delta_e + (L_{1m0} - L_{1m\infty})\delta_{1m} \tag{6.109}$$

or $$V^{(2)}_{ym\infty} = W_t\delta_t + (L_{2m\infty} - L_{2m0})\delta_{2m} \tag{6.110}$$

$$V^{(1)}_{ym\infty} = V^{(2)}_{ym\infty} = V_{ym\infty} \tag{6.111}$$

where L_{1m0} = initial length of the onshore profile, when the division between onshore and offshore profile is taken at the location of s_{ym}

$L_{1m\infty}$ = equilibrium length of the onshore profile, when the division

between onshore and offshore profile is taken at the location of s_{ym}.

The definitions of L_{2m0} and $L_{2m\infty}$ are similar to those of L_{1m0} and $L_{1m\infty}$, with that difference that the offshore profile is now under consideration.

$V^{(1)}_{ym\infty}$ = total volume of sand passing the location of s_{ym} in time, calculated with the aid of the variation in volume onshore of that point

$V^{(2)}_{ym\infty}$ = same definition as for $V^{(1)}_{ym\infty}$, with the exception that the variation in volume offshore of location of s_{ym} is used.

The values of $L_{1m\infty}$ and $L_{2m\infty}$ can be found from the form of the equilibrium profile, as given by equation (6.12). Furthermore it is possible to determine the total volume of sand passing the location of s_{ym} by integration of equation (6.35):

$$V^{(3)}_{ym\infty} = \int_0^{\infty} s_{ym} \left(W_m - (L_2 - L_1)_{mt}\right) dt \qquad (6.112)$$

where $V^{(3)}_{ym\infty}$ = total volume of sand passing the location of s_{ym} in time, as found from the integration of the transport (equation (6.35))

W_m = value of W at the location of s_{ym}

$(L_2-L_1)_{mt}$ = value of $(L_2 - L_1)_t$ at the location of s_{ym}.

The integration in equation (6.112) yields:

$$V^{(3)}_{ym\infty} = \frac{\delta_{1m}\,\delta_{2m}}{\delta}\left(W_m - (L_2 - L_1)_{m0}\right) + W_e \frac{\delta_{2m}\delta_e}{\delta} + W_t \frac{\delta_{1m}\delta_t}{\delta} \qquad (6.113)$$

$$V^{(3)}_{ym\infty} = V_{ym\infty} \qquad (6.114)$$

where $(L_2 - L_1)_{m0}$ = value of $(L_2 - L_1)_0$ at location of s_{ym}.

For time $t = t_m$ it now follows that:

$$V^{(3)}_{ymt_m} = f\, V^{(1)}_{ym\infty} \tag{6.115}$$

where $$V^{(3)}_{ymt_m} = \int_0^{t_m} s_{ym} \left[W_m - (L_2 - L_1)_{mt} \right] dt \tag{6.116}$$

= total volume of sand passing the location of s_{ym} up to the time t_m

$$V^{(3)}_{ym\infty} - V^{(3)}_{ymt_m} = (1-f)\, V^{(2)}_{ym\infty} \tag{6.117}$$

where $$V^{(3)}_{ym\infty} - V^{(3)}_{ymt_m} = \int_{t_m}^{\infty} s_{ym} \left[W_m - (L_2 - L_1)_{mt} \right] dt \tag{6.118}$$

= total volume of sand passing the location of s_{ym} between the time $t = t_m$ and $t = \infty$.

Furthermore the schematized profile length $(L_2 - L_1)_{mt}$ can either be found from equation (6.92), or as shown below:

$$(L_{2mt_m} - L_{2m0})\, \delta_{2m} + (V_t)_{t_m} = f\, V^{(1)}_{ym\infty} \tag{6.119}$$

where $(V_t)_{t_m}$ = total volume of sand passing the lower limit of the D-profile until time $t = t_m$

$$= \int_0^{t_m} S_t\, dt$$

$$= W_t \delta_t \left(1 - \exp\left(-\frac{s_t t_m}{\delta_t}\right)\right) \qquad \text{(see equation (4.83))} \tag{6.120}$$

Thus it follows from equation (6.119) that

$$L_{2mt_m} = L_{2m0} + \frac{1}{\delta_{2m}} \left(f\, V^{(1)}_{ym\infty} - (V_t)_{t_m} \right) \tag{6.121}$$

In the same manner it follows that:

$$(L_{1m0} - L_{1mt_m})\,\delta_{1m} + (V_e)_{t_m} = f\,V^{(2)}_{ym\infty} \tag{6.122}$$

where $(V_e)_{t_m}$ = total volume sand passing the upper limit of the D-profile until time $t = t_m$

$$= \int_0^{t_m} S_e\,dt$$

$$= W_e\delta_e\,(1 - \exp\,(-\frac{s_e t_m}{\delta_e})) \tag{6.123}$$

(see equation (4.72))

It follows from equation (6.122) that:

$$L_{1mt_m} = L_{1m0} + \frac{1}{\delta_{1m}}((V_e)_{t_m} - f\,V^{(2)}_{ym\infty}) \tag{6.124}$$

Combination of equations (6.121) and (6.124) yields:

$$(L_2 - L_1)_{mt_m} = (L_2 - L_1)_{m0} + \frac{1}{\delta_{2m}}\left[f\,V^{(1)}_{ym\infty} - (V_t)_{t_m}\right] - \frac{1}{\delta_{1m}}\left[(V_e)_{t_m} - f\,V^{(2)}_{ym\infty}\right] \tag{6.125}$$

As a matter of fact, equation (6.125) is equal to equation (6.92), when $t = t_m$ is substituted into the latter equation. The equations (6.115) and (6.116), (6.117) and (6.118), and (6.92) and (6.125) yield 3 equations, which, together with the earlier-mentioned equations (6.95), (6.97), (6.101) and (6.105) form a set of 7 non-linear equations. From these equations the unknown quantities s_e, s_t, W_e, W_t, s_{y3}, s_{y4} and t_m can be found.

For any location in the D-profile with onshore and offshore layer thicknesses of δ_{1i} and δ_{2i} respectively, the value of s_{yi} can now be found by considering the situation when a fraction f_i of the total transport up to equilibrium had occurred, viz.:

$$f_i\,(W_e\delta_e + (L_{10} - L_{1\infty})_i\delta_{1i}) = V^{(3)}_{yt_i} \tag{6.126}$$

$$\text{and } (1 - f_i)\,(W_t\delta_t + (L_{2\infty} - L_{20})_i\,\delta_{2i}) = V^{(3)}_{y\infty} - V^{(3)}_{yt_i} \tag{6.127}$$

$$\text{where } V^{(3)}_{yt_i} = \int_0^{t_i} s_{yi}\left[W_i - (L_2 - L_1)_i\right]dt \tag{6.128}$$

= total volume of sand passing the location of s_{yi} up to time t_i

$$V^{(3)}_{y\infty} = \int_0^{\infty} s_{yi}\left[W_i - (L_2 - L_1)_i\right]dt \tag{6.129}$$

= total volume of sand passing the location of s_{yi} up to time t = infinity.

Subscript i denotes the profile quantities at the location of s_{yi}, i.e. where the onshore and offshore profile thicknesses are δ_{1i} and δ_{2i} respectively. The only two unknown quantities in equations (6.126) and (6.127) are s_{yi} and t_i. By repeating this procedure at various locations in the D-profile the distribution of s_y across the D-profile can be found.

In a three-dimensional case the value of s_{ym}, as determined for the two-dimensional case, must be increased with the aid of equation (6.88) before applying the above-mentioned procedure.

In the same manner as for the case where offshore transport was calculated, step (8) will now yield the distribution of $(L_2 - L_1)$ across the D-profile for any wanted time t.

The form of the time-dependent D-profile can be determined from the variation in $(L_2 - L_1)$ across the D-profile, in the same manner as was done to arrive to equation (3.63). That equation was derived for equilibrium conditions, however, the derivation was based purely on geometrical conside-

rations and consequently it can be applied to any time-dependent profile, as long as W_r and W_k are replaced by $(L_2 - L_1)_r$ and $(L_2 - L_1)_k$, i.e.:

$$Y_k = \left\{ (L_2 - L_1)_r \left(\frac{Z_r - Z_m}{Z_0 - Z_m}\right) - (L_2 - L_1)_k \left(\frac{Z_k - Z_m}{Z_0 - Z_m}\right) \right\} \left(\frac{Z_0 - Z_k}{Z_{k-1} - Z_k}\right) + \frac{\sum_{i=1}^{k-1} Y_i \, (Z_{i-1} - Z_i)}{Z_{k-1} - Z_k} \qquad (6.130)$$

where Y_k = the ordinate in zone k of the D-profile at time t at an elevation $Z = 1/2 \, (Z_{k-1} + Z_k)$, i.e. at the average elevation of the k^{th} zone, as measured from the zero line. The zero line is the vertical line through the schematized position of the sediment in the area of the profile defined by $Z_0 \geqslant Z \geqslant Z_r$

$(L_2 - L_1)_r$ = value of $(L_2 - L_1)$ at time t when the division between the onshore and offshore profiles lies at a height Z_r above the reference level

$(L_2 - L_1)_k$ = value of $(L_2 - L_1)$ at time t when the division between the onshore and offshore profiles lies at a height Z_k above the reference level.

The dimensionless form of the equilibrium D-profile can be determined by substitution of the values of W/W_r from equation (6.20) into equation (6.12). When the reference level is chosen at the lower limit of the D-profile, equation (6.12) reduces to equation (6.14).
Equation (6.20) can then be written as:

$$\frac{W}{W_r} = 0.7 \left(\frac{h_m}{\delta} - \frac{Z}{\delta}\right) + 1 + 3.97 * 10^7 b \, D_{50}^2 \left(\frac{h_m}{\delta} - \frac{Z}{\delta}\right)^{1.36 * 10^4 D_{50}}$$

$$= 0.7 \, (h_r - z) + 1 + P \, (h_r - z)^E$$

$$= Q - 0.7 \, z + P \, (h_r - z)^E \qquad (6.131)$$

where $h_r = \frac{h_m}{\delta}$ (6.132)

= dimensionless position of the water line relative to the lower limit of the D-profile

$z = \frac{Z}{\delta}$ (6.133)

= dimensionless position in the D-profile measured relative to the lower limit of the D-profile

$Q = 0.7\, h_r + 1$ (6.134)

$P = 3.97 * 10^7 b\, D_{50}^2$ (6.135)

$E = 1.36 * 10^4 D_{50}$ (6.136)

Substitution of equations(6.131) ... (6.133) into equation (6.14) yields:

$$Y/W_r = h_r + \frac{\partial}{\partial z}\left[(Q - 0.7z + P\,(h_r - z)^E)\,(z - z^2)\right] \quad (6.137)$$

When the differentiation in equation (6.137) is performed, the dimensionless equilibrium D-profile results, viz.:

$$Y/W_r = h_r + (1 - 2z)\left[Q - 0.7z + P\,(h_r - z)^E\right] - (z - z^2) * * \left[0.7 + E\,P\,(h_r - z)^{E-1}\right]$$

$$= (h_r + Q) + 2.1z^2 - (1.4 + 2Q)z + P\,(1 - 2z)\,(h_r - z)^E + + E\,P(z^2 - z)\,(h_r - z)^{E-1} \quad (6.138)$$

Y is measured relative to the schematized position of the sediment in the area of the equilibrium profile defined by $Z_0 \geqslant Z \geqslant Z_r$. When calculating time-dependent profiles, however, it will be more convenient to calculate the Y-ordinates at any time t ($t \leqslant \infty$) relative to some fixed zero line. This choice will depend upon the specific situation in each application of the theory.

C. Derivation of scale relationships

An investigation into the consequences of the results of the present study for the scale relationships in small-scale hydraulic models is a study apart. As such, the scale relationships for geometrical distortion and offshore sediment transport, which can be derived from the empirical formulae given in this report, will not be studied in detail at this stage. These aspects are still the subject of continued research. At the moment it will only be stated that the scale relationship for geometrical distortion can be derived with the aid of equations (6.20) and (6.32), while the offshore sediment transport scale in a small-scale hydraulic model can be found with the aid of the equations (6.20), (6.32), (6.40), (6.44), (6.47) ... (6.49), (6.92) and (6.108).

LIST OF REFERENCES

1 ARTHUR, R.S.
A note on the dynamics of rip currents;
Journal of Geophysical Research, Vol. 67, No. 7, pp. 2777 - 2779, July, 1962.

2 BAKKER, W.T.
The dynamics of a coast with a groyne system;
Proceedings, 11th Conference on Coastal Engineering, London, Chapter 31, pp. 492 - 517, 1968.

3 BAKKER, W.T.
The influence of the longshore variation of the wave height on the littoral current;
Study Report WWK 71 - 19, Department for Coastal Research, Division of Water Management and Hydraulic Research, Ministry of Public Works (Rijkswaterstaat), The Hague, 1971.

4 BATTJES, J.A.
"Golfoploop en golfoverslag" (Wave run-up and wave overtopping);
Den Haag, Technische Adviescommissie voor de Waterkeringen, January, 1972.

5 BHATTACHARYA, P.K.
Sediment suspension in shoaling waves;
Iowa City, The University of Iowa, Ph. D. Thesis,100 pp., 1971.

6 BONNEFILLE, R. and PERNECKER, L.
"Le début d'entrainement des sédiments sous l'action de la houle";
Bulletin du Centre de Recherches et d'Essais de Chatou, No. 15, Mars, 1966.

7 BOWEN, A.J.
Rip currents (Theoretical Investigations);
Journal of Geophysical Research, Vol. 74, No. 23, October, 1969.

LIST OF REFERENCES (continued)

8 BOWEN, A.J., INMAN, D.L. and SIMMONS, V.P.
Wave "set-down" and set-up;
Journal of Geophysical Research, 73, No. 8, pp. 2569 - 2577,
April, 1968.

9 BIJKER, E.W.
Some considerations about scales for coastal models with movable bed;
Delft Hydraulics Laboratory, Publication No. 50, 142 pp., November, 1967.

10 DELFT HYDRAULICS LABORATORY
Gold Coast, Queensland, Australia-Coastal erosion and related problems;
Volume II, Part 2: Investigations (Figures), Report R 257, 1970.

11 EAGLESON, P.S. and JOHNSON, J.W.
Coastal processes;
in: Estuary and Coastline Hydrodynamics, editor: A.T. Ippen,
Chapter 9, McGraw-Hill Book Company, Inc., June, 1966.

12 EAGLESON, P.S., GLENNE, B. and DRACUP, J.A.
Equilibrium characteristics of sand beaches;
Proceedings, ASCE, Journal of the Hydraulics Div., 89, Paper No. 3387,
pp. 35 - 57, January, 1963.

13 EINSTEIN, H.A.
The bed-load function for sediment transportation in open channel flow;
Washington, U.S. Department of Agriculture, Techn. Bull. No. 1026,
71 pp., 1950.

14 FRIJLINK, H.C.
Discussion des formules de débit solide de Kalinske, Einstein et
Meyer-Peter et Mueller compte tenue des mesures récentes de transport
dans les rivières Néerlandaises;
2me Journ. Hydraulique, Soc. Hydr. de France, Grenoble, pp. 98 - 103, 1952.

15 GODDET, J.
"Etude du début d'entrainement des matériaux mobiles sous l'action de la
houle":,
La Houille Blanche, No. 2, pp. 122 - 135, Mars - Avril, 1960.

LIST OF REFERENCES (continued)

16 HALD, A.
Statistical theory with engineering applications;
John Wiley and Sons, Inc., New York, 783 pp., 1952.

17 HALD, A.
Statistical tables and formulas;
John Wiley and Sons, Inc., New York, 97 pp., 1952.

18 HATTORI, M.
The mechanics of suspended sediment due to standing waves;
Coastal Engineering in Japan, Volume XII, pp. 69 - 81, December, 1969.

19 HOM-MA, M. and HORIKAWA, K.
Suspended sediment due to wave action;
Proceedings, 8th Conference on Coastal Engineering, Mexico City,
Mexico, pp. 168 - 193, November, 1962.

20 HORIKAWA, K. and KUO, C.T.
A study of wave transformation inside surf zone;
Proceedings, 10th Conference on Coastal Engineering, Tokyo, Chapter 15,
pp. 217 - 233, 1966.

21 HULSBERGEN, C.H.
Origin, effect and suppression of secondary waves;
Proceedings, 14th Conference on Coastal Engineering, Copenhagen, 1974.

22 HUNT, I.A.
Design of seawalls and breakwaters;
Proceedings, ASCE, Journal of the Waterways and Harbours Division, 85,
No. WW3, paper 2172, pp. 123 - 152, September, 1959.

23 IVERSEN, H.W.
Waves in shoaling water;
in: Manual of Amphibious Oceanography, ed. R.L. Wiegel, Univ. of
California, Contract N 7 onr-29535, Office of Naval Research, 1951.

LIST OF REFERENCES (continued)

24 IVERSEN, H.W.
Waves and breakers in shoaling water;
Proceedings, 3rd Conference on Coastal Engineering, 1952.

25 IWAGAKI, Y. and NODA, H.
Laboratory study of scale effects in two-dimensional beach processes;
Proceedings, 8th Conference on Coastal Engineering, Mexico, Chapter 14, pp. 194 - 210, November, 1962.

26 JOHNSON, J.W.
Scale effects in hydraulic models involving wave motion;
Transactions, American Geophysical Union, Vol. 30, (4), pp. 517 - 525, 1949.

27 JONSSON, I.G.
Measurements in the turbulent wave boundary layer;
Proceedings, 10th I.A.H.R. Congress, London, Volume I, Paper I - 12, pp. 85 - 92, 1963.

28 JONSSON, I.G.
Wave boundary layers and friction factors;
Proceedings, 10th Conference on Coastal Engineering, Tokyo, Volume I, Chapter 10, pp. 127 - 148, 1966.

29 KALINSKE, A.A.
Movement of sediment as bed load in rivers;
Transactions, American Geophysical Union, Volume 28, No. 4, pp. 615 - 620, 1947.

30 KEMP, P.H.
The relationship between wave action and beach profile characteristics;
Proceedings, 7th Conference on Coastal Engineering, Volume 1, Chapter 14, pp. 262 - 277, 1960.

31 LAITONE, E.V.
The second approximation of cnoidal and solitary waves;
Journal of Fluid Mechanics, Volume 9, 1961.

LIST OF REFERENCES (continued)

32 LARRAS, J.
Variations de la periode des lames au cours de leur deferlement;
Proceedings, 10th I.A.H.R. Congress, London, Volume 1, Subject I, No. 43, pp. 351 - 352, 1963.

33 LONGUET-HIGGINS, M.S.
Mass transport in water waves;
Phil. Transactions of the Royal Society, London, A 245, No. 903, pp. 535 - 581, 1953.

34 LONGUET-HIGGINS, M.S. and STEWART, R.W.
Radiation stresses in water waves, a physical discussion with applications;
Deep-sea Research, 11, No. 4, pp. 529 - 562, August, 1964.

35 MEYER-PETER, E. and MUELLER, R.
Formulas for bed load transport;
Proceedings, 2nd I.A.H.R. Congress, Stockholm, Volume 2, Paper 2, 1948.

36 MOTTA, V.F.
"A Questao da Correlacão entre a Esbeltez das Ondas do Mar e seu Eferto Erosivo ou Construtivo sôbre os Perfis de Praia";
Inst. de Pesquisas Hidr., Univ. do Rio Grande do Sul. Mem. apres. ao 1° Congr. Bras. de Transp. Maritimos e Construçao Naval, Rio de Janeiro, Outubro, 1963.

37 NAKAMURA, M., SHIRAISHI, H. and SASAKI, J.
Wave decaying due to breaking;
Proceedings, 10th Conference on Coastal Engineering, Tokyo, Chapter 16, pp. 234 - 253, 1966.

38 PATRICK, D.A. and WIEGEL, R.L.
Amphibian Tractors in the Surf;
1st Conference on Ships and Waves, Chapter 29, 1955.

LIST OF REFERENCES (continued)

39 PELNARD-CONSIDERE, R.
Essai de théorie de l'évolution des formes de rivages en plages de sable et de galets;
Quatrième Journées de l'Hydraulique, Paris, Les Energies de la Mer, Question III, 13 - 15 Juin,1954.

40 PRANDTL, L.
Gesammelte Abhandlungen zur angewandten Mechanik, Hydro- und Aerodynamik, Dritter Teil;
Springer - Verlag, Berlin/Göttingen/Heidelberg, 1961.

41 RECTOR, R.L.
Laboratory study of equilibrium profiles of beaches;
Beach Erosion Board,Technical Memorandum No. 41, Washington, 38 pp., August, 1954.

42 SAVILLE, T. (jr.)
Wave run-up on shore structures;
Proceedings, ASCE, 82, No. WW2, April, 1956.

43 SAVILLE, T. (jr.)
Scale effects in two-dimensional beach studies;
Transactions, I.A.H.R., 7th General Meeting, Paper A3, pp. 1 - 10, 1957.

44 SCOTT, T.
Sand movement by waves;
Beach Erosion Board, Technical Memorandum No. 48, 37 pp., August, 1954.

45 SHINOHARA, K. and TSUBAKI, T.
Laboratory study of sand movement and equilibrium profiles of beaches;
Coastal Engineering in Japan, Volume 2, pp. 29 - 34, 1959.

46 SHINOHARA, K., TSUBAKI, T., YOSHITAKA, M. and AGEMORI, C.
Sand transport along a model sandy beach by wave action;
Kyushu University, Japan, Research Institute for Applied Mechanics, 6, No. 21, 23 pp., 1958.

LIST OF REFERENCES (continued)

47 SITARZ, J.A.
Contribution à l'étude de l'évolution des plages à partir de la connaissance des profils d'équilibre;
Lab. de Chatou, 20 pp., 1963.

48 SWART, D.H.
Die effek van verwringing op kusprofiele (The effect of distortion on coastal profiles; in Afrikaans);
M. Eng. Thesis, University of Stellenbosch, South Africa, 176 pp., March, 1971.

49 SWART, D.H.
Long-duration tests of coastal profile development;
Delft Hydraulics Laboratory, Report S246, to be published in 1975.

50 U.S. ARMY COASTAL ENGINEERING RESEARCH CENTER.
Shore Protection, Planning and Design;
Technical Report No. 4, 3rd edition, 1966.

51 WATERS, C.H.
Equilibrium slopes of sea beaches;
M.Sc.thesis, Dept. of Engng., University of California, 1939.

52 WATTS, G.M.
Laboratory study of the effect of varying periods on beach profiles;
Beach Erosion Board, Technical Memorandum No. 53, 19 pp., December, 1954.

53 WIEGEL, R.L.
Oceanographical Engineering;
Englewood Cliffs, New Jersey, Prentice Hall, 532 pp., 1964.

54 ZWAMBORN, J.A. and VAN WYK, W.
Some positive results in reproducing coastal processes in models;
Symposium on Coastal Engineering, Stellenbosch, 16 pp., June, 1969.

Table I

Breaker type p (-)	Wave energy dissipation $1-(H_{b2}/H_{b1})^2$ (-)	Breaker type p (-)	Wave energy dissipation $1-(H_{b2}/H_{b1})^2$ (-)
0	0	.60	.57
.10	.23	.30	.47
.20	.23	.50	.60
.30	.29	.10	.26
.40	.39	.70	.39
.50	.47	.30	.19
.60	.62	.30	.41
.70	.69	.20	.34
.80	.78	.80	.85
.90	.90	.75	.88
1.00	.98	.60	.51
.56	.59	.70	.51
.05	.07	.45	.47
.10	.08	.40	.47
.47	.76	.30	.52
0	.07	.35	.52
.30	.44	.70	.74
.15	.31	.75	.74

REMARK: All measurements were performed during test 7301.

Table I: Relation between breaker type p and energy dissipation.

Table II

Test no.	Breaker type p (-)	Deepwater wave steepness H_o/λ_o (-)	cot α (-)	Breaker index γ (-)
7112 A	1.00	.0469	7.56	1.075
	1.00		25.45	.746
	.90		9.80	.800
	.90		17.35	.812
	.85		18.00	.654
	.80		23.50	.518
	.80		20.95	.670
	.65		15.15	.610
	.60		13.16	.585
	.55		14.59	.544
	.50		16.67	.443
	.50		11.16	.572
	.50		12.88	.572
	.50		13.16	.572
	.50		13.16	.605
	.30		14.33	.618
	0		18.63	.525
7112 B	1.00	.0454	11.43	1.024
	1.00		16.71	.815
	.85		22.50	.718
	.80		28.40	.488
	.80		24.00	.737
	.80		22.40	.683
	.65		14.52	.650
	.53		10.80	.657
	.50		12.27	.667
	.50		18.62	.424
	.35		11.32	.730
	.35		16.88	.759
	.30		23.00	.492
	.20		12.00	.689
	0		46.00	.428
	0		30.37	.515

Table II (continued)

Test no.	Breaker type p (-)	Deepwater wave steepness H_o/λ_o (-)	cot α (-)	Breaker index γ (-)
7112 C	1.00	.0464	12.61	.962
	1.00		14.55	1.043
	1.00		20.00	.672
	1.00		22.40	.792
	1.00		24.55	.706
	1.00		22.40	.778
	1.00		24.55	.647
	1.00		22.40	.778
	1.00		22.40	.754
	1.00		22.40	.754
	1.00		22.40	.820
	1.00		24.55	.730
	.95		24.55	.706
	.93		21.82	.808
	.87		24.55	.752
	.80		32.07	.603
	.80		24.55	.706
	.77		13.24	.733
	.75		19.18	.738
	.50		14.55	.767
	.50		11.67	.806
	.50		22.40	.658
	.40		53.33	.469
	.40		56.00	.414
7301 A	.60	.0419	19.05	.686
	.30		15.63	.606
	.10		6.80	.540
	.10		10.75	.567
	.10		11.75	.479
	.10		20.96	.552
	.05		20.50	.456
	0		13.50	.407
7301 B	.50	.0419	27.50	.500
	.47		10.10	.837
	.35		28.00	.535
	.15		10.00	.463
	.15		26.00	.508

Table II (continued)

Test no.	Breaker type p (-)	Deepwater wave steepness H_o/λ_o (-)	cot α (-)	Breaker index γ (-)
7301 B	.15	.0419	25.46	.488
	.15		31.11	.527
	.15		12.83	.508
	.10		35.00	.419
	.10		25.65	.442
	.07		20.00	.527
	.05		15.88	.470
	.05		15.00	.430
	.03		19.36	.430
7301 C	.56	.0419	10.74	.670
	.40		15.90	.640
	.35		15.49	.404
	.15		8.50	.508
	.15		20.82	.476
	.10		15.48	.536
	.08		8.93	.483
	.07		17.41	.416
	.07		13.07	.440
	.05		21.78	.383
	.05		13.80	.440
	.05		11.80	.483
	.05		15.63	.492
7301 D	1.00	.0419	7.42	.885
	.90		10.86	.960
	.80		14.29	.925
	.75		9.23	.828
	.70		10.52	.814
	.60		8.33	.770
	.50		12.70	.718
	.40		8.19	.725
	.30		14.29	.640
	.20		7.04	.637
	.15		10.38	.604
	.14		13.83	.632
	.12		17.86	.568
	.10		5.07	.572
	.10		10.50	.536

Table II (continued)

Test no.	Breaker type p (-)	Deepwater wave steepness H_o/λ_o (-)	cot α (-)	Breaker index γ (-)
7301 D	.05	.0419	9.37	.532
	.05		8.00	.523
	0		4.76	.533
7112 B	.80	.0454	-	.647
	.75		-	.807
	.20		-	.608
7112 C	1.00	.0464	-	.750
	.80		-	.827
	.70		-	.525
	.60		-	.622
	.50		-	.777
	.30		-	.400
	.30		-	.527
	.20		-	.575
	.10		-	.425

Table II: Determination of breaker index γ

Table III

Test no. (run no.)	Deepwater wave height H_o (m)	Median particle diameter D_{50} (mm)	Wave period T (sec)	Dimensionless upper limit h_o/D_{50}
6902 A	.103	.227	1.55	440
6902 B	.107	.227	1.55	396
6902 C	.101	.227	1.55	308
6902 D	.107	.227	1.55	308
6903 A	.111	.224	1.55	268
6903 B	.111	.224	1.55	313
6903 C	.104	.163	1.55	368
6903 D	.104	.163	1.55	368
7001 A	.082	.221	1.55	317
7001 B	.086	.221	1.55	317
7001 C	.081	.163	1.55	368
7001 D	.081	.163	1.55	368
7005 A	.080	.221	1.55	317
7005 B	.078	.221	1.55	317
7005 C	.073	.163	1.55	368
7005 D	.077	.163	1.55	368
7006 A	.088	.220	1.55	273
7006 B	.088	.220	1.55	273
7006 C	.088	.160	1.55	250
7006 D	.088	.160	1.55	375
7016 A	.129	.220	1.55	478
7017 A	.129	.220	1.55	455
7109 A	.114	.220	1.15	250
7109 B	.114	.160	1.15	344
7111 A	.107	.220	1.15	205
7111 B	.112	.160	1.15	281
7112 A	.096	.220	1.15	182
7112 B	.093	.160	1.15	250
7112 C	.095	.110	1.15	434
7114 A	.086	.220	1.15	227
7114 B	.086	.160	1.15	344
7114 C	.086	.110	1.15	482
7115 A	.096	.220	1.15	227
7115 B	.092	.160	1.15	282

Table III (continued)

Test no. (run no.)	Deepwater wave height H_o (m)	Median particle diameter D_{50} (mm)	Wave period T (sec)	Dimensionless upper limit h_o/D_{50}
7115 C	.097	.110	1.15	455
7116 A	.094	.220	1.15	182
7116 B	.095	.160	1.15	219
7116 C	.091	.110	1.15	409
7201 A	.098	.220	1.15	250
7201 B	.096	.160	1.15	250
7201 C	.097	.110	1.15	400
721 A	.038	.220	.844	114
721 B	.038	.160	.844	63
722 A	.051	.220	.844	73
722 B	.053	.160	.844	69
723 A	.064	.220	.844	114
723 B	.064	.160	.844	125
724 A	.065	.220	1.038	182
724 B	.063	.160	1.038	207
725/1 A	.082	.220	1.038	205
725/1 B	.085	.160	1.038	238
725/2 A	.081	.220	1.038	227
725/2 B	.085	.160	1.038	238
726 A	.097	.220	1.038	155
726 B	.097	.160	1.038	175
726/1 A	.095	.220	1.038	205
726/1 A	.097	.160	1.038	275
727 A	.074	.220	1.146	273
727 B	.075	.160	1.146	269
728 A	.095	.220	1.146	173
728 B	.095	.160	1.146	244
729 A	.113	.220	1.146	227
729 B	.114	.160	1.146	256
1101 A	.082	.220	1.08	318
1101 B	.082	.220	1.08	341
1101 C	.082	.220	1.08	341
1101 D	.082	.170	1.08	438

Table III (continued)

Test no. (run no.)	Deepwater wave height H_o (m)	Median particle diameter D_{50} (mm)	Wave period T (sec)	Dimensionless upper limit h_o/D_{50}
301 A	.200	.220	1.67	682
301 B	.200	.220	1.67	614
301 C	.200	.220	1.67	591
301 D	.200	.170	1.67	750
7301 A	.070	.220	1.04	182
7301 B	.070	.170	1.04	188
7301 C	.070	.170	1.04	188
7301 D	.070	.220	1.04	182
HoHA 301171	4.65	.220	7.65	5909
HoHB 301171	4.65	.220	7.65	5455
HoHC 301171	4.65	.220	7.65	6364
DSE 300765	1.22	.350	7.5	3833
DSE 300865	1.52	.350	7.5	3833
DNE 220365	2.93	.350	9.5	5000
DNE 150365	3.05	.350	8.5	4181
DNE 250365	1.22	.350	9.4	3484
DNE 260365	1.52	.350	9.4	3484
Qζ 0766	1.57	.202	7.00	4528
Qζ 0667	1.61	.202	7.00	4528
Qζ 09/1067	1.38	.202	7.00	4528
Qζ 0868	1.54	.202	7.00	4528
Qζ 1268	1.38	.202	7.00	4528
Qδ 0766	1.38	.211	7.00	4028
Qδ 0768	1.38	.211	7.00	4028
Qβ 1068	1.01	.204	7.00	3162
Qβ 0967	.97	.204	7.00	3646

REMARK: For location of the prototype cases, see Table IX

Table III: Upper limit of D-profile.

Table IV

Test no. (run no.)	Deepwater wave height H_o (m)	Median particle diameter D_{50} (mm)	Wave period T (sec)	Dimensionless lower limit h_m/λ_o
6902 A	.103	.227	1.55	.0480
6902 B	.107	.227	1.55	.0427
6902 C	.101	.227	1.55	.0427
6902 D	.107	.227	1.55	.0480
6903 A	.111	.224	1.55	.0507
6903 B	.111	.224	1.55	.0560
6903 C	.104	.163	1.55	.0480
6903 D	.104	.163	1.55	.0587
7001 A	.082	.221	1.55	.0400
7001 B	.086	.221	1.55	.0427
7001 C	.081	.163	1.55	.0400
7001 D	.081	.163	1.55	.0400
7005 A	.080	.221	1.55	.0374
7005 B	.078	.221	1.55	.0400
7005 C	.073	.163	1.55	.0374
7005 D	.077	.163	1.55	.0374
7006 A	.088	.220	1.55	.0480
7016 A	.129	.220	1.55	.0747
7017 A	.129	.220	1.55	.0747
7109 A	.114	.220	1.15	.1357
7109 B	.114	.160	1.15	.1357
7111 A	.107	.220	1.15	.1163
7111 B	.112	.160	1.15	.1308
7112 A	.096	.220	1.15	.1114
7112 B	.093	.160	1.15	.1114
7114 B	.086	.160	1.15	.1212
7115 A	.096	.220	1.15	.1212
7115 B	.092	.160	1.15	.1212
7115 C	.097	.110	1.15	.1357
7201 A	.098	.220	1.15	.1018
7201 B	.096	.160	1.15	.1114
721 A	.038	.220	.844	.0810
721 B	.038	.160	.844	.0810

Table IV (continued)

Test no. (run no.)	Deepwater wave height H_o (m)	Median particle diameter D_{50} (mm)	Wave period T (sec)	Dimensionless lower limit h_m/λ_o
722 A	.051	.220	.844	.0990
722 B	.053	.160	.844	.1080
723 A	.064	.220	.844	.1170
723 B	.064	.160	.844	.1260
724 A	.065	.220	1.038	.0952
724 B	.063	.160	1.038	.0952
725/1 A	.082	.220	1.038	.1072
725/1 B	.085	.160	1.038	.1131
725/2 A	.081	.220	1.038	.1072
725/2 B	.085	.160	1.038	.1072
726 A	.097	.220	1.038	.1132
726 B	.097	.160	1.038	.1191
727 A	.074	.220	1.146	.0732
727 B	.075	.160	1.146	.0825
728 A	.095	.220	1.146	.0969
728 B	.095	.160	1.146	.1019
729 B	.114	.160	1.146	.1212
1101 A	.082	.220	1.08	.1044
1101 B	.082	.220	1.08	.1044
1101 C	.082	.220	1.08	.0990
1101 D	.082	.170	1.08	.1156
7301 A	.070	.220	1.04	.1071
7301 B	.070	.170	1.04	.1071
7301 C	.070	.170	1.04	.1131
7301 D	.070	.220	1.04	.1071
Qβ average	2.37	.204	7.0	.0956
Qγ average	2.62	.200	7.0	.0876
Qδ average	2.88	.211	7.0	.0917
Qζ average	3.28	.202	7.0	.1036
Qδ 0766	1.38	.211	7.0	.0438
Qδ 0567	1.64	.211	7.0	.0518
Qδ 0768	1.38	.211	7.0	.0399
Qδ 1168	1.27	.211	7.0	.0399

Table IV (continued)

Test no. (run no.)	Deepwater wave height H_o (m)	Median particle diameter D_{50} (mm)	Wave period T (sec)	Dimensionless lower limit h_m/λ_o
Qχ 1168	1.15	.200	7.0	.0438
Qχ 0567	1.49	.200	7.0	.0478
Qχ 0967	1.08	.200	7.0	.0438
Qχ 0668	1.29	.200	7.0	.0478
Qζ 0766	1.57	.200	7.0	.0558
Qζ 0667	1.61	.202	7.0	.0518
Qζ 09/1067	1.38	.202	7.0	.0478
Qζ 0868	1.54	.202	7.0	.0558
Qζ 1268	1.38	.202	7.0	.0517
DSE 300865	1.52	.350	7.5	.0417
DSE 030965	3.17	.350	10.0	.0410
DSE 160965	1.37	.350	7.0	.0479
DNE 110365	1.22	.350	6.6	.0493
DNE 120365	1.83	.350	8.5	.0339
DNE 150365	3.05	.350	8.5	.0523
DNE 170365	1.22	.350	8.5	.0314
DNE 180365	.92	.350	7.5	.0348
DNE 190365	1.83	.350	8.0	.0413
DNE 220365	2.93	.350	9.5	.0455
DNE 230365	2.93	.350	8.5	.0614
DNE 240365	2.01	.350	9.5	.0347
DNE 250365	1.22	.350	9.4	.0243
DNE 260365	1.52	.350	9.4	.0243

REMARK: For location of the prototype cases, see Table IX

Table IV: Lower limit of D-profile.

Property	Model I				Model II			
Flume length (measured from wave board)	17 m				25 m			
Height of walls relative to wave-generator floor	0.50 m				0.70 m			
Possibility to introduce water-level variation	no				yes			
Flume number	A	B	C	D	A	B	C	D
Flume width (m)	1.23	1.23	1.23	1.23	1.14	1.14	1.14	0.91

Table V: General information: two-dimensional models.

Model no.	Test no.	Initial profile no.[1]	Initial distance wave board ⟶ still-water line	Type of wave generation	Still-water depth h[2] (m)	Test duration (hours)	Number of bottom soundings	Deepwater wave height H_o (m)	Wave period T (sec)	Deepwater wave steepness H_o/λ_o (-)	Particle diameter D_{50} (mm)	Ursell-parameter U_r[3] (-)	Orbital velocity at bed u_o[3] (m/sec)	$1.2 \times u_{cr}$ (Goddet [15]) (m/sec)	Remarks
I	6902 B	1	12.3	trans/rot	0.38	135	11	.107	1.55	.0274	.227	13.02	.199	.205	
	6902 C	1	12.5	trans/rot	0.38	135	11	.101	1.55	.0258	.227	12.24	.187	.205	
	6902 D	1	12.6	trans/rot	0.38	135	11	.107	1.55	.0274	.227	13.02	.199	.205	
	6903 A	2	13.3	trans/rot	0.38	200	9	.111	1.55	.0284	.224	13.42	.205	.205	
	6903 B	2	13.3	trans/rot	0.38	200	9	.111	1.55	.0284	.224	13.42	.205	.205	
	6903 C	2	13.3	trans/rot	0.38	200	9	.104	1.55	.0266	.163	12.64	.191	.192	
	6903 D	2	13.3	trans/rot	0.38	200	9	.104	1.55	.0266	.163	12.64	.191	.192	
	7001 B	2	14.7	trans/rot	0.38	205	13	.086	1.55	.0220	.221	10.42	.159	.205	
	7001 C	2	14.7	trans/rot	0.38	205	13	.081	1.55	.0207	.163	9.76	.149	.192	
	7001 D	2	14.7	trans/rot	0.38	205	13	.081	1.55	.0207	.163	9.76	.149	.192	
II	7109 A	3	18.8	trans/rot	0.38	225^{45}	14	.114	1.15	.0552	.220	6.10	.161	.184	
	7109 B	3	18.8	trans/rot	0.38	225^{45}	14	.114	1.15	.0522	.160	6.10	.161	.172	
	7111 A	3	20.0	trans/rot	0.38	225^{45}	10	.107	1.15	.0518	.220	5.74	.152	.184	
	7111 B	3	20.0	trans/rot	0.38	225^{45}	10	.112	1.15	.0543	.160	5.98	.158	.172	
	7112 A	4	18.8	trans/rot	0.38	848^{30}	21	.096	1.15	.0465	.220	5.16	.137	.184	
	7112 B	4	18.8	trans/rot	0.38	848^{30}	21	.093	1.15	.0451	.160	4.98	.132	.172	
	7114 B	4	18.8	trans/rot	0.38 ± 0.025	240^{36}	13	.086	1.15	.0417	.160	5.46	.132	.172	tidal cycle
	7115 A	5	20.3	trans	0.38 ± 0.025	209^{50}	13	.096	1.15	.0465	.220	6.10	.147	.184	period = 1 hr
	7115 B	4	18.8	trans	0.38 ± 0.025	209^{50}	13	.092	1.15	.0446	.160	5.82	.140	.172	
	7115 C	4	18.8	trans	0.38 ± 0.025	209^{50}	13	.097	1.15	.0470	.110	6.16	.149	.155	
	7209 A	6	21.2	trans/rot	0.45	114	5	.113	1.15	.0551	.220	4.00	.133	.184	
	7209 B	6	21.8	trans/rot	0.45	114	5	.114	1.15	.0557	.160	4.04	.134	.172	
	7301 A	7	17.5	trans	0.45	3878	106	.070	1.04	.0417	.220	1.84	.070	.176	
	7301 B	7	17.5	trans	0.45	3878	106	.070	1.04	.0417	.170	1.84	.070	.166	
	7301 C	7	16.5	trans	0.45	3878	106	.070	1.04	.0417	.170	1.84	.070	.166	
	7301 D	7	16.5	trans	0.45	3878	106	.070	1.04	.0417	.220	1.84	.070	.176	

REMARKS: 1) see Figure 51
2) in front of wave generator
3) at point of wave generation

Table VI: Boundary conditions: two-dimensional small-scale tests.

Model no.	Test no.	Still-water depth $h^{1)}$ (m)	Deepwater wave height H_o (m)	Wave period T (sec)	Deepwater wave steepness H_o / λ_o (-)	Littoral current (m^3/sec)	Ursell-parameter $U_r^{2)}$ (-)	Orbital velocity at bed $u_o^{2)}$ (m/sec)	$1.2 \pm u_{cr}$ (Goddet [15]) (m/sec)
III	14	0.38	.100	1.55	.0267	.020	12.17	.186	.205
	17	0.38	.107	1.55	.0285	.048	13.02	.199	.205
	19	0.38	.086	1.55	.0229	.025	10.42	.159	.205
	26	0.38	.081	1.55	.0216	.055	9.76	.149	.205
	27	0.38	.110	1.15	.0533	.055	6.98	.169	.172
	33	0.38 $\pm$ 0.25	.109	1.15	.0528	.050	6.92	.167	.172

Test no.	Initial profile no.$^{3)}$	Initial distance wave board still-water line (m)	Test duration (hours)	Number of bottom soundings	Particle diameter D_{50} (mm)	Mean sand supply (m^3/hr)	Mean amount of trapped sand (m^3/hr)	Remarks
14	1	11.5	60	9	.220	.111	.148	
17	2	13.0	56^{30}	8	.220	.096	.132	
19	3	12.7	50	7	.220	.082	.065	
26	4	12.7	50	8	.220	.061	.120	
27	5	13.1	40	4	.220	.094	.090	
33	6	13.5	30	6	.220	.070	.082	tidal cycle period = 1 hr

REMARKS:
1) in front of wave generator
2) at point of wave generation
3) see Figure 52
4) angle of wave incidence = 10^o at point of wave generation
5) type of wave generation = trans./rot. for all tests

Table VII: Boundary conditions: three-dimensional small-scale tests.

Test no.	Initial beach slope	Still-water depth $h^{1)}$ (m)	Test duration (hours)	Number of bottom soundings	Deepwater wave height H_o (m)	Wave period T (sec)	Deepwater wave steepness H_o/λ_o (-)	Particle diameter D_{50} (mm)	Ursell-parameter $U_r^{2)}$ (-)	Orbital velocity at bed $u_o^{2)}$ (m/sec)	$1.2 \pm u_{cr}$ (Goddet [15]) (m/sec)
CERC 102	1:15	4.57	12	4	1.07	11.33	.0054	.200	73.3	.893	.422
CERC 302	1:15	4.27	50	10	1.39	11.33	.0069	.200	110.6	1.214	.422
CERC 402	1:15	4.42	40	9	1.71	5.60	.0350	.200	20.8	.972	.325
CERC 404	1:15	4.42	40	9	1.71	5.60	.0350	.400	20.8	.972	.386
CERC 502	1:15	4.57	60	11	1.59	3.75	.0725	.200	5.9	.602	.280

REMARKS: 1) in front of wave generator
2) at point of wave generation
3) tank width = 4.57 m
4) these data are used with courtesy of the Coastal Engineering Research Center

Table VIII: Boundary conditions: C.E.R.C.-tests.

Table IX

Run no.[1]	Deepwater wave height[2] H_o (m)	Wave period T (sec)	Deepwater wave steepness H_o/λ_o (-)	Median particle diameter D_{50} (mm)	Location of measurements
Qβ average	2.37	7	.0310	.204	β-lines, Queensland, Australia[3]
Qɣ average	2.62	7	.0342	.200	ɣ-lines, Queensland, Australia[3]
Qδ average	2.88	7	.0377	.211	δ-lines, Queensland, Australia[3]
Qε average	3.20	7	.0418	.213	ε-lines, Queensland, Australia[3]
Qζ average	3.28	7	.0429	.202	ζ-lines, Queensland, Australia[3]
Qβ 0666	1.16	7	.0152	.204	β-lines, Queensland, Australia
Qβ 0567	1.34	7	.0175	.204	
Qβ 0967	.97	7	.0127	.204	
Qβ 0568	1.34	7	.0175	.204	
Qβ 1068	1.01	7	.0131	.204	
Qɣ 0666	1.29	7	.0168	.200	ɣ-lines, Queensland, Australia
Qɣ 0567	1.49	7	.0196	.200	
Qɣ 0967	1.08	7	.0141	.200	
Qɣ 0668	1.29	7	.0169	.200	
Qɣ 1168	1.15	7	.0150	.200	
Qδ 0766	1.38	7	.0180	.211	δ-lines, Queensland, Australia
Qδ 0567	1.64	7	.0214	.211	
Qδ 0768	1.38	7	.0180	.211	
Qδ 1168	1.27	7	.0166	.211	
Qε 0767	1.53	7	.0200	.213	ε-lines, Queensland, Australia
Qε 1067	1.36	7	.0178	.213	
Qε 0968	1.32	7	.0172	.213	
Qε 1168	1.40	7	.0183	.213	
Qζ 0766	1.57	7	.0205	.202	ζ-lines, Queensland, Australia
Qζ 0667	1.61	7	.0210	.202	
Qζ 09/1067	1.38	7	.0180	.202	
Qζ 0868	1.54	7	.0201	.202	
Qζ 1268	1.38	7	.0180	.202	

Run no.[1] (-)	Deepwater wave height[2] H_o (m)	Wave period T (sec)	Deepwater wave steepness H_o/λ_o (-)	Median particle diameter D_{50} (mm)	Location of measurements
DSE 300765	1.22	7.5	.0139	.350	West Street Jetty, Durban, South Africa[4]
DSE 300865	1.52	7.5	.0173	.350	
DSE 030965	3.17	10.0	.0203	.350	
DSE 160965	1.37	7.0	.0179	.350	
DNE 110365	1.22	6.6	.0180	.350	West Street Jetty, Durban, South Africa
DNE 120365	1.83	8.5	.0162	.350	
DNE 150365	3.05	8.5	.0271	.350	
DNE 170365	1.22	8.5	.0108	.350	
DNE 180365	.92	7.5	.0105	.350	
DNE 190365	1.83	8.0	.0183	.350	
DNE 220365	2.93	9.5	.0208	.350	
DNE 230365	2.93	8.5	.0260	.350	
DNE 240365	2.01	9.5	.0143	.350	
DNE 250365	1.22	9.4	.0089	.350	
DNE 260365	1.52	9.4	.0111	.350	
HoHA 301171	4.65	7.65	.0509	.220	Artificial beach, Hook of Holland, the Netherlands
HoHB 301171	4.65	7.65	.0509	.220	
HoHC 301171	4.65	7.65	.0509	.220	

REMARKS: 1) If 6 figures follow the letters in the run number, they indicate the day, month and year respectively, when the measurement was performed (eg. 030965 = 3rd September, 1965). If only 4 figures follow the letters, only the month and year are mentioned (eg. 0666 = June, 1966).

2) Significant wave heights were used.

3) All Queensland data were obtained from Delft Hydraulics Laboratory [10].

4) All Durban data were obtained from Zwamborn and van Wyk [54].

Table IX: Boundary conditions: prototype cases.

Table IX (continued)

Table X

Test no.	Dimensionless location Δ_r (-)	Median particle diameter D_{50} (mm)	Ratio W/W_r (-)
6903 A	-.158	.224	.848
	-.058		.947
	.042		1.033
	.142		1.257
	.242		1.411
	.342		1.440
6903 B	-.158	.224	.795
	-.058		.919
	.042		1.060
	.242		1.288
	.342		1.333
	.642		1.508
7001 B	-.200	.221	.990
	-.100		.958
	0		1.000
	.100		1.089
	.200		1.201
	.300		1.418
	.400		1.464
	.500		1.809
	.600		2.341
7109 A	-.072	.220	.957
	.028		1.020
	.128		1.119
	.228		1.218
	.328		1.314
	.428		1.412
	.528		1.572
	.628		1.761
	.728		2.125

Table X (continued)

Test no.	Dimensionless location Δ_r (-)	Median particle diameter D_{50} (mm)	Ratio W/W_r (-)
7109 B	-.061	.160	.980
	.039		1.013
	.139		1.081
	.239		1.163
	.339		1.253
	.439		1.360
	.539		1.443
	.639		1.680
7111 A	.033	.220	1.014
	.133		1.104
	.233		1.159
	.333		1.291
	.433		1.430
	.533		1.658
	.633		2.298
	.733		2.680
7111 B	-.061	.160	.955
	.039		1.024
	.139		1.129
	.239		1.214
	.339		1.348
	.439		1.512
	.539		1.669
	.639		1.820
	.739		2.064
7112 A (old)	-.043	.220	.965
	.057		1.048
	.157		1.137
	.257		1.260
	.357		1.424
	.457		1.628
	.557		1.880
	.657		2.176
	.757		2.494

Table X (continued)

Test no.	Dimensionless location Δ_r (-)	Median particle diameter D_{50} (mm)	Ratio W/W_r (-)
7112 B (old)	-.043	.160	.963
	.057		1.054
	.157		1.142
	.257		1.182
	.357		1.232
	.457		1.312
	.557		1.452
	.657		1.540
	.757		1.646
7112 B (new)	-.067	.160	.942
	.033		1.010
	.133		1.094
	.233		1.187
	.333		1.242
	.433		1.331
	.533		1.479
	.633		1.698
	.733		1.970
7114 B	-.060	.160	.960
	.040		1.025
	.140		1.124
	.240		1.238
	.340		1.362
	.440		1.470
	.540		1.577
	.640		1.680
	.740		1.730
7115 A	-.079	.220	.990
	.021		1.009
	.121		1.080
	.221		1.194
	.321		1.359
	.421		1.559
	.521		1.728
	.621		1.958
	.721		2.776

Table X (continued)

Test no.	Dimensionless location Δ_r (-)	Median particle diameter D_{50} (mm)	Ratio W/W_r (-)
7115 B	-.085	.160	.952
	.015		1.009
	.115		1.096
	.215		1.210
	.315		1.338
	.415		1.424
	.515		1.502
	.615		1.593
	.715		1.689
7115 C	-.038	.110	.976
	.062		1.045
	.162		1.119
	.262		1.185
	.362		1.252
	.462		1.311
7209 A	-.072	.220	.945
	.028		1.026
	.128		1.109
	.228		1.179
	.328		1.266
	.628		1.720
	.728		2.094
7301 A	-.060	.220	1.000
	.040		1.000
	.140		1.115
	.240		1.150
	.340		1.255
	.440		1.395
	.540		1.680
	.640		2.135
	.740		2.900
7301 B	-.080	.170	.992
	.020		1.032
	.120		1.062
	.220		1.092
	.320		1.151

Table X (continued)

Test no.	Dimensionless location Δ_r (-)	Median particle diameter D_{50} (mm)	Ratio W/W_r (-)
7301 B	.420	.170	1.240
	.520		1.369
	.620		1.538
	.720		1.752
7301 C	-.080	.170	.992
	.020		1.032
	.120		1.067
	.220		1.117
	.320		1.200
	.420		1.340
	.520		1.508
	.620		1.701
	.720		2.114
7301 D	-.060	.220	.960
	.040		1.027
	.140		1.113
	.240		1.219
	.340		1.339
	.440		1.518
	.540		1.748
	.640		2.040
	.740		2.562

Table X: Distribution of W/W_r (two-dimensional model tests).

Table XI

Test no.	Dimensionless location Δ_r (-)	Median particle diameter D_{50} (mm)	Ratio W/W_r (-)
17	.010	.220	1.005
	.110		1.075
	.210		1.186
	.310		1.313
	.410		1.371
19	.010	.220	1.011
	.110		1.096
	.210		1.196
	.310		1.333
	.410		1.488
	.510		1.696
	.610		1.992
	.710		2.400
	.810		2.366
27	-.214	.220	.879
	-.143		.914
	-.071		.953
	0		1.000
	.071		1.051
	.143		1.106
	.214		1.166
	.286		1.236
	.357		1.317
	.429		1.427
	.500		1.567
	.571		1.763
	.643		2.051
	.714		2.485

Table XI (continued)

Test no.	Dimensionless location Δ_r (-)	Median particle diameter D_{50} (mm)	Ratio W/W_r (-)
33	-.100	.220	.954
	0		1.000
	.100		1.058
	.200		1.135
	.300		1.244
	.400		1.329
	.500		1.464
	.600		1.745
	.700		2.579

Table XI: Distribution of W/W_r (three-dimensional model tests).

Table XII

Run no.[1]	Dimensionless location Δ_r (-)	Median particle diameter D_{50} (mm)	Ratio $(L_2 - L_1)/(L_2 - L_1)_r$ (-)	Type of profile[2]
Qβ 0567	.017	.204	.997	A
	.117		1.264	
	.217		1.452	
	.317		1.705	
	.417		1.780	
	.517		1.808	
	.617		1.877	
Qβ 0967	.017	.204	1.020	A
	.117		1.172	
	.217		1.322	
	.317		1.583	
	.417		1.798	
	.517		1.967	
	.617		2.224	
Qβ 0568	.017	.204	1.016	A
	.117		1.142	
	.217		1.318	
	.317		1.452	
	.417		1.698	
	.517		1.948	
	.617		2.290	
Qβ 1068	.017	.204	1.018	A
	.117		1.138	
	.217		1.279	
	.317		1.388	
	.417		1.572	
	.517		1.816	
	.617		2.125	

Table XII (continued)

Run no.[1]	Dimensionless location Δ_r (-)	Median particle diameter D_{50} (mm)	Ratio $(L_2 - L_1)/(L_2 - L_1)_r$ (-)	Type of profile [2]
QX 0567	.018	.200	1.008	E
	.129		1.118	
	.241		1.168	
	.352		1.270	
	.463		1.536	
	.574		2.200	
QX 0967	.018	.200	1.018	E
	.129		1.132	
	.241		1.211	
	.352		1.360	
	.463		1.492	
	.574		1.700	
QX 0668	.018	.200	1.010	E
	.129		1.100	
	.241		1.228	
	.352		1.413	
	.463		1.408	
	.574		1.413	
QX 1168	.018	.200	1.008	E
	.129		1.092	
	.241		1.166	
	.352		1.238	
	.463		1.287	
	.574		1.363	

Table XII (continued)

Run no.[1]	Dimensionless location Δ_r (-)	Median particle diameter D_{50} (mm)	Ratio $(L_2 - L_1)/(L_2 - L_1)_r$ (-)	Type of profile[2]
Qδ 0567	.014	.211	1.012	E
	.097		1.082	
	.182		1.173	
	.264		1.198	
	.347		1.255	
	.431		1.289	
	.514		1.382	
	.597		1.555	
	.681		1.669	
Qδ 0768	.014	.211	1.013	E
	.097		1.100	
	.182		1.207	
	.264		1.221	
	.347		1.244	
	.431		1.305	
	.514		1.387	
	.597		1.520	
	.681		1.553	
Qδ 1168	.014	.211	1.019	E
	.097		1.087	
	.182		1.130	
	.264		1.088	
	.347		1.090	
	.431		1.141	
	.514		1.275	
Qε 0767	.017	.213	1.010	E
	.117		1.117	
	.217		1.204	
	.317		1.262	
	.417		1.271	
	.517		1.301	
	.617		1.199	

Table XII (continued)

Run no.[1]	Dimensionless location Δ_r (-)	Median particle diameter D_{50} (mm)	Ratio $(L_2 - L_1)/L_2 - L_1)_r$ (-)	Type of profile [2]
Qε 1067	.017	.213	1.000	E
	.117		1.058	
	.217		1.042	
	.317		1.222	
	.417		1.259	
	.517		1.362	
	.617		1.452	
Qε 0968	.017	.213	1.009	E
	.117		1.077	
	.217		1.171	
	.317		1.185	
	.417		1.198	
	.517		1.252	
	.617		1.350	
Qε 1168	.017	.213	1.007	E
	.117		1.063	
	.217		1.139	
	.317		1.144	
	.417		1.205	
	.517		1.290	
	.617		1.416	
Qε 0667	.017	.202	1.016	E
	.117		1.112	
	.217		1.142	
	.317		1.220	
	.417		1.363	
	.517		1.453	
	.617		1.713	

Table XII (continued)

Run no.[1]	Dimensionless location Δ_r (-)	Median particle diameter D_{50} (mm)	Ratio $(L_2 - L_1)/(L_2 - L_1)_r$ (-)	Type of profile [2]
Qζ 09/1067	.017	.202	1.012	E
	.117		1.080	
	.217		1.183	
	.317		1.307	
	.417		1.393	
	.517		1.563	
	.617		1.872	
Qζ 0868	.017	.202	1.010	E
	.117		1.098	
	.217		1.198	
	.317		1.347	
	.417		1.410	
	.517		1.483	
	.617		1.521	
Qζ 1268	.017	.202	1.015	E
	.117		1.097	
	.217		1.184	
	.317		1.226	
	.417		1.327	
	.517		1.492	
	.617		1.632	

REMARKS: 1) For an explanation of the run numbers, see Table IX
2) Eroding (E) or accreting (A)

Table XII: Distribution of $(L_2 - L_1)/(L_2 - L_1)_r$ (prototype cases).

Table XIII

Test no. (run no.)	Deepwater wave height H_o (m)	Median particle diameter D_{50} (mm)	Deepwater wave steepness H_o/λ_o (-)	Schematized slope m_r (-)
6902 C	.101	.227	.0258	.0366
6902 D	.107	.227	.0274	.0312
6903 A	.111	.224	.0284	.0392
6903 B	.111	.224	.0284	.0360
6903 C	.104	.163	.0266	.0299
6903 D	.104	.163	.0266	.0280
7109 A	.114	.220	.0552	.0640
7109 B	.114	.160	.0552	.0307
7111 A	.107	.220	.0518	.0489
7111 B	.112	.160	.0543	.0363
7112 A (old)	.096	.220	.0465	.0409
7112 B (old)	.093	.160	.0451	.0287
7112 B (new)	.093	.160	.0451	.0312
7114 B	.086	.160	.0417	.0345
7115 A	.096	.220	.0465	.0423
7115 B	.092	.160	.0446	.0336
7115 C	.097	.110	.0470	.0287
7209 A	.113	.220	.0551	.0405
7209 B	.114	.160	.0557	.0326
7301 A	.070	.220	.0417	.0549
7301 B	.070	.170	.0417	.0314
7301 C	.070	.170	.0417	.0324
7301 D	.070	.220	.0417	.0607
14	.100	.220	.0267	.0400
17	.100	.220	.0267	.0314
19	.080	.220	.0213	.0422
26	.075	.220	.0200	.0450
27	.110	.220	.0533	.0545
33	.100	.220	.0485	.0589

Table XIII (continued)

Test no. (run no.)	Deepwater wave height H_o (m)	Median particle diameter D_{50} (mm)	Deepwater wave steepness H_o/λ_o (-)	Schematized slope m_r (-)
Qβ average	2.37	.204	.0310	.0122
Qɣ average	2.62	.200	.0342	.0163
Qδ average	2.88	.211	.0377	.0153
Qε average	3.20	.213	.0418	.0204
Qζ average	3.28	.202	.0429	.0122
Qβ 0666	1.16	.204	.0152	.0128
Qβ 0567	1.34	.204	.0175	.0146
Qβ 0967	.97	.204	.0127	.0170
Qβ 0568	1.34	.204	.0175	.0182
Qβ 1068	1.01	.204	.0131	.0128
Qɣ 0666	1.29	.200	.0168	.0184
Qɣ 0567	1.49	.200	.0196	.0184
Qɣ 0967	1.08	.200	.0141	.0115
Qɣ 0668	1.29	.200	.0169	.0153
Qɣ 1168	1.15	.200	.0150	.0124
Qδ 0766	1.38	.211	.0180	.0200
Qδ 0567	1.64	.211	.0214	.0200
Qδ 0768	1.38	.211	.0180	.0150
Qδ 1168	1.27	.211	.0166	.0150
Qε 0767	1.53	.213	.0200	.0128
Qε 1067	1.36	.213	.0178	.0170
Qε 0968	1.32	.213	.0172	.0146
Qε 1168	1.40	.213	.0183	.0128
Qζ 0766	1.57	.202	.0205	.0170
Qζ 0667	1.61	.202	.0210	.0204
Qζ 09/1067	1.38	.202	.0180	.0204
Qζ 0868	1.54	.202	.0201	.0146
Qζ 1268	1.38	.202	.0180	.0138

Table XIII: Determination of the schematized slope m_r at the water line.

Test no.	Deepwater wave height H_o (m)	Deepwater wave steepness (H_o/λ_o) (-)	Ratio (H_o/h_m) (-)	Wave period T (sec)	Median particle diameter D_{50} (mm)	$\frac{s_{ym}\ T}{D_{50}}$ (-)
6902 B	.107	.0274	.535	1.55	.227	.0147
6902 C	.101	.0258	.505	1.55	.227	.0136
6902 D	.107	.0274	.535	1.55	.227	.0127
6903 C	.104	.0266	.433	1.55	.163	.0199
7001 B	.086	.0220	.358	1.55	.221	.0073
7001 C	.081	.0207	.312	1.55	.163	.0037
7001 D	.081	.0207	.312	1.55	.163	.0051
7109 A	.114	.0552	.475	1.15	.220	.0119
7109 B	.114	.0552	.439	1.15	.160	.0047
7111 A	.107	.0518	.428	1.15	.220	.0095
7111 B	.112	.0543	.430	1.15	.160	.0068
7112 A (old)	.096	.0465	.320	1.15	.220	.0016
7112 B (old)	.093	.0451	.310	1.15	.160	.0023
7112 B (new)	.093	.0451	.372	1.15	.160	.0036
7114 B	.086	.0417	.366	1.15	.160	.0055
7115 A	.096	.0465	.376	1.15	.220	.0050
7115 B	.092	.0446	.375	1.15	.160	.0053
7115 C	.097	.0470	.353	1.15	.110	.0172
7209 A	.113	.0551	.471	1.15	.220	.0121
7209 B	.114	.0557	.438	1.15	.160	.0043
7301 A	.070	.0417	.333	1.04	.220	.0006
7301 B	.070	.0417	.318	1.04	.170	.0013
7301 C	.070	.0417	.318	1.04	.170	.0011
CERC 102	1.074	.0054	.534	11.33	.200	6.5210
CERC 302	1.386	.0069	.758	11.33	.200	6.0631
CERC 402	1.714	.0350	.750	5.60	.200	2.9859
CERC 404	1.714	.0350	.703	5.60	.400	1.3607
CERC 502	1.590	.0725	.435	3.75	.200	.4843

Table XIV: Determination of s_{ym}.

Table XV

Test no.	Deepwater wave height H_o (m)	Ratio H_o/h_m (-)	Dimensionless location Δ_{2m} (-)
6902 B	.107	.535	.90
6902 C	.101	.505	.90
6902 D	.107	.535	.90
6903 C	.104	.433	.70
6903 D	.104	.320	.60
7109 A	.114	.475	.60
7109 B	.114	.439	.60
7111 A	.107	.428	.50
7111 B	.112	.430	.60
7112 A (old)	.096	.320	.29
7112 B (old)	.093	.310	.43
7112 B (new)	.093	.372	.50
7114 B	.086	.366	.40
7115 A	.096	.376	.40
7115 B	.092	.375	.40
7115 C	.097	.353	.40
7209 A	.113	.471	.80
7209 B	.114	.438	.80
7301 A	.070	.333	.50
7301 B	.070	.318	.40
7301 C	.070	.318	.40
CERC 102	1.074	.534	.50
CERC 302	1.386	.758	.50
CERC 402	1.714	.750	.50
CERC 404	1.714	.703	.60
CERC 502	1.590	.435	.40

Table XV: Position of s_{ym}.

Table XVI

Test no. (-)	Dimensionless location Δ_m (-)	Deepwater wave steepness H_o/λ_o (-)	Ratio H_o/h_m (-)	Ratio s_y/s_{ym} (-)
6902 B	0	.0274	.535	1.000
	.1			.555
	.2			.193
	.3			.109
	.4			.063
	.5			.035
	.6			.031
	.7			.032
	.8			.032
6902 C	0	.0258	.505	1.000
	.1			.490
	.2			.284
	.3			.211
	.4			.187
	.5			.183
	.6			.189
	.7			.190
	.8			.160
6902 D	0	.0274	.535	1.000
	.1			.430
	.2			.190
	.3			.140
	.4			.113
	.5			.095
	.6			.087
	.7			.071
	.8			.056

Table XVI (continued)

Test no. (-)	Dimensionless location Δ_m (-)	Deepwater wave steepness H_o/λ_o (-)	Ratio H_o/h_m (-)	Ratio s_y/s_{ym} (-)
6903 C	0	.0266	.433	1.000
	.2			.390
	.3			.317
	.4			.328
	.5			.315
	.6			.294
	.7			.266
6903 D	0	.0266	.433	1.000
	.1			.302
	.2			.252
	.3			.225
	.4			.194
	.5			.161
7001 D	0	.0207	.312	1.000
	.1			.987
7109 A	0	.0552	.475	1.000
	.1			.965
	.2			.652
	.3			.399
	.4			.244
	.5			.124
7109 B	0	.0552	.439	1.000
	.1			.914
	.2			.720
	.3			.533
	.4			.265
	.5			.052

Table XVI (continued)

Test no. (-)	Dimensionless location Δ_m (-)	Deepwater wave steepness H_o/λ_o (-)	Ratio H_o/h_m (-)	Ratio s_y/s_{ym} (-)
7111 A	0	.0518	.428	1.000
	.1			.901
7111 B	0	.0518	.430	1.000
	.1			.976
	.2			.854
	.3			.623
	.4			.650
	.5			.320
7112 A (old)	0	.0465	.320	1.000
	.1			.885
	.2			.774
7112 B (old)	0	.0451	.310	1.000
	.1			.884
	.2			.784
	.3			.695
7112 B (new)	0	.0451	.372	1.000
	.1			.916
	.2			.872
	.3			.781
	.4			.608
7114 B	0	.0417	.366	1.000
	.1			.986
	.2			.912
	.3			.733
7115 A	0	.0465	.376	1.000
	.1			.870
	.2			.566
	.3			.259

Table XVI (continued)

Test no. (-)	Dimensionless location Δ_m (-)	Deepwater wave steepness H_o/λ_o (-)	Ratio H_o/h_m (-)	Ratio s_y/s_{ym} (-)
7115 B	0	.0446	.375	1.000
	.1			.968
	.2			.861
	.3			.638
7115 C	0	.0470	.353	1.000
	.1			.911
	.2			.791
	.3			.622
7209 A	0	.0551	.471	1.000
	.3			.254
	.4			.294
	.5			.146
	.6			.055
7209 B	0	.0557	.438	1.000
	.1			.957
	.2			.756
	.3			.714
	.4			.577
7301 A	0	.0417	.333	1.000
	.1			.919
	.2			.799
	.3			.719
	.4			.461
	.5			.229
	.6			.250
7301 B	0	.0417	.318	1.000
	.1			.911
	.2			.801
	.3			.694
	.4			.440

Table XVI (continued)

Test no. (-)	Dimensionless location Δ_m (-)	Deepwater wave steepness H_o/λ_o (-)	Ratio H_o/h_m (-)	Ratio s_y/s_{ym} (-)
7301 C	0	.0417	.318	1.000
	.1			.947
	.2			.810
	.3			.710
	.4			.494
CERC 502	0	.0725	.435	1.000
	.1			.797
	.2			.595
	.3			.282

Table XVI: Distribution of s_y/s_{ym} (onshore branch).

Table XVII

Test no. (-)	Dimensionless location Δ_m (-)	Deepwater wave steepness H_o/λ_o (-)	Ratio H_o/h_m (-)	Ratio s_y/s_{ym} (-)
6902 B	0	.0274	.535	1.000
6902 C	0	.0258	.505	1.000
6902 D	0	.0274	.535	1.000
6903 C	0	.0266	.433	1.000
	.1			.569
6903 D	0	.0266	.433	1.000
	.1			.739
	.2			.672
	.3			.740
7001 C	0	.0207	.312	1.000
	.1			.592
	.2			.513
	.3			.461
	.4			.343
	.5			.209
	.6			.040
7001 D	0	.0207	.312	1.000
	.1			.915
	.2			.755
	.3			.577
	.4			.365
	.5			.141
	.6			.026
7109 A	0	.0552	.475	1.000
	.1			.804
	.2			.907
	.3			.432

Table XVII (continued)

Test no. (-)	Dimensionless location Δ_m (-)	Deepwater wave steepness H_o/λ_o (-)	Ratio H_o/h_m (-)	Ratio s_y/s_{ym} (-)
7109 B	0	.0552	.439	1.000
	.1			.982
	.2			.540
	.3			.185
7111 A	0	.0518	.428	1.000
	.1			.964
	.2			.802
	.3			.208
	.4			.182
7111 B	0	.0518	.430	1.000
	.1			.929
	.2			.619
	.3			.323
7112 A (old)	0	.0465	.320	1.000
	.1			.957
	.2			.868
	.3			.736
	.4			.510
	.5			.326
	.6			.154
7112 B (old)	0	.0451	.310	1.000
	.1			.930
	.2			.723
	.3			.439
	.4			.289
7112 B (new)	0	.0451	.372	1.000
	.1			.982
	.2			.736
	.3			.446
	.4			.236

Table XVII (continued)

Test no. (-)	Dimensionless location Δ_m (-)	Deepwater wave steepness H_o/λ_o (-)	Ratio H_o/h_m (-)	Ratio s_y/s_{ym} (-)
7114 B	0	.0417	.366	1.000
	.1			.986
	.2			.998
	.3			.914
	.4			.681
	.5			.513
7115 A	0	.0465	.376	1.000
	.1			.902
	.2			.763
	.3			.774
	.4			.573
	.5			.131
7115 B	0	.0446	.375	1.000
	.1			.956
	.2			.925
	.3			.839
	.4			.627
	.5			.454
7115 C	0	.0470	.353	1.000
	.1			.985
	.2			.858
	.3			.644
	.4			.496
	.5			.411
7209 B	0	.0557	.438	1.000
	.1			.622
7301 A	0	.0417	.333	1.000
	.1			.822
	.2			.465
	.3			.262
	.4			.169

Table XVII (continued)

Test no. (-)	Dimensionless location Δ_m (-)	Deepwater wave steepness H_o/λ_o (-)	Ratio H_o/h_m (-)	Ratio s_y/s_{ym} (-)
7301 B	0	.0417	.318	1.000
	.1			.930
	.2			.682
	.3			.449
	.4			.303
	.5			.182
7301 C	0	.0417	.318	1.000
	.1			.806
	.2			.520
	.3			.329
	.4			.209
	.5			.129
CERC 502	0	.0725	.435	1.000
	.1			.983
	.2			.628
	.3			.272
	.4			.041

Table XVII: Distribution of s_y/s_{ym} (offshore branch).

Table XVIII

Test no.	δ_1/δ	$s_{y_{3D}}$	$\overline{(\frac{\tau_{wc}}{\tau_w})}$ (crest)	$\overline{(\frac{\tau_{wc}}{\tau_w})}$ (crest + trough)	$\frac{s_{y_{3D}}}{s_{y_{2D}}}$
19	.1	.0285	-	-	-
	.2	.0315	1.221	1.175	3.93
	.3	.0386	1.195	1.147	3.54
	.4	.0431	1.235	1.180	2.64
	.5	.2270	1.273	1.213	8.90
	.6	.2050	1.316	1.251	6.72
	.7	.1500	1.356	1.287	7.89
	.8	.0632	1.358	1.287	5.80
	.9	.0380	1.361	1.292	5.56
26	.1	.0080	-	-	-
	.2	.0137	1.185	1.127	2.61
	.3	.0229	1.268	1.169	3.80
	.4	.0243	1.322	1.193	3.49
	.5	.0310	1.379	1.221	3.43
	.6	.0341	1.442	1.255	2.53
	.7	.3200	1.834	1.770	12.21
	.8	.1880	1.854	1.788	3.80
	.9	.0995	1.829	1.763	4.56
33	.1	.1125	-	-	-
	.2	.2128	2.099	2.059	20.66
	.3	.3927	2.246	2.212	29.31
	.4	.5537	2.151	2.103	29.93
	.5	.3372	2.055	1.996	12.68
	.6	.3692	1.753	1.678	10.23
	.7	.3241	1.417	1.340	9.70
	.8	.2018	1.154	1.112	9.30
	.9	.0558	1.052	1.033	4.70

Table XVIII: Increase in coastal constant s_y.

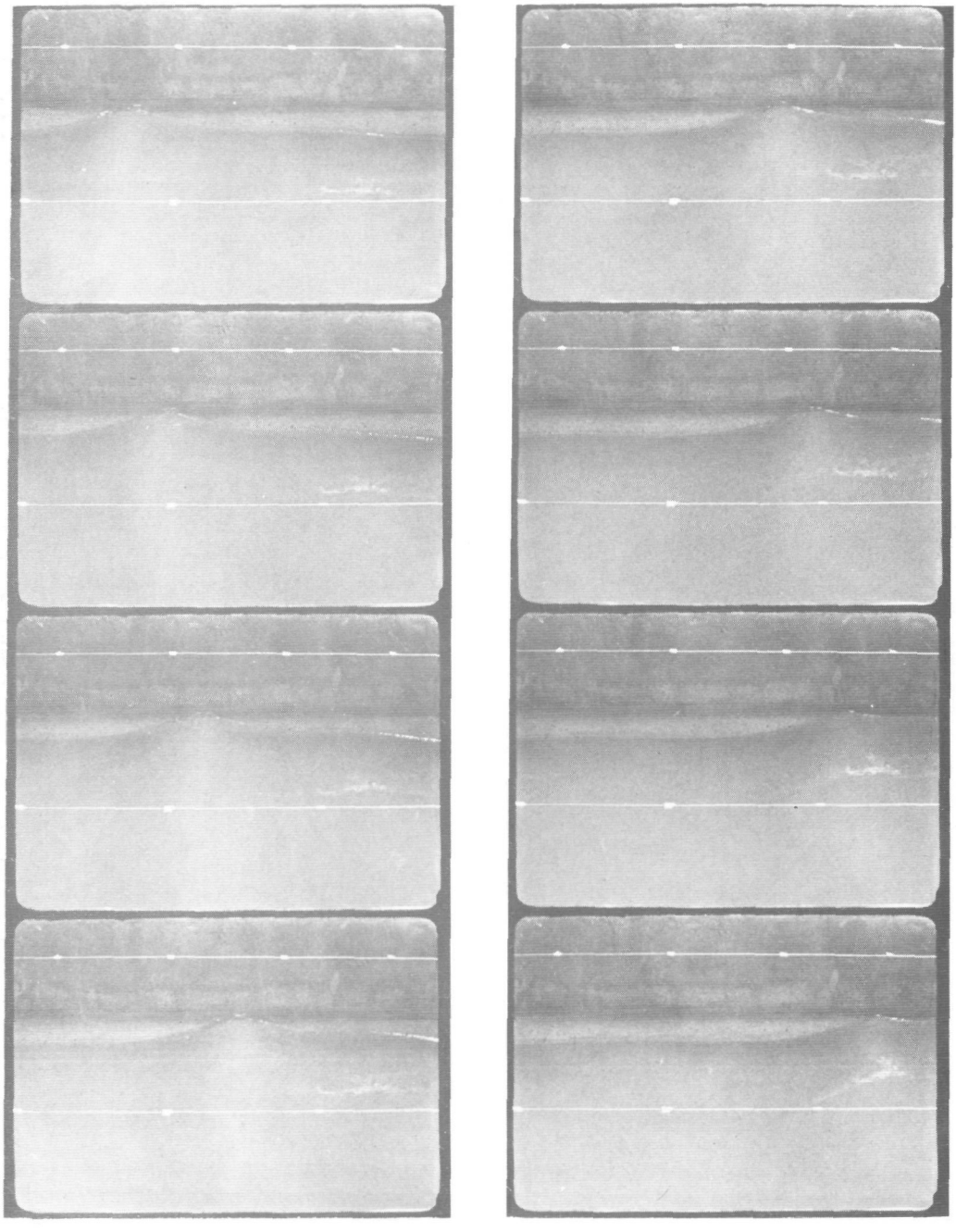

visually determined p = 0
calculated energy loss = 0 %
breaker index γ = 0.533; $\frac{H_0}{\lambda_0}$ = 0.042; tan α = 0.210

1. Breaking wave: p = 0

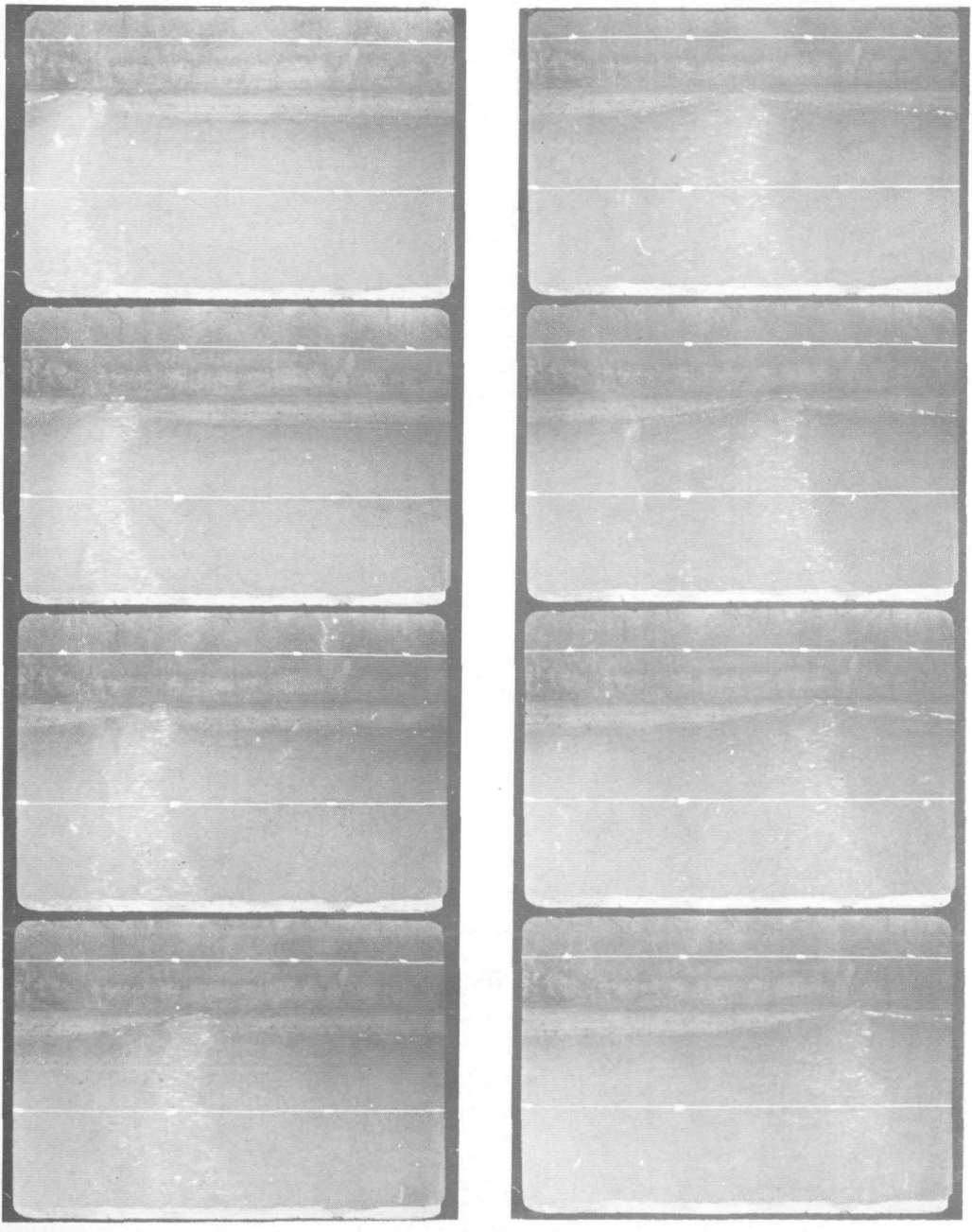

visually determined $p = 0.1$
calculated energy loss = 23 %
breaker index $\gamma = 0.572$; $\frac{H_0}{\lambda 0} = 0.042$; $\tan \alpha = 0.197$

2. Breaking wave: $p = .1$

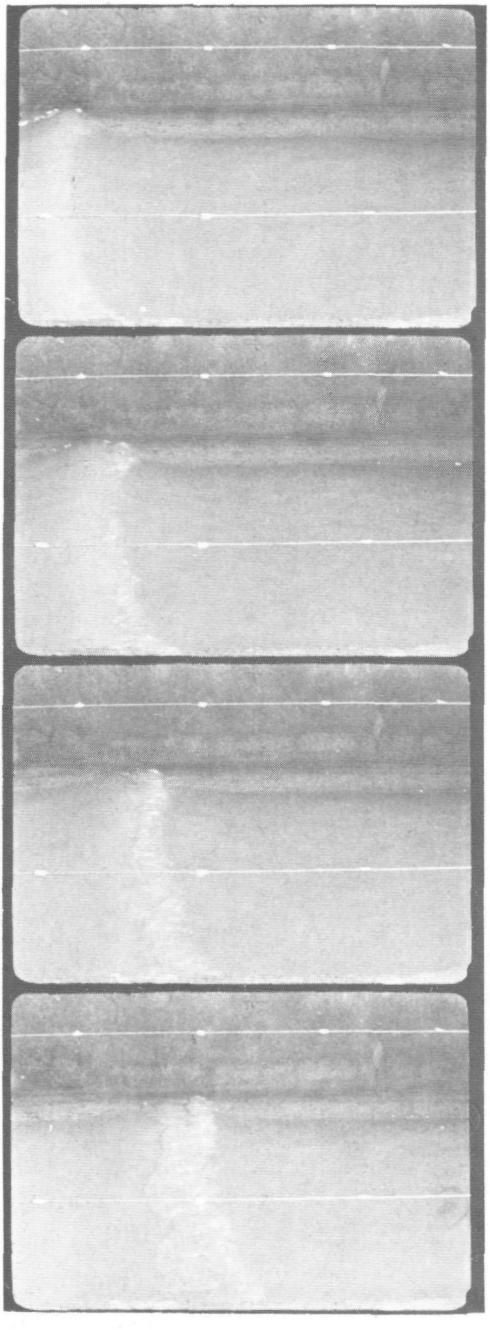

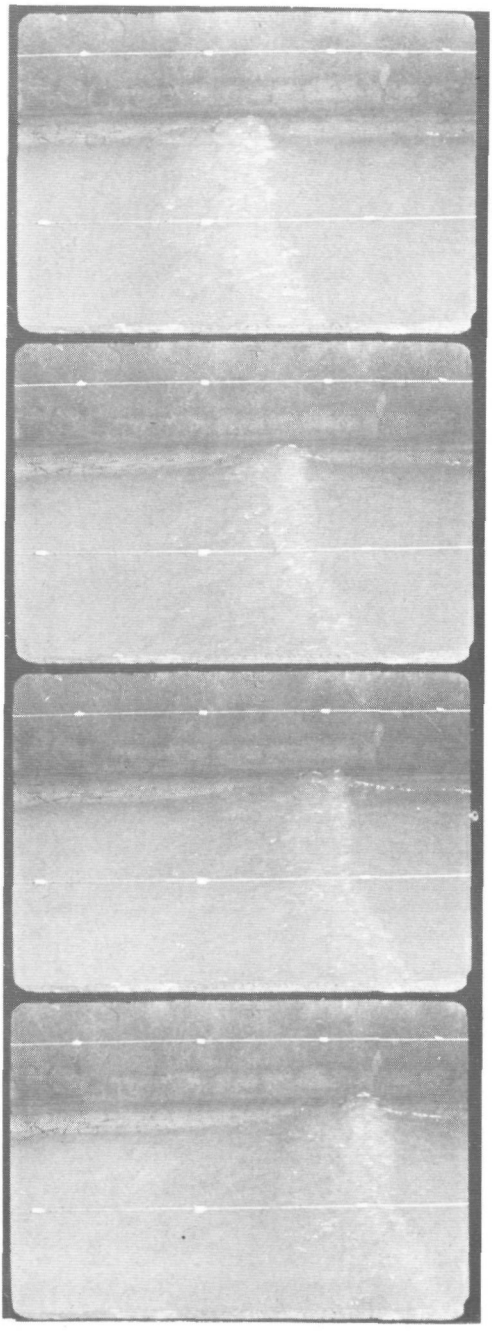

visually determined p = 0.2
calculated energy loss = 23 %
breaker index γ = 0.637; $\frac{H_0}{\lambda_0}$ = 0.042; tan α = 0.142

3. Breaking wave: p = .2

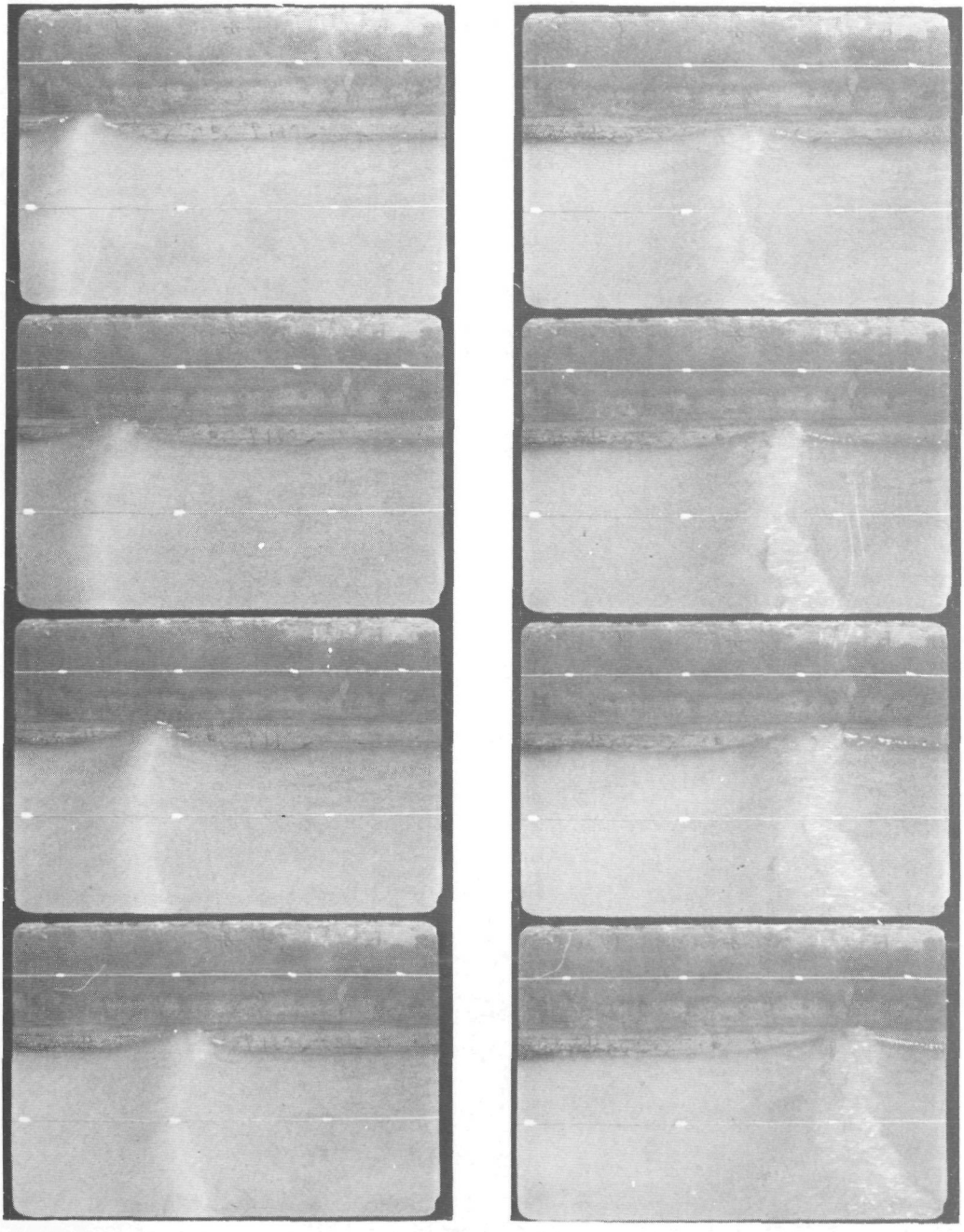

visually determined p = 0.3
calculated energy loss = 29 %
breaker index γ = 0.640; $\frac{H_0}{\lambda_0}$ = 0.042; tan α = 0.070

4. Breaking wave: p = .3

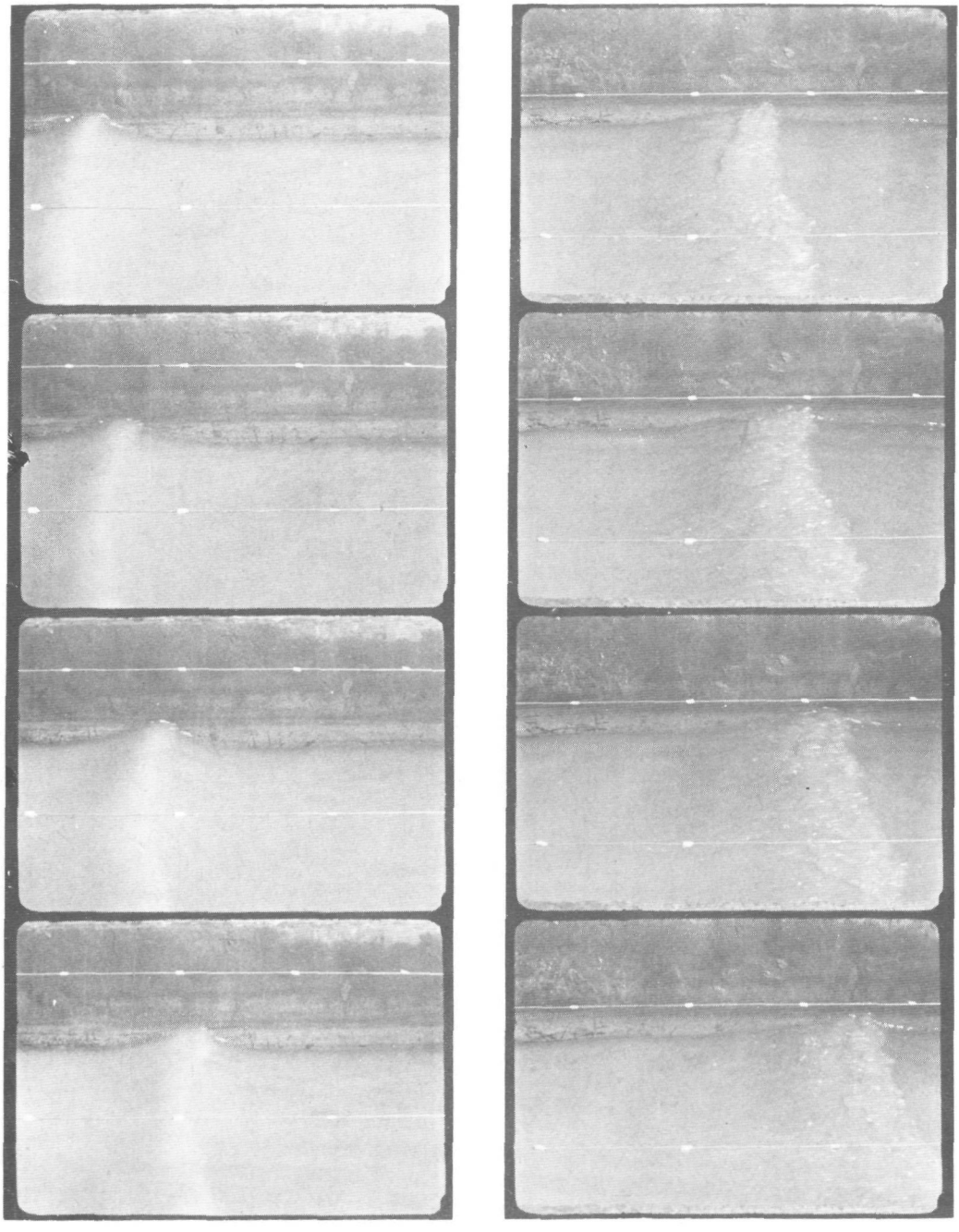

visually determined $p = 0.4$
calculated energy loss = 39 %
breaker index $\gamma = 0.725$; $\frac{H_0}{\lambda_0} = 0.042$; $\tan \alpha = 0.122$

5. Breaking wave: $p = .4$

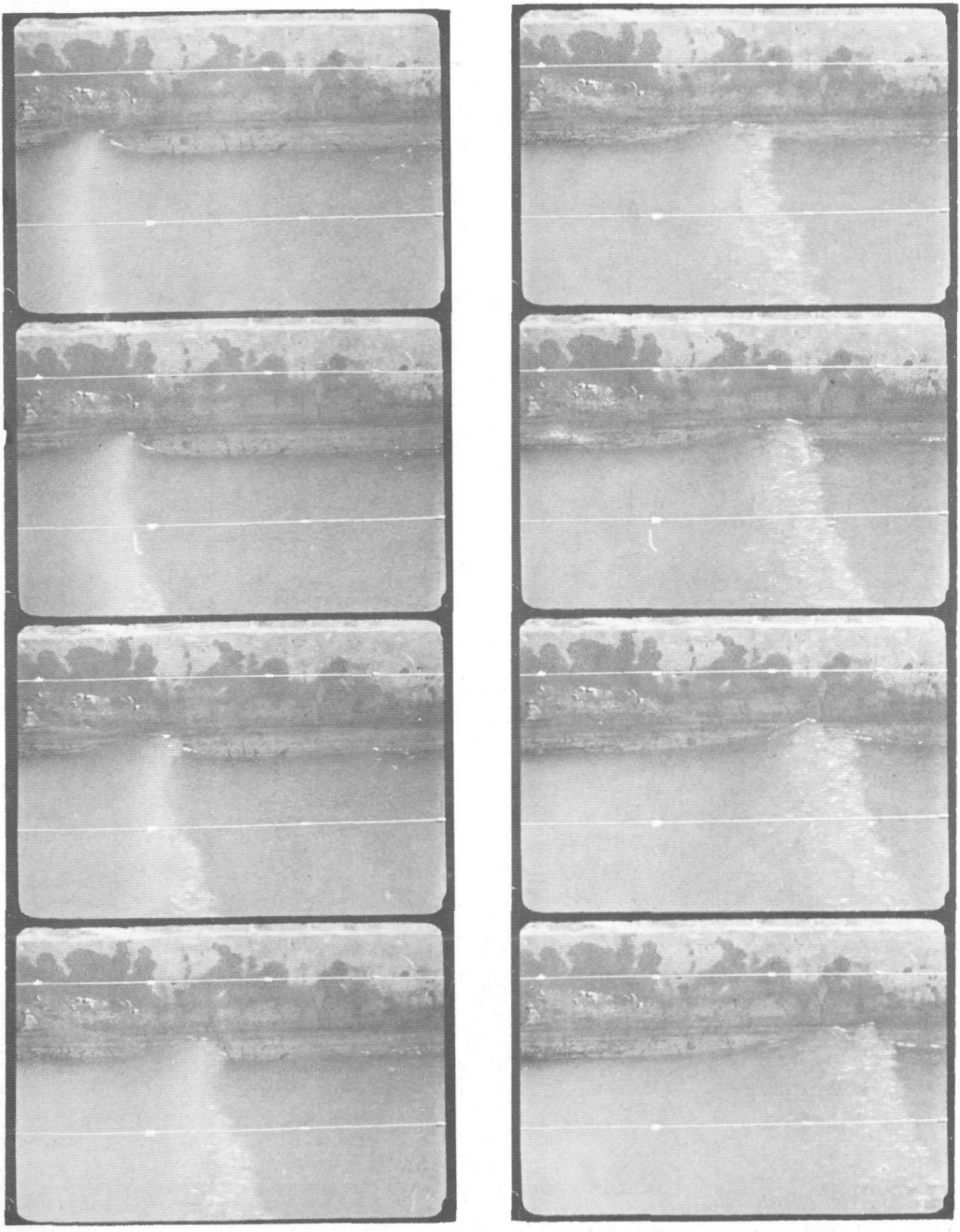

visually determined p = 0.5
calculated energy loss = 47 %
breaker index γ = 0.718; $\frac{H_0}{\lambda_0}$ = 0.042; tan α = 0.079

6. Breaking wave: p = .5

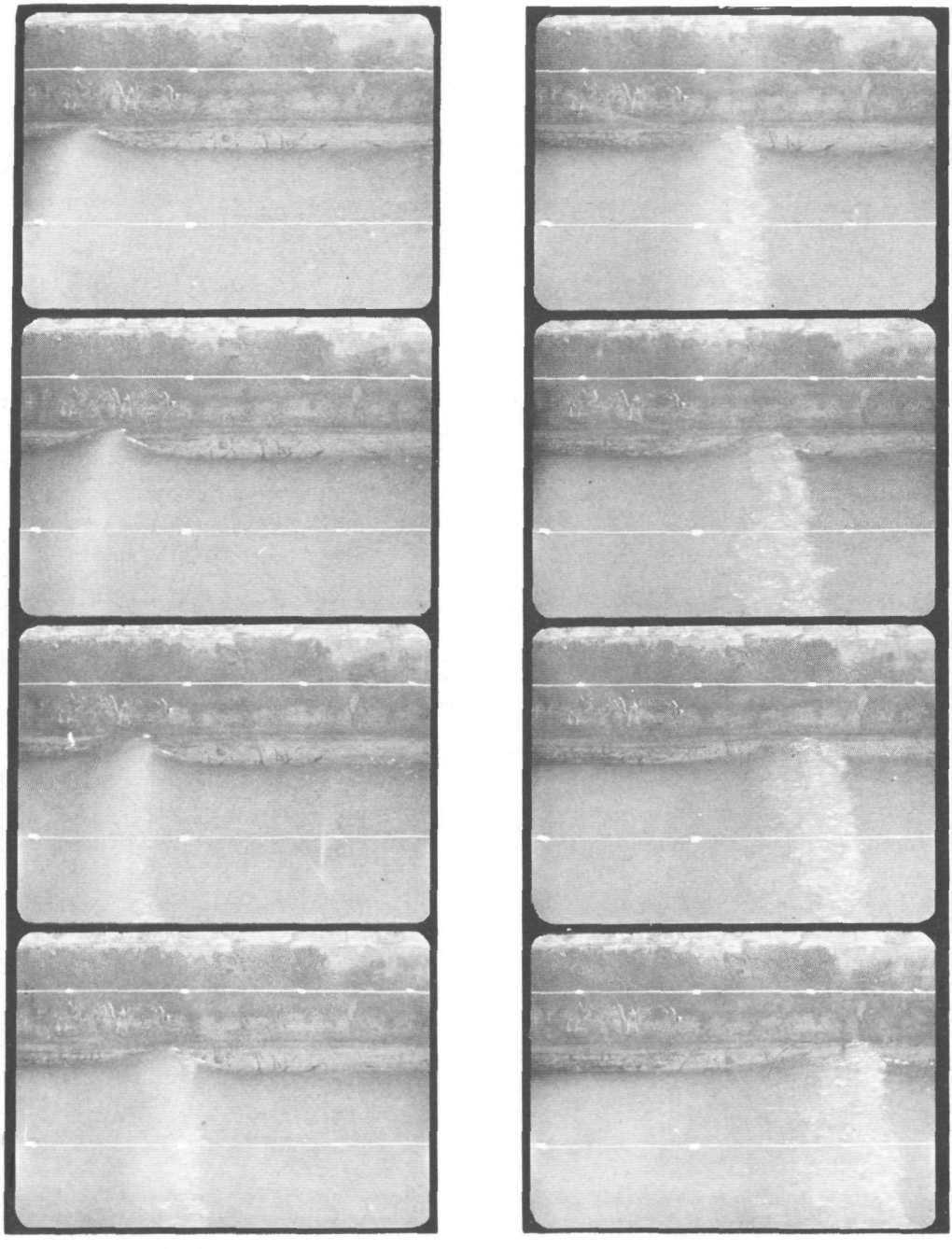

visually determined p = 0.6
calculated energy loss = 62 %
breaker index γ = 0.770; $\frac{H_0}{\lambda_0}$ = 0.042; tan α = 0.120

7. Breaking wave p = .6

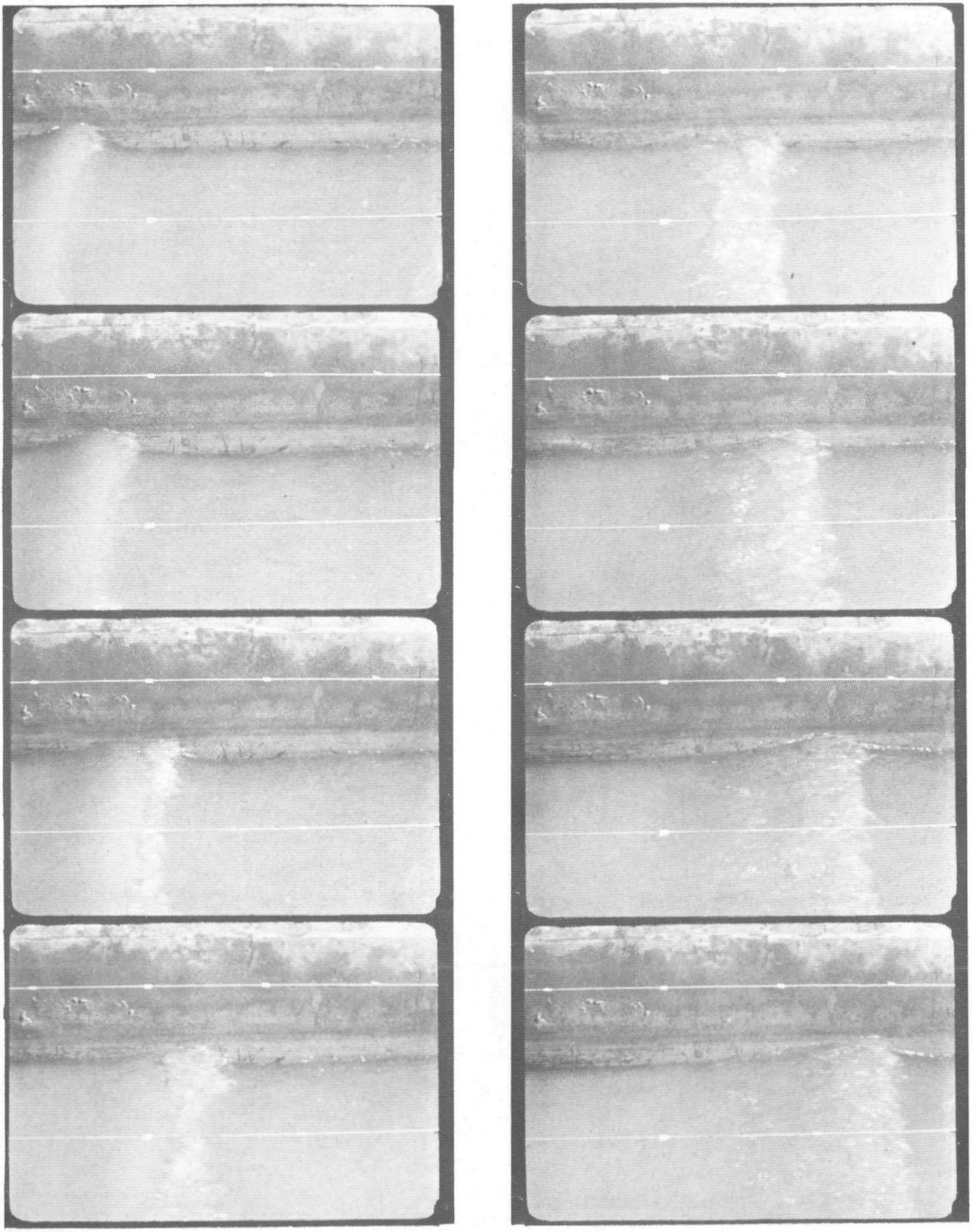

visually determined p = 0.7
calculated energy loss = 69 %
breaker index γ = 0.814; $\frac{H_0}{\lambda_0}$ = 0.042; tan α = 0.095

8. Breaking wave p = .7

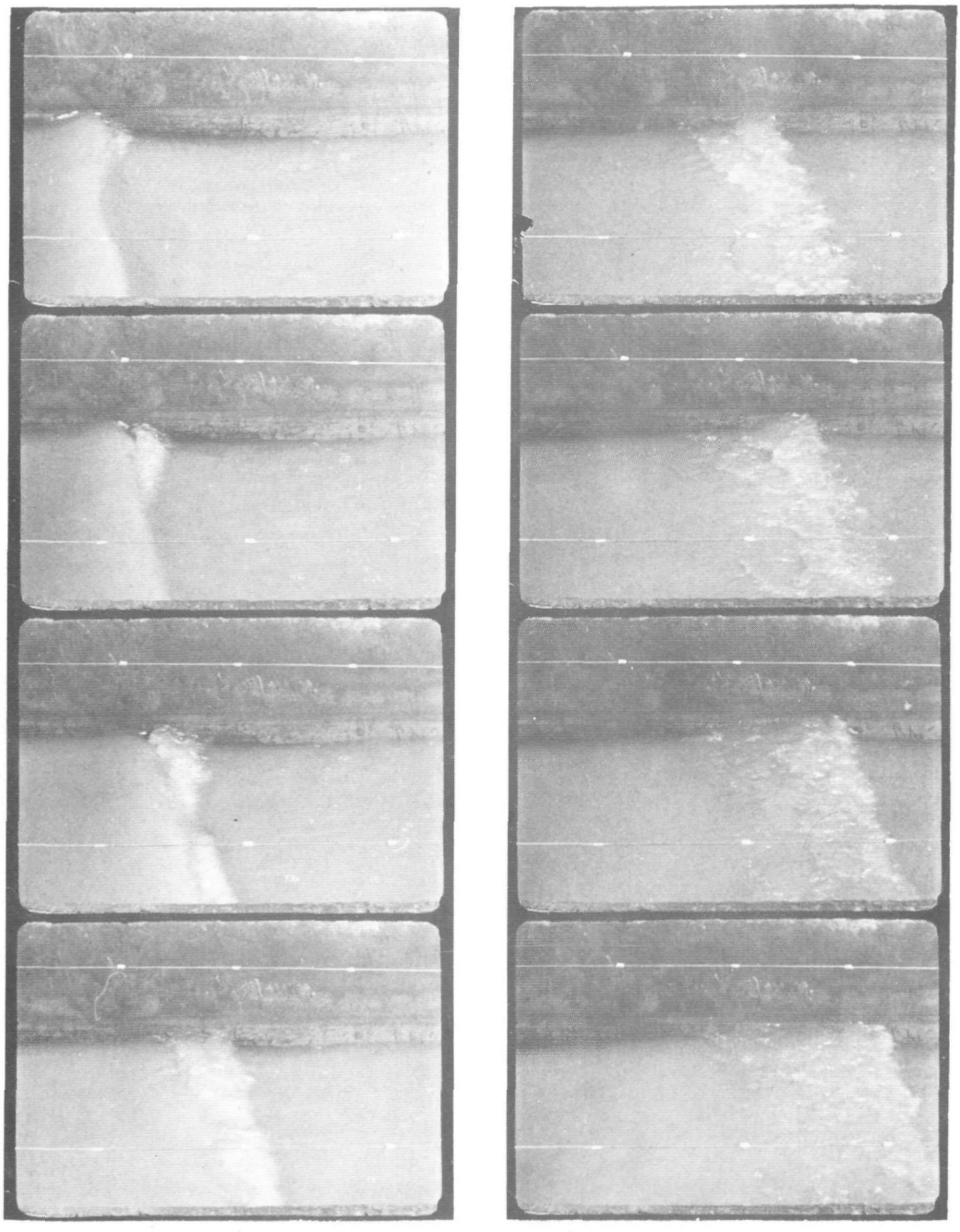

visually determined p = 0.8
calculated energy loss = 78 %
breaker index γ = 0.925; $\frac{H_0}{\lambda_0}$ = 0.042; tan α = 0.070

9. Breaking wave: p = .8

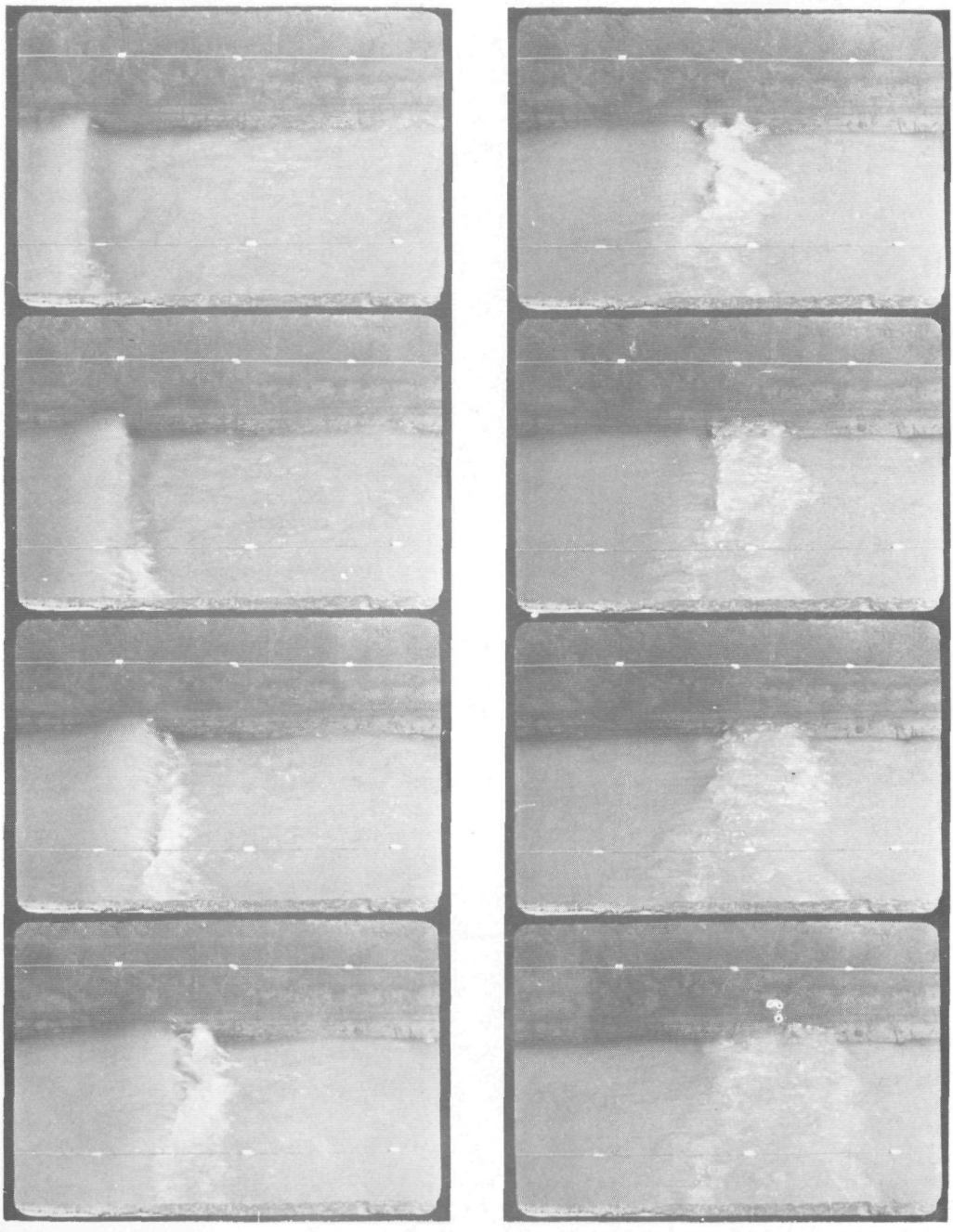

visually determined p = 0.9
calculated energy loss = 90 %
breaker index $\gamma = 0.960$; $\frac{H_0}{\lambda_0} = 0.042$; $\tan \alpha = 0.092$

10. Breaking wave: p = .9

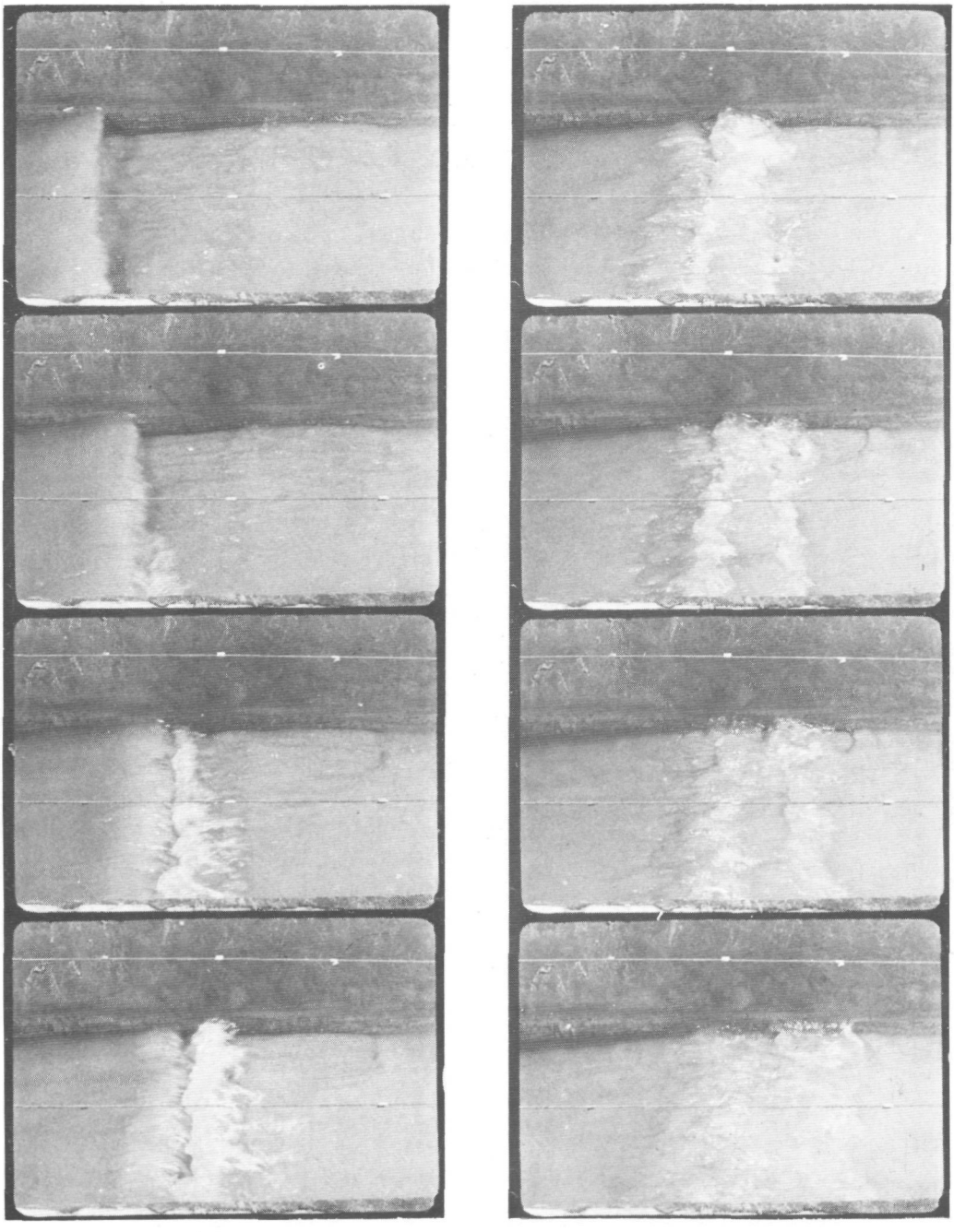

visually determined p = 1.0
calculated energy loss = 98 %
breaker index γ = 0.885; $\frac{H_0}{\lambda_0}$ = 0.042; tan α = 0.135

11. Breaking wave: p = 1.0

SAMENVATTING

Indien het snelheidsveld en het sedimentgehalte van het water in het kustgebied exact bekend zijn in termen van golf-, bodem- en sedimenteigenschappen, kan de grootte van het sedimenttransport loodrecht op de kust (dwarstransport) exact worden berekend. Het onderzoek naar het interne mechanisme van de sedimentbeweging is echter nog niet zover gevorderd dat een dergelijke berekening via het interne mechanisme van het sedimenttransport mogelijk is. De voortgang van dat onderzoek zal in grote mate worden bepaald door het beschikbaar komen van betere meetapparatuur. In hoofdstuk 2 wordt aangetoond op welke wijze het dwarstransport kan worden bepaald indien de concentratieverdeling en het snelheidsveld voldoende bekend zouden zijn.

Met een proef, die in totaal 3878 uur duurde, is aangetoond dat een kustprofiel onder inwerking van golven na langere tijd een evenwichtsligging en evenwichtsvorm zal bereiken. Dit resultaat en de bovengenoemde analyse in hoofdstuk 2 leiden tot de conclusie dat het dwarstransport op een tijdstip t evenredig is aan het verschil tussen het profiel op dat tijdstip t en het evenwichtsprofiel.

In hoofdstuk 3 wordt nagegaan op welke wijze de schematisatie, die uit hoofdstuk 2 volgt, het beste kan worden toegepast om met behulp van beschikbare resultaten van modelproeven te komen tot een voorspelling van de grootte van het dwarstransport. Hieruit blijkt dat het bepalen van de grenzen waarbinnen de schematisatie zal gelden, uitermate belangrijk is. Dat gebied wordt het D-profiel genoemd. De bovenbegrenzing van het D-profiel wordt gelijkgesteld aan het peil van de maximale golfoploop, terwijl de benedenbegrenzing wordt gerelateerd aan het punt van begin van beweging van het bodemmateriaal.

De tijdsafhankelijke transportcapaciteiten in de gebieden boven de grens van golfoploop en beneden de ondergrens van het D-profiel worden in hoofdstuk 4 berekend op grond van fysische overwegingen en de gekozen profielschematisatie. Deze transporten dienen als randvoorwaarden voor de veranderingen in het D-profiel.

In hoofdstuk 5 worden de gegevens, die gebruikt zijn om te komen tot fysisch-gegronde empirische verbanden, vermeld. Deze gegevens omvatten alle daarvoor

geschikte in het Waterloopkundig Laboratorium aanwezige resultaten van twee- en driedimensionale modelproeven inzake de ontwikkeling van kustprofielen. Hierbij inbegrepen zijn een aantal proeven op grote schaal (golfhoogte ≈ 1 à 2 m), gedaan door de U.S. Army Coastal Engineering Research Center te Washington. Verder zijn die prototypemetingen, waarbij met voldoende zekerheid de randvoorwaarden bekend zijn, ook bij de verwerking betrokken.

In hoofdstuk 6 zijn de verkregen resultaten gecorreleerd aan de randvoorwaarden. Hierdoor wordt het mogelijk om met behulp van de gevonden relaties het dwarstransport zowel als de tijdsafhankelijke profielen en eventuele evenwichtsprofielen van kusten te berekenen. In het algemeen is in een tweedimensionaal geval het dwarstransport een functie van het kustprofiel, de golfhoogte en golfsteilheid op diep water, de golfperiode, het type brekende golf en de korreldiameter van het bodemmateriaal, terwijl het evenwichtsprofiel wordt bepaald door de golfhoogte en golfsteilheid op diep water, de golfperiode en de korreldiameter van het bodemmateriaal. Het effect van driedimensionaliteit (scheefinvallende golven) is eveneens onderzocht. In dit geval neemt de schuifspanning aan de bodem toe als gevolg van de aanwezigheid van een stroom evenwijdig aan de kust, wat een vergroting van het dwarstransport ten gevolge heeft. Het evenwichtsprofiel onder driedimensionale omstandigheden is echter bij benadering gelijk aan dat onder tweedimensionale omstandigheden.

Aangezien in vrijwel alle beschikbare proeven kusterosie optrad, gelden de in dit proefschrift gevonden relaties in eerste instantie alleen voor zeewaarts gericht dwarstransport.

In hoofdstuk 6.5 wordt de toepassing van de schematisatie beschreven.

STELLINGEN

I

Als het sedimentgehalte van het water en het snelheidsveld in het kustgebied exact bekend worden in termen van golf-, bodem- en sedimenteigenschappen, kan de in dit proefschrift gegeven benadering van de grootte van het sedimenttransport loodrecht op de kust (dwarstransport) worden vervangen door een exacte berekening ervan volgens de in hoofdstuk 2 getoonde werkwijze.

II

Proeven in een grote goot zijn een noodzakelijke volgende stap in het realiseren van een exacte voorspelling van het sedimenttransport loodrecht op de kust. Het is echter niet zo dat de resultaten die verkregen worden uit proeven in een grote goot, direct naar het prototype vertaalbaar zullen zijn. Het effect van driedimensionaliteit moet dan nog worden onderzocht.

III

Met behulp van de invloed van de bodemruwheid op de snelheidsverticaal onder een golf, zoals gehanteerd in hoofdstuk 6.4, en door aanpassing van de coëfficiënt van Von Kármán aan de veranderde energieverdeling en het turbulentiepatroon in een stromingstoestand met sedimentbeweging, kan de formule voor het bepalen van het langstransport, zoals gegeven door Bijker (Bijker, E.W., Proceedings, ASCE, Journal of the Waterways, Harbours and Coastal Engineering Division, WW4, pp. 687 - 701, November, 1971), worden verbeterd.

IV

Indien de waterbeweging in de omgeving van een constructie aan de kust voldoende bekend is, kan een combinatie van de langstransportformule van Bijker (Bijker, E.W., Proceedings, ASCE, Journal of the Waterways, Harbours and Coastal Engineering Division,WW4, pp. 687 - 701, November, 1971) en de verbanden voor dwarstransport, zoals deze zijn afgeleid in dit proefschrift, een beter inzicht verschaffen in de door de constructie veroorzaakte bodemveranderingen, dan tot nu toe via langstransportberekeningen alleen kon worden verkregen.

V

Aangezien de vergelijking voor de bodemhelling, gegeven door Eagleson en Johnson (Eagleson, P.S. and Johnson, J.W. Coastal processes, in: Estuary and Coastline Hydrodynamics, editor: A.T. Ippen, Chapter 9, McGraw-Hill Book Company, Inc., June, 1966), en die voor het evenwichtsprofiel, zoals gegeven in dit proefschrift, verschillende toepassingsgebieden hebben, kan een combinatie van genoemde twee vergelijkingen leiden tot een beschrijving van het profiel landwaarts van het punt van begin van beweging, die volledi-ger is dan tot nu toe mogelijk was.

VI

Een voorwaarde voor een juiste weergave van de golfoploop in een hydraulisch model is dat de verticale en horizontale schaal aan elkaar gelijk zijn (Hunt, I.A., Design of seawalls and breakwaters; Proceedings, ASCE, Journal of the Waterways and Harbours Division, 85, No. WW3, paper 2172, pp.123 - 152, September, 1951). Aangezien in een kustmodel met beweeglijke bodem deze schalen ongelijk aan elkaar zijn, zullen schaaleffecten optreden in het gebied tussen de stille waterspiegel en de grens van maximale golfoploop.

VII

In een morfologisch model van een riviermond zijn er veelal gebieden te onderkennen, waar het sedimenttransport wordt veroorzaakt door alleen stroom en door stroom en golven tezamen. Op grond van de respectieve transportformules van Frijlink en Bijker (Bijker, E.W., Proceedings, ASCE, Journal of the Waterways, Harbours and Coastal Engineering Division, WW4, pp. 687 - 701, November, 1971) moet worden geconcludeerd, dat als gevolg van de verschillende bodemruwheden de transportschalen in deze twee gebieden niet gelijk zullen zijn. Daardoor is een juiste weergave van de bodemligging in het overgangsgebied niet mogelijk.

VIII

Op grond van fysisch inzicht, gesteund door zowel praktijkgegevens als modelonderzoekingen, moet het aanleggen van z.g. "low-weir sections" in havendammen, met als doel de afvoer van een gedeelte van het langstransport, worden ontraden.

IX

Voor een goede uitvoering van een waterloopkundig modelonderzoek levert een bezoek ter plaatse door de projectingenieur veelal een waardevolle bijdrage tot de oplossing van het probleem.

X

Om een optimaal gebruik te kunnen maken van een beschikbaar computerprogramma, moet de gebruiker volledig op de hoogte zijn van de mogelijkheden van dat programma en de beginselen die eraan ten grondslag liggen.

XI

Het zou tot de aanvaarde normen moeten behoren, dat de samensteller van een empirisch verband de beperkingen van het toepassingsgebied van de door hem gevonden relatie duidelijk vermeldde.

XII

De kustwaterbouwkunde in het algemeen is een relatief jonge tak der technische wetenschappen; het volledig beschrijven van alle processen zal daarom nog enkele tientallen jaren vergen. Als ingenieur is een kustwaterbouwkundige echter wel verplicht om adviezen uit te brengen, ook op korte termijn. Daarom moet hij zich vaak verlaten op meer of minder betrouwbare benaderingsmethodieken (the skill of engineering is to draw sufficient conclusions from insufficient data).

XIII

Milieuproblemen zouden makkelijker kunnen worden opgelost als de terminologieën van de vertegenwoordigers van de verschillende erbij betrokken vakdisciplines (biologen, sociologen, planologen, ingenieurs, enz.) beter op elkaar zouden zijn ingesteld.

XIV

Het bestuur van een vereniging kan pas dan effectief functioneren als het ook daadwerkelijk bij de verenigingsactiviteiten betrokken is.